Author:
Doungsong, Nettraporn

Title:
Synthesis and Characterization of Poly(acrylic acid) based Microgels for Formulation Applications

Synthesis and Characterization of Poly(acrylic acid) based Microgels for Formulation Applications

Nettraporn Doungsong

A dissertation submitted to the University of Bristol in accordance with the requirements for award of the degree of Doctor of Philosophy in the Faculty of Science

School of Chemistry

September 2018

Synthesis and Characterization of Poly(acrylic acid) based Microgels for Formulation Applications

Nettraporn Doungsong

A dissertation submitted to the University of Bristol in accordance with the requirements for award of the degree of Doctor of Philosophy in the Faculty of Science

School of Chemistry

September 2018

Word Count: 38,979

To my parents Wilai and Torn Doungsong

Without whom, in many respects,

this thesis would not have been written.

Author's Declaration

I declare that the work in this dissertation was carried out in accordance with the requirements of the University of Bristol. This work is original, except where indicated by special reference in the text, and no part of the dissertation has been submitted for any other academic award. Any views expressed in the dissertation are those of the author.

Signed …….

Date ……

Abstract

pH-responsive microgels are cross-linked polymer latex particles which can swell / deswell in response to pH and salt concentration of their external surroundings. This project focuses on pH-responsive microgels, particularly based on poly(acrylic acid) (PAA) hydrophobically modified with poly(ethers) *i.e.* poly(propylene glycol) (PPG) and poly(tetrahydrofuran) (PTHF). PAA is well known as pH-responsive and hydrophilic polymer due to the presence of ionizable carboxyl group, whilst PPG and PTHF are considered as hydrophobic polymers. Interestingly, these poly(ethers) are not widely used to incorporate in PAA based hydrogels yet.

With chemical cross-linking, we present a two-step method to prepare well-defined PAA micro-spherical hydrogels with either poly(propylene glycol) diacrylate (PPGDA) or poly(tetrahydrofuran) diacrylate (PTHFDA) as macro cross-linkers. Firstly, poly(*tert*-butyl acrylate) (P*t*BA) microparticles were produced by surfactant free emulsion polymerization with KPS as ionic initiator in aqueous medium. Then, the *tert*-butyl group of P*t*BA was hydrolyzed to carboxylic acid with trifluoroacetic acid (TFA) in dichloromethane (DCM) so PAA microgels were obtained. The chemical structure of resulting PAA microgels was confirmed by ^{1}H-, ^{13}C-, and HSQC-NMR. The effect of cross-linking density on the swelling of the microgels was investigated by varying the molar ratio of monomer to cross-linker at 50:1, 75:1 and 100:1 for PAA/PPG and at 100:1 and 300:1 for PAA/PTHF microgels. At high pH, the carboxylic acid (-COOH) of PAA was ionized to carboxylate anions (COO^{-}) so electrostatic repulsion between these negatively charged groups contributed to the swelling of the PAA microgels. In some cases, a small effect of cross-linking density was observed so that the swelling is larger for particles with a lower cross-linking density. In addition, the shape factor ($\rho = R_G/R_H$) obtained by the combination of DLS and SLS informed that the structure of P*t*BA particles was consistent with homogeneous hard spheres (ρ = 0.775); for PAA particles, somewhat lower values were found, which is commonly the case for microgel particles containing a dense core with a loose shell. For 100:1 PAA/PPG microgels in pH 4.5 solutions, the addition of salt resulted in the shrinkage of the microgels due to salt screening effect, while the addition of low M_w PEO increases the particle size of the microgels possibly due to the association between PAA and PEO through hydrogen bonding.

Additionally, physical association between PAA and poly(ethers) in solutions was investigated using various techniques (^{1}H-NMR, DOSY NMR and T_2 proton solvent relaxation). In our experiment, the mixture of PAA/PEO was prepared in acidic solution, but due to the limited water solubility of PTHF the mixture of PAA/PTHF was prepared in methanol. We found the aggregates formed by very high M_w PAA/PEO solutions, while the other solutions were homogeneous and did now show any precipitate. The effect of M_w and weight ratio between PAA and poly(ethers) (PEO and PTHF) on the physical interaction was also considered. From ^{1}H-NMR spectra, we could not follow the carboxylic acid proton (-COO**H**) of PAA hydrogen bonded with the oxygen of poly(ethers) to observe the change of chemical shift ($\Delta\delta$) as a consequence of H-bonding. Instead, we found an upfield shift to lower ppm of protons in polymer main chains with $\Delta\delta$ = 0.05 ppm for low M_w PAA/PEO solutions and with $\Delta\delta$ = 0.17 ppm for PAA/PTHF solutions, but no upfield shift was seen for very high M_w PAA/PEO solutions. As the $\Delta\delta$ values are very small, ^{1}H-NMR might not be a helpful technique to probe the association of PAA/poly(ethers) in our experiments. DOSY results gave such potential evidence for association both for low M_w and very high M_w of PAA/PEO solutions, while the results from T_2 solvent relaxation only reveal the association of very high M_w PAA/PEO solutions.

Due to the limited amount of PAA microgels prepared previously, we first tried to perform preliminary experiments using a dialysis method to investigate the release of active ingredients (AIs; benzyl alcohol and paracetamol) from Carbopol® 690, commercial PAA hydrogels, as a function of pH. UV-Vis spectroscopy was used to measure the content of AIs loaded and released from the Carbopol® 690. It is seen that the release of AIs from the Carbopol® 690 was significantly sustained comparing with the control samples. However, the effect of pH (or the swelling of Carbopol® 690) on the release of AIs is rather unclear.

This work shows how to prepare and characterize amphiphilic PAA/poly(ethers) based microgels which might be further used as carriers for both hydrophilic and hydrophobic active ingredients with controlled-release response triggered by pH and salt concentration.

Acknowledgements

First of all, I would like to thank my main supervisor, Jeroen S van Duijneveldt and my co-supervisor, Terence Cosgrove for the opportunity to be a part of their research group. Without their encouragement, endless academic and moral support throughout, I wouldn't have made it this far.

I am thankful for Ministry of Science and Technology in Thailand for the full-time PhD funding.

I appreciate all advice on synthetic sections from Dr Erol Hason and Dr Worawat Niwetmarin, and technical support from John Jones (TEM), Dr Craig Butts and Paul Lawrence (NMR).

Many thanks to my colleagues in the laboratory: Emma, Phil, Jess, Claudia, Will, Ellen, Laura, Sian and Andy for helping me one way or another and being patient with my English. I would also like to thank my Thai friends for their authentic Thai foods and joyful atmosphere.

I am very grateful for Adam and the Brady family, Catherine and Christopher Richards for being kind and encouraging during my PhD study.

SLS data analysis benefited from SasView software, originally developed by the DANSE project under NSF award DMR-0520547 (see website: http://www.sasview.org/).

Contents

List of Figures

List of Tables

List of Symbols

Q	swelling ratio
α	degree of ionization
a, r	radius of spherical particle
A_2	second virial coefficient
B	baseline offset
B_0	strength of applied filed in the z-direction
bkg	background level
B_x	strength of applied filed in the x-direction
c^*	the overlap concentration
C_i	concentrations of mobile ions
D	diffusion coefficient ($m^2\ s^{-1}$)
Δ	diffusion time (ms)
Δ'	the corrected diffusion time
δ	chemical shift (ppm), gradient diffusion length (ms)
$\Delta\delta$	difference in chemical shift
$\Delta\rho$	difference in scattering length density between a particle and the matrix
D_s	self-diffusion or translational diffusion coefficient
E	scattered electric fields.
f_0	friction coefficient
g	gradient strength (G/m)
γ	gyromagnetic ratio
$h, \hbar$	Planck constant
I	intensity
k_B	Boltzmann's constant (1.38065×10^{-23} J/K)
K_f^s	the first virial coefficient
λ	wavelength of the light source
λ^3	volume-swelling ratio (a ratio of fully swollen gel volume to its condensed volume)
l	rod length
M	molar mass (g/mol)

M_0	transverse magnetization immediately after the initial excitation of 90° pulse
M_e	effective molecular weight between crosslinks
M_w	molecular weight, molar mass
$\overline{M_w}$	weight average molecular weight
$\overline{M_v}$	viscosity average molecular weight
M_{xy}	transverse magnetization
n, N	number of repeating units or degree of polymerization
N_A	Avogadro number
n_D	refractive index of solvent
n_m	molarity of monomer
n_p	molarity of polymer
N_P	number of particles
π	osmotic pressure
P(Q)	particle form factor
pK_a	acid dissociation constant
P_s	fraction of solvent molecules absorbed on a surface phase
θ	scattering angle
Q	scattering vector
Q_v	volume-swelling ratio,
Q_w	weight-swelling ratio
ρ	shape factor
R	radius of microparticle
$\rho(r)$	cross-linking density distribution as a function of distance from the centre of a particle
R_2	relaxation rate of spin-spin relaxation
R_2^0	relaxation rate of a referent sample or bulk solvent
R_{2sp}	specific relaxation rate constant
R_G	radius of gyration
R_H	hydrodynamic radius
σ	polydispersity
S	amplitude of spin echo or stimulated echo signal
S_0	amplitude in the absence of the diffusion (the reference intensity)
scale	volume fraction or scale factor
SD	standard deviation

sld	scattering length density
T	absolute temperature (K)
T_1	spin-lattice (or longitudinal) relaxation time
T_2	spin-spin (or transverse) relaxation time
T_{2F}	relaxation time of 'free' solvent molecules in bulk solution
T_{2S}	relaxation time of 'restricted' solvent molecules on surface phase
V	volume
V_P	volume of a particle
W	weight of polymer gel
W_{dry}	weight of polymer gels in dry state
$W_{swollen}$	weight of polymer gels in swollen state
ξ	correlation length
x_{mean}	mean size
η	viscosity
υ	the scaling exponent
ζ	zeta potential

List of Abbreviations

^{13}C-NMR	carbon-13 nuclear magnetic resonance nuclear magnetic resonance
^{1}H-NMR	proton nuclear magnetic resonance nuclear magnetic resonance
AA	acrylic acid
ACVA	4,4'-azobis(4-cyanopentanoic acid)
AIBN	2,2'-azobis isobutyronitrile
AIs	active ingredients
APS	ammonium persulfate
ATR-FTIR	attenuated total reflection fourier transform infrared spectroscopy
BIS	bis[2-(2′-bromoisobutyryloxy) ethyl] disulfide
BnOH	benzyl alcohol
CBP	carbopol®
CMC	carboxymethyl cellulose
CMT	critical micellization temperature
CPMG	standard Carr-Purcell-Meiboom-Gill sequence
D_2O	deuterated water
DCl	deuterium chloride
DCM	dichloromethane
DLS	dynamic light scattering
DOSY	diffusion ordered NMR Spectroscopy
EGDMA	ethylene glycol dimethacrylate
EP	emulsion polymerization
H_2SO_4	sulfuric acid
HBL	hydrophilic-lipophilic balance
H-bonding	hydrogen bonding
HCl	hydrochloric acid
HPMC	hydroxy propyl methyl cellulose
HSQC	heteronuclear single quantum correlation spectroscopy
IPNs	interpenetrating polymer networks

K_2CO_3	potassium carbonate
KCl	potassium chloride
KCps	kilo counts per second
KH_2PO_4	potassium phosphate monobasic
MA	methacrylic anhydride
MBA	N,N'-methylene bisacrylamide
m-DIB	m-diisopropenyl-benzene
MeOD	deuterated methanol
MEP	microemulsion polymerization
NaCl	sodium chloride
$NaHCO_3$	sodium hydrogen carbonate
NaOH	sodium hydroxide
P	paracetamol
PAA	poly(acrylic acid)
PAAm	poly(acrylamide)
PAANa	sodium polyacrylate
PAN	poly(acrylonitrile)
PCS	photon correlation spectroscopy
PD	polydispersity
PDAC	poly(diallyldimethylammonium chloride)
PEA	poly(ethyl acrylate)
PEAA	poly(2-ethylacrylic acid)
PEG	poly(ethylene glycol)
PEO	poly(ethylene oxide)
PFG-SSE or STE	pulsed field gradient stimulated spin echo
PGSE	pulsed gradient spin echo
PHEMA	poly(hydroxyethylmethacrylate)
Pluronic	triblock copolymers of PEO-PPO-PEO
PMA	poly(methyl acrylate)
PMAA	poly(meth-acrylic acid)
PMMA	poly(methyl methacrylic acid)
PNIPAm	poly(*N*-isopropylacrylamide)
PP	precipitation polymerization
PPG	polypropylene glycol
PPGDA	poly(propylene glycol) diacrylate
PPO	poly(propylene glycol)

PS	poly(styrene)
PSS	poly(styrene sulfonate)
P*t*BMA	poly(*tert*-butyl methacrylate)
PTHDMA	poly(tetrahydrofuran) dimethacrylate
PTHF	poly(tetrahydrofuran)
PTHFDA	poly(tetrahydrofuran) diacrylate
PTMEG	poly(tetramethylene ether glycol)
PTSA	*p*-toluenesulfonic acid
PVP	poly(N-vinylpyrrolidone)
PVS	poly(vinylsulfonic acid)
PVTAC	poly(4-vinylbenzyl trimethylammonium chloride)
QELS	quasi-elastic light scattering
RAFT	reversible addition-fragmentation chain transfer polymerization
RF	radiofrequency
RGD	Rayleigh-Gans-Debye theory
SANS	small angle neutron scattering
SAXS	small angle x-ray scattering
SDS	sodium dodecyl sulfate
SFEP	surfactant free emulsion polymerization
sld	scattering length density
SLS	static light scattering
SPS	sulfonated polystyrene
*t*BA	*tert*-butyl acrylate
TEA	triethylamine
TEM	transmission electron microscopy
TFA	trifluoroacetic acid
TMS	tetramethylsilane
XLD	cross-linking density

Chapter 1

Introduction

Polymer microgels are cross-linked particles which can swell to absorb a large amount of solvent, under favourable solvent conditions. The presence of cross-links does however restrict the maximum extent of swelling for such a particle. As a result, a key factor for preparing the microgels is to create the cross-linking networks by employing physical and /or chemical interactions. In addition, for stimuli-responsive gels or smart gels containing certain functional groups on their main chains, the swelling behaviour of these gels can be sensitive to external conditions such as pH, ionic strength and temperature. For example, pH-sensitive microgels can be prepared from polyacids such as poly(carboxylic acid) and poly(sulfonic acid), and polybase such as poly(amine). For temperature-sensitive microgels, they are typically prepared from poly(acrylamides) such as poly(*N*-isopropyl-acrylamide). With the stimuli-sensitive swelling of these gels, they consequently have been widely used in many applications such as delivery systems, cell encapsulation, and tissue engineering.

In this chapter, we provide an overview of microgel particles: definition, type, synthesis methods, stimulus-responsive microgels particularly based on poly(carboxylic acid), swelling theory of polyelectrolyte gels, and a literature review of polyacid/poly(ether) microparticles and the use of pH-sensitive microgels for delivery systems. Finally, the last two sections consist of project aims and thesis overview.

1.1 Polymer gels

Polymer gels are cross-linked polymer networks with a potential to absorb a large amount of solvents and swell without the destruction of their shape. The term 'superabsorbent polymer' is also commonly used for hydrophilic polymer gels with a high performance to imbibe water up to 10-1000 times their dried weight or volume.[1,2] Specifically, the term 'hydrogels' is defined as the polymer gels which are greatly swollen in aqueous solution. The term 'microgel particles' will be normally used in our study and it refers to cross-linked latex particles which can form stable colloidal dispersions. The size of microgel particles is typically in the range of 10-1000 nm, while the size of nanogels is less than 100 nm in diameter.[3-5] For stimuli-responsive microgel particles, the swelling or de-swelling of the particles can be controlled by change in external conditions such as pH, ionic strength, temperature and electric field as shown in **Figure 1.1**.

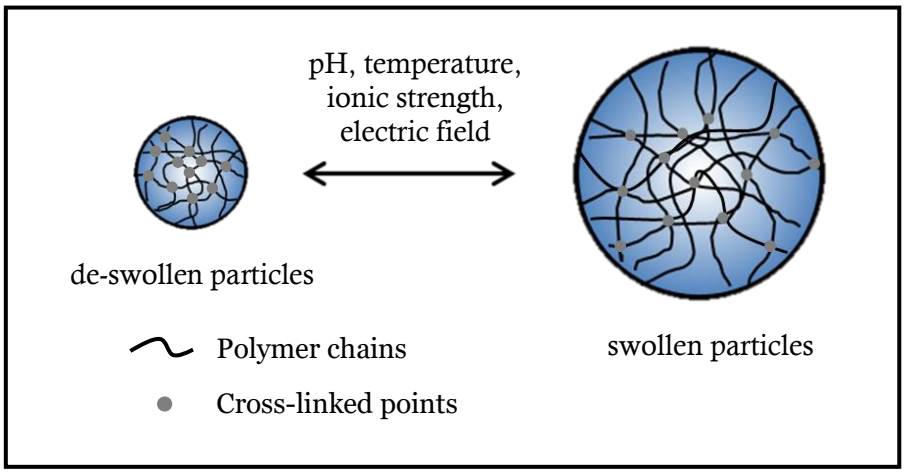

Figure 1.1 Stimulus-response behavior of microgel particles in response to various external stimuli.

To quantify the absorption efficiency, the 'swelling ratio (Q)' is generally expressed as the ratio of weight or volume of the swollen gel over the dry mass or volume of collapsed gel, following Equation (1.1) and Equation (1.2):[6,7]

$$Q_w = \frac{W_s}{W_d} \qquad (1.1)$$

Here, Q_w is the weight-swelling ratio, W is the weight of polymer gels and the subscripts 's' and 'd' refer to the swollen and dry states, respectively.

$$Q_v = \frac{V_{swollen}}{V_{collapsed}} = (\frac{R_{swollen}}{R_{collapsed}})^3 \qquad (1.2)$$

Here, Q_v is the volume-swelling ratio, V is the volume of polymer gels, R is the radius of gel particles, and the subscript 'swollen' and 'collapsed' refer to the swollen and collapsed states, respectively.

In our experiments, light scattering is employed to measure the radius of microgel particles. Therefore, we generally use the term radius-swelling ratio; $R_{swollen}/R_{collapsed}$ from which a volume-swelling ratio can then be obtained using Equation (1.2) above.

1.1.1 Polyelectrolyte gels

Polyelectrolyte (PE) gels are cross-linked polymer networks specifically containing acidic or basic pendant groups. They can be divided into two types: strong and weak polyelectrolytes.[8] For strong PE gels, the acidic (or basic) groups are deprotonated (or protonated) in the typical range of pH values so that their charge densities are normally insensitive to a change in pH, thus the volume transition and thermodynamics are attributed to salt concentration and valency of salt *e.g.* strong polyanions are poly(vinylsulfonic acid) (PVS) and sulfonated polystyrene (SPS), and strong polycations are poly(diallyldimethylammonium chloride) (PDAC) and poly(4-vinylbenzyl trimethyl-ammonium chloride) (PVTAC).[8,9] In contrast, the weak PE gels are partially charged in solutions so the charge densities are greatly dependent on the acid disassociation constant (pK_a) of the ionizable groups, resulting in the reversible swelling behaviour driven by changes in pH and salt concentration or ionic strength. For instance, weakly anionic PE gels dramatically swell at high pH (above the pK_a) due to increasing in negatively charged groups, whilst the weakly cationic PE gels are better swollen at low pH (below the pK_a) owing to rising in positively charged groups.[1,10-12]

Typical functional groups for weakly anionic gels are carboxylic acid (-COOH) and phosphoric acid (-PO_3H_2), while weakly cationic gels can be obtained using primary amines (-NH_2).[1,3] With either negatively or positively charged groups, the PE gels are more hydrophilic and can imbibe a substantial amount of water into their networks up to ~1000 times the polymer weight.[13,14] For example, Askari *et al.*[15] prepared the weakly anionic gels based on partially neutralized poly(acrylic acid) with ethylene glycol dimethacrylate (EGDMA) as cross-linker by inverse suspension polymerization and reported that the weight-swelling ratio is 929 g/g in water at 0.055 mole% of cross-linker to monomer.

1.1.1.1 Poly(carboxylic acid) gels

As mentioned previously, a poly(carboxylic acid) based gel is weakly anionic and thus it can be swollen in basic solutions.[16] At pH above its pK_a (*i.e.* pK_a = 4.5 – 5 for poly(acrylic acid)),[17-19] the carboxyl groups (-COOH) are ionized to carboxylate anions (-COO^-), therefore electrostatic repulsion between the adjacent charged groups causes the gel to expand. However, when the pH decreases the negatively charged groups are protonated and the gel collapses. Moreover, salt addition also contributes to the shrinkage of the swollen gel due to a decrease in the difference of osmotic pressure between the interior of the gel and the surrounding solution. Well-known examples of poly(carboxylic acid) gels are prepared from poly(acrylic acid) (PAA), poly(meth-acrylic acid) (PMAA) and poly(2-ethylacrylic acid) (PEAA).

1.2 Synthesis methods

Gelation is the process for creating gels in which polymer chains are linked together, resulting in three-dimensional networks of soluble polymers. In terms of flow properties, gelation is a phase transformation which turns a liquid solution or suspension into a 'gel' by forming three-dimensional networks. The critical point where a gel first appears is called the 'gel point'.[20] Gelation can be achieved by physical and / or chemical cross-linking, so any techniques, which can create cross-linked networks in polymer structures, can be used to prepare hydrogels.

Types of microgels can be classified by different aspects such as type of cross-linking, environmental response, preparation method, and morphology.[5,21,22] In this section, microgels are mainly categorized into two types: physical and chemical microgels according to the type of cross-linking. The cross-linking of physical microgels is formed by physical interactions such as hydrophobic interaction, ionic interaction, block copolymer micelles and hydrogen bonding, which are reversible depending on external conditions such as pH, temperature, and ionic strength. In contrast, the cross-linking of chemical microgels is non-reversible and formed by covalent bonds. In addition, interpenetrating polymer networks (IPNs) prepared from polymer blending are also included here.

1.2.1 Physical cross-linking

Recently, physical gels have gained interest because they do not require a cross-linking agent to form the cross-linked networks. Instead, the polymer chains are held together by reversible association such as cross-linked or entangled networks of linear homopolymers, linear copolymers and block / graft copolymers, polyion-multivalent ion, polyion-polyion, H-bonding, hydrophilic networks stabilized by hydrophobic segments, interpenetrating polymer networks (IPNs) or physical blends, and crystallite formation.[21-24]

1.2.1.1 Ionic interaction

The key to this method is to have an interaction between two different charges. **Figure 1.2** illustrates two procedures to prepare physical hydrogels through ionic interaction. The first one involves ionotropic hydrogels created by association between polyelectrolyte chains and di- or multi-valent counterions which are the opposite charges of the polyelectrolyte. The second one is complex coacervate or polyion complex hydrogels formed by association between polyanions and polycations.

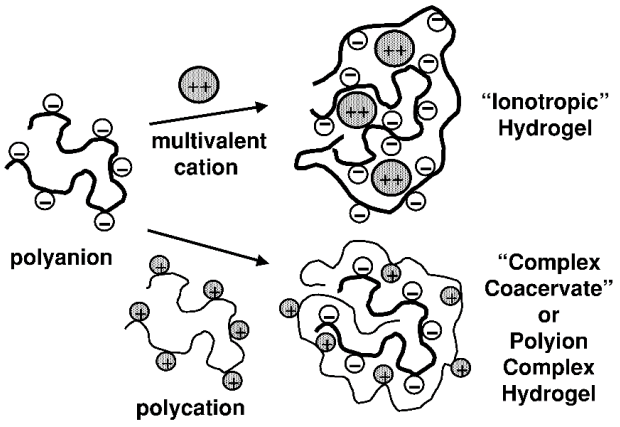

Figure 1.2 Schematic method for forming physical cross-linking from two types of ionic interactions: between polyanion and multivalent cation, and between polyanion and polycation.[24] Reprinted from [24]. Copyright (2012) by Advanced Drug Delivery Reviews.

Alginate is the most common example of an ionotropic hydrogel.[22,23,25] The hydrogel is formed by adding divalent cations *i.e.* Ca^{2+} into the aqueous solution of sodium alginate (Na^+ alginate$^-$) at room temperature and physiological pH as shown in **Figure 1.3**. Moreover, this interaction can be destabilized by extraction of Ca^{2+} from the hydrogel by a chelating agent. For polyion complex gels, examples are the mixture of polyanionic

xanthan with polycationic chitosan,[26,27] and polyanionic poly(styrenesulfonate) (PSS) with polycationic poly(diallyldimethyl-ammonium) (PDADMA).[28]

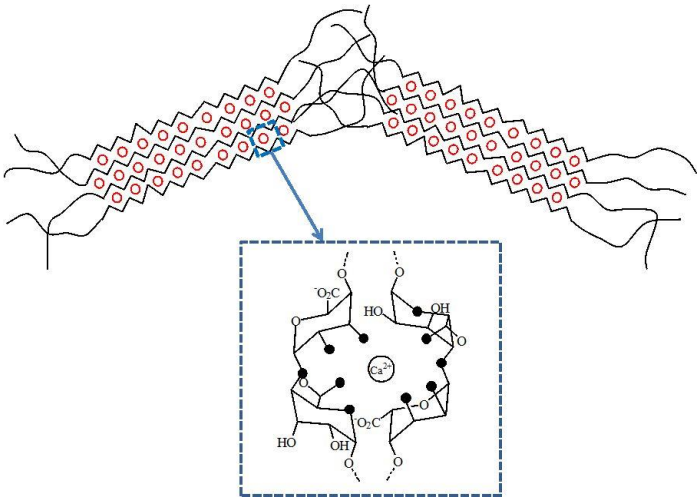

Figure 1.3 Ionotropic hydrogel formed by interaction between anionic groups on alginate (COO^-) with calcium ions (Ca^{2+}).[22] Reprinted from [22]. Copyright (2011) by IntechOpen Limited.

1.2.1.2 Hydrogen bonding interaction

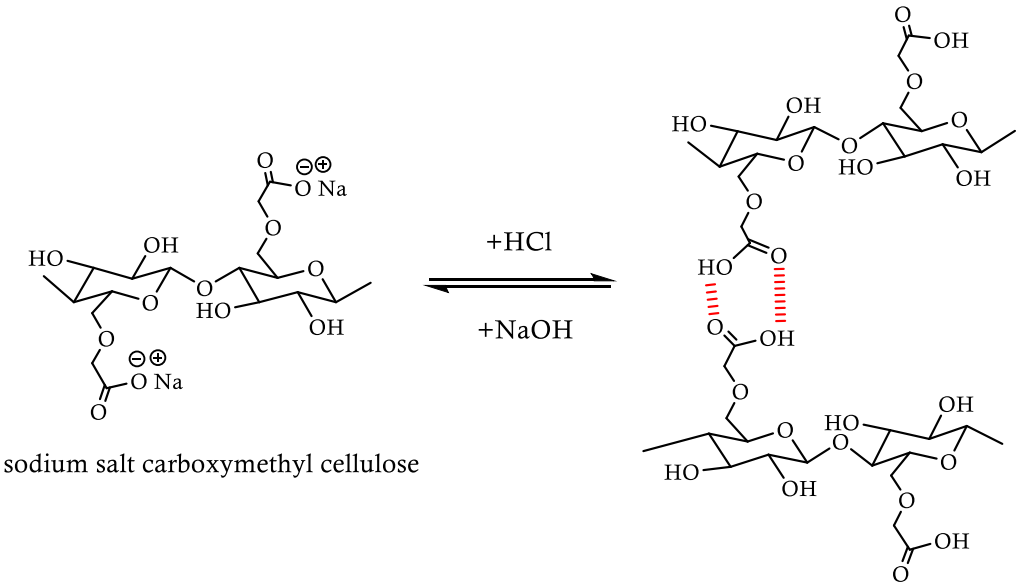

Figure 1.4 Carboxymethyl cellulose (CMC) hydrogel formed by intramolecular hydrogen bonding at low pH.

Hydrogels can also be formed by hydrogen bonding of polymers carrying carboxylic groups at low pH in aqueous solution. An example of such hydrogels is shown in **Figure 1.4**. The mechanism starts with the protonation of sodium carboxymethyl cellulose (CMC) in acid solution. The resulting carboxyl group (-COOH) shows self-association via hydrogen bonding which can be broken in basic solution.[22] Also, poly(acrylic acid) (PAA) or poly(methacrylic acid) (PMAA) can form complexes with poly(ethylene glycol) (PEG) via the carboxyl group of PAA or PMAA and the ether oxygen of PEG at low pH.[29,30]

1.2.1.3 Hydrophobic interaction

This type of physical hydrogel is prepared from amphiphilic block or graft copolymers containing both hydrophilic and hydrophobic segments in one polymer chain.[21,23] At low temperature, the copolymers are water soluble but at elevated temperature the hydrophobic domains will link together and form aggregates to reduce the surface area between themselves and bulk water. Therefore, the structure of polymeric micelles or hydrogels is obtained. The temperature to form the hydrophobic interaction (or gelation temperature) depends on the concentration of polymer solution, the length of the hydrophobic segment and chemical structure of the polymer. The increasing hydrophobicity enhances the driving force to form aggregates and the gelation temperature is consequently decreased. **Figure 1.5** shows the hydrophobicity-driven gelation of amphiphilic block copolymer at a high temperature. For instance, triblock copolymers of poly(ethylene oxide)-poly(propylene oxide)-poly(ethylene oxide) (PEO_{101}-PPO_{56}-PEO_{101} or Pluronic 407) are viscous liquids at 25%w/v in aqueous solution at room temperature or lower. When temperature increases to body temperature (37 °C) a network can be formed due to the aggregation of hydrophobic PPO domains.[21]

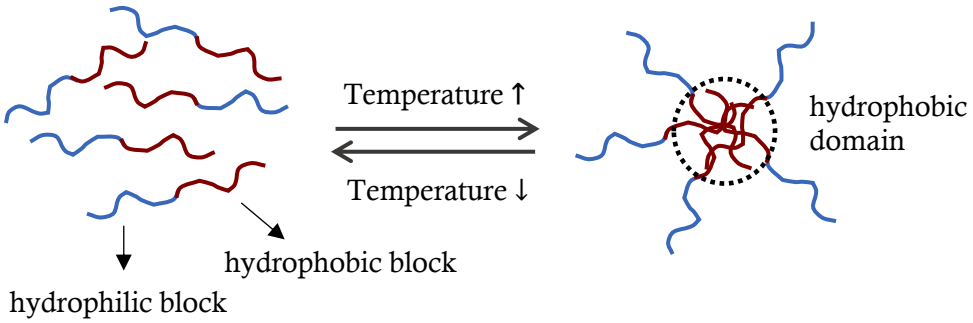

Figure 1.5 Physical hydrogel formed by hydrophobic interaction of amphiphilic block copolymer.

1.2.2 Chemical cross-linking

Many polymerization techniques have been used to prepare hydrogels such as bulk, suspension, solution and radiation polymerization, reversible addition-fragmentation chain transfer (RAFT) polymerization and free radical polymerization.

Generally, hydrogels are prepared by copolymerization and cross-linking free-radical polymerization using mainly hydrophilic monomers, initiator and multifunctional cross-linkers.[1,2] However, different preparation methods result in different sizes and structures of hydrogels. Macroscopic gels (or bulk gels) can be established by bulk polymerization which is an easy method however without size control, whilst microgels and nanogels are commonly prepared by anionic copolymerization, emulsion polymerization, inverse (mini) emulsion, inverse micro-emulsion polymerization, and dispersion polymerization by an uncontrolled free radical polymerization process.[31,32] Bonham *et al.*[33] reported that the typical particle size of microgels prepared by microemulsion polymerization (MEP) is rather small in a range of 10-100 nm, while the particle sizes for emulsion polymerization (EP), surfactant free emulsion polymerization (SFEP) and precipitation polymerization (PP) are in a range of 50-1000 nm, whilst dispersion polymerization (DP) yields rather large particles in the range of 1,000–15,000 nm.

More detail of each method is provided next.

1.2.2.1 Bulk polymerization

Bulk polymerization is the simplest technique to prepare hydrogels formed by many types of vinyl monomers, monomer-soluble initiators, and a small amount of cross-linker which is added during hydrogel formation. The resulting hydrogel is a glassy, transparent polymer which is hard, but it becomes softer and more flexible after it is immersed in water.

1.2.2.2 Solution polymerization

The system of solution copolymerization or cross-linking involves ionic or neutral monomers, multifunctional cross-linkers, initiator and solvent. The reaction is thermally initiated by UV-irradiation or by a redox initiator system. The presence of solvents (such as water, ethanol, water-ethanol mixtures, benzyl alcohol) can reduce heat generation during polymerization which is a limitation of bulk polymerization. After the reaction is complete, the resulting hydrogels need to be washed with distilled water to remove

reactants and other impurities. Examples of macro hydrogel prepared by solution polymerization are poly(acrylamide-*co*-acrylic acid) (PAM-*co*-PAA) hydrogels,[34] and graft copolymerization of cross-linked poly(acrylamide) (PAM) chains onto carboxymethyl cellulose (CMC) and poly(vinyl alcohol) (PVA).[35]

1.2.2.3 Suspension polymerization

This polymerization method is used to prepare spherical hydrogels in a size range of 1 μm to 1 mm. The monomer solution is dispersed in an organic solvent, so fine monomer droplets can be formed and stabilized by adding stabilizer. The polymerization is initiated by thermal decomposition of an initiator into radicals. Fang *et al.*[36] prepared microporous poly(HEMA–MMA) particles by suspension copolymerization which contains monomers of HEMA and MMA, cross-linker (EGDMA), initiator (AIBN), and pore forming agent (1-octanol) dispersed in organic phase. Then, this phase was transferred into sodium dodecyl sulfate (SDS) aqueous solution. The result showed that the introduction of highly porous structures improves the swelling capacity of these particles. However, recently water-in-oil (W/O) suspension polymerization or inverse suspension polymerization has been widely used for preparing of poly(acrylamide) based hydrogels since it is easier to remove the hazardous residual acrylamide monomer.[1]

For example, Kiatkamjornwong *et al.*[37] synthesized pH-responsive PAM-*co*-PAA beads by inverse suspension polymerization in which their size depends on hydrophilic-lipophilic balance (HLB) of type and concentration of suspending agent. In addition, Askari *et al.*[15] prepared partially neutralized poly(acrylic acid) based hydrogels by inverse suspension polymerization. The aqueous phase contained monomer, NaOH solution, water-soluble initiator, and this phase was subsequently added dropwise into the continuous phase (toluene) containing water-in-oil surfactant before heating and then, an oil soluble cross-linker was added. The reaction was carried out at 80 °C for 1.5 h and the particle size of resulting beads was in a range of 50-500 microns.

1.2.2.4 Dispersion polymerization

The ingredients for dispersion polymerization consist of monomer, stabilizers, and initiators which can be soluble in the continuous phase. Although the polymerization is initiated in a homogeneous solution, after the particles are formed the solution becomes milky white dispersed in the continuous phase. The resulting particle size is in the range of 1,000-15,000 nm.[31,33] However, when the polymerization is carried out in organic solvents, the effect of electrostatic stabilization is insignificant. Therefore, soluble polymer chains

are always used to graft onto particles to stabilize and avoid the coagulation, and cross-linkers should be added into the reaction after the particles are formed.[33]

For example, Zhou and Chu[38] prepared poly(methacrylic acid-*co*-*N*-isopropyl-acrylamide) (poly(MAA-*co*-NIPAm)) microgels via dispersion polymerization with sodiumdodecyl sulfate (SDS) as surfactant, methylenebisacrylamide (BIS) as crosslinker, and ammonium persulfate (APS) as initiator in aqueous solution at pH of 3.1±0.2 and temperature of 70 °C. The results show that small amount of SDS can improve the colloidal stability and leads to a nearly monodisperse size distribution of the microgel particles, while the small amount of charged MAA monomer did not enhance the colloidal stability since it is too hydrophilic and not absorbed on the surface of nuclei. In addition, the swelling ratio and the critical transition pH of the microgels are increased with the increasing PMAA content.

1.2.2.5 Precipitation polymerization

This technique employs monomer which is soluble in solvent initially, but after initiation and propagation steps the polymer chains are chemically cross-linked so the polymer networks become insoluble and precipitate out of the solvent.[31,33] The advantages of this method are that it does not require external stabilizers since the stability of particles employs the use of low concentration of monomer, the mechanism is carried out in single step and the reaction is reasonably fast. However, the resulting microgels are not well-defined with high polydispersity.

For example, Mackova and Horak[39] prepared poly(*N*-isopropylacrylamide) (PNIPAm) based microspheres by using two different methods: precipitation and dispersion polymerization. For the precipitation method, PNIPAm spheres were prepared by using a single step which the reaction contains NIPAm monomer, MBAAm cross-linker and APS initiator dissolved in distilled water. Similarly, for dispersion polymerization, NIPAm monomer in water was stabilized with poly(N-vinylpyrrolidone) (PVP) stabilizer, whilst this monomer in toluene/heptane co-solvent was stabilized with Shellvis 50 and Kraton G 1650, and AIBN was used as an initiator. The particle size of microspheres from precipitation method controlled by solvency of polymer chains is about 0.2-1 μm, while the size of microspheres from dispersion method stabilized by two different stabilizers in toluene/heptane is in the range of 1-2 μm.

1.2.2.6 Emulsion polymerization

Emulsion polymerization usually involves monomer, cross-linker, surfactant, water, and water-soluble initiator. The surfactant will form micelles, used as micro-reactor, which controls the size of the obtained particles. The final product is a milky latex stabilized by surfactant and dispersed in the aqueous medium, and it is reported that the resulting microparticles may have non-uniform cross-linking or core-shell structure.[33] In addition, the removal of the residual surfactant is inconvenient, and this may cause coagulation or flocculation of the latex.[32,40,41] For microemulsion polymerization, the monomer is effectively stabilized within surfactant micelles, and there are no droplets of monomer present unlike in emulsion polymerization. However, it is recommended to use a co-surfactant for this method.[33] Recently, Tiwari *et al.*[42] prepared well-defined poly(meth-acrylic acid) (PMAA) microgels with ethylene glycol dimethacrylate (EGDMA) as cross-linker, and sodium dodecyl sulfate (SDS) as surfactant via emulsion polymerization and acid-hydrolysis of P*t*BMA. They found that at a mole ratio of monomer to cross-linker of 100, increasing the content of SDS from 0.5 mM to 4 mM reduces the hydrodynamic radius (R_H) of P*t*BMA latex obtained by DLS from 130 nm to 83 nm. The effect of cross-linking density (the mole ratio of monomer to cross-linker) in a range of 0 – 500 is insignificant on the particle size of P*t*BMA latex. However, such an effect is more obvious after hydrolysis of P*t*BMA to PMAA latex. For instance, the R_H value of P*t*BMA latex with two different cross-linking densities (the mole ratio of monomer to cross-linker is 10 ($PtBMA_{E10}$) and 500 ($PtBMA_{E500}$)) is similar about 155 nm. However, after hydrolysis, the R_H value of $PMAA_{E500}$ (less cross-linked) is 200 nm which is larger than 180 nm of the $PMAA_{E10}$ in the collapsed state (at pH =3).

1.2.2.7 Surfactant Free Emulsion polymerization

Unlike emulsion polymerization, surfactant free emulsion polymerization (SFEP) can be used to prepare monodisperse latex particles without the added surfactant. Consequently, this method only requires monomers and ionic initiators (*e.g.* KPS, ACVA) and a continuous phase having a high dielectric constant (*e.g.* water). The mechanism of SFEP is shown in **Figure 1.6**.

The decomposition of KPS ionic initiator produces free radicals which then react with monomers. In the propagation step, more monomers react with the growing radicals. Then, when charged oligomers become longer and more hydrophobic, they will act as surfactant to form nuclei and stabilize the growing particles.[32,40] Notably, charges on

initiator molecules play an important role in colloidal stability of the resulting particles.[43] In addition, the particle size can be controlled by the amount of monomer and initiator.[20, 23,24] Moreover, it is suggested that rapid stirring should be applied during the reaction to maintain the small droplets of monomers dispersed in aqueous medium, and to reproduce the similar particle size in other batches the stirring condition should keep constant.[40]

SFEP has been used for the preparation of poly(styrene) (PS), poly(methyl-methacrylate) (PMMA) and poly(*N*-isopropylacrylamide) (PNIPAm) microparticles.

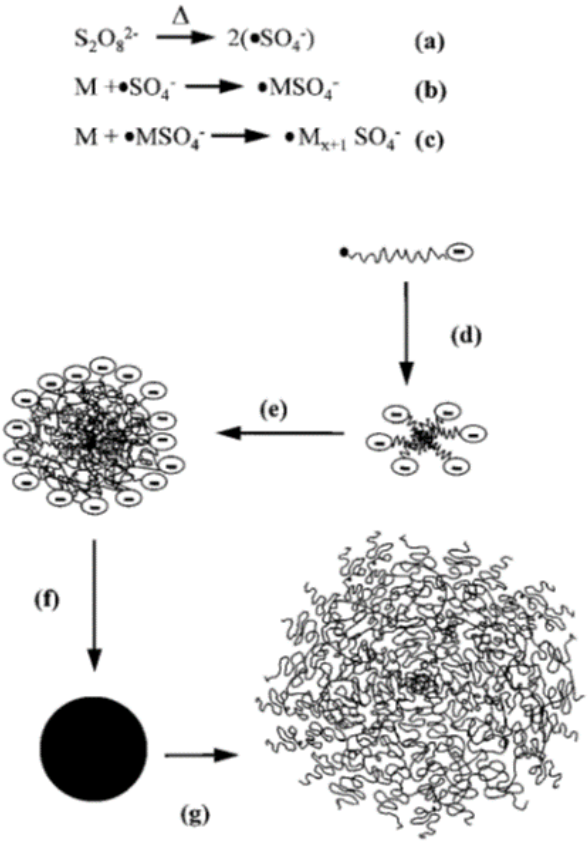

Figure 1.6 Mechanism for the preparation of microgel particles by SFEP. The steps shown are (a) initiator decomposition, (b) initiation, (c) propagation, (d) particle nucleation, (e) particle aggregation, (f) particle growth in poor solvent, and (g) particle swelling in a good solvent. The counter-cations and particles charges for steps (f) and (g) have been omitted for clarity. M represents a vinyl group of monomer.[32] Reprinted from [32]. Copyright (1999) by Advances in Colloid and Interface Science.

1.2.3 Interpenetrating polymer networks (IPNs)

Interpenetrating polymer networks (IPNs) are a type of polymer blends where at least one component is polymerized or cross-linked to be a pre-polymerized hydrogel. IPNs can be formed by the presence of monomer, initiator with cross-linker to create new cross-linking networks trapped inside the pre-hydrogels and it is called a 'fully interpenetrating network (full IPNs)'. Without cross-linker, linear polymer chains are trapped inside the pre-hydrogels and it is called a 'semi IPNs' as shown in **Figure 1.7**. The most important benefit of IPNs is the improved physical properties compared with normal polymer blends of their components.[21,44]

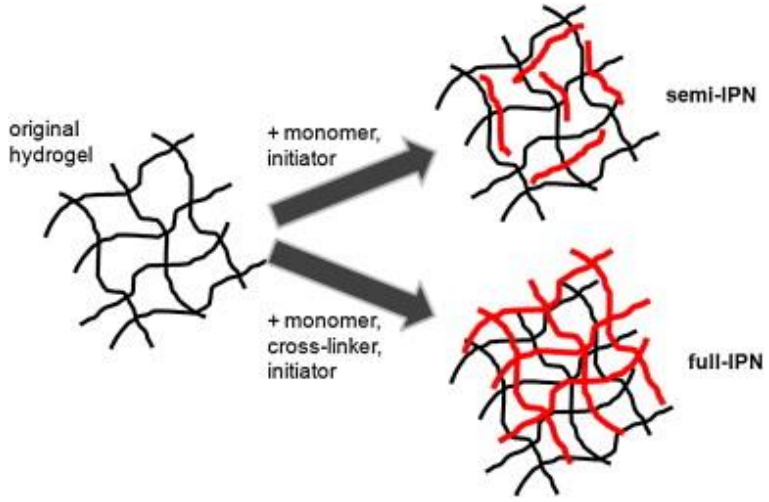

Figure 1.7 The formation and structure of semi- and full- interpenetrating polymer networks (IPNs).[21] Reprinted from [21]. Copyright (2008) by Polymer.

1.3 Cross-linking distribution

Light scattering techniques (dynamic (DLS) and static (SLS)) can be used to characterize particle size. The hydrodynamic radius (R_H) obtained from DLS is determined from the translational diffusion coefficient. The Stokes-Einstein equation then yields an equivalent sphere radius. The radius of gyration (R_G) is obtained from SLS and is a measure of the mass distribution inside a particle.[45,46] More detail on these light scattering techniques is given in Appendix A. With the combination of DLS and SLS data, a shape factor (ρ) defined as the ratio of R_G/R_H can be obtained and this provides information about the shape and internal structure of particles. For example, the ρ value is 0.775, 1.0, 1.5-1.8 and greater than 2, for homogeneous hard spheres, hollow spheres, random coils in theta solvent, and very elongated particles such as nanotubes, respectively.[47-51]

For spherical microgel particles, it has been reported that the cross-linking density distribution throughout the particle is non-uniform so that the cross-linking density (XLD) is constant up to a certain radius, however, above this radius the XLD decreases exponentially due to the presence of dangling chains or loops in the surface region as shown in **Figure 1.8** (case B).[47-49,52]

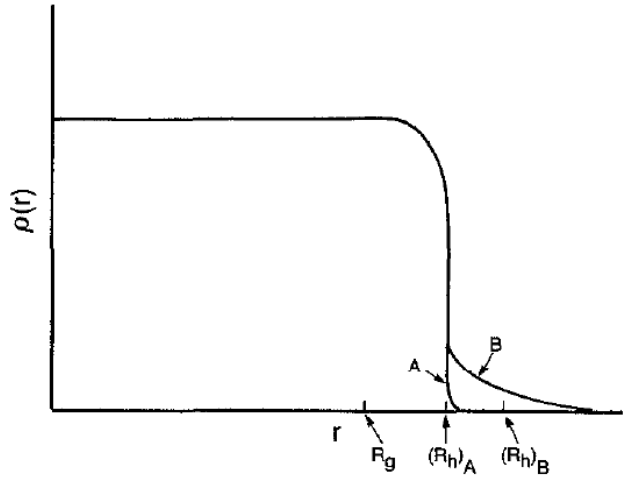

Figure 1.8 Plot of cross-linking density distribution ($\rho(r)$) as a function of distance from the centre of sphere (r). Case A refers to microgels with uniform XLD having a sudden decrease in XLD near the surface. Case B refers to microgels with low XLD tails at the surface.[49] Reprinted from [49]. Copyright (1989) by Journal of Colloid and Interface Science.

Wu *et al.,*[53] Scheffold *et al.*,[54] and Boon and Schurtenberger[55] found that the PNIPAm microgel particles prepared with emulsion or surfactant free emulsion polymerization have a core-shell structure (a highly cross-linked core surrounding with a hairy shell). They suggested that the rate of the cross-linking reaction is initially faster than the polymerization and this results in a more densely cross-linked network formed at the beginning compared to the end of polymerization.

Since SLS is sensitive to the dense center of the particle (R_G) and DLS is sensitive to both dense core and hairy surface (R_H), the shape factor (R_G/R_H) for microgels with the non-uniform XLD distribution is generally lower than the hard sphere value (0.775). Examples of the shape factor of spherical microgels are 0.49-0.58 for poly(butyl-methacrylate) (PBMA) microgels prepared by emulsion polymerization,[48] 0.3-0.8 for pH- and salt-responsive poly(ethyl acrylate)/poly(methacrylic acid) (PEA/PMAA) copolymer microgels prepared by semi-continuous emulsion polymerization,[52] 0.58-0.79 for

poly(styrene) (PS) prepared from microemulsion polymerization, and 0.56-0.73 for poly(*N*-isopropyl acrylamide) (PNIPAm) microgels prepared by surfactant free emulsion polymerization.[56] Considering the effect of cross-linking density, Wolfe and Scopazzi[49] prepared PMMA microgels by emulsion polymerization with various contents of ethylene glycol dimethacrylate (EGDMA) cross-linker in a range of 0.25 to 0.4%wt. They showed that the increasing content of EGDMA contributes to the increasing ρ value of resulting PMMA microgels from 0.55 to 0.67 approaching the hard sphere value (0.775). Antonietti *et al.*[57] also found that with high cross-linking density the PS microparticles prepared by microemulsion polymerization with *m*-diisopropenyl benzene (*m*-DIB) as cross-linker behave like a homogeneous hard sphere (the ρ value = 0.74-0.79) and the reduction of cross-linking density causes the decrease in the ρ value (the lowest value is 0.58).

Rodriguez *et al.*[52] studied the non-uniform swelling of ionizable PEA/PMAA microgels as a function of degree of neutralization with and without salt. The presence of PMAA enables the microgels to be pH- and salt-sensitive. At a high degree of neutralization, electrostatic repulsion between adjacent ionized carboxyl groups causes the swelling of the microgel particles. However, a non-uniform swelling is observed since the core can swell much less than the shell. This results in a significant decrease of the ρ value from 0.8 (at collapsed state) to the minimum value of 0.3 at 50% degree of neutralization and then the ρ value rises to around 0.5 at above 100% degree of neutralization. However, the presence of 0.1 M NaCl dramatically reduces the swelling of the ionized particles observed in a range of 0-200% degree of neutralization. Therefore, the ρ value is found to be around 0.7 – 0.75 which is very close to the homogeneous hard sphere value.

Similarly, **Figure 1.9** illustrates that in the collapsed state the PNIPAm microgel particles can be assumed to be homogeneous spheres. However, in the swollen state a core-shell model is more appropriate, and therefore it is expected that its swelling behavior is heterogeneous as the center region swells less than the shell region.[54-57]

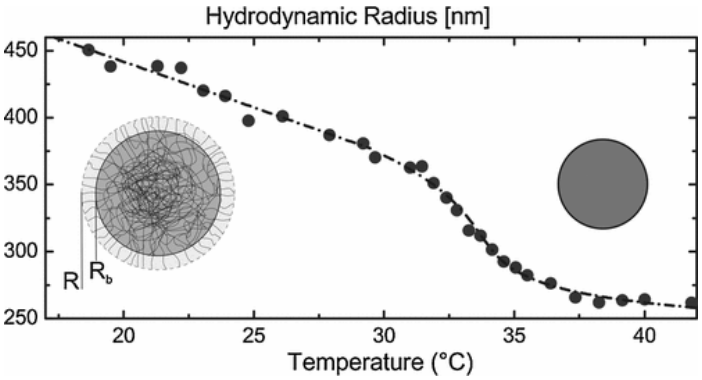

Figure 1.9 Plot of hydrodynamic radius (R) of PNIPAm microgels as a function of temperature, and a sketch of the microgels with core-shell-like structure consisting of densely cross-linked core (R_b) and an uncross-linked shell with the shell thickness of R-R_b under good solvent conditions in the swollen state (low temperature) and the homogeneous hard sphere in the collapsed state (elevated temperature).[54] Reprinted from [54]. Copyright (2010) by Physical Review Letters.

As the examples above, the non-uniform swelling could contribute to a difficulty in modelling the swelling of microgel particles. We must consider not only the solvent conditions but also the internal structure of the particles.

1.4 Swelling theory

Swelling/de-swelling is one of the most important properties of microgel particles which enables them to be used in various applications. Factors affecting the swelling efficiency of microgels are the chemical structure of the repeating unit (in some cases, with specific functional groups the microgels are external stimuli-responsive), network structure (type of cross-linking, type of cross-linker, cross-linking density distribution), and the condition of the surrounding medium (type of medium, pH, salt concentration, temperature).[1,6,58]

In general, swelling theory for hydrogels without ionic moieties is based on the free energy change due to the mixing of polymer chains with solvent molecules (*i.e.* Flory-Huggins theory), and the stretching or elastic configuration of polymer chains. For ionic gels (or polyelectrolyte gels), the swelling equilibrium is more complicated due to the additional effects of the degree of ionization for ionizable groups and ionic strength of the external solution.[12,59-62] Consequently, the equilibrium swelling conditions can be derived by minimising the total Gibbs free energy change of dissolving an ionic gel as following Equation (1.3):[12,62]

$$\Delta G_{Total} = \Delta G_{Mixing} + \Delta G_{Elastic} + \Delta G_{Ionic} \quad (1.3)$$

where ΔG_{Total} is the change of total free energy, ΔG_{Mixing} is the free energy due to the mixing of polymer chains with solvent, $\Delta G_{Elastic}$ is the free energy change due to elastic or deformation contributions, and ΔG_{Ionic} is the free energy change due to ion/solvent mixing and the electrostatic effect of ionic groups.

An ionic gel is subjected to an osmotic pressure (π) which consists of three components similar to the total free energy, following Equation (1.4):[12,60-62]

$$\pi = \pi_{Mixing} + \pi_{Elastic} + \pi_{Ionic} \quad (1.4)$$

where π_{Mixing} is the osmotic pressure due to the mixing of solvent with polymer, $\pi_{Elastic}$ is the osmotic pressure due to elastic force of the hydrogel, and π_{Ionic} is the osmotic pressure due to the ionic contribution resulting from the difference of osmotic pressure between mobile ions in the ionic hydrogel and in the external solution.[63,64] At equilibrium swelling, π is zero.

The ionic contribution to the osmotic pressure (π_{Ionic}) is given by:[12,62,65]

$$\pi_{ion} = RT[\Phi \sum_i \overline{C}_i - \phi \sum_i C_i] \quad (1.5)$$

where C_i and $\overline{C}_i$ are the concentrations of mobile ions in the external solution and in the gel phase, ϕ and Φ are the corresponding osmotic coefficients, respectively.

Due to the non-ideal behaviour of the ionic gels, the osmotic coefficient (Φ) for the gel phase is given by: $\Phi = \pi_p/\pi_{ideal}$. π_{ideal} is the ideal osmotic pressure of salt-free polyelectrolyte gels given by Van't Hoff expression; $\pi_{ideal} = RT\left(n_m\alpha + n_p\right)$, while $\pi_p = RT(n_m\alpha\phi_p + n_p)$. Here, n_m is the molarity of monomer, n_p is the molarity of the polymer, α is the degree of ionization, and ϕ_p is a correction factor called the osmotic coefficient. With the combination of the above equations, the osmotic coefficient (Φ) is therefore expressed as:[62]

$$\Phi = \left(\phi_p + \frac{n_p}{n_m\alpha}\right)/(1 + \frac{n_p}{n_m\alpha}) \quad (1.6)$$

1.4.1 Effect of pH

As mentioned previously, the swelling behaviour of polyelectrolyte gels is strongly dependent on pH and salt concentration. **Figure 1.10** illustrates the effect of pH and cross-linking density on the volume-equilibrium swelling (λ^3), which is defined as a ratio of fully swollen gel volume to its condensed volume, of pH-sensitive poly(methacrylic acid-*co*-acrylic acid) (PMAA-*co*-PAA)-based microgels. $1/Nv$ denotes the number of monomers between cross-linked points so that a greater value of $1/Nv$ means a lower density of cross-links. A greater swelling of microgels is seen at higher pH of the external solution. This can be explained by two mechanisms: an increase in the difference of osmotic pressure due to the different concentration of ions between inside the gels and the surrounding medium, and an increase in electrostatic repulsion between the negative charges of the ionized gels.[66] In addition, the swelling ratio of the microgels is lessened with increasing cross-linking density.[1,58,67-69]

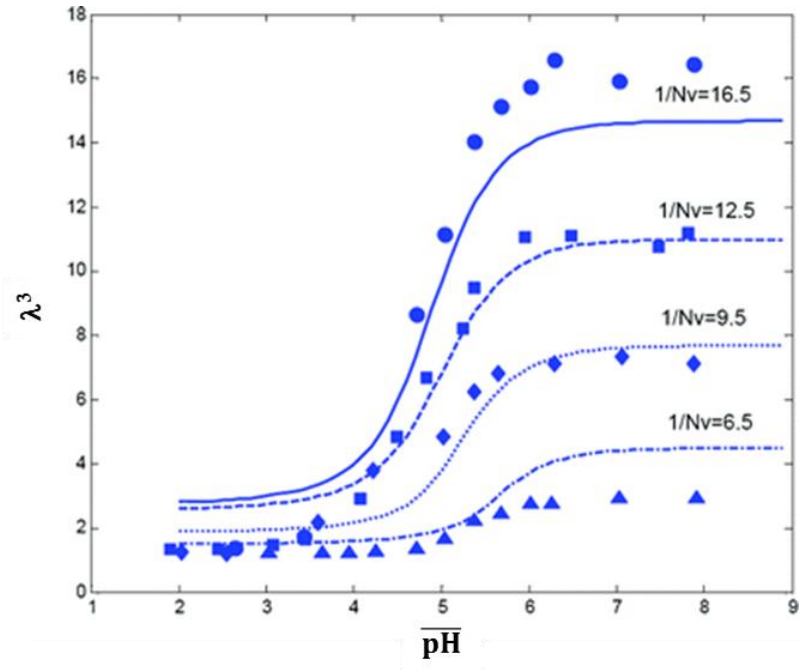

Figure 1.10 Plot of the volume-swelling ratio (λ^3) as a function of pH for pH-sensitive poly(methacrylic acid-*co*-acrylic acid)-based microgels at four different cross-linking densities. Experimental data were measured by Eichenbaum *et al.*[67] and theoretical prediction was performed by Marcombe *et al.*[70] $1/Nv$ denotes the number of monomers per polymer chain between cross-links. Reprinted from [70]. Copyright (2010) by Soft Matter.

1.4.2 Effect of salt

Generally, an increasing salt concentration decreases the equilibrium swelling ratio of the anionic gels.[8,61,63,70-72] This can be explained by (i) condensation of mobile counter-ions (positive charges) around the negative charges of anionic gels resulting in the reduction of osmotic pressure, (ii) combination of mobile counter-ions with the negative charges of anionic gels causing the neutral complexation and thus the decrease in negative charges along the anionic gels, and (iii) change in chemical potential of solvent with concentration of mobile-ions leading to variation in Flory–Huggins parameter.[66]

Figure 1.11 illustrates the swelling behaviour of PAA based ionic gels depending on pH and salt concentration of the external solution. At pH 8.7, the increasing salt concentration results in the de-swelling of the negatively charged gels consisting with the decreasing degree of ionization. However, at pH 6.5 as more salt is added the degree of ionization increases. Eventually, this leads to an increased swelling of the gels, but above a maximum concentration further addition of salt causes gel shrinkage.[8,61,63,68,70,73]

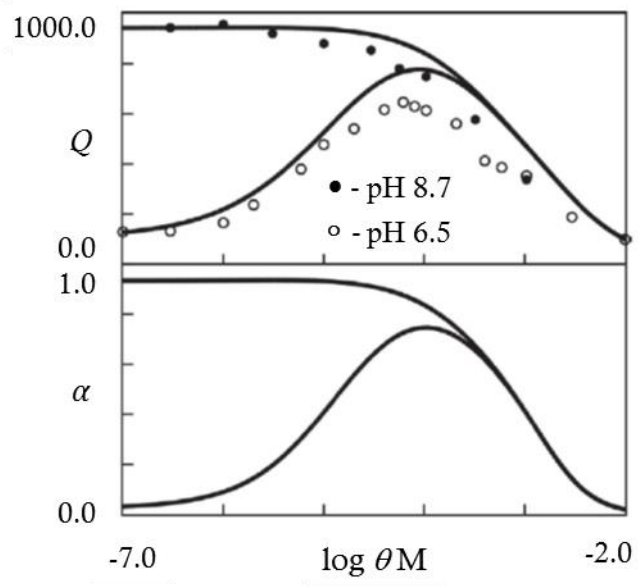

Figure 1.11 Plot of degree of volume-swelling (Q) (above) and degree of ionization (α) (below) for poly(acrylamide-*co*-acrylic acid) gel as function of salt concentration (θ) in solutions at pH 6.5 (open circles) and 8.7 (solid circles). Solid lines are the results of simulation.[73] Reprinted from [73]. Copyright (2016) by Materials Today Communications.

1.5 Hydrophobically modified PAA microgels and applications

With ionizable carboxyl groups (-COOH), PAA microgels are hydrophilic resulting in high-efficiency water absorption and their swelling / deswelling is sensitive to pH and salt concentration. Therefore, PAA based microgels have been extensively used for various applications[1,21,22] such as agriculture,[72,74-76] drug delivery,[21,77-79] or tissue engineering.[80-82] Especially in delivery systems, PAA based microgels are suitable as a carrier for hydrophilic active ingredients. However, for hydrophobic active ingredients such as anti-cancer drugs such an approach is generally problematic due to their low solubility in water and poor compatibility with the hydrophilic microgels resulting in the limited loading capacity of the active ingredients.[83] One effective approach to improve the hydrophobicity is to incorporate hydrophobic polymers into the PAA microgels.[77,83]

In this section, we are giving examples of PAA based microgels for pharmaceutical and agricultural applications.

1.5.1 Pharmaceutical applications

Using controlled-release carriers can improve drug effectiveness, reliability and safety.[84] For instance, Bromberg *et al.*[77,85-87] prepared a series of hydrophobically modified PAA microgels through physical and chemical association with Pluronic (polyethylene-polypropylene-polyethylene; PEO-PPO-PEO copolymer) for drug delivery applications.

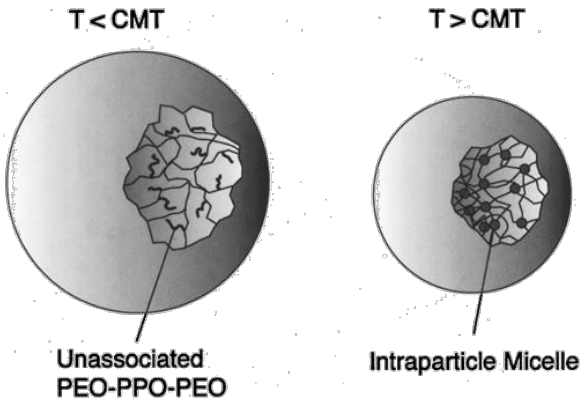

Figure 1.12 Schematic of temperature-sensitive aggregation of Pluronic dangling chains attached inside the PAA microgels.[85] Reprinted from [85]. Copyright (2002) by Langmuir.

For example, they prepared loosely cross-linked PAA microgels grafted with Pluronic, and ethylene glycol dimethacrylate (EGDMA) was used as cross-linker. The results show that hydrophilic drugs (doxorubicin, mitoxantrone, and mitomycin C which are mono-, di-, and trivalent cationic weak bases, respectively) can be effectively loaded within the cross-linked PAA networks through Donnan ion-exchange equilibrium (to balance the ion chemical potential between inside the gels and the external solvent). In addition, the drug uptake capacity is remarkedly dependent on size, hydrophilicity and net charge of drug, consequently the uptake values: mitomycin C > mitoxantrone > Doxorubicin. To evaluate the effect of temperature and pH on the equilibrium loading of doxorubicin, the drug uptake was measured at a fixed temperature of 37 °C whilst varying pH (pH 2-9) and at fixed pH 7 whilst varying temperature (15 – 45 °C). It is seen that at high pH the uptake is increased due to the swelling of the microgels as a result of the increasing ionization of carboxyl groups of PAA, whilst at elevated temperature (above the critical micellization temperature (CMT) of Pluronic) the microgels are collapsed as the PPO domains are aggregated as shown in **Figure 1.12**, and the drug uptake is therefore decreased. For a hydrophobic drug (Taxol), the uptake value is less than 1000 times that of a hydrophilic drug since its loading mechanism is different from the hydrophilic ones. They suggested that Taxol is loaded into the microgels via hydrophobic association with the PPO domains of Pluronic dangling chains attached to the PAA networks. Consequently, the uptake value of Taxol is enhanced at elevated temperature (above CMT) due to the dominant hydrophobicity of the PPO aggregation. They concluded that these microgels are suitable for both hydrophilic and hydrophobic drugs and might be promising to be used as controlled-release carriers *i.e.* in stomach (acidic pH) the drug is encapsulated inside the microgels, however, when pH suddenly increases in the small intestine (basic pH) the microgels become swollen, hence the drugs can be released.

Carbopol® is a trade name of high M_w poly(acrylic acid) based hydrogels cross-linked with allyl sucrose or allyl pentaerythritol cross-linker which is manufactured by Lubrizol. Carbopol® is widely used as pharmaceutical and multifunctional ingredients for controlled-release systems,[88-90] bioadhesive formulation[91, 92] and rheology modifier in a broad range of product types for household, industrial and institutional applications.[93, 94] Barreiro-Iglesias *et al.*[88] studied the use of Carbopol® 934 associated with various types of surfactant (Pluronic F-127, Tween, sodium dodecylsulfate (SDS), or benzalkonium chloride (BkCl)) as drug carriers for poor water-soluble drug (estradiol). The result shows that the hydrophobic drug can solubilise best in the aggregates formed by Carbopol® with SDS and Carbopol® with Tween 80. In addition, the release of estradiol from both

aggregates was evaluated in four different receptor media: 0.3% and 1.0% SDS aqueous solution (pH 4), NaCl solution (0.001%) and phosphate buffer (pH 7.5). It is seen that the release of estradiol from both Carbopol®/SDS and Carbopol®/Tween 80 can be sustained for more than 1 week and Carbopol®/SDS can release more estradiol than Carbopol® /Tween 80 in all receptor media except 1%SDS. Particularly, the release of estradiol is very low in phosphate buffer (pH 7.5) perhaps due to the restricted diffusion of estradiol through the swollen gels. In contrast, Rizi *et al.*[90] studied the release of hydrocortisone from microcapsules of Eudragit L100 (PMAA/PMMA copolymer gels) incorporated within Carbopol®/hydroxy propyl methyl cellulose (HPMC) aqueous gels and found that the release of hydrocortisone in basic pH (pH 7) is much greater than in pH 5 (below10% release of hydrocortisone) in 5 h. This indicates that these carriers are a good candidate to be used as drug carries of hydrocortisone triggered by pH in which specifically target for diseased skin having pH ~ 6 or above while pH of heathy skin is in the range of 5.0 to 5.9.

1.5.2 Agricultural applications

Due to the world population growth, agricultural land decreases whilst food demand increases. The overuse of land consequently causes the poor quality of soil, and in addition climate change and insufficient water resources also have a negative impact on food productivity.[74,76] PAA based hydrogels are beneficial for agricultural applications as the existence of hydrophilic PAA can absorb and retain a large amount of water. Apart from mixing the hydrogels with soil to decrease water draining, they can be used for coating seeds and improving the efficient use of fertilizers or other agricultural compounds during planting.[1,72,74,75,95]

For example, Olad *et al.*[72] prepared hydrogel nanocomposites from a copolymer of poly(acrylic acid) and poly(acrylamide) using *N,N'*-methylene bisacrylamide (MBA) as cross-linker onto a maize bran (MB) backbone with the presence of clay mineral (clinoptilolite; clino) and NPK fertilizers. For the neat hydrogel, it illustrates the swelling behavior as a function of pH so that the hydrogel is suddenly swollen when the pH value is increased from 2 to 5, then it gradually swells until reaching the highest value at pH 7. Afterwards, it starts shrinking slowly at pH 7 - 12. The swelling behavior of hydrogel composites (hydrogel/clino) is rather similar to the neat hydrogel. Interestingly, the addition of clino enhances the swelling ratio by a factor of two compared to the neat hydrogel and the maximum swelling is shifted to pH 10 before the composite gel is swiftly de-swollen. In general, the equilibrium swelling ratio of the hydrogels decreases with increasing concentration of salt solutions, and this is found for all type of salts (NaCl,

$CaCl_2$, and $FeCl_3$). Especially, the swelling ratio is also dependent on the type of salt so that the hydrogels can swell better in $Na^+ > Ca^{2+} > Fe^{3+}$ salt solutions. Additional ionic cross-linking formed by association between multivalent cations and carboxylate anions of PAA increases the content of cross-linking and electrostatic attraction inside the hydrogel networks and consequently reduces the swelling ratio. For the release behavior of NPK fertilizer, the results show that more than 90% of untreated NPK compound is rapidly released in aqueous medium within 5 hours in water and 98% of NPK is released in 4 hours in soil. For hydrogel/NPK and hydrogel/clino/NPK formulations, they exhibit a delayed release of NPK in both media. Within 1 month, the release of NPK is found at 88.5% and 72.9% in water, and at 90.1% and 77% in soil for hydrogel/NPK and hydrogel/clino/NPK, respectively. The results indicate that these hydrogels and hydrogel composites significantly promote the water retention and slow release of NPK in soil.

An example of commercial PAA based hydrogels for agricultural applications is Bountigel® manufactured by mOasis Inc, US. There are a few patents[96-100] of mOasis Inc, US about hydrogels consisting of high M_w poly(acrylic acid) (PAA; M_w 250,000 - 1,000,000 or 400,000 - 600,000), low M_w poly(tetramethylene ether glycol) (PTMEG or poly(tetra-hydrofuran) (PTHF); M_w 650 - 2000 or 500 - 1000), and other monomers such as acrylic acid or acrylamide with/without carboxymethyl cellulose (CMC). One possible method[96] for preparing Bountigel® is to mix up solution A (3 kg of acrylic acid dissolved in 4.5 L of water) with solution B (1.62 kg of KOH dissolved in 4.5 cold water) under stirring. Then, 9.0 g of *N,N'*-methylene bis(acrylamide) (MBA; cross-linker) and 45 g of potassium persulfate (KPS; initiator) are added into the mixture. After that, 30 g of PAA and 60 g of PTHF are also added into the mixture under stirring. The reactor is heated up to 50-55 °C for 3 hours. The resulting hydrogels are cut and dried at 70 °C. The water absorbency is about 200-250 times their dry weight. It is claimed that Bountigel® can enormously enhance the efficient use of water in soil since it possesses very high capacities of water absorption and water retention. In addition, it can improve seed germination and delay the release of fertilizers, and crop yield and quality are therefore enhanced.

1.6 Project Aims

The original idea of this project was to study polymer gels for controlled-release applications. A commercial example of such a material is Bountigel® supplied by mOasis Inc., US (referred to above). This type of hydrogels (as reported in the patent literature)[96-100] is based on poly(acrylic acid) (PAA; polycarboxylic acid) and poly(tetrahydrofuran) (PTHF; poly(ether)). They are intended for agricultural application to improve the efficient water usage and delay the release of fertilizer before leaching out of the root zone. However, they do not mention the pH-responsive behaviour of Bountigel® in the patents or for advertising.

We decided to focus on PAA/poly(ethers) based polymer gels. PAA is well known as a pH-sensitive polymer and the presence of poly(ethers) might enhance the compatibility with hydrophobic active ingredients. We expect that such polymer gels may further be of interest as a model delivery vehicle triggered by changes in pH and salt concentration for agrochemicals, or pharmaceuticals, for instance. Previously, PAA chemically or physically associated with poly(ethers) such as poly(ethylene oxide) (PEO) and Pluronics (PEO-PPO-PEO) had been used to prepare hydrogels.[77,85,101-106] Here, we prefer to explore a new polymer system consisting of PAA and commercial poly(propylene glycol) diacrylate (PPGDA) or end-group modified poly(tetrahydrofuran) (PTHF) called PTHFDA as hydrophobic-macro cross-linkers.

Consequently, the main aim of this project is to prepare hydrophobically modified PAA microgel particles with poly(ethers) as cross-linkers. The two-step method of surfactant free emulsion polymerization and hydrolysis is used to prepare the well-define microgel particles. We then proceed to investigate the swelling behaviour of the resulting PAA microgels controlled by changes in pH and salt concentration. In addition, we attempt to prepare complexes formed by hydrogen bonding between PAA and poly(ethers) (PEO and PTHF) in aqueous and methanol solutions, and to examine the possibility of using ^{1}H-NMR, DOSY-NMR and T_2 solvent relaxation to monitor this association.

Finally, we perform some preliminary experiments for controlled release using commercial PAA hydrogel triggered by changes in pH.

1.7 Thesis Overview

The remainder of this thesis is organised as follows.

In chapter 2, we show that well-defined PAA microgel particles cross-linked with hydrophobic poly(ethers) can be successfully prepared through surfactant free emulsion polymerization and acid-hydrolysis of poly(*tert*-butyl acrylate) (P*t*BA). The chemical structure of P*t*BA before and after hydrolysis to PAA microparticles is characterized with ^{1}H-NMR, ^{13}C-NMR and Heteronuclear Single Quantum Correlation spectroscopy (HSQC -NMR). In addition, the morphology of these particles is illustrated by TEM images.

Chapter 3 studies the effect of cross-linking density by varying the mole ratio of monomer to cross-linker and type of cross-linker on the swelling behaviour of the microparticles. The particle size of the microparticles is measured using light scattering techniques (both DLS and SLS). The SLS data is further analysed with the SasView software and polydisperse sphere and core-shell models, and the radius of particle and polydispersity are then obtained. The combined results of DLS and SLS inform the shape and cross-linking distribution of the particles through the shape factor which is the ratio between radius of gyration (R_G)/hydrodynamic radius (R_H). For P*t*BA microparticles, the swelling ratio in three different solvents (water, acetone and THF) is investigated, while for PAA microparticles, the swelling behaviour as a function of pH and salt concentration as well as the association with low M_w PEO is observed.

In chapter 4, we probe the association between PAA and two different types of poly(ethers) (PEO and PTHF) using a variety of different experimental techniques: ^{1}H-NMR, DOSY-NMR and T_2 solvent relaxation as well as visual observations.

Chapter 5 which is the final experimental chapter presents our attempt to set up an experiment to investigate the use of commercial PAA hydrogels as a controlled release device. Active ingredient (AI) is loaded in the hydrogels in the swollen state. The content of active ingredient loaded and released from the hydrogels to an external solution is measured as a function of pH using UV-visible spectroscopy.

Finally, a conclusion of the results and suggestions for further work are provided in chapter 6. In addition, we present a brief background information on the techniques used in the experimental chapters in Appendix A.

Bibliography

1. W. A. Laftah, S. Hashim, A. N. Ibrahim. *Polymer-Plastics Technology and Engineering* **2011**, *50*, 1475-1486.

2. E. M. Ahmed. *Journal of Advanced Research* **2013**, *6*, 105-121.

3. S-K. Ahn, R. M. Kasi, S. C. Kim, N. Sharma, Y. Zhou. *Soft Matter* **2008**, *4*, 1151-1157.

4. J. K. Oh, R. Drumright, D. J. Siegwart, K. Matyjaszewski. *Progress in Polymer Science* **2008**, *33*, 448-477.

5. H. Kawaguchi. *Polymer International* **2014**, *63*, 925-932.

6. O. Okay, In Hydrogel Sensors and Actuators; Gerlach, G., Arndt, K. F., Editors.; Springer-Verlag: Berlin Heidelberg **2010**, pp 1-14.

7. J. H. Lee, D. G. Bucknall. *Journal of Polymer Science Part B: Polymer Physics* **2008**, *46*, 1450-1462.

8. G. S. Longo, M. O. de la Cruz, I. Szleifer. *Macromolecules* **2011**, *44*, 147-158.

9. J. Choi, M. F. Rubner. *Macromolecules* **2005**, *38*, 116-124.

10. P. Gupta, K. Vermani, S. Garg. *Drug Discovery Today* **2002**, *7*, 569-579.

11. G. Kocak, C. Tuncer, V. Butun. *Polymer Chemistry* **2017**, *8*, 144-176.

12. G. R. L. Deen, Xian Jun. *Gels* **2018**, *4*, 13.

13. H. J. Kwon, Y. Osada, J. P. Gong. *Polymer Journal* **2006**, *38*, 1211-1219.

14. Y. Osada, J. P. Gong. *Advanced Materials* **1998**, *10*, 827-837.

15. F. Askari, S. Nafiai, H. Omidian, S. A. Hashemi. *Journal of Applied Polymer Science* **1993**, *50*, 1851-1855.

16. A. R. Khare, N. A. Peppas. *Biomaterials* **1995**, *16*, 559-567.

17. Y. Guan, W. W. Jiang, W. C. Zhang, G. X. Wan, Y. X. Peng. *Journal of Polymer Science Part B: Polymer Physics* **2001**, *39*, 1784-1790.

18. E. Jabbari, S. Nozari. *European Polymer Journal* **2000**, *36*, 2685-2692.

19. T. Swift, L. Swanson, M. Geoghegan, S. Rimmer. *Soft Matter* **2016**, *12*, 2542-2549.

20. M. Rubinstein, R. H. Colby. Polymer Physics; Oxford University Press: Oxford, **2003**.

21. T. R. Hoare, D. S. Kohane. *Polymer* **2008**, *49*, 1993-2007.

22. S. K. H. Gulrez, S. Al-Assaf, G. O. Phillips. Hydrogels: methods of preparation, characterisation and applications; Prof. Angelo Carpi (Editor); In tech: UK, **2011**.

23. W. E. Hennink, C. F. van Nostrum. *Advanced Drug Delivery Reviews* **2012**, *64*, 223-236.

24. A. S. Hoffman. *Advanced Drug Delivery Reviews* **2012**, *64*, 18-23.

25. K. Y. Lee, D. J. Mooney. *Progress in Polymer Science* **2012**, *37*, 106-126.

26. F. Chellat, M. Tabrizian, S. Dumitriu, E. Chornet, P. Magny, C. H. Rivard, L. Yahia. *Journal of Biomedical Materials Research* **2000**, *51*, 107-116.

27. N. Popa, O. Novac, L. Profire, C. E. Lupusoru, M. I. Popa. *Journal of Materials Science-Materials in Medicine* **2010**, *21*, 1241-1248.

28. Q. F. Wang, J. B. Schlenoff. *Macromolecules* **2014**, *47*, 3108-3116.

29. F. E. Bailey JR, R. D. Lundberg, R. W. Callard. *Journal of Polymer Science: Part A* **1964**, *2*, 845-851.

30. Pradip, C. Maltesh, P. Somasundaran, R. A. Kulkarni, S. Gundiah. *Langmuir* **1991**, *7*, 2108-2111.

31. F. Sultana, Manirujjaman, M. Imran-Ul-Haque, M. Arafat, S. Sharmin. *Journal of Applied Pharmaceutical Science* **2013**, *3*, S95-S105.

32. B. R. Saunders, B. Vincent. *Advances in Colloid and Interface Science* **1999**, *80*, 1-25.

33. J. A. Bonham, M. A. Faers, J. S. van Duijneveldt. *Soft Matter* **2014**, *10*, 9384-9398.

34. Z. Chen, M. Liu, S. Ma. *Reactive & Functional Polymers* **2004**, *62*, 85-92.

35. A. K. Bajpai, A. Giri. *Reactive & Functional Polymers* **2002**, *53*, 125-141.

36. D. Y. Fang, Q. M. Pan, G. L. Rempel. *Journal of Applied Polymer Science* **2007**, *103*, 707-715.

37. S. Kiatkamjornwong, P. Phunchareon. *Journal of Applied Polymer Science* **1999**, *72*, 1349-1366.

38. S. Q. Zhou, B. Chu. *Journal of Physical Chemistry B* **1998**, *102*, 1364-1371.

39. H. Mackova, D. Horak. *Journal of Polymer Science Part A: Polymer Chemistry* **2006**, *44*, 968-982.

40. J. W. Goodwin, J. Hearn, C. C. Ho, R. H. Ottewill. *British Polymer Journal* **1973**, ***5***, 347-362.

41. S. Dai, P. Ravi, K. C. Tam. *Soft Matter* **2008**, *4*, 435-449.

42. R. Tiwari, T. Heuser, E. Weyandt, B. C. Wang, A. Walther. *Soft Matter* **2015**, *11*, 8342-8353.

43. J. A. Bonham, F. Waggett, M. A. Faers, J. S. van Duijneveldt. *Colloid and Polymer Science* **2017**, *295*, 479-486.

44. A. K. Bajpai, S. K. Shukla, S. Bhanu, S. Kankane. *Progress in Polymer Science* **2008**, *33*, 1088-1118.

45. Y. Sun, 'Different particle information obtained from static and dynamic laser light scattering', Master of Science Thesis, Simon Fraser University, Canada **2004**.
46. C. Fraschini, G. Chauve, J. F. Le Berre, S. Ellis, M. Methot, B. O'Connor, J. Bouchard. *Nordic Pulp & Paper Research Journal* **2014**, *29*, 31-40.
47. M. Schmidt, D. Nerger, W. Burchard. *Polymer* **1979**, *20*, 582-588.
48. D. Kunz, A. Thurn, W. Burchard. *Colloid and Polymer Science* **1983**, *261*, 635-644.
49. M. S. Wolfe, C. Scopazzi. *Journal of Colloid and Interface Science* **1989**, *133*, 265-277.
50. B. M. Tande, N. J. Wagner, M. E. Mackay, C. J. Hawker, M. Jeong. *Macromolecules* **2001**, *34*, 8580-8585.
51. S. Bhattacharjee. *Journal of Controlled Release* **2016**, *235*, 337-351.
52. B. E. Rodriguez, M. S. Wolfe, M. Fryd. *Macromolecules* **1994**, *27*, 6642-6647.
53. X. Wu, R. H. Pelton, A. E. Hamielec, D. R. Woods, W. McPhee. *Colloid and Polymer Science* **1994**, *272*, 467-477.
54. F. Scheffold, P. Diaz-Leyva, M. Reufer, N. Ben Braham, I. Lynch, J. L. Harden. *Physical Review Letters* **2010**, *104*, 4.
55. N. Boon, P. Schurtenberger. *Physical Chemistry Chemical Physics* **2017**, *19*, 23740-23746.
56. M. Reufer, P. Diaz-Leyva, I. Lynch, F. Scheffold. *European Physical Journal E* **2009**, *28*, 165-171.
57. M. Antonietti, W. Bremser, M. Schmidt. *Macromolecules* **1990**, *23*, 3796-3805.
58. A. M. Rumyantsev, A. Pan, S. G. Roy, P. De, E. Y. Kramarenko. *Macromolecules* **2016**, *49*, 6630-6643.
59. L. Brannon-Peppas, N. A. Peppas. *Chemical Engineering Science* **1991**, *46*, 715-722.
60. M. Shibayama, T. Tanaka. *Advances in Polymer Science* **1993**, *109*, 1-62.
61. M. Quesada-Perez, J. A. Maroto-Centeno, J. Forcada, R. Hidalgo-Alvarez. *Soft Matter* **2011**, *7*, 10536-10547.
62. F. Ganji, S. Vasheghani-Farahani, E. Vasheghani-Farahani. *Iranian Polymer Journal* **2010**, *19*, 375-398.
63. J. Ricka, T. Tanaka. *Macromolecules* **1984**, *17*, 2916-2921.
64. B. A. Firestone, R. A. Siegel. *Journal of Biomaterials Science-Polymer Edition* **1994**, *5*, 433-450.
65. E. Vasheghanifarahani, J. H. Vera, D. G. Cooper, M. E. Weber. *Industrial & Engineering Chemistry Research* **1990**, *29*, 554-560.
66. A. D. Drozdov, J. D. Christiansen. *Modelling and Simulation in Materials Science and Engineering* **2015**, *23*, 38.

67. G. M. Eichenbaum, P. F. Kiser, A. V. Dobrynin, S. A. Simon, D. Needham. *Macromolecules* **1999**, *32*, 4867-4878.

68. J. Ostroha, M. Pong, A. Lowman, N. Dan. *Biomaterials* **2004**, *25*, 4345-4353.

69. X. Jin, Y. L. Hsieh. *Polymer* **2005**, *46*, 5149-5160.

70. R. Marcombe, S. Q. Cai, W. Hong, X. H. Zhao, Y. Lapusta, Z. G. Suo. *Soft Matter* **2010**, *6*, 784-793.

71. W. F. Zhao, R. W. N. Nugroho, K. Odelius, U. Edlund, C. S. Zhao, A. C. Albertsson. *ACS Applied Materials and Interfaces* **2015**, *7*, 4202-4215.

72. A. Olad, H. Gharekhani, A. Mirmohseni, A. Bybordi. *Journal of Polymer Research* **2016**, *23*, 14.

73. A. D. Drozdov, C. G. Sanporean, J. D. Christiansen. *Materials Today Communications* **2016**, *6*, 92-101.

74. Y. L. Ma, Y. J. Sun, Y. J. Fu, G. Z. Fang, X. R. Yan, Z. H. Guo. *Chemosphere* **2016**, *163*, 610-619.

75. H. A. Essawy, M. B. M. Ghazy, F. Abd El-Hai, M. F. Mohamed. *International Journal of Biological Macromolecules* **2016**, *89*, 144-151.

76. K. Zhong, Z. T. Lin, X. L. Zheng, G. B. Jiang, Y. S. Fang, X. Y. Mao, Z. W. Liao. *Carbohydrate Polymers* **2013**, *92*, 1367-1376.

77. L. Bromberg, M. Temchenko, T. A. Hatton. *Langmuir* **2003**, *19*, 8675-8684.

78. E. S. Gil, S. M. Hudson. *Progress in Polymer Science* **2004**, *29*, 1173-1222.

79. A. K. Bajpai, S. K. Shukla, S. Bhanu, S. Kankane. *Progress in Polymer Science* **2008**, *33*, 1088-1118.

80. R. A. Stile, W. R. Burghardt, K. E. Healy. *Macromolecules* **1999**, *32*, 7370-7379.

81. D. L. Taylor, M. I. H. Panhuis. *Advanced Materials* **2016**, *28*, 9060-9093.

82. F. Wang, Z. Q. Li, M. Khan, K. Tamama, P. Kuppusamy, W. R. Wagner, C. K. Sen, J. J. Guan. *Acta Biomaterialia* **2010**, *6*, 1978-1991.

83. E. Larrañeta, S. Stewart, M. Ervine, R. Al-Kasasbeh, R. F. Donnelly. *Journal of Functional Biomaterials* **2018**, *9*, 13.

84. H. Almeida, M. H. Amaral, P. Lobão. *Journal of Applied Pharmaceutical Science* **2012**, *2*, 01-10.

85. L. Bromberg, M. Temchenko, T. A. Hatton. *Langmuir* **2002**, *18*, 4944-4952.

86. L. E. Bromberg, E. S. Ron. *Advanced Drug Delivery Reviews* **1998**, *31*, 197-221.

87. L. Bromberg, T. A. Hatton, R. Barreiro-Iglesias, C. Alvarez-Lorenzo, A. Concheiro. *Drug Development and Industrial Pharmacy* **2007**, *33*, 607-615.

88. R. Barreiro-Iglesias, C. Alvarez-Lorenzo, A. Concheiro. *Journal of Controlled Release* **2003**, *93*, 319-330.
89. C. Rodriguez-Tenreiro, L. Diez-Bueno, A. Concheiro, J. J. Torres-Labandeira, C. Alvarez-Lorenzo. *Journal of Controlled Release* **2007**, *123*, 56-66.
90. K. Rizi, R. J. Green, M. X. Donaldson, A. C. Williams. *Pharmaceutical Research* **2011**, *28*, 2589-2598.
91. Z. Pavelic, N. Skalko-Basnet, R. Schubert. *International Journal of Pharmaceutics* **2001**, *219*, 139-149.
92. S. Salah, G. E. A. Awad, A. I. A. Makhlouf. *European Journal of Pharmaceutical Sciences* **2018**, *114*, 255-266.
93. Carbopol. [online] Available at: https://www.lubrizol.com/Carbopol (accessed 19 July 2018, 2018).
94. Carbopol life sciences products. [online] Available at: https://www.lubrizol.com/Life-Sciences/Products/Carbopol-Polymer-Products (accessed 19 July 2018, 2018).
95. L. H. Xie, M. Z. Liu, B. L. Ni, X. Zhang, Y. F. Wang. *Chemical Engineering Journal* **2011**, *167*, 342-348.
96. N. Li, M. C. Williams (Moasis Inc., USA) Patent US 2013/0303665 A1, **2013**.
97. N. Li, C. Blackford (Moasis Inc., USA) Patent US 2015/0299975 A1, **2015**.
98. N. Li, J. C. Wu (Moasis Inc., USA) Patent US 2015/0225646 A1, **2015**.
99. N. Li, J. C. Wu (Moasis Inc., USA) Patent US 2016/0219871 A1, **2016**.
100. N. Li, M. C. Williams (mOasis Inc., USA) Patent US 2018/0086913 A1 **2018**.
101. G. H. Chen, A. S. Hoffman, B. Kabra, K. Randeri. *Poly(Ethylene Glycol): Chemistry and Biological Applications* **1997**, *680*, 441-457.
102. L. Bromberg, M. Temchenko, G. D. Moeser, T. A. Hatton. *Langmuir* **2004**, *20*, 5683-5692.103. L. Bromberg, M. Temchenko, V. Alakhov, T. A. Hatton. *International Journal of Pharmaceutics* **2004**, *282*, 45-60.
104. S. S. Jang, W. A. Goddard, M. Y. S. Kalani. *Journal of Physical Chemistry B* **2007**, *111*, 1729-1737.
105. K. T. Oh, T. K. Bronich, V. A. Kabanov, A. V. Kabanov. *Biomacromolecules* **2007**, *8*, 490-497.
106. T. Swift, C. C. Seaton, S. Rimmer. *Soft Matter* **2017**, *13*, 8736-8744.

Chapter 2

Synthesis and chemical characterization of poly(acrylic acid) microgels

Abstract

Surfactant free emulsion polymerization (SFEP) is a promising method to create microparticles with a well-controlled particle size and structure. The method commonly involves monomer(s), water-soluble initiator and cross-linker(s) dispersed in water. In this chapter, we present the use of SFEP to prepare microparticles of poly(acrylic acid) (PAA) cross-linked with two types of hydrophobic poly(ethers). Firstly, poly(*tert*-butyl acrylate) (P*t*BA) microparticles were made using SFEP with potassium persulfate (KPS) as initiator, and poly(propylene glycol) diacrylate (PPGDA) or poly(tetrahydrofuran) diacrylate (PTHF-DA) as cross-linker. Subsequently, with acid-hydrolysis, the *tert*-butyl ester groups of P*t*BA were transformed to carboxyl groups so PAA microgels were obtained. In addition, we varied the molar ratios of *t*BA monomer and cross-linker. This allows the effect of cross-linking density on the swelling behaviour of the microgels to be studied (Chapter 3). FT-IR and NMR spectra as well as TEM images show that well-defined PAA microgels were successfully produced. Due to the amphiphilic structure of PAA microparticles cross-linked with poly(ethers), these particles might be used in model studies of polyelectrolyte interactions with active ingredients and may also be of interest as a controlled delivery vehicle with pH-trigger.

2.1 Introduction

Poly(acrylic acid) (PAA) is a well-known pH responsive polymer due to its ionizable carboxyl groups along the polymer chains. Traditionally, PAA with a narrow molecular weight distribution is made via anionic polymerization and hydrolysis of polyacrylates such as poly(methyl acrylate) (PMA) and poly(*tert*-butyl acrylate) (P*t*BA).[1-3] For example, first P*t*BA is polymerized and then the deprotection of *tert*-butyl ester group of P*t*BA into a carboxyl group is performed to obtain PAA using trifluoroacetic acid (TFA) in dichloromethane (DCM),[4-6] hydrochloric acid (HCl) in dioxane,[7-9] or sulfuric acid (H_2SO_4) in water/methanol co-solvent.[10]

The preparation method is one of the key factors in the size and structure of hydrogels. Babic and Horak[11] prepared poly(N,N-dimethylacrylamide) based microgels by heterogeneous polymerizations including inverse suspension, inverse emulsion and dispersion polymerization. The microgels obtained by inverse suspension polymerization are 100 μm in diameter, while the gels formed by inverse emulsion polymerization are 0.13-1 μm in diameter with a broad size distribution. In contrast, they report that the dispersion polymerization is effective to create monodisperse microgels with the size of 1-2 μm by using Kraton G 1650 as stabilizer.

A number of previous studies report preparation of PAA-based homo-polymer or co-polymer gels by precipitation polymerization, inverse suspension polymerization, emulsion polymerization, and miniemulsion polymerization which mainly contain hydrophobic monomers, initiator and multifunctional cross-linkers.[12,13] Askari *et al.*[14] synthesized PAA microgels via inverse suspension polymerization using toluene as the organic phase, potassium persulfate (KPS) as initiator, Span 80 as surfactant, and ethylene glycol dimethacrylate as cross-linker. The resulting particles are lump-like beads with an average diameter of 2-3 mm which consist of particles of 50-500 μm fused together. However, after the particles were protected from adhering to each other by adding ethyl cellulose as macromolecular emulsifiers, an average particle diameter of about 300 μm was obtained. Philippova *et al.*[15] used N,N'-methylenebisacrylamide (MBA) cross-linker and 2,2'-azobisisobutyronitrile (AIBN) initiator to prepare hydrophobically modified PAA gels with n-alkyl acrylates via free radical polymerization in N,N-dimethyl formamide. Es-haghi *et al.*[16] prepared cross-linked PAA macrogels via precipitation polymerization in a co-solvent of ethyl acetate/n-hexane using MBA as cross-linker and AIBN as initiator. Yu *et al.*[17] prepared microcrystalline PAA gels via emulsion polymerization. The reaction

consisted of AA monomer, MBA as cross-linker, ammonium persulfate/sodium sulfite as a redox initiator system, and sodium dodecyl sulfate (SDS) as emulsifier. Zhang *et al.*[18] prepared PAA microgels via miniemulsion polymerization and basic hydrolysis of poly(acrylonitrile) (PAN) microgels. They reported that the particle size of PAN nanoparticles was about 105 nm in diameter with a narrow size distribution. However, after base-hydrolysis to convert nitrile (–CN) groups of PAN into carboxyl (-COOH) groups, the particle size of the PAA microgels became broad with a range of 100-500 nm in diameter.

For the examples above, the synthetic method plays a key role in the size and size distribution of cross-linked PAA gels. Unfortunately, these methods were fairly complicated and the control of particle size is limited. Recently, Tiwari *et al.*[19] prepared well-defined poly(methacrylic acid) (PMAA) microgels with ethylene glycol dimeth-acrylate (EGDMA) as cross-linker, and sodium dodecyl sulfate (SDS) as surfactant via emulsion polymerization and acid hydrolysis of poly(*tert*-butyl methacrylate) (P*t*BMA). They found that the higher SDS concentration leads to the smaller size of P*t*BMA latex, while effect of cross-linking density (the mole ratio of monomer to cross-linker is varied in a range of 0 – 500) on the size of P*t*BMA latex is not visible. In addition, after hydrolysis of P*t*BMA, the hydrodynamic radius of resulting PMAA latex becomes larger from 155 nm to 180 nm and effect of cross-linking density on the particle size is noticeable as found that the less cross-linking density results in the larger size of PMAA latex at pH 3 (collapsed state). However, many studies[20-22] mention the difficulty to remove the residual surfactant which may lead to the coagulation of the latex.

2.1.1 Surfactant free emulsion polymerization (SFEP)

The detailed background and mechanism of this method were discussed previously in Chapter 1 introduction. To summarize, SFEP requires only hydrophobic monomer and cross-linker, and soluble ionic initiator in aqueous medium. Importantly, since surfactant is not required for SFEP (unlike emulsion polymerization), the latex particles are stabilized to be able to disperse in the medium by charges on polymer chains initiated from the ionic initiator. Moreover, the particle size of the latex is dependent on the amount of monomer and initiator[21,23,24] and the stability of the particles is dependent on type of initiator.[25] pH responsive hydrogels prepared from poly(acids) copolymerized with hydrophilic poly(ethers) such as poly(ethylene glycol) (PEG) and Pluronic or Poloxamer (PEO-PPO-PEO) have been widely studied for drug delivery applications, scaffolds and sensors.[26-36]

Besides the pH response of PAA, we are interested in the preparation of amphiphilic structures containing hydrophilic PAA cross-linked with hydrophobic poly(ethers). We intend to use polypropylene glycol (PPG) and poly(tetrahydrofuran) (PTHF), which are both more hydrophobic than PEG, as macro cross-linkers. Few studies have been done using these polymers.[37-39] The increase of hydrophobicity of microgels can enhance the compatibility between the polymer gels as carriers and hydrophobic active ingredients for controlled release applications.

Beneficially, SFEP only requires monomer, ionic initiator, and cross-linker dispersed in water. Charges on the polymer networks formed by the ionic initiator can efficiently stabilize and prevent the aggregation of microparticles dispersed in water.[40-42] However, acrylic acid (AA) monomer is unsuitable for SFEP because it is water-soluble. Instead, we use *tert*-butyl acrylate (*t*BA) monomer, which dissolves sparingly in water, and can subsequently be acid-hydrolysed into PAA. In this chapter, we present a novel method to prepare very well-defined PAA microgels cross-linked with hydrophobic poly(ethers) through SFEP and acid-hydrolysis of P*t*BA microparticles. The chemical structures of cross-linked microparticles were characterized by FT-IR and NMR spectroscopy. Morphology and particle size of the microparticles were investigated by TEM.

2.2 Experimental

2.2.1 Materials

tert-butyl acrylate (*t*BA, Aldrich) was purified with a pre-packed column for removing monomethyl ether hydroquinone prior to use. Poly(propylene glycol diacrylate) (PPGDA M_n 800, Aldrich), poly(tetrahydrofuran) (PTHF M_n 1000, Aldrich), methacrylic anhydride (MA, Aldrich), acrylic acid (AA, Merck), triethylamine (TEA, Fisher Scientific), *p*-toluenesulfonic acid (PTSA, Acros Organics), hydroquinone (Acros Organics), and potassium persulfate (KPS, Aldrich) were used without further purification. Deionized (DI) water with a resistivity greater than 18.2 MΩ·cm was obtained from a Milli-Q Plus system from Millipore. Trifluoroacetic acid (TFA, Aldrich) and all solvents were used as received. Cellulose membrane dialysis tubing with a cut-off molecular weight of 14,000 (Sigma-Aldrich) was used to purify the microparticles.

2.2.2 End-group modification of PTHF

Two types of poly(ethers) are used as cross-linkers to prepare PAA microgels. One is poly(propylene glycol) (PPG) having vinyl acrylate groups at its two chain ends which is commercially available (referred to as PPGDA). Unfortunately, we cannot purchase poly(tetrahydrofuran) (PTHF) having such end groups. Therefore, we modified PTHF to have vinyl end groups via two different routes using either methacrylic anhydride (MA) or acrylic acid (AA).

2.2.2.1 Esterification of PTHF with methacrylic anhydride (MA)

The reaction was carried out in a 250 mL round-bottom flask with magnetic stirrer bar. 15.0 g of PTHF (M_w 1000 g/mol, 15 mmol) and 8.4 mL of triethylamine as catalyst (TEA, 60 mmol) were dissolved in 210 mL of dry DCM. Then 9 mL of methacrylic anhydride (MA, 60 mmol) was added into the reactor dropwise. The mixture was stirred overnight at room temperature and then washed thrice with saturated $NaHCO_3$ (200 mL). The organic phase was concentrated *in vacuo*. The resulting product was characterized using FT-IR and ^{1}H-NMR.

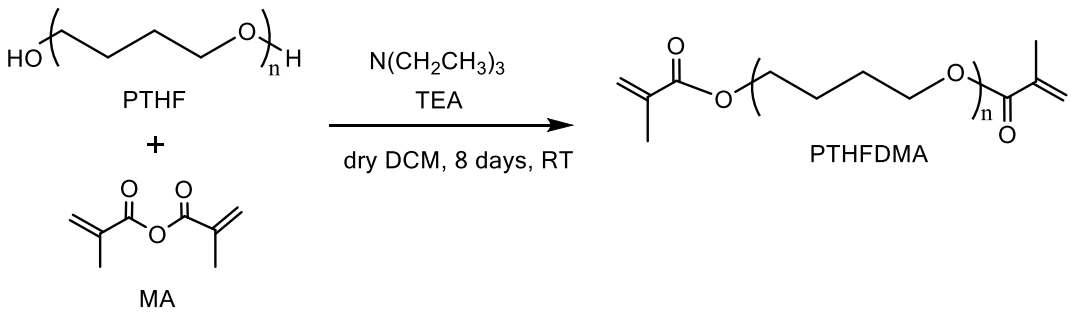

Figure 2.1 Schematic of esterification of PTHF with methacrylic anhydride (MA) to obtain PTHF with dimethacrylate (PTHDMA).

2.2.2.2 Esterification of PTHF with acrylic acid (AA)

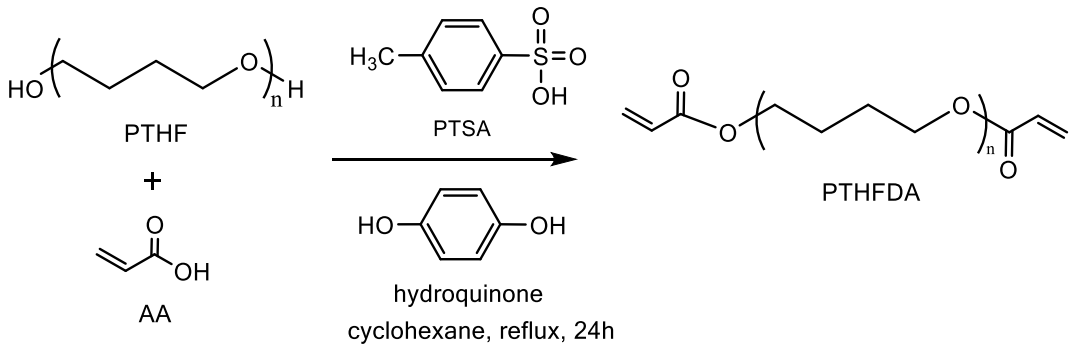

Figure 2.2 Schematic of esterification of PTHF with acrylic acid (AA), PTSA as catalyst and hydroquinone as inhibitor to obtain PTHF with diacrylate (PTHFDA).

The esterification of poly(tetrahydrofuran) (PTHF) with AA in cyclohexane has been reported previously by Guan *et al.*[43] 5 g of PTHF (M_w 1000 g/mol, 5 mmol), 0.89 mL of acrylic acid (AA, 13 mmol), 0.086 g of *p*-toluenesulfonic acid as catalyst (PTSA, 0.45 mmol), and 0.017 g of hydroquinone as inhibitor (0.15 mmol) were dissolved in 83 mL of cyclohexane. The mixture was stirred in a 250-mL flask equipped with a Dean–Stark water collector and a magnetic stirring bar. The reaction mixture was carried out for 24 h with reflux at ~170 °C. To eliminate the catalyst and free acrylic acid, the reaction mixture was treated with 0.138 g potassium carbonate (K_2CO_3, 1.0 mmol) with stirring for a further 20 mins and was then filtered. The solvent was evaporated in a vacuum rotary evaporator until constant weight was reached. The crude product was dissolved in 80 mL of DCM and washed three times with 1 M of NaOH to remove the inhibitor until the washing solution was colourless. Afterward, it was washed three times with distilled water to remove NaOH. At last, it was dried under vacuum at room temperature for 3 days. The success of the reaction can be studied using FT-IR and ^{1}H-NMR.

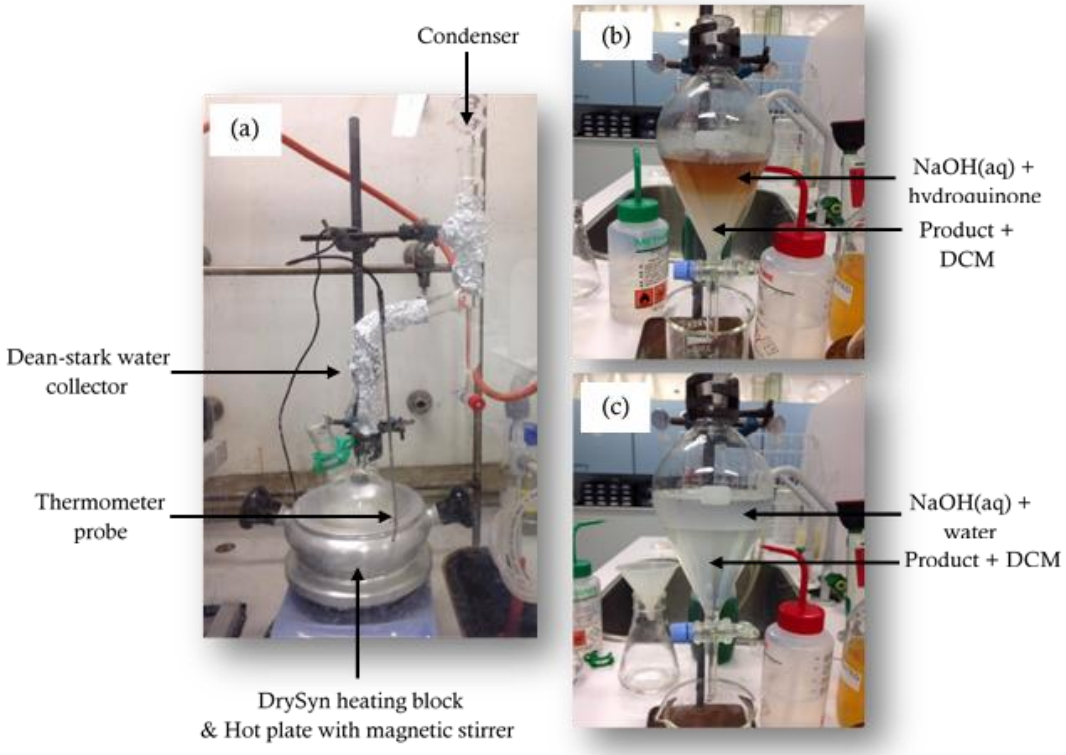

Figure 2.3 Experimental set-up for (a) esterification of PTHF with acrylic acid (AA) at 170 °C, (b) the removal of hydroquinone inhibitor with NaOH(aq) and (c) the removal of NaOH(aq) with DI water (top) from the final product dissolved in DCM (bottom).

2.2.3 Synthesis of P*t*BA microparticles

The preparation of P*t*BA microparticles was reported previously in the literature.[41] The reaction was carried out in a one-litre, three-neck round-bottom flask fitted with an air condenser, overhead stirrer and an Argon gas (Ar) bubbler. A mixture of DI water (444 ml), *t*BA monomer and cross-linker was added into the flask and then the reactor was heated up to 70 °C and stirred at 300 rpm under Ar atmosphere. Then, KPS solution (0.1 g in 36.42 g of DI water) was added into the reactor dropwise. After 24 h, the resulting latex was filtered through glass wool to remove coagulum and then purified by dialysis for 2 weeks in DI water which was replaced daily to remove unreacted reactants.

Table 2.1 List of chemicals used to prepare P*t*BA microparticles.

Microparticles	Molar ratio *t*BA : cross-linker	*t*BA* monomer (g)	M_w of cross-linker (g/mol)	Cross-linker (g)
P*t*BA/PPG	50 : 1	19.23	800	2.4
	75 : 1	19.23	800	1.6
	100 : 1	19.23	800	1.2
P*t*BA/PTHF	100 : 1	19.23	1105	1.93**
	300 : 1	19.23	1105	0.64**

*M_w of *t*BA = 128.2 g/mol

**calculation based on 86% esterification of PTHF to PTHFDA

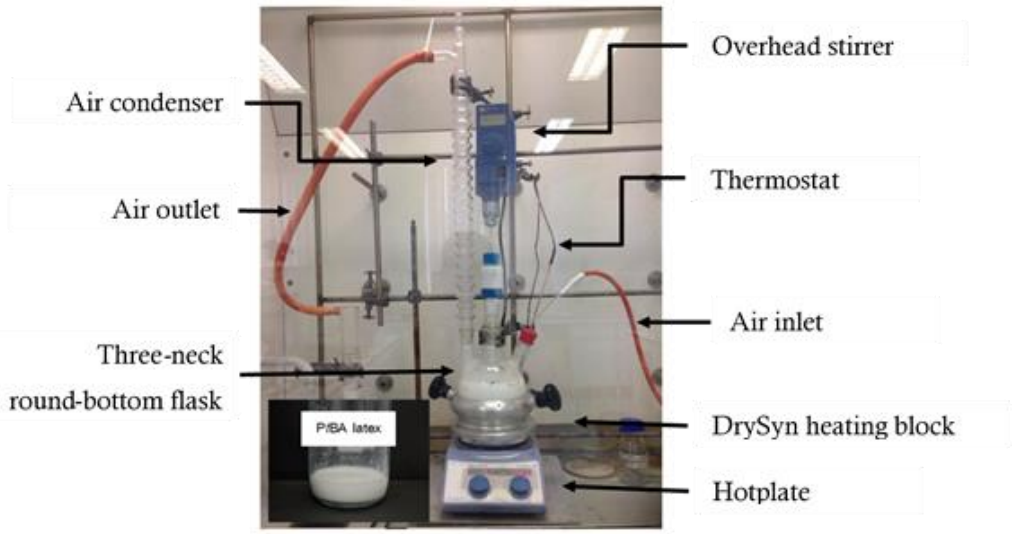

Figure 2.4 Experimental set-up for synthesis of P*t*BA microparticles.

2.2.4 Hydrolysis of P*t*BA to PAA microgels

Since the P*t*BA latex is already dispersed in water, we simply attempted to hydrolyze the latex by adding acid such as acetic acid (CH_3COOH), trifluoroacetic acid (TFA), hydrochloric acid (HCl), and HCl in water/methanol co-solvent.[10] In addition, we hydrolyzed freeze-dried P*t*BA microparticles with TFA in DCM[4-6] and with HCl in 1,4-dioxane.[7-9] In this part, P*t*BA/PPG microparticles at a molar ratio of *t*BA monomer to PPGDA cross-linker = 100:1 were used to study the possibility of using a hydrolysis reaction to convert the *tert*-butyl ester groups of cross-linked P*t*BA microparticles to carboxyl groups in order to obtain PAA microgels. A summary of hydrolysis conditions used is given in **Figure 2.5**.

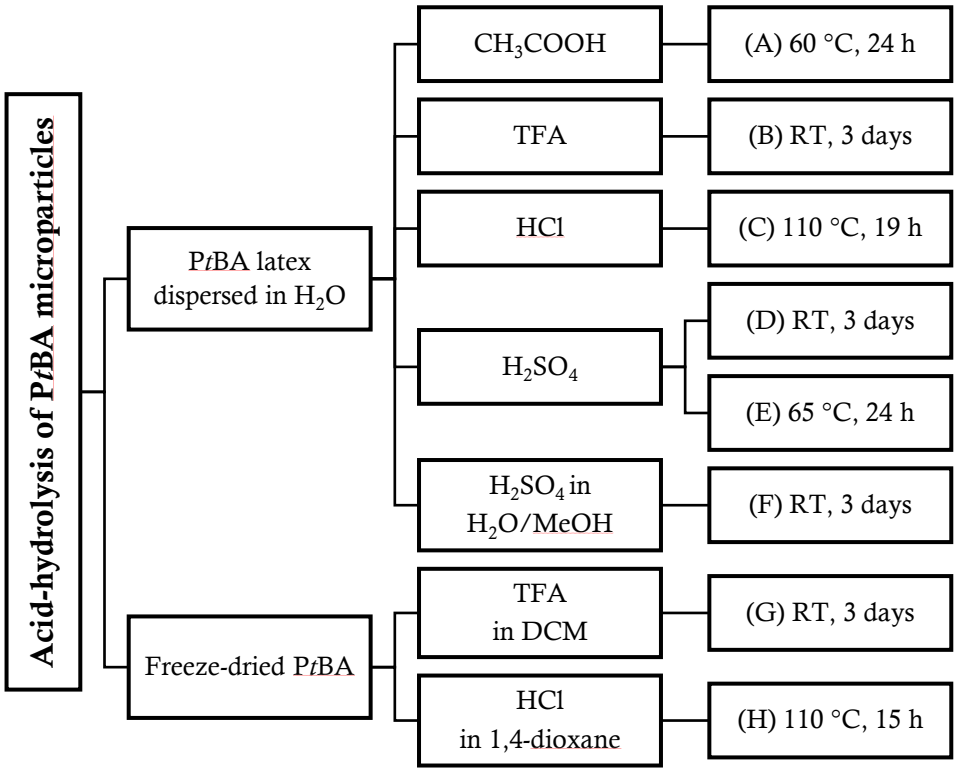

Figure 2.5 Acid-hydrolysis conditions for P*t*BA microparticles.

(A) P*t*BA latex/CH_3COOH: 1 g of 10%wt P*t*BA latex dispersed in water was added into 9 g of 99%wt acetic acid with stirring and then the mixture was heated up to 60 °C for 24 h. The coagulated latex was purified by dialysis against deionized water.

(B) P*t*BA latex/TFA: A tenfold excess of TFA (with respect to *tert*-butyl ester) was added into 25 g of 0.2%wt P*t*BA latex dispersed in water. The mixture was stirred at room temperature for 3 days. The coagulated latex was purified by dialysis against deionized water.

(C) P*t*BA latex/HCl/110 °C: 20 mL of 35%wt HCl was added into 100 mL of 0.13%wt/v P*t*BA latex dispersed in water. The mixture was heated with reflux at 110 °C for 19 h and then dialysed against deionized water.

(D) P*t*BA latex/H_2SO_4/RT: 5 mL of 11%wt P*t*BA latex dispersed in water was diluted into 50 mL. Then 95%wt H_2SO_4 was added into the solution until pH of 1. The mixture was stirred at room temperature for 3 days and then was purified by dialysis against deionized water.

(E) P*t*BA latex/H_2SO_4/65 °C: 10 mL of 11%wt P*t*BA latex dispersed in water was diluted into 50 mL. Then 95%wt H_2SO_4 was added into the solution until pH of 1. The solution temperature was raised to 65 °C. After 3 h, the same amount of 95%wt H_2SO_4 was fed into the solution. The solution was cooled down after 24 h in total, and then was purified by dialysis against deionized water.

(F) P*t*BA latex/H_2SO_4/MeOH: 5 mL of 11%wt P*t*BA latex dispersed in water was diluted into 50 mL. Then 20 mL of methanol was added into the mixture. After that, 95%wt H_2SO_4 was added into the solution until pH of 1. The mixture was stirred at room temperature for 3 days and then was purified by dialysis against deionized water.

(G) freeze-dried P*t*BA/TFA/DCM: P*t*BA latex was freeze-dried using a VirTis BenchTop Pro freeze-dryer for 2 days. 0.1 g of freeze-dried P*t*BA microparticles was dispersed into DCM (25 ml) by a probe sonicator (QSonica Q125, 125 Watt 20 KHz, amplitude 50%) in pulse mode (pulse on 5 sec/off 5 sec) for 15 mins. Then, a tenfold excess of TFA (0.6 ml, with respect to one mole of *tert*-butyl ester group) was slowly added into the mixture. After stirring at room temperature for 3 days, the reaction mixture was poured into cold hexane (250 ml) and the precipitate was collected and dried in a vacuum oven at 60 °C overnight until a constant weight was achieved.

(H) freeze-dried P*t*BA/HCl/1,4-dioxane: P*t*BA latex was freeze-dried using a VirTis BenchTop Pro freeze-dryer for 2 days. 0.1 g of freeze-dried P*t*BA microparticles was dispersed into 1,4-dioxane (0.1%w/v) by a probe sonicator (QSonica Q125, 125 Watt 20 KHz, amplitude 50%) in pulse mode (pulse on 5 sec/off 5 sec) for 15 mins. Then, 12 g of 35%wt HCl was added into the mixture slowly with stirring. The mixture was heated up to 110 °C with reflux for 15 h. The final mixture was precipitated into cold n-hexane and then was dried by rotary evaporator at 60 °C until a constant weight was achieved.

2.2.5 ATR-FTIR

Attenuated Total Reflection Fourier Transform Infrared (ATR FT-IR) spectra were obtained with a Perkin Elmer spectrum 100 FTIR spectrometer in the wavenumber range 600–3400 cm^{-1} with a resolution of 8 cm^{-1}.

2.2.6 ^{1}H-, ^{13}C- and HSQC-NMR

Proton (^{1}H-), carbon (^{13}C-) and 2D heteronuclear single quantum correlation (2D-HSQC) NMR spectra of the particles in THF-d_8 were measured using a Bruker Advance III HD spectrometer operating at 500 MHz. P*t*BA microparticles were freeze-dried for two days and PAA microgels were dried in a vacuum oven at 60 °C overnight before preparing the solutions. The NMR samples were prepared by dispersing 10 mg of dry particles in 0.8 mL of THF-d_8. The experiments were recorded at 25 °C and the number of scan for ^{1}H-, ^{13}C-, and HSQC-NMR was 64, 1024, and 4, respectively.

2.2.7 TEM

TEM images were obtained using a JEOL JEM 1400. The electron beam accelerating voltage was set at 120 kV. A drop of dilute solution of the particles in DI water was dropped onto a carbon coated copper grid and then the grid was dried at 40 °C overnight before being placed into the TEM specimen holder.

2.3 Results and Discussion

2.3.1 End-group modification of PTHF

Apart from poly(propylene glycol) (PPG), we were also interested in using poly(tetra-hydrofuran) (PTHF), which is more hydrophobic than PPG, as a cross-linker. Two different pathways were followed in an attempt to prepare PTHF with vinyl acrylate end groups.

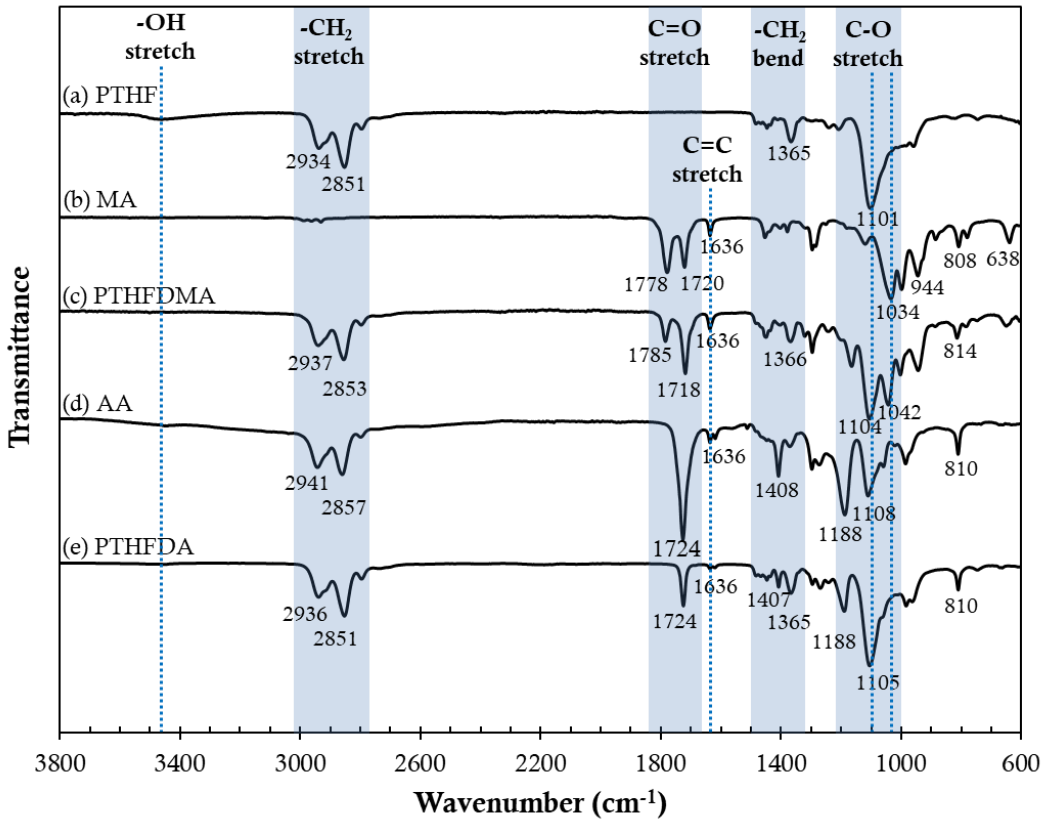

Figure 2.6 FT-IR spectra of (a) PTHF, (b) methacrylic anhydride (MA), (c) PTHF having dimethacrylate end groups (PTHFDMA), (d) acrylic acid (AA), and (e) PTHF having diacrylate end groups (PTHFDA).

The FTIR spectrum of PTHF clearly show CH_2 stretching at 2934 and 2851 cm^{-1}, CH_2 bending at 1500-1300 cm^{-1}, and C-O-C stretching of ether at 1101 cm^{-1}.[44-46] The bands of methacrylic anhydride (MA) appear at 1778 and 1720 cm^{-1} owing to C=O stretching of anhydride, at 1636 cm^{-1} owing to C=C stretching, at 1034 cm^{-1} owing to C-O-C stretching, at 944 cm^{-1} owing to $=CH_2$ wagging, and at 808 and 638 owing to $=CH_2$ twisting of

methacrylate groups.[47] Comparing with PTHF and MA, FT-IR bands of PTHF-dimethacrylate (PTHFDMA) are according to the combination of PTHF and MA with a small shift as expected as shown in **Figure 2.6**(c).

The FT-IR bands of AA appear at 1724 cm^{-1} according to C=O stretching, at 1636 cm^{-1} according to C=C stretching, and at 1188 and 1108 cm^{-1} according to C-O stretching. After esterification of PTHF with AA, the FT-IR bands of PTHF-diacrylate (PTHFDA) are similar to the combination of PTHF and AA spectra as shown in **Figure 2.6**(e). However, it is evident that a characteristic peak at 3470 cm^{-1} corresponding to hydroxyl end groups (-OH) of PTHF disappears in PTHFDMA and PTHFDA spectra as a result of the transformation of hydroxyl to acrylate groups.[43]

The characteristic peaks of PTHF and MA are clearly observed in **Figure 2.7**(a, b), respectively. Comparing to the PTHF and MA spectra, we found the new peaks of protons (d', e', f') according to the presence of acrylate groups in PTHFDMA spectrum - see **Figure 2.7**(c). We also found another peak at 4.15 ppm (a') in the PTHFDMA spectrum which is shifted from 3.62 ppm (a) and is attributed to the methylene protons ($-CH_2$) which were originally attached to the hydroxyl end groups (-OH) of PTHF and then converted to acrylate end groups. However, from the remaining peak at 3.62 ppm in the PTHFDMA spectrum it is evident that the esterification is incomplete.

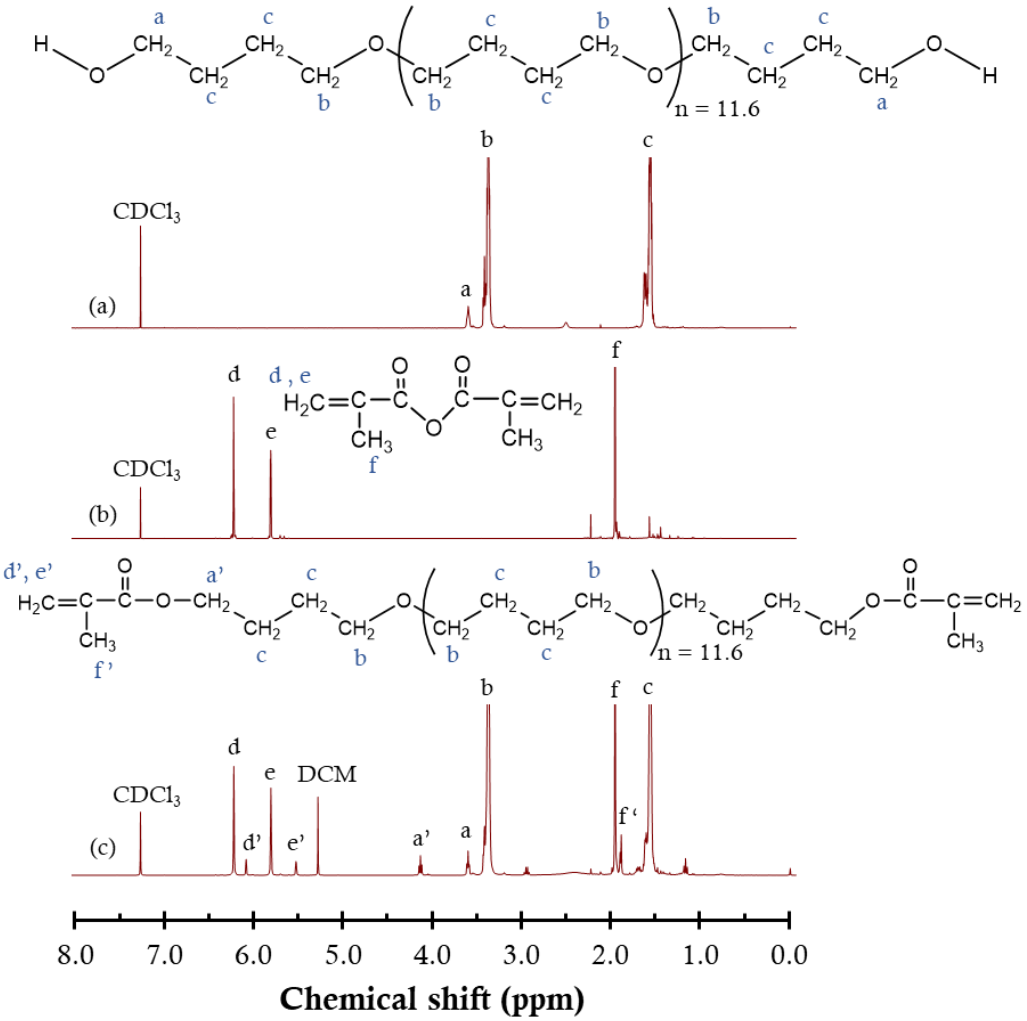

Figure 2.7 ^{1}H-NMR spectra of (a) PTHF, (b) methacrylic anhydride (MA) and (c) PTHF-dimethacrylate (PTHFDMA).

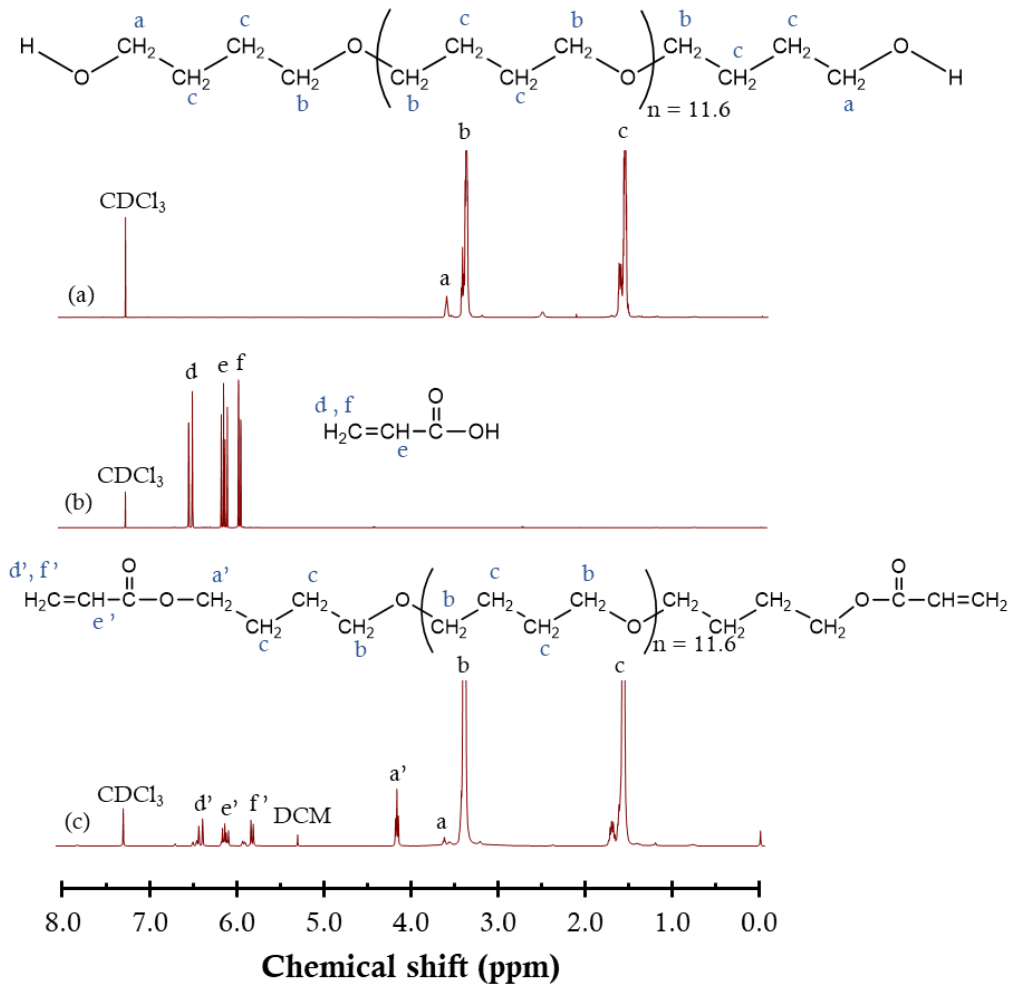

Figure 2.8 ^{1}H-NMR spectra of (a) PTHF, (b) acrylic acid (AA), and (c) PTHF-diacrylate (PTHFDA).

The characteristic peaks of PTHF and AA are shown in **Figure 2.8**(a, b), respectively. Three new peaks (d', e', f') are clearly visible, at 6.35, 6.10 and 5.80 ppm, as a result of the acrylate groups attached to PTHF. In addition, we found another new peak (a') at 4.15 ppm and a remaining peak at 3.62 ppm which can be explained as above.

By using integration to find the area under a proton signal, we can estimate the percentage of esterification of PTHF to PTHFDMA or PTHFDA using Equation (2.1), where methylene protons (-C**H**$_2$) in the main chains of PTHF at 1.60 ppm are set as a reference with integral area = 1.

$$\text{Esterification} = \frac{A_{4.15\ \text{ppm}}}{A_{4.15\ \text{ppm}} + A_{3.62\ \text{ppm}}} \times 100 \qquad (2.1)$$

where $A_{4.15\ \text{ppm}}$ and $A_{3.62\ \text{ppm}}$ are the areas under the proton signals at 4.51 ppm (a') and 3.26 ppm (a), respectively. This equation is based on the number of methylene protons (-C**H**$_2$)

attached to acrylate end groups at 4.51 ppm (a') compared to the unmodified methylene protons at 3.62 ppm (a). We can conclude that the approach using acrylic acid (AA) is more successful than the one using methacrylate anhydride (MA) for modifying the hydroxyl end groups of PTHF to vinyl acrylate end groups. %Esterification of PTHF to PTHFDMA and PTHFDA is 43% and 86%, respectively.

Therefore, PTHFDA with 86%esterification was used as the cross-linker to prepare P*t*BA/PTHF microparticles in further experiments.

Table 2.2 Calculation of %esterification of PTHF.

Sample	Chemical shift (ppm)	Assignment	Integral	%esterification
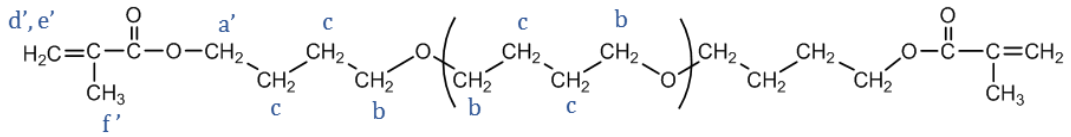				
PTHFDMA	3.26 ppm (a)	H in –C**H**$_2$-OH (remaining)	0.04	**43%**
	4.15 ppm (a')	H in –C**H**$_2$-acrylate (modified)	0.03	
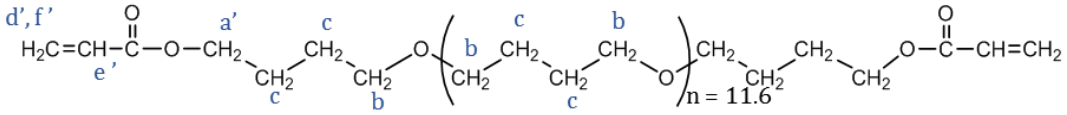				
PTHFDA	3.26 ppm (a)	H in –C**H**$_2$-OH (remaining)	0.01	**86%**
	4.15 ppm (a')	H in –C**H**$_2$-acrylate (modified)	0.06	

2.3.2 SFEP of P*t*BA microparticles

Taking advantage of the benefits of SFEP, we proceeded to make poly(*tert*-butyl acrylate) (P*t*BA) microparticles cross-linked with poly(propylene) (PPG) or poly(tetrahydrofuran) (PTHF) in aqueous media.

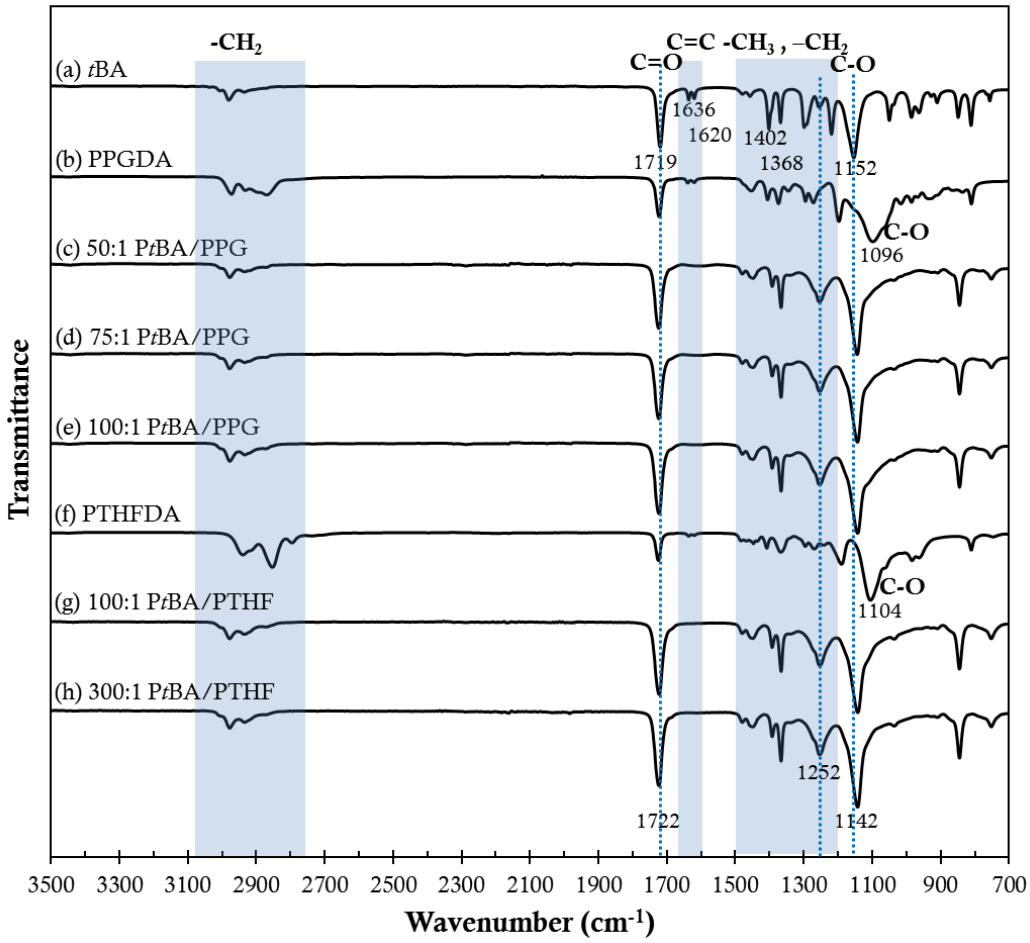

Figure 2.9 FT-IR spectra of (a) *t*BA monomer, (b) poly(propylene glycol) diacrylate (PPGDA) cross-linker, P*t*BA microparticles cross-linked with PPGDA at the molar ratio of monomer to cross-linker (c) 50:1, (d) 75:1, (e) 100:1, and (f) poly(tetrahydrofuran) diacrylate (PTHFDA) cross-linker, P*t*BA microparticles cross-linked with PTHFDA at the molar ratio of monomer to cross-linker (g) 100:1 and (h) 300:1.

For the chemical characterization of *t*BA monomer, PPGDA and PTHFDA cross-linkers, P*t*BA/PPG and P*t*BA/PTHF microparticles with the different molar ratios of monomer to cross-linker, ATR-FTIR spectra were taken -see **Figure 2.9**. The characteristic peaks of *t*BA monomer appear at 3100–2750, 1719, 1500-1200, and 1152 cm^{-1} according to -CH_2 stretching, C=O stretching, -CH_2 and –CH_3 bending, and C-O-C stretching,

respectively.[48,49] Considering the chemical structures of PPGDA and PTHFDA cross-linkers, their characteristic peaks *i.e.* -CH_2, -CH_3, -C=O, and -C=C groups are similar to *t*BA monomer except we found the broader and stronger peaks at 1096 and 1104 cm^{-1} according to ether groups (C-O-C stretching) in PPGDA and PTHFDA, respectively.

Compared to *t*BA monomer and two cross-linkers, the peaks at 1636 cm^{-1} and 1620 cm^{-1} attributed to C=C stretching are absent in the spectra of cross-linked P*t*BA/PPG and P*t*BA/PTHF microparticles due to the success of polymerization illustrated by **Figure 2.9**(c-e, g-h). Especially, we found strong and broad peaks at 1252 cm^{-1} (-CH_2, -CH_3 bending) and at 1142 cm^{-1} (C-O-C stretching shifted from 1152 cm^{-1} of *t*BA) which may be the consequence of the combined peaks of P*t*BA and cross-linkers.

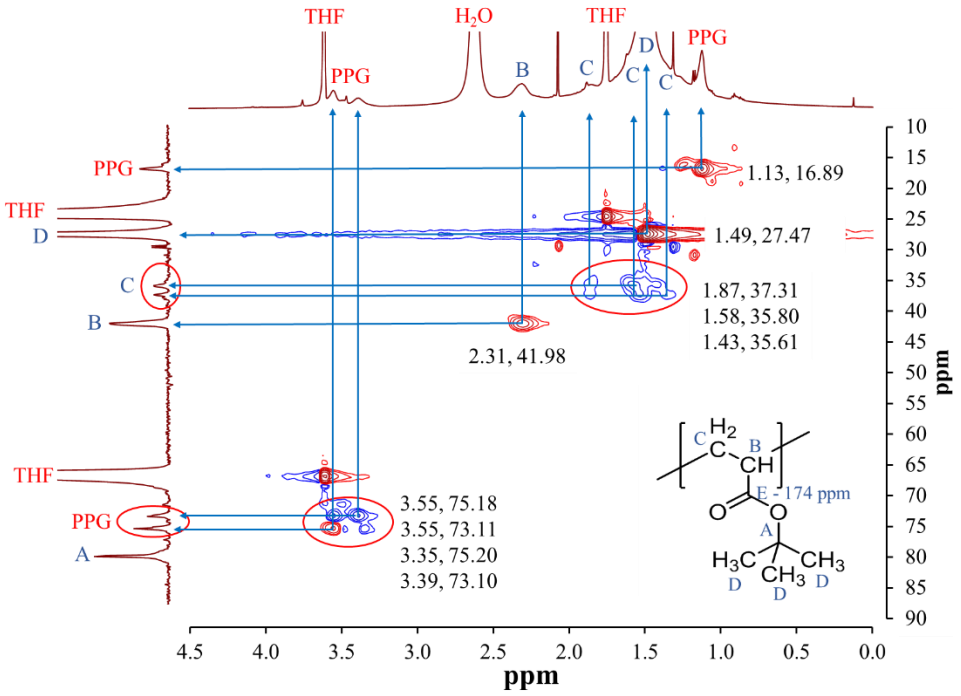

Figure 2.10 2D-HSQC spectrum of P*t*BA microparticles cross-linked with PPG (molar ratio of *t*BA monomer to cross-linker = 100:1).

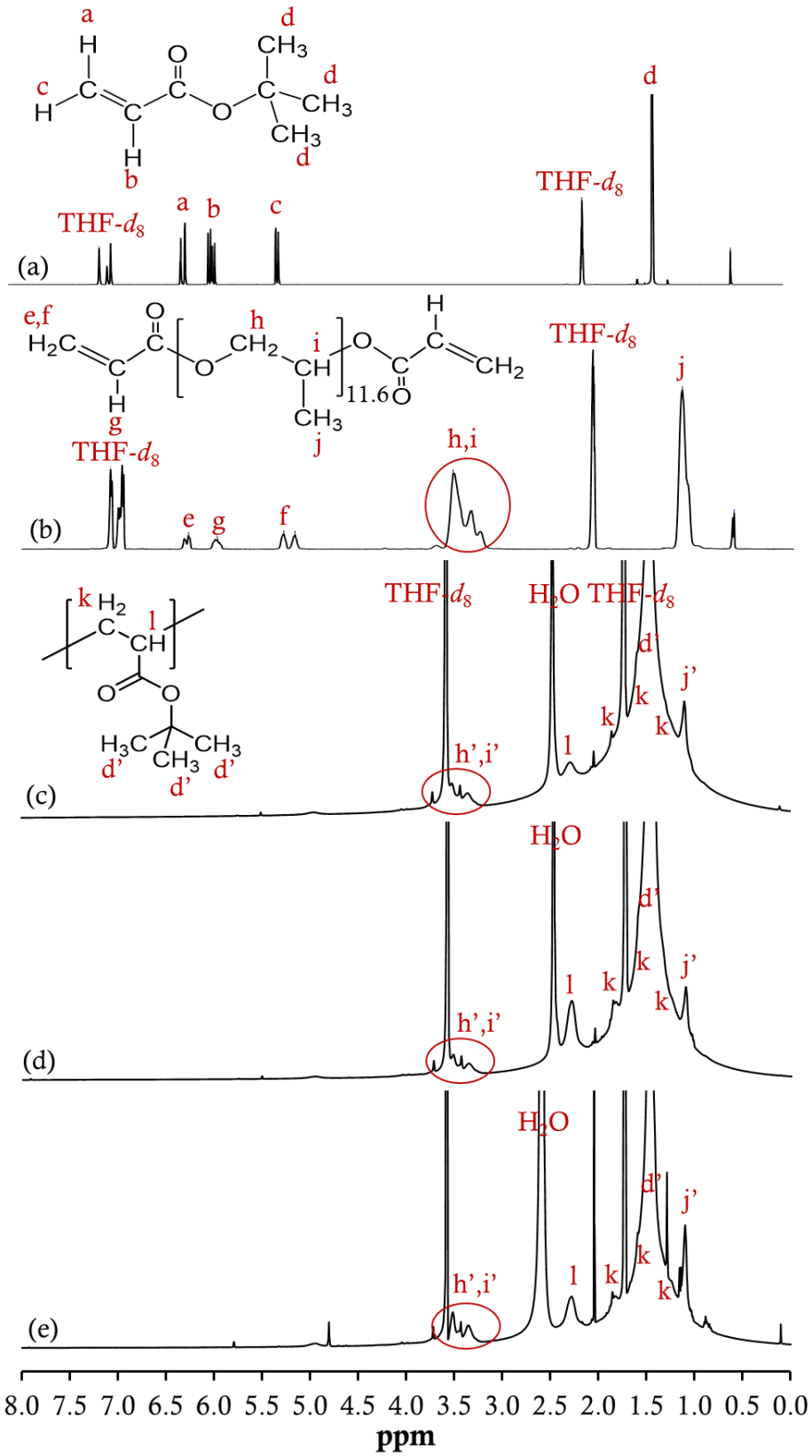

Figure 2.11 ^{1}H-NMR spectra of (a) *t*BA monomer in toluene-d_8, (b) PPGDA cross-linker in toluene-d_8, and P*t*BA microparticles cross-linked with PPGDA at the molar ratio of monomer to cross-linker (c) 50:1, (d) 75:1 and (e) 100:1 in THF-d_8.

In addition to ^{1}H- and ^{13}C-NMR, 2D-HSQC NMR is a very informative technique to obtain the chemical shift correlation between ^{13}C nuclei and their adjacent ^{1}H. Hence, the complicated molecular structures of cross-linked P*t*BA can be precisely assigned using these three experiments of NMR spectroscopy together.

From **Figure 2.10**, the 2D-HSQC spectrum provides the correlation between the carbons and their associated protons of cross-linked P*t*BA/PPG microparticles. Although the peaks of methyl protons (-C**H**$_{3}$) in *tert*-butyl group and the methine proton (-C**H**) in the P*t*BA main chain can be simply assigned in the ^{1}H-NMR spectrum at 1.49 ppm and 2.32 ppm, respectively, the location of the methylene protons (-C**H**$_{2}$) is still unclear. With 2D-HSQC NMR, we are able to determine that the methylene protons interfered with the signal of the methyl protons in the P*t*BA main chain at 1.43, 1.58, 1.87 ppm. In addition, a strong water peak was found at 2.47 ppm for 50:1 and 75:1 and at 2.59 ppm for 100:1 P*t*BA/PPG microparticles.

For *t*BA monomer, we found the methylene protons (-C**H**$_{2}$) and the methine proton (-C**H**) attached to the double bond at 6.20, 5.93 and 5.26 ppm while the methyl protons (-C**H**$_{3}$) in *tert*-butyl ester appear at 1.36 ppm. For PPGDA cross-linker, the vinyl protons appear at 6.28, 5.98 and 5.17 ppm, the strong broad peaks of the methylene protons (-C**H**$_{2}$) and the methine protons (-C**H**) in the backbone appear at 3.53, 3.33 and 3.25 ppm and the methyl protons (-C**H**$_{3}$) in the side chain at 1.15 ppm. After SFEP and purification to remove unreacted reactants, the vinyl protons (C**H**$_{2}$=C**H**-) from *t*BA monomer and PPGDA cross-linker disappear from the spectra of P*t*BA/PPG microparticles for all conditions as shown in **Figure 2.11**(c-e). Since we still found the characteristic peaks of the PPG main chain in the P*t*BA microparticles spectrum, this indicates the network structure of P*t*BA was cross-linked with PPG.

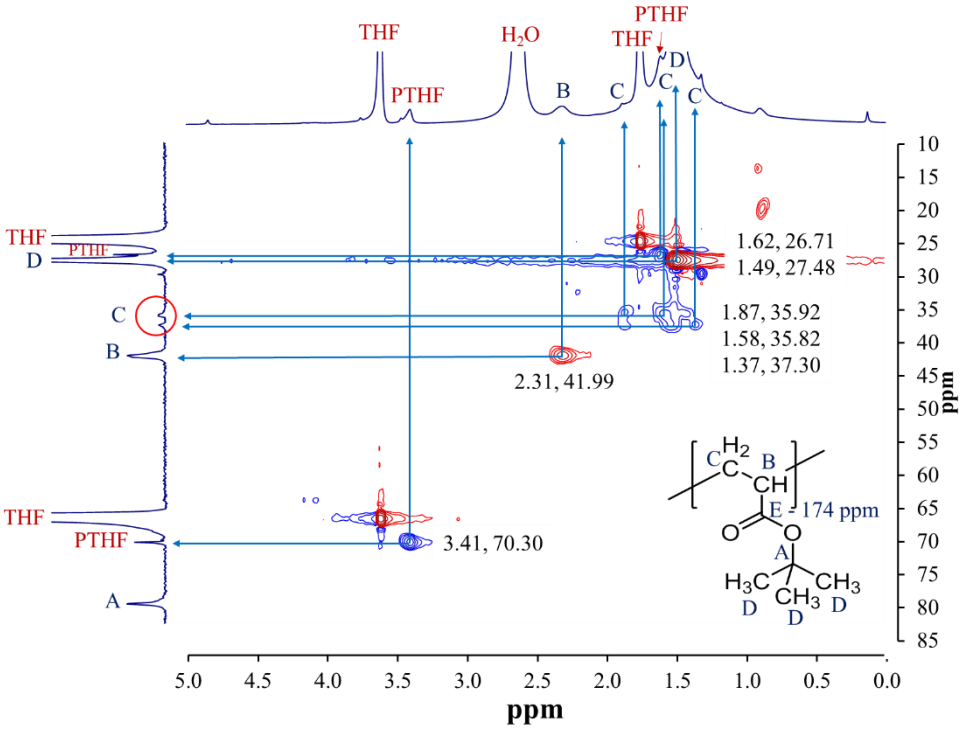

Figure 2.12 2D-HSQC spectrum of P*t*BA microparticles cross-linked with PTHF (molar ratio of *t*BA monomer to cross-linker = 100:1).

From **Figure 2.12**, the 2D-HSQC spectrum shows the correlation between the carbons and their associated protons of cross-linked P*t*BA/PTHF microparticles. Similar to P*t*BA/PPG, with 2D-HSQC NMR we now can precisely locate the methylene protons (-C**H**$_2$) at 1.87, 1.58, 1.37 ppm in the P*t*BA main chain and the strong peak of water at 2.59 ppm for 100:1 and at 2.48 ppm for 300:1 P*t*BA/PTHF microparticles. For PTHFDA cross-linker, the vinyl protons appear at 6.35, 6.10 and 5.80 ppm. In addition, we found the two strong peaks of the methylene protons in PTHF main chain at 3.40 and 1.61 ppm. After SFEP and purification, the vinyl protons (C**H**$_2$=C**H**-) from *t*BA monomer and PTHFDA cross-linker disappear due to the complete polymerization and we found the peaks of PTHF in the spectrum of P*t*BA microparticles at 3.36 ppm as shown in **Figure 2.13**(c-d). This indicates the network structure of P*t*BA was cross-linked with PTHF.

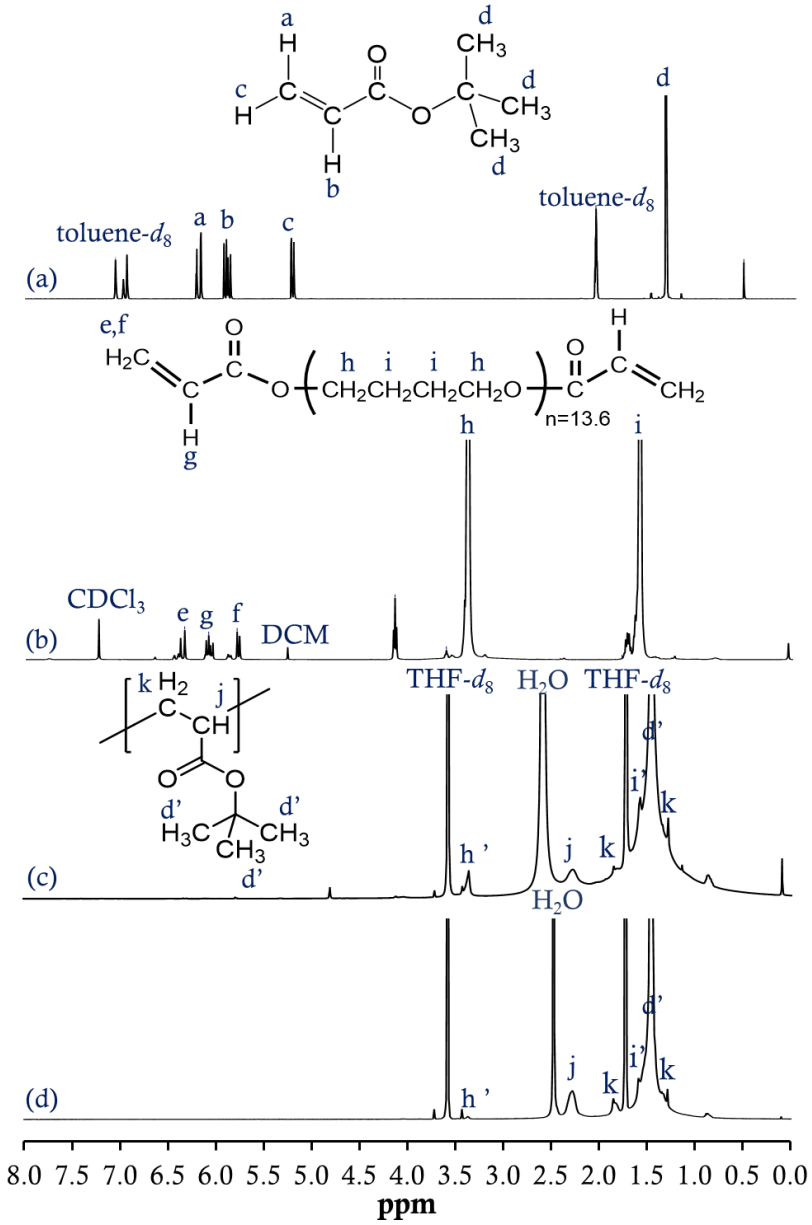

Figure 2.13 ^{1}H-NMR spectra of (a) *t*BA monomer in toluene-d_8 (b) PTHFDA cross-linker in toluene-d_8 and P*t*BA microparticles cross-linked with PTHFDA at the molar ratio of monomer to cross-linker (c) 100:1 and (d) 300:1 in THF-d_8.

Interestingly, after freeze drying for two days we still found the strong peaks of water in the spectra of P*t*BA/PPG and P*t*BA/PTHF microparticles. It is possible that water is trapped inside the network structures and even the freeze dryer cannot completely remove it.

Theoretically, the area under each signal is proportional to the number of protons giving the signal so it is feasible to probe the degree of cross-linking by using ^{1}H-NMR integration[50,51] following by Equation (2.2).[52]

$$\text{Degree of cross} - \text{linking} = \frac{\text{number of cross}-\text{links}}{\text{number of polymer repeating units}} \qquad (2.2)$$

To gauge the number of cross-links in P*t*BA/PPG microparticles, we make use of the methyl protons (-C**H**$_3$) in a PPGDA molecule (which give a peak in the NMR spectrum at 1.10 ppm). On average, each PPG molecule has 11.6×3 = 34.8 of these protons - see **Figure 2.11**. For the P*t*BA polymer main chain, we make use of the peak at 1.46 ppm which is attributed to both -C**H**$_2$ and -C-(C**H**$_3$)$_3$ protons in *t*BA. One *t*BA monomer contains a total of 11 of such protons. Therefore, the crosslink density for P*t*BA/PPG microparticles can be expressed as Equation (2.2a):

$$\text{Degree of cross} - \text{linking} = \frac{\text{Peak area at 1.10 ppm} \,/\, 34.8}{\text{Peak area at 1.46 ppm} \,/\, 11} \qquad (2.2a)$$

In case of P*t*BA/PTHF microparticles, we consider the methylene protons (-C**H$_2$**) closest to the ether oxygens in a PTHFDA molecule giving the peak at 3.41 ppm. On average, each PTHFDA molecule contains 4×13.6 =54.4 of these protons – see **Figure 2.13**. For the P*t*BA polymer main chain, we make use of the peak at 1.49 ppm which is attributed to both -C**H**$_2$ and -C-(C**H**$_3$)$_3$ protons in *t*BA so one *t*BA monomer has a total of 11 of such protons. Therefore, the crosslink density for P*t*BA/PTHF microparticles can be expressed as Equation (2.2b):

$$\text{Degree of cross} - \text{linking} = \frac{\text{Peak area at 3.41 ppm} \,/\, 54.4}{\text{Peak area at 1.49 ppm} \,/\, 11} \qquad (2.2b)$$

Table 2.3 illustrates degree of cross-linking calculated by the reagent feeding and ^{1}H-NMR integration. The observed degree of cross-linking of P*t*BA microparticles is typically different from predicted on the basis of the reagent ratios used in the polymerization step. It is likely that the integration under the peaks of microparticles cannot be accurate due to the more rigid protons in cross-linked networks leading to the less sensitivity and more broadening of the signals than small molecules or linear soluble polymers in solvents.[53,54] Nevertheless, there is an encouraging trend of the observed degree of cross-linking increasing with the increase of the amount of cross-linker added to the reaction.

Table 2.3 Degree of cross-linking for P*t*BA microparticles.

Mole ratio (loading)	**Degree of cross-linking**			
PPGDA : *t*BA	**Predicted**	**^{1}H-NMR**		
		$A_{1.10\ ppm}$	**$A_{1.46\ ppm}$**	**Observed**
1 : 50	0.020	1	10.85	0.03
1 : 75	0.013	1	16.03	0.02
1 : 100	0.010	1	18.25	0.02
PTHFDA : *t*BA	**Predicted**	**$A_{3.41\ ppm}$**	**$A_{1.49\ ppm}$**	**Observed**
1 : 100	0.010	1	28.72	0.01
1 : 300	0.003	1	396.29	0.001

2.3.3 Hydrolysis of P*t*BA to PAA microparticles

The mechanism for hydrolysis of P*t*BA to PAA is shown in **Figure 2.14**. The *tert*-butyl ester group of P*t*BA is transformed into a carboxyl group to obtain PAA by using an acid catalyst such as hydrochloric acid (HCl) in 1,4-dioxane, trifluoroacetic acid (TFA) in dichloromethane (DCM), or sulphuric acid (H_2SO_4) in water/methanol co-solvents.

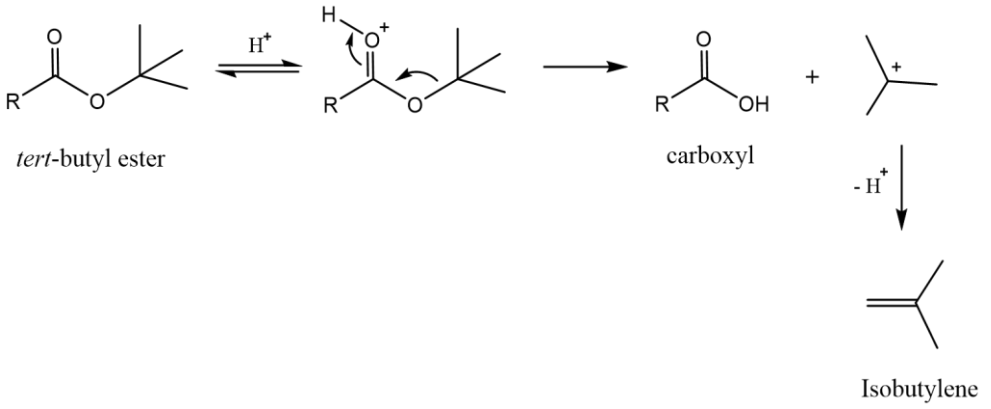

Figure 2.14 Mechanism of acid-catalysed hydrolysis of *tert*-butyl ester.[55]

FTIR spectra of P*t*BA latex hydrolyzed in aqueous solutions in **Figure 2.15**(a-f) still show strong peaks at 1722 cm^{-1} due to C=O stretching, 1368 cm^{-1} due to -CH_3 bending, 1252 cm^{-1} due to -CH_2 bending, 1142 cm^{-1} due to C-O stretching, and 845 cm^{-1} due to CH_3 bending. Nevertheless, for acid-hydrolysis of freeze-dried P*t*BA microparticles, the characteristic peaks of *tert*-butyl group at 1368 and 845 cm^{-1} due to CH_3 bending disappear completely in **Figure 2.15**(g, h). The absence of these characteristic peaks demonstrates that the *tert*-butyl groups of P*t*BA were successfully transformed into carboxyl groups, and hence PAA microparticles were obtained. In addition, we found that the C=O stretching is slightly shifted from 1722 cm^{-1} (of the *tert*-butyl ester group) to 1698 cm^{-1} appropriate for carboxyl groups (-COOH), which is consistent with the carboxyl group in linear PAA. From the FT-IR spectra, the acid-hydrolysis reaction is promising when we hydrolyzed freeze-dried P*t*BA microparticles in organic solvents (DCM and 1,4-dioxane) with acids. However, it was difficult to disperse the microparticles in the organic solvents as a result of the network structure of P*t*BA microparticles so here we decided to use DCM as the solvent for further experiments because the particles can be dispersed in DCM better than in 1,4-dioxane.

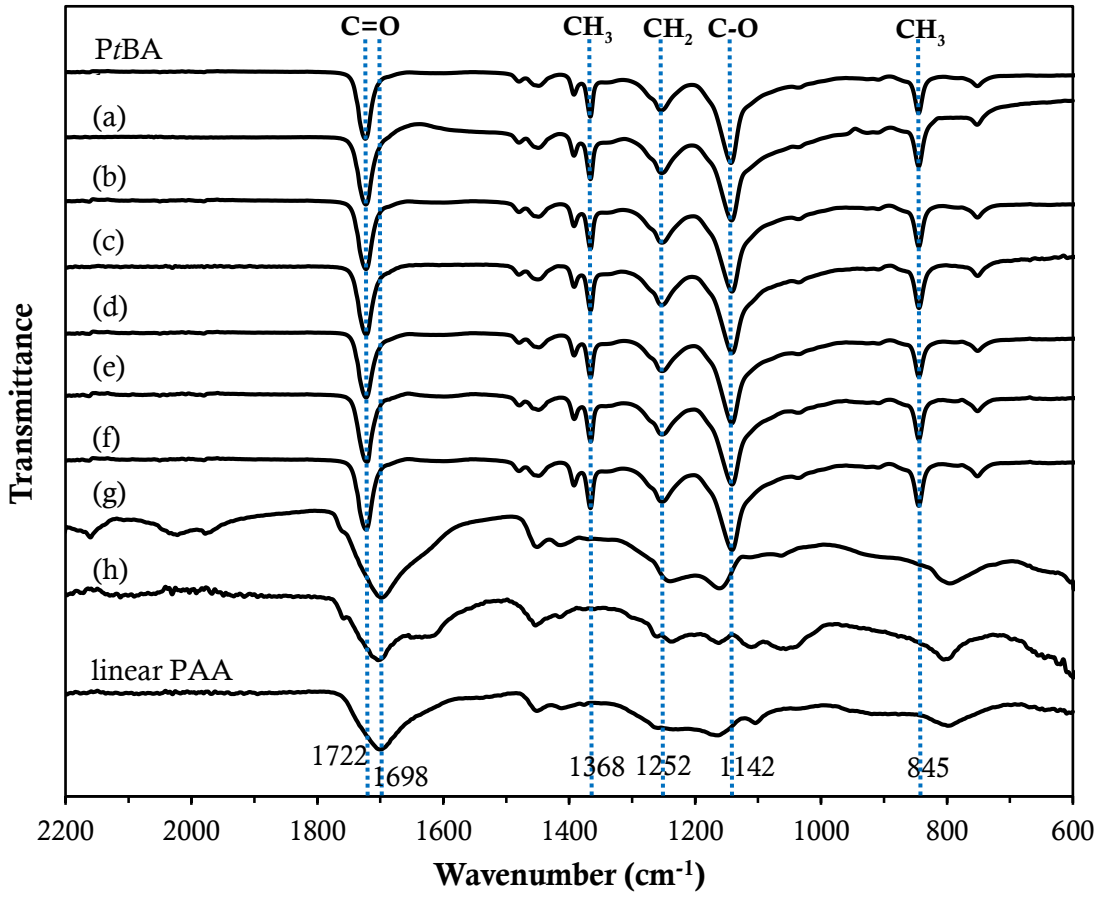

Figure 2.15 FT-IR spectra of dried P*t*BA microparticles, the hydrolysis of P*t*BA latex dispersed in DI water using (a) CH_3COOH, (b) TFA, (c) HCl at 110 °C, (d) H_2SO_4, (e) H_2SO_4 at 65 °C, (f) H_2SO_4 in H_2O/MeOH, and the hydrolysis of freeze-dried P*t*BA microparticles using (g) TFA in DCM, (h) HCl in 1,4-dioxane at 110 °C, and linear PAA M_n 5000.

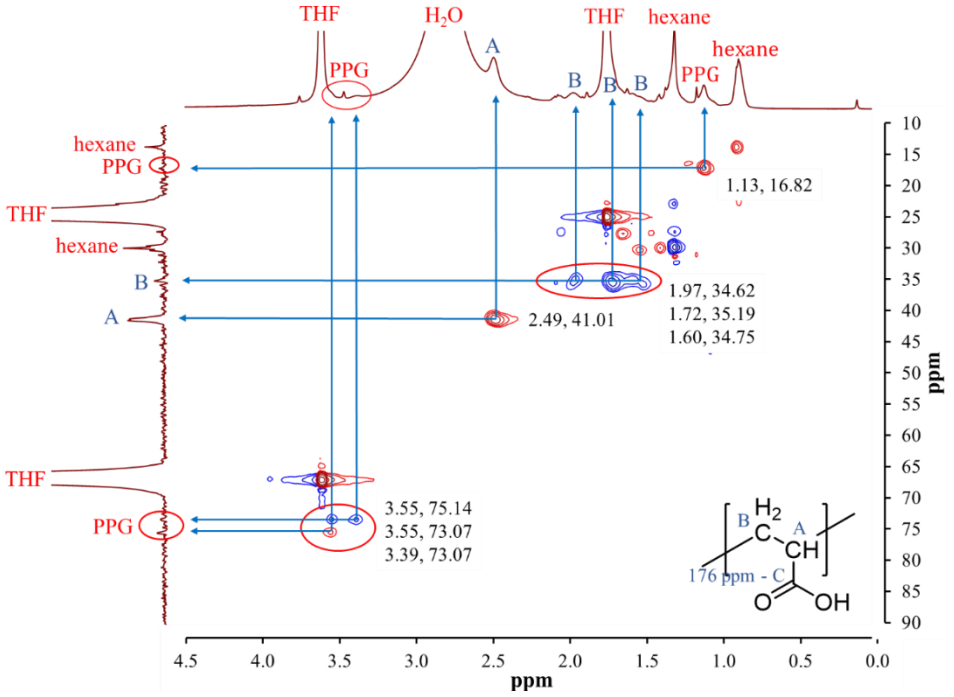

Figure 2.16 2D-HSQC spectra of PAA microparticles cross-linked with PPG (molar ratio of *t*BA monomer to cross-linker = 100:1).

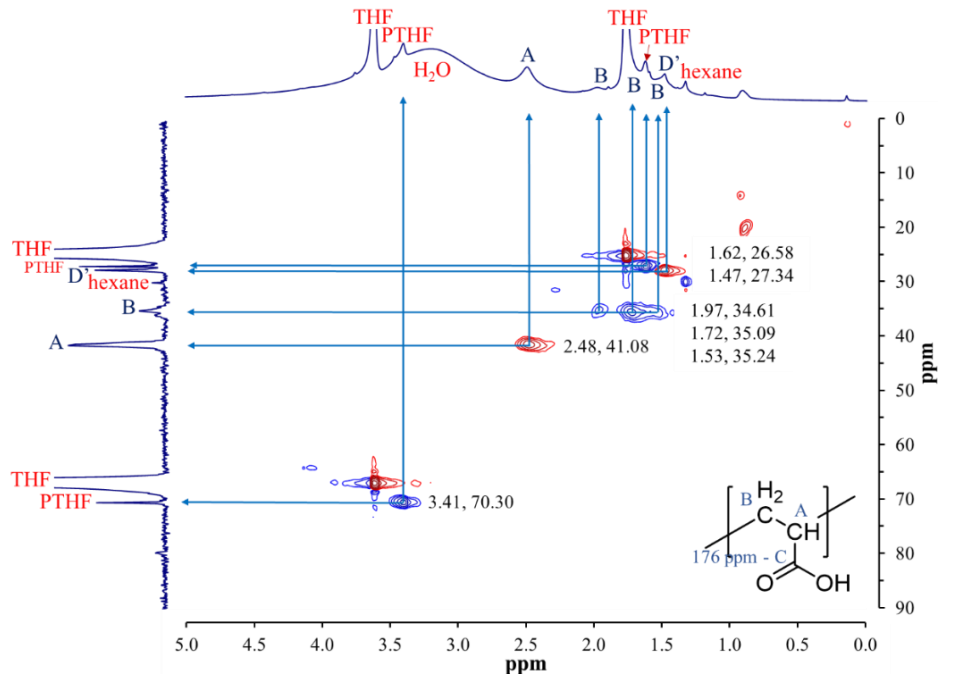

Figure 2.17 2D-HSQC spectra of PAA microparticles cross-linked with PTHF (molar ratio of *t*BA monomer to cross-linker = 100:1).

From the 2D-HSQC spectrum of 100:1 PAA/PPG microparticles, the methyl protons (-C**H**$_3$) of *tert*-butyl groups at 1.49 ppm are absent as shown in **Figure 2.16** so that 100:1 P*t*BA/PPG microparticles were successfully converted to PAA/PPG microparticles. However, there is a very tiny signal of *tert*-butyl groups at 1.47 ppm in the spectrum of 100:1 PAA/PTHF as shown in **Figure 2.17** since the hydrolysis was mostly complete.

Inspecting the structure shown in **Figure 2.18**, we can now relate the average degree of polymerisation between cross-links to the cross-link density (XLD). From Equation (2.2), XLD = number of cross-links/number of polymer repeating units = 1/2z or z = 1/(2×XLD), where each cross-linker connects two bits of P*t*BA chain with z monomers on average. In other words, z = 25 if XLD = 0.02.

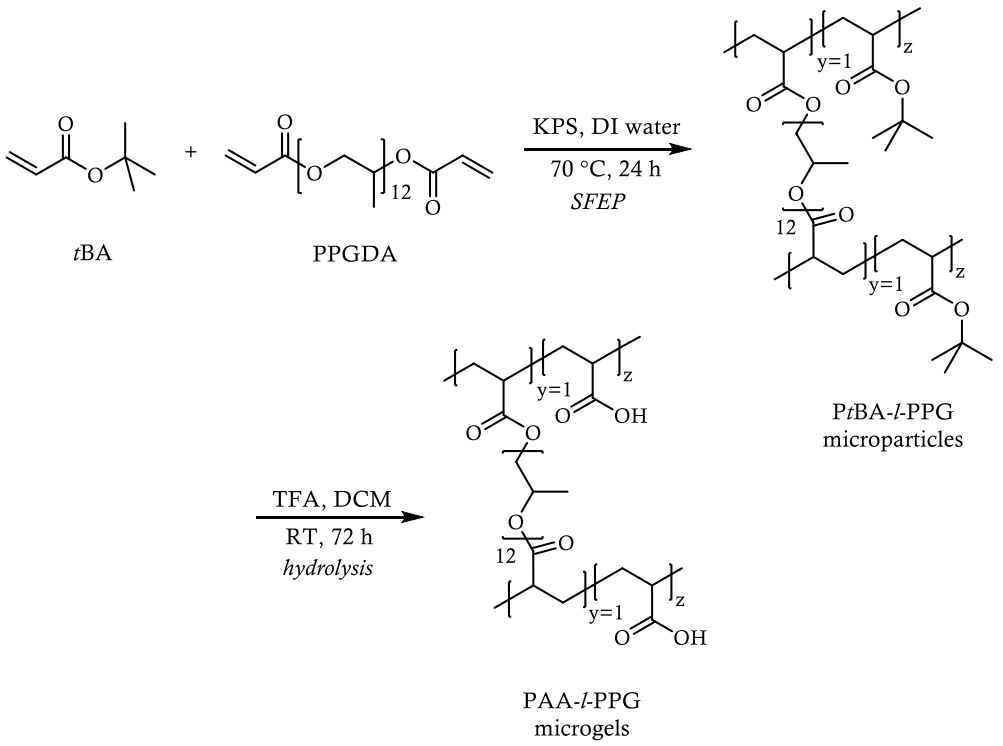

Figure 2.18 Schematic illustration of synthesis of PAA/PPG microgels.

2.3.3.1 Effect of degree of cross-linking

We proceed to discuss the chemical structure of the P*t*BA microparticles hydrolysed to PAA using TFA in DCM. FT-IR spectra of P*t*BA hydrolysed to PAA in **Figure 2.19**(b, c) show that the hydrolysis reaction was complete due to the absence of CH_3 bending at 1368 and 845 cm^{-1}, while the FT-IR spectra in **Figure 2.19**(d, f, g) show the characteristic peaks of PAA as discussed previously, but also tiny peaks at 1368 cm^{-1} of C=O of *tert*-butyl ester groups still appear as a result of the mostly complete acid-hydrolysis.

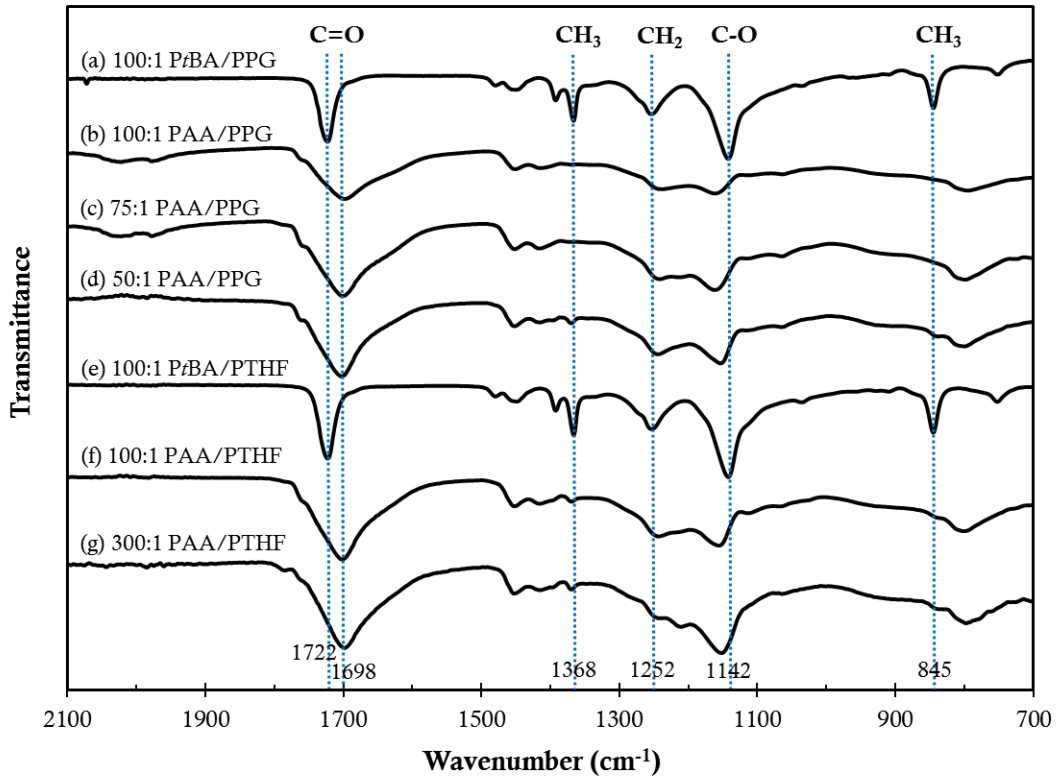

Figure 2.19 FT-IR spectra of (a) P*t*BA/PPG microparticles (molar ratio of *t*BA monomer to PPGDA cross-linker = 100:1), PAA/PPG microparticles with molar ratio of monomer to PPGDA cross-linker (b) 100:1, (c) 75:1, and (d) 50:1, (e) P*t*BA/PTHF microparticles (molar ratio of *t*BA monomer to PTHFDA cross-linker = 100:1), and PAA/PTHF microparticles with molar ratio of (f) 100:1, (g) 300:1 prepared from acid-hydrolysis with TFA in DCM.

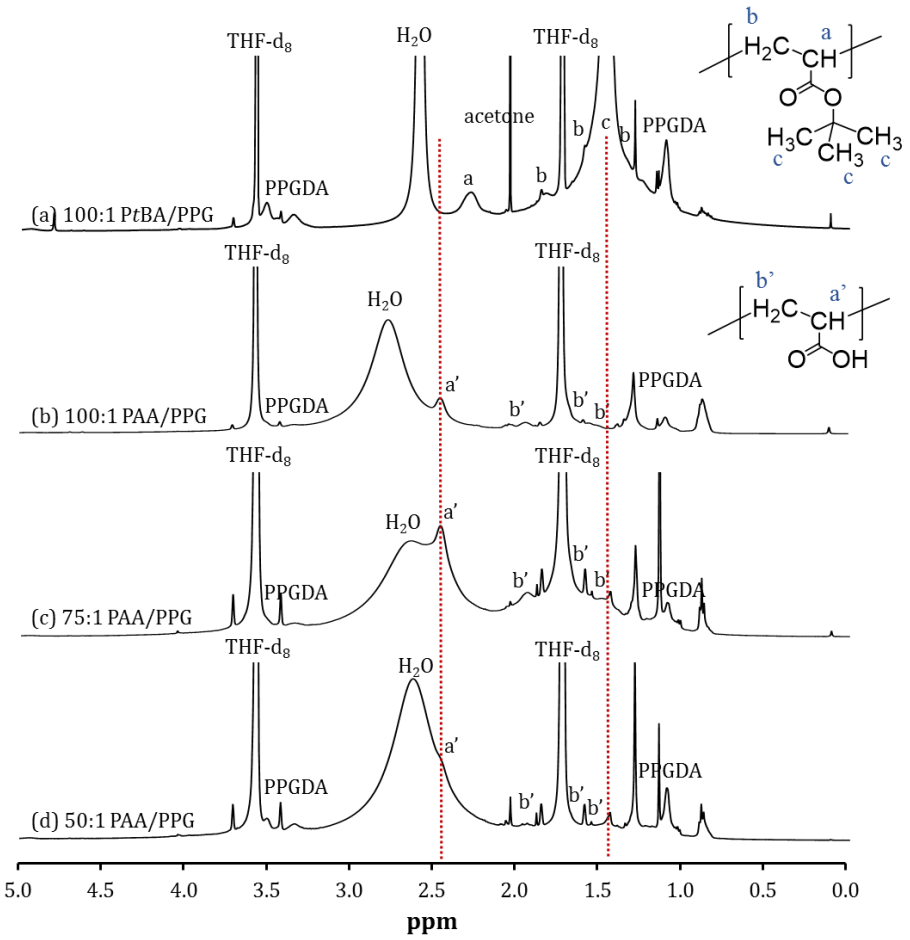

Figure 2.20 ^{1}H-NMR spectra of (a) P*t*BA/PPG microparticles (molar ratio of *t*BA monomer to PPGDA cross-linker = 100:1), and PAA/PPG microparticles with molar ratio of monomer to PPGDA cross-linker (d) 100:1, (e) 75:1, and (f) 50:1 prepared from acid-hydrolysis of P*t*BA/PPG with TFA in DCM.

The methyl proton (-C**H**$_3$) signal of *tert*-butyl groups disappears in **Figure 2.20**(b) when 100:1 P*t*BA/PPG was hydrolysed to 100:1 PAA/PPG indicating the complete hydrolysis. However, we still found tiny peaks of methyl proton (-C**H**$_3$) in 75:1 and 50:1 PAA/PPG spectra as shown in **Figure 2.20**(c, d) and in 100:1 and 300:1 PAA/PTHF spectra as shown in **Figure 2.21**(b, c). Compared to the very strong peaks of methyl protons of P*t*BA/PPG or P*t*BA/PTHF, it is reasonable to say that the hydrolysis reaction of these P*t*BA microparticles to PAA was successful. In addition, we found that all samples show the downfield shift of methyl protons (-C**H**-) from 2.31 ppm in P*t*BA to 2.48 ppm in PAA microparticles.

It is seen that PTHF is in the structure of 100:1 PAA/PTHF microparticles as shown in **Figure 2.21**(b) but the peak of PTHF in 300:1 PAA/PTHF in **Figure 2.21**(c) interferes with the water peak so it is hard to detect. However, with the 2D-HSQC measurement we confidently confirm that PTHF is incorporated into 300:1 PAA/PTHF microparticles.

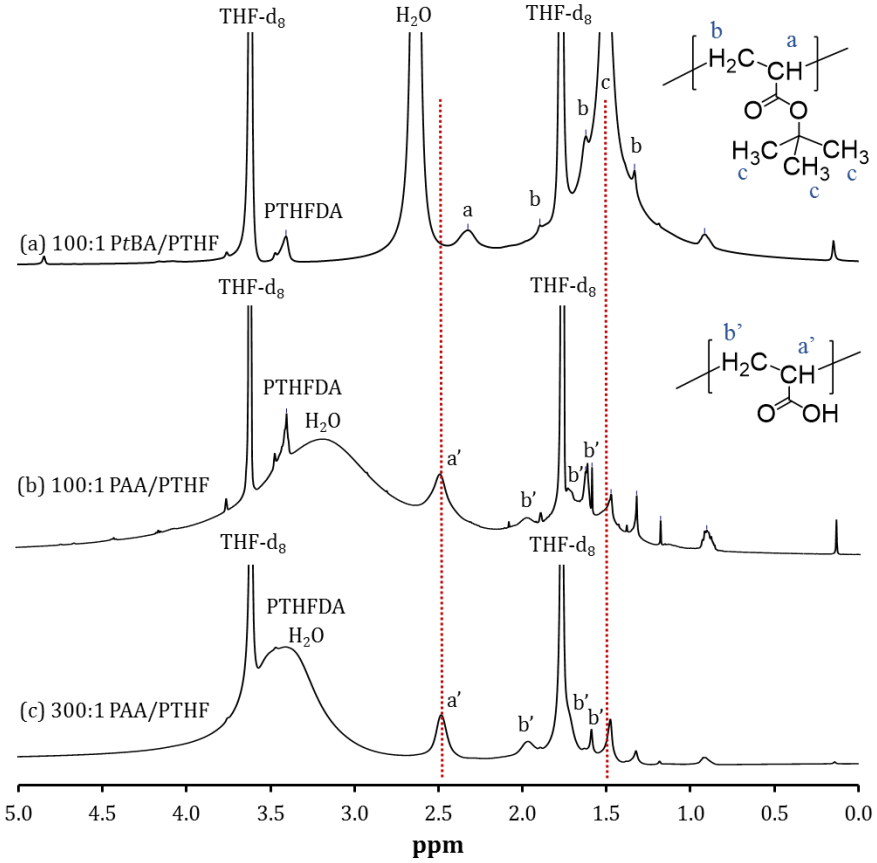

Figure 2.21 ^{1}H-NMR spectra of (a) P*t*BA/PTHF microparticles (molar ratio of *t*BA monomer to PTHFDA cross-linker = 100:1), and PAA/PTHF microparticles with molar ratio of monomer to PTHFDA cross-linker (d) 100:1 and (e) 300:1 prepared from acid-hydrolysis of P*t*BA/PTHF with TFA in DCM.

TEM images in **Figure 2.22** illustrate that well-defined PAA microparticles were prepared via SFEP followed by acid-hydrolysis of P*t*BA. The microparticles cross-linked with PTHF are larger than those particles cross-linked with PPG as a result of the longer chains of PTHF than PPG cross-linkers at the same molar ratio of monomer to cross-linker. After the hydrolysis, the particle size of resulting PAA microparticles is smaller than that of P*t*BA microparticles due to the deprotection of *tert*-butyl groups of P*t*BA to carboxyl groups to obtain PAA. The molar mass of the repeating unit of P*t*BA is 128.17 g/mol while that of PAA is 72.06 g/mol. Theoretically, by assuming that the bulk density remains the

same after hydrolysis, the molar mass of the repeating unit is decreased by 1.8 times so that the volume of the particles should be reduced by the same factor. This results in calculated diameters of PAA/PPG and PAA/PTHF microparticles of about 175 nm and 314 nm, both of which are a little smaller than the diameters obtained from TEM images (189 nm and 369 nm), respectively. It is likely that the higher size seen in the TEM images is a result of PAA microgels being swollen in water before drying on the carbon grid so that the PAA microgels may be somewhat deformed (flattened) as shown in **Figure 2.22**(d).

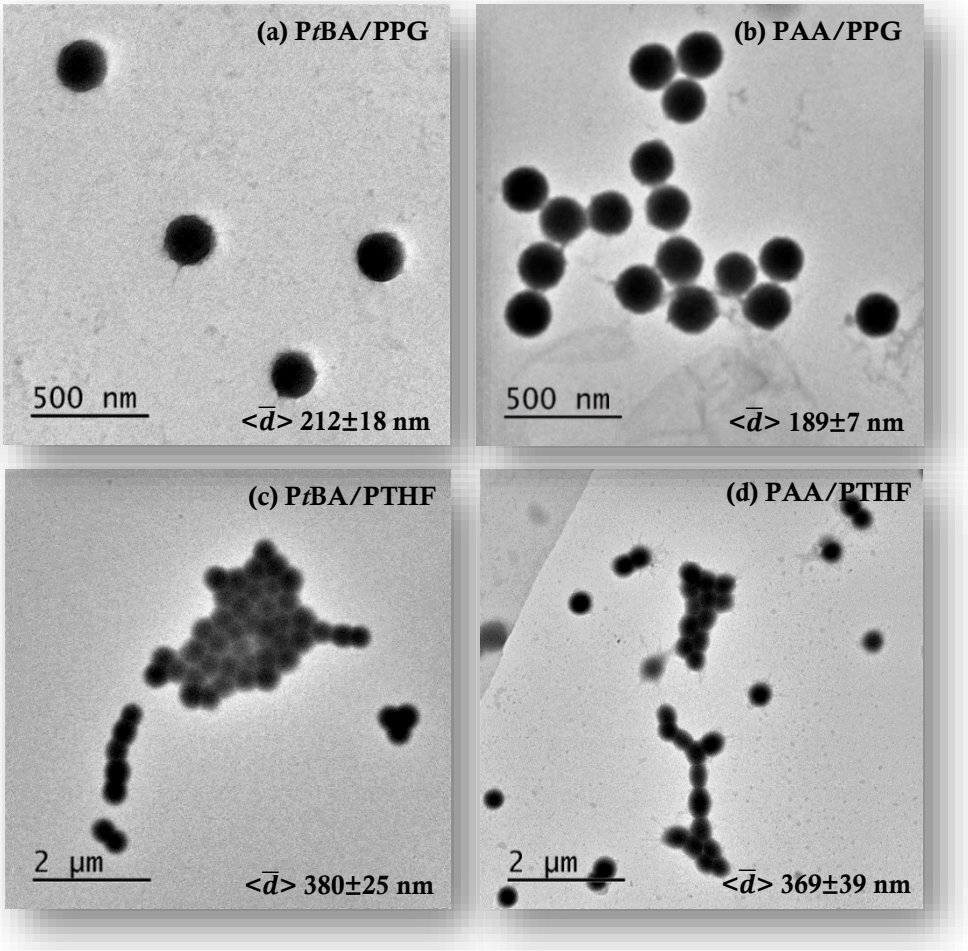

Figure 2.22 TEM images of (a) 100:1 P*t*BA/PPG, (b) 100:1 PAA/PPG, (c) 100:1 P*t*BA/PTHF and (d) 100:1 PAA/PTHF microparticles.

Conclusion

Two types of hydrophobic poly(ethers) were used as macro cross-linkers in the preparation of amphiphilic poly(acrylic acid) (PAA) microparticles. Poly(propylene glycol) having divinyl acrylate end groups (PPGDA) is commercially available, while poly(tetrahydrofuran) (PTHF) having such end groups were prepared by two different esterification reactions. From ^{1}H-NMR integration, the %esterification of hydroxyl end groups of PTHF reacted with methacrylate anhydride (MA) and acrylic acid (AA) to obtain PTHFDMA and PTHFDA are 43% and 86%, respectively.

Firstly, P*t*BA microparticles cross-linked with PPGDA and PTHFDA were prepared via surfactant free emulsion polymerization (SFEP) in aqueous media. Degree of cross-linking was varied by varying the molar ratio of *t*BA monomer to cross-linker. The chemical structure of P*t*BA microparticles was characterized with FT-IR and NMR. Especially, with 2D-HSQC NMR we can precisely assign the proton and carbon signals in cross-linked networks of P*t*BA so this enables us to probe the degree of cross-linking using ^{1}H-NMR integration comparing with the reactant ratios added in the polymerization step. Even though the observed degrees of cross-linking are rather different from predicted ones, we found the satisfying trend of the observed degree of cross-linking increasing with the increase of the amount of cross-linker added to the reaction. Then, the various acid-hydrolysis conditions to convert *tert*-butyl groups of P*t*BA to carboxyl groups to obtain PAA were performed. We found that the best condition was to disperse freeze-dried P*t*BA microparticles in DCM before hydrolyzed with TFA at room temperature for 3 days. The chemical structure of resulting PAA microparticles was confirmed from the absence of the *tert*-butyl groups in their FT-IR and NMR spectra. TEM images illustrated the spherical morphology of P*t*BA and PAA microparticles with a narrow size distribution. The size of P*t*BA/PPG and P*t*BA/PTHF microparticles were 212±18 nm and 380±25 nm in diameter, and after the acid-hydrolysis the particle sizes were reduced to 189±7 nm and 369±39 nm of PAA/PPG and PAA/PTHF microparticles respectively.

With these promising results, we can assert that well-defined PAA microparticles can be prepared via SFEP and acid-hydrolysis of P*t*BA. The swelling behaviors of the resulting amphiphilic PAA/PPG and PAA/PTHF microparticles with various degrees of cross-linking will be studied in the next chapter.

Bibliography

1. A. Katchalsky, H. Eisenberg. *Journal of Polymer Science* **1951**, *6*, 145-154.

2. J. Ji, L. Jia, L. Yan, P. R. Bangal. *Journal of Macromolecular Science Part A: Pure and Applied Chemistry* **2010**, *47*, 445-451.

3. A. Kubotera, R. Saito. *Polymer Journal* **2016**, *48*, 611-619.

4. Z. H. Lu, G. J. Liu, F. T. Liu. *Journal of Applied Polymer Science* **2003**, *90*, 2785-2793.

5. S. Abraham, C. S. Ha, I. Kim. *Journal of Polymer Science Part A: Polymer Chemistry* **2005**, *43*, 6367-6378.

6. H. R. Yang, Y. L. Su, H. J. Zhu, H. Zhu, B. Q. Xie, Y. Zhao, Y. M. Chen, D. J. Wang. *Polymer* **2007**, *48*, 4344-4351.

7. K. A. Davis, K. Matyjaszewski. *Macromolecules* **2000**, *33*, 4039-4047.

8. M. Fernandez-Garcia, J. L. de la Fuente, M. L. Cerrada, E. L. Madruga. *Polymer* **2002**, *43*, 3173-3179.

9. B. Y. Li, Y. Shi, W. C. Zhu, Z. F. Fu, W. T. Yang. *Polymer Journal* **2006**, *38*, 387-394.

10. P. Corpart, D. Charmot, T. Biadatti, S. Zard, D. Michelet, S. Z. Zard (Rhodia Chim) Patent WO 9858974-A1, **2000**.

11. M. Babic, D. Horak. *Macromolecular Reaction Engineering* **2007**, *1*, 86-94.

12. W. A. Laftah, S. Hashim, A. N. Ibrahim. *Polymer-Plastics Technology and Engineering* **2011**, *50*, 1475-1486.

13. E. M. Ahmed. *Journal of Advanced Research* **2013**, *6*, 105-121.

14. F. Askari, S. Nafiai, H. Omidian, S. A. Hashemi. *Journal of Applied Polymer Science* **1993**, *50*, 1851-1855.

15. O. E. Philippova, D. Hourdet, R. Audebert, A. R. Khokhlov. *Macromolecules* **1997**, *30*, 8278-8285.

16. H. Es-haghi, H. Bouhendi, G. Bagheri-Marandi, M. J. Zohurian-Mehr, K. Kabiry. *Polymer-Plastics Technology and Engineering* **2010**, *49*, 1257-1264.

17. Q. B. Yu, X. F. Wang, Y. H. Shen, Y. L. Tao, A. J. Xie. *Russian Journal of Physical Chemistry A* **2013**, *87*, 2100-2104.

18. J. A. Zhang, Z. Q. Lu, M. Y. Wu, Q. Y. Wu, J. J. Yang. *RSC Advances* **2015**, *5*, 58889-58894.

19. R. Tiwari, T. Heuser, E. Weyandt, B. C. Wang, A. Walther. *Soft Matter* **2015**, *11*, 8342-8353.

20. J. W. Goodwin, J. Hearn, C. C. Ho, R. H. Ottewill. *British Polymer Journal* **1973**, ***5***, 347-362.

21. B. R. Saunders, B. Vincent. *Advances in Colloid and Interface Science* **1999**, *80*, 1-25.

22. S. Dai, P. Ravi, K. C. Tam. *Soft Matter* **2008**, *4*, 435-449.

23. A. Kotera, K. Furusawa, Y. Takeda. *Kolloid-Zeitschrift and Zeitschrift Fur Polymere* **1970**, *239*, 677-681.

24. Y. G. Feng, S. H. Huang, F. Teng. *Polymer Journal* **2009**, *41*, 266-271.

25. J. A. Bonham, F. Waggett, M. A. Faers, J. S. van Duijneveldt. *Colloid and Polymer Science* **2017**, *295*, 479-486.

26. L. Bromberg, M. Temchenko, T. A. Hatton. *Langmuir* **2002**, *18*, 4944-4952.

27. L. Bromberg, M. Temchenko, T. A. Hatton. *Langmuir* **2003**, *19*, 8675-8684.

28. L. Bromberg, M. Temchenko, G. D. Moeser, T. A. Hatton. *Langmuir* **2004**, *20*, 5683-5692.

29. L. Bromberg, M. Temchenko, V. Alakhov, T. A. Hatton. *International Journal of Pharmaceutics* **2004**, *282*, 45-60.

30. S. Naficy, G. M. Spinks, G. G. Wallace. *Acs Applied Materials & Interfaces* **2014**, *6*, 4109-4114.

31. G. Bonacucina, M. Cespi, G. Mencarelli, G. Giorgioni, G. F. Palmieri. *Polymers* **2011**, *3*, 779-811.

32. S. Dutta, D. Cohn. *Journal of Materials Chemistry B* **2017**, *5*, 9514-9521.

33. F. Zhang, F. Meng, J. Lubach, J. Koleng, N. A. Watson. *European Journal of Pharmaceutics and Biopharmaceutics* **2016**, *105*, 97-105.

34. K. T. Oh, T. K. Bronich, V. A. Kabanov, A. V. Kabanov. *Biomacromolecules* **2007**, *8*, 490-497.

35. T. G. O'Lenick, N. X. Jin, J. W. Woodcock, B. Zhao. *Journal of Physical Chemistry B* **2011**, *115*, 2870-2881.

36. K. Kabiri, S. Lashani, M. J. Zohuriaan-Mehr, M. Kheirabadi. *Journal of Polymer Research* **2011**, *18*, 449-458.

37. Y. Guan, W. W. Jiang, W. C. Zhang, G. X. Wan, Y. X. Peng. *Journal of Polymer Science Part B: Polymer Physics* **2001**, *39*, 1784-1790.

38. S. J. Kim, K. J. Lee, S. I. Kim, Y. M. Lee, T. D. Chung, S. H. Lee. *Journal of Applied Polymer Science* **2003**, *89*, 2301-2305.

39. N. Li, M. C. Williams (W&L Polymer, Ltd.) Patent WO2012064787 A2, **2012**.

40. R. H. Pelton, P. Chibante. *Colloids and Surfaces* **1986**, *20*, 247-256.

41. S. Kirsch, A. Doerk, E. Bartsch, H. Sillescu, K. Landfester, H. W. Spiess, W. Maechtle. *Macromolecules* **1999**, *32*, 4508-4518.

42. J. A. Bonham, M. A. Faers, J. S. van Duijneveldt. *Soft Matter* **2014**, *10*, 9384-9398.

43. Y. Guan, W. C. Zhang, G. X. Wan, Y. X. Peng. *Journal of Polymer Science Part a-Polymer Chemistry* **2000**, *38*, 3812-3820.

44. R. Schafer, J. Kressler, R. Neuber, R. Mulhaupt. *Macromolecules* **1995**, *28*, 5037-5042.

45. A. Fidalgo, L. Ilharco. *Journal of Sol-Gel Science and Technology* **1998**, *13*, 433-437.

46. A. R. Guo, W. X. Yang, F. Yang, R. Yu, Y. X. Wu. *Macromolecules* **2014**, *47*, 5450-5461.

47. G. Mertz, T. Fouquet, C. Becker, F. Ziarelli, D. Ruch. *Plasma Processes and Polymers* **2014**, *11*, 728-733.

48. A. Kawasaki, J. Furukawa, T. Tsuruta, G. Wasai, T. Makimoto. *Makromolekulare Chemie* **1961**, *49*, 76-111.

49. G. Gratzl, C. Paulik, S. Hild, J. P. Guggenbichler, M. Lackner. *Materials Science & Engineering C: Materials for Biological Applications* **2014**, *38*, 94-100.

50. M. A. Gauthier, J. Luo, D. Calvet, C. Ni, X. X. Zhu, M. Garon, M. D. Buschmann. *Polymer* **2004**, *45*, 8201-8210.

51. Y. Zhang, P. C. Zhu, D. Edgren. *Journal of Polymer Research* **2010**, *17*, 725-730.

52. D. Capitani, M. A. Nobile, G. Mensitieri, A. Sannino, A. L. Segre. *Macromolecules* **2000**, *33*, 430-437

53. D. Doskocilova, B. Schneider. *Pure and Applied Chemistry* **1982**, *54*, 575-584.

54. F. J. Wende, S. Gohil, L. I. Nord, A. H. Kenne, C. Sandstrom. *Carbohydrate Polymers* **2017**, *157*, 1525-1530.

55. P. Bisel, L. Al-Momani, M. Muller. *Organic & Biomolecular Chemistry* **2008**, *6*, 2655-2665.

Chapter 3

pH- and salt- responsive behaviour of poly(acrylic acid) (PAA) microgels

Abstract

The pH- and salt-responsive behaviour of polymer gels is attributed to the presence of certain pendant groups such as carboxyl groups (–COOH), sulfonic acid groups (-SO_3H), and amine groups (-NH_2). In this chapter, we investigate the effect of solvents on the swelling of P*t*BA microparticles and the effect of pH and ionic strength on the swelling behaviour of PAA microgels. This includes the effect of type of cross-linker and the cross-linking density. We employed light scattering techniques (both dynamic and static) to measure the particle size and also measured the zeta potential of the microgels. Hydrophobic P*t*BA microparticles swell in THF and acetone but not in water, consistent with the decreasing dielectric constant and Hansen solubility parameters of solvents: water > acetone > THF.

The swelling behaviour of PAA microgels is sensitive to the change in pH and ionic strength. At high pH, the carboxyl groups are ionized to carboxylate anions and the electrostatic repulsion between the adjacent ionized groups causes the swelling of the microgels, while the presence of salt results in some deswelling of PAA microgels. In some cases, a small effect of crosslink density was seen, with the extent of swelling being larger for particles with a lower crosslink density. The shape factor (ratio of radius of gyration over hydrodynamic radius) in the case of P*t*BA particles in all solvents was around 0.6 - 0.8, in reasonable agreement with the value expected for solid spheres; for PAA particles, somewhat lower values were found, which is commonly the case for microgel particles where the crosslink density is higher near the particle centre.

3.1 Introduction

3.1.1 Micro(hydro)gels

Micro(hydro)gels are cross-linked polymer latex particles that are swollen in water with a particle size in a range of 10 – 1000 nm.[1] These particles are called stimulus-responsive or smart. The gels exhibit a phase transition or rapid volume change in response to small changes in external conditions such as pH, ionic strength, temperature, magnetic field, or exposure to UV/visible light. This characteristic of stimulus responsive gels has been very useful in many applications such as delivery systems, cell encapsulation, and tissue engineering.[2,3]

3.1.2 pH- and salt-responsive microgels

pH-responsive microgels can be classified into two categories by the nature of pendant groups: (1) polyacid gels with weak acid groups such as carboxylic (-COOH) and sulfonic acid (-SO_3H), and (2) polybase gels with weak basic groups such as amine (-NH_2) in the network.

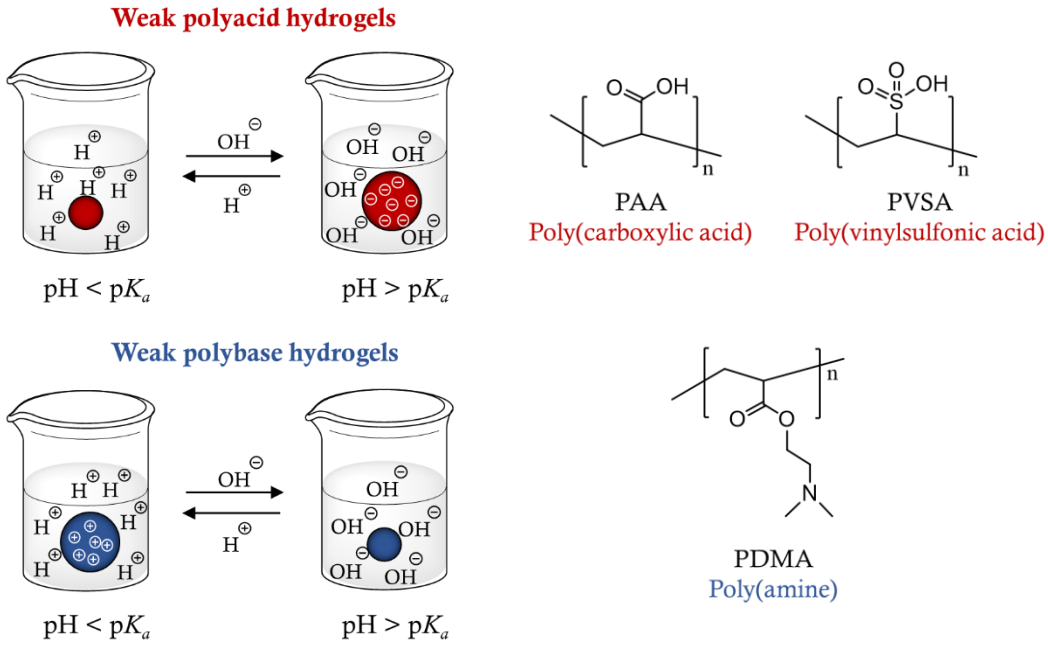

Figure 3.1 Swelling-deswelling behaviour of polyacid and polybase hydrogels.

A volume transition from a collapsed into a swollen gel can arise because these functional pendant groups are ionized to anions (-) or cations (+) at certain pH values. Electrostatic repulsion forces between these charges cause an increased osmotic pressure difference between the external solution and the microgel network, therefore the microgels are swollen. In **Figure 3.1**, polyacid gels containing carboxylic acid groups (-COOH) are ionized to carboxylate anions ($-COO^-$) at a high pH so the gels are swollen. In contrast, for polybase hydrogels, their tertiary amine groups ($-NR_2$) become protonated to tertiary ammonium cations ($-NR_2H^+$) at a low pH causing the swelling of the gels.[3,4]

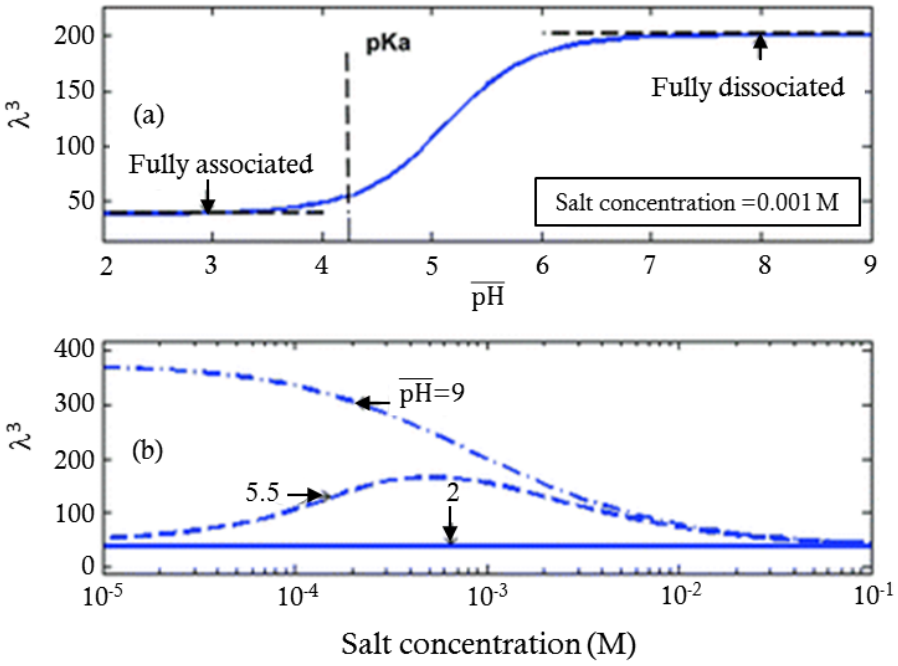

Figure 3.2 The volume-swelling ratio (λ^3) is plotted as a function of (a) $\overline{pH}$ for a fixed salt concentration, and as a function of (b) salt concentration at several values of $\overline{pH}$.[7] Modified from [7]. Copyright (2010) by Soft Matter.

In general, the swelling behaviour of pH-responsive gels is also sensitive to salt concentration.[5-10] The volume-swelling ratio (λ^3) of pH-responsive microgels as a function of salt concentration at a certain pH of external solution ($\overline{pH}$) is shown in **Figure 3.2**(b). In the collapsed state at $\overline{pH}$ = 2, the gels are fully protonated, and the swelling is independent of salt concentration. However, in the swollen state at $\overline{pH}$ = 9, the gels are fully ionized and electrostatic interactions are dominant, therefore, the increasing salt concentration causes the shrinkage of the gels due to charge screening. When $\overline{pH}$ = 5 (around their pK_a or intermediate value) the swelling behaviour of the gels is non-monotonous. Increasing salt concentration initially induces the swelling of the gels since

disassociation of the acidic groups is promoted, reaching a plateau. Subsequently, the additional salt decreases the difference of osmotic pressure between the inside of the gels and the external solution, so the gels are deswelling.

3.1.3 Hydrophobically modified PAA microgels

Poly(acrylic acid) (PAA) contains carboxylic acid as a side group which enables PAA to be hydrophilic and pH-responsive. Amphiphilic structures based on hydrophobically modified PAA hydrogels have been extensively studied, focussing on the swelling behaviour,[11,12] the morphology and especially potential applications as drug carriers.[13,14]

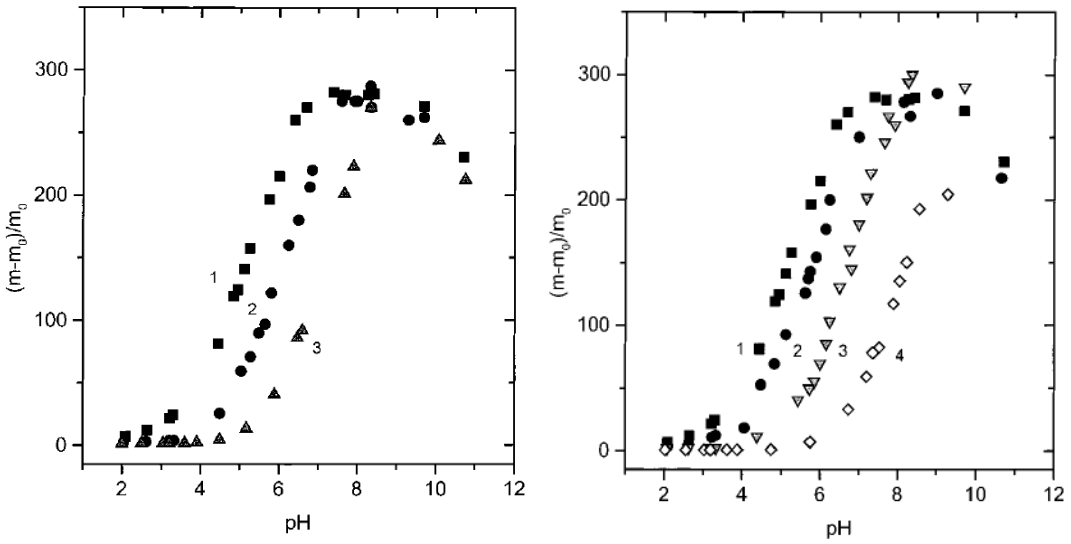

Figure 3.3 (a) Degree of swelling of (1) PAA gels and of the modified PAA gels with (2) C8-5%, (3) C12-5%, and (b) degree of swelling of (1) PAA gels and of the modified PAA gels with (2) C8-2.5%, (3) C8-10% and (4) C8-20% mole of acrylates (n=8) as a function of pH solution.[11] Reprinted from [11]. Copyright (1997) by the Macromolecules.

For example, Philippova *et al.*[11] prepared hydrophobically modified PAA hydrogels by adding *n*-alkyl acrylates (n=8, 12, 18). For PAA modified with 5%mol of *n*-octyl (C-8) or *n*-dodecyl (C-12) acrylates, the volume transition shifts to a higher pH according to the increasing hydrophobicity (C-12 > C-8) of PAA hydrogels as shown in **Figure 3.3**(a). Similarly, increasing the content of C-8 causes a shift of volume transition pH to a higher value as shown in **Figure 3.3**(b). In addition, the degree of swelling of PAA hydrogels modified with 20%mole of C-8 acrylates is significantly lower than for lower contents.

Guan *et al.*[12] prepared PAA hydrogels cross-linked with PTHF (PAA-*l*-PTHF) via free-radical polymerization. The swelling behavior was investigated as a function of solvent, pH and cross-linking density. In water, the swelling ratio of PAA-*l*-PTHF hydrogels decreases with increasing PTHF content (%wt PTHF segment in PAA-*l*-PTHF), whilst in cyclohexane the swelling ratio increases with increasing PTHF content and the relationship between the swelling ratio and the %wt PTHF segment can be expressed with a linear equation. The presence of PAA causes the hydrogels to be pH-sensitive and their pK_a is about 5. Therefore, when pH is greater than 5, the hydrogels significantly swell and the swelling ratio decreases with an increase in %wt PTHF.

Bromberg *et al.*[13] prepared PAA-*g*-Pluronic (PEO-PPO-PEO) microgels lightly cross-linked with ethylene glycol dimethacrylate (EGDMA) to be used as drug carriers. The swelling behaviour of these microgels is sensitive to changes in pH and temperature attributed to the PAA and Pluronic segments, respectively. The degree of crosslinking (XL) is controlled by the mole ratio of EGDMA to acrylic acid monomer and increasing XL leads to a decrease in swelling ratio. In addition, the microgels are swollen at high pH, and at fixed pH = 7 when temperature is higher than critical micellization temperature (CMT), the microgels are shrinking due to aggregation of Pluronic which improves the association with hydrophobic drug such as taxol. In addition, at high pH the uptake efficiency of positively charged drugs such as doxorubicin increases due to the swelling of ionized PAA segment. Consequently, the amphiphilic structure allows PAA-*g*-Pluronic microgels to be used as drug carrier for various types of drug.

3.1.3 Radius of gyration (R_G) and hydrodynamic radius (R_H)

The radius of gyration (R_G) is typically measured by static light scattering (SLS) in which the scattering intensity is measured as a function of angle, while the hydrodynamic radius (R_H) is measured by dynamic light scattering (DLS) which characterises the time fluctuations in the scattered light. For suitably small particles, the SLS data can be analysed with a Zimm plot, Berry plot or Guinier plot in order to obtain the root mean-square radius of gyration $< R_G^2 >^{1/2}$. The R_G of particles is defined as the mass weighted average distance from the center of mass to every atom within the particle.[15, 16] For a solid sphere, $R_G = \sqrt{3/5}\, R$ where R = radius of sphere. The R_H of particles is obtained from the normalized time auto-correlation function of the scattered light and is defined as the radius of an equivalent hard sphere diffusing at the same rate as the observed particles following the Stokes-Einstein equation. In addition, the shape factor is defined as the ratio of R_G/R_H. It characterises the compactness and shape of the dispersed particles. For instance, for solid

spheres the value is ~0.78, it is 1.5–2.1 for random polymer coils and greater than 2 for very elongated particles such as nanotubes.[15,17-19]

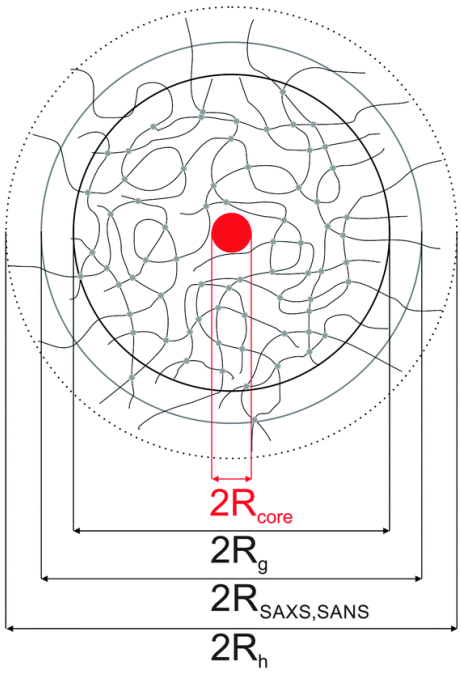

Figure 3.4 Soft sphere structure of Au–PNIPAM core–shell particles with the gold as core (red circle) and PNIPAM microgel as shell. The black, solid lines represent linear polymer chains and the cross-linker points are highlighted by grey circles. The radii are determined from DLS (R_H), SLS (R_G), SAXS and SANS ($R_{SAXS,\,SANS}$) and the Au core radius from SAXS and TEM (R_{CORE}).[20] Reprinted from [20]. Copyright (2015) by the Physical Chemistry Chemical Physics.

Figure 3.4 illustrates that different scattering techniques provide different information on the radii of microgel particles. It is seen that R_G from SLS is mainly sensitive to the dense core of the particle, whilst R_H from DLS is not only sensitive to this dense part but also to the thin outer layer, consisting of weakly cross-linked dangling chains. Consequently, for microgels with such a heterogeneous distribution of cross-linking, the shape factor is smaller than the value for homogeneous hard spheres (0.775).[20-22]

3.2 Experimental

3.2.1 Materials

PAA microgels crosslinked with PPG and PTHF with different crosslinking densities were prepared as described in chapter 2. Hydrochloric acid (36%wt HCl, VWR), sodium hydroxide (NaOH, Fisher Scientific UK), and sodium chloride (NaCl, Fisher Scientific UK) were used without further purification. Deionized (DI) water with a resistivity greater than 18.2 MΩ·cm was obtained from a Milli-Q Plus system from Millipore. All solvents were used as received.

3.2.2 Light scattering

The particle size was measured using a Malvern Auto-sizer 4800 which was designed for both dynamic (DLS) and static light scattering (SLS) equipped with a laser with wavelength 532 nm. For DLS, scattering data were measured at 90° and the intensity correlation functions ($g_2(t)$) were analyzed using a multimodal analysis. The correlation functions provide the diffusion coefficient (D) of the particles. Then, the hydrodynamic radius (R_H) was calculated using the Stokes-Einstein equation as $R_H = k_B T/6\pi\eta D$, where D is the diffusion coefficient, k_B is the Boltzmann constant, T is the absolute temperature and η is the viscosity of the solvent.

For SLS, the light intensity was measured for scattering angles of 30-140° and the radii of the particles (R) were calculated using the SasView software with the polydisperse sphere model. Scattering intensities were determined in arbitrary units (no calibration was done to obtain absolute scattering data) and therefore we set the scattering length density (sld) at 1 and o for microgels and solvent, respectively. Background, scale, radius and polydispersity (standard deviation in size / mean size) were left free whilst fitting the scattering data. However, the sphere model cannot properly fit the scattering data of 300:1 PAA/PTHF microgels so we tried a core-shell model to fit them, setting the sld of the shell at 2, 0.5 or leaving it to vary. For homogeneous spheres, the radius of gyration (R_G) and the radius of particles (R) are related as $R_G = 0.775R$. The swelling ratio is calculated as Equation (3.1):

$$\text{Swelling ratio} = \frac{R}{R_0} \tag{3.1}$$

where R and R_0 are the radius of microgels in the swollen and collapsed states, respectively.

3.2.2.1 Sample preparation

Effect of solvent

P*t*BA latex was diluted in the solvents (water, acetone, THF) and the count rate of all samples were kept below 800 KCps (kilo counts per second) in order to reduce the error of measurement generated by multiple scattering and viscosity effects. The refractive index is 1.331, 1.356 and 1.405, and the viscosity is 0.891 cP, 0.302 cP, and 0.481 cP for water, acetone[23] and THF[24] at 25 °C, respectively.

Effect of pH

Dry particles were dispersed at a concentration of 0.1 mg/mL in 1 mM NaCl using a probe sonicator (QSonica Q125, 125 Watt 20 KHz, amplitude 50%) in pulse mode (pulse on 5 sec/off 5 sec) for 15 mins and then the solutions were filtered through a 2 μm controlled pore filter (Whatman® Cyclopore, polycarbonate and polyester membranes). To determine the pH responsive behaviour, the pH of the solutions was adjusted with 0.1 M HCl or NaOH and the solutions were held for 30 mins to achieve swelling/de-swelling equilibrium before measurements were taken.

Effect of salt

Dry particles of 100:1 PAA/PPG were dispersed at a concentration of 0.06 %wt in DI water using a probe sonicator (QSonica Q125, 125 Watt 20 KHz, amplitude 50%) in pulse mode (pulse on 5 sec/off 5 sec) for 15 mins and then the solutions were filtered through a 2 μm controlled pore filter (Whatman® Cyclopore, polycarbonate and polyester membranes). The pH of sample solution was 4.5 before adding 10 mM NaCl aqueous solution (0.1 mL/time) into the cell. After 15 mins, the particle size of PAA microgels was measured by DLS.

Effect of PEO

PEO (M_w 200) was added into 0.1%wt 100:1 PAA/PPG microgels dispersed in DI water at different weight ratio of PAA: PEO of 1:5, 1:10, 1:15, 1:35, and 1:50. The sample solutions were mixed by sonicator probe for 15 mins and centrifuged for 5 mins (10k rpm). The pH of the aqueous solution containing PAA microgels was 4.5 before the addition of PEO. The particle size of PAA microgels was measured by DLS.

3.2.3 Zeta potential

Zeta potentials of the particles were measured using a Malvern Zetasizer Nano Z, using the Smoluchowski equation. Samples were prepared by dispersing dry particles in DI water at concentration of 0.1 mg/mL. The pH of samples was adjusted with 0.1 M HCl or NaOH and the solutions were held for 15 mins before measurements were taken.

3.3 Results and discussion

3.3.1 Swelling behaviour of P*t*BA microparticles

3.3.1.1 Effect of solvent

Poly(*tert*-butyl acrylate) (P*t*BA) microparticles were prepared using surfactant free emulsion polymerization (SFEP) in aqueous solution with two different cross-linkers: poly(propylene glycol) (PPG, -$[CH_2CH_2O]_n$-) and poly(tetrahydrofuran) (PTHF, -$[CH_2CH_2CH_2CH_2O$-$]_n$-). For P*t*BA/PPG microparticles, we varied the molar ratio of monomer to cross-linker = 50:1, 75:1 and 100:1, and for P*t*BA/PTHF microparticles the molar ratio is 100:1 and 300:1, respectively.

Due to the *tert*-butyl acrylate (-COOC-$(CH_3)_3$) of P*t*BA, these particles are hydrophobic and are deswollen in water. We therefore investigated the swelling of these particles by dispersing in organic solvents (acetone and THF) and measuring the radius of particles using DLS and SLS techniques.

Table 3.1 Summary of dielectric constant (ε) and Hansen solubility parameters of the solvents used for the swelling of P*t*BA microgels.

Solvent	Dielectric constant (ε)	Hansen solubility parameters[26] ($Pa^{1/2}$)			
		δ_{Total}	δ_D	δ_P	δ_H
THF	7.5[25]	19.5	16.8	5.7	8.0
Acetone	21.3[27]	20.0	15.6	10.4	7.0
Water	80.0[27]	47.9	15.6	16.0	42.3
P*t*BA	-	18.4	15.3	8.4	5.7

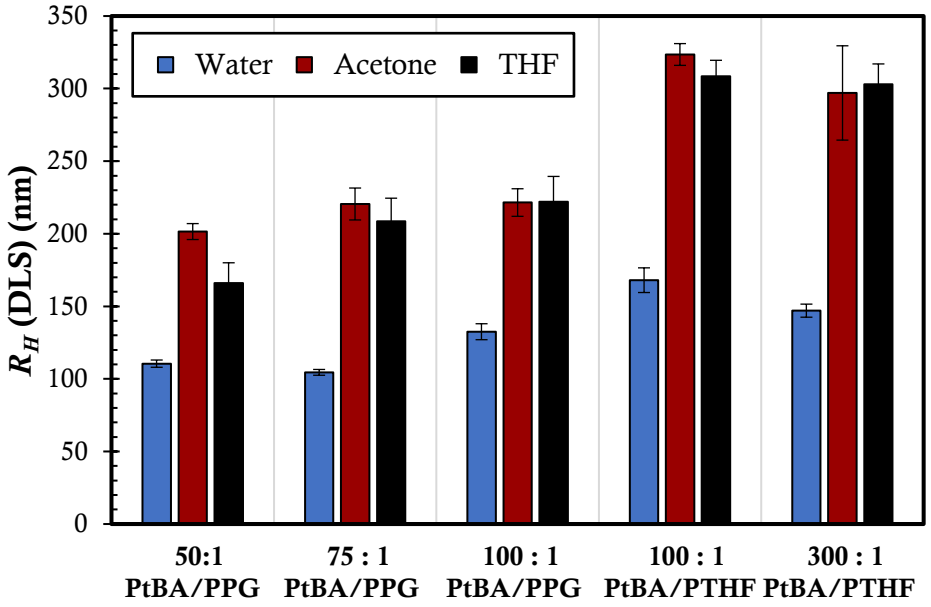

Figure 3.5 Hydrodynamic radius (R_H) from DLS of P*t*BA microparticles cross-linked with PPG at molar ratio of monomer to cross-linker = 50:1, 75:1 and 100:1, and cross-linked with PTHF at molar ratio of monomer to cross-linker = 100:1 and 300:1, respectively.

The hydrodynamic radius (R_H) from DLS experiments of P*t*BA microparticles cross-linked with PPG or PTHF dispersed in water, acetone and THF are shown in **Figure 3.5**. It is clear that the P*t*BA microparticles are shrinking in water due to the hydrophobicity of *tert*-butyl groups in P*t*BA. It is worth noting that the particles swell well in acetone and THF, which have Hansen solubility parameters close to that of the P*t*BA polymer – see **Table 3.1**. The R_H of P*t*BA microparticles in acetone is rather similar to that in THF with a high standard deviation. Whilst measuring swollen microparticles with DLS, we noticed that the baseline of the correlation curves of swollen particles was not a horizontal line, which means the data need to be interpreted with care.

We anticipate that the microparticles swell less with increasing cross-linking density. However, the effect of cross-linking density on the swollen size is not obvious for both P*t*BA/PPG and P*t*BA/PTHF microparticles except for 50:1 P*t*BA/PPG for which the swollen size is smaller than for 75:1 and 100:1 P*t*BA/PPG.

Using two different cross-linkers, PPG and PTHF, we can consider the effect of type of cross-linker at fixed mole ratio of monomer to cross-linker = 100:1. We suggest that PTHF cross-linker is more hydrophobic than PPG cross-linker due to the lower polarity and longer chains of PTHF (M_w of PTHF and PPG is 1105 and 800 g/mol and number of

repeating units = 14 and 12, respectively). In fact, neither of these particles swell in water, but both do swell when dispersed in acetone or THF.

Then, we measured the particle sizes using SLS and the scattering intensity curves were analysed with the SasView program using the polydisperse sphere model. It is seen that this model can fit all curves very well as shown in **Figure 3.6**.

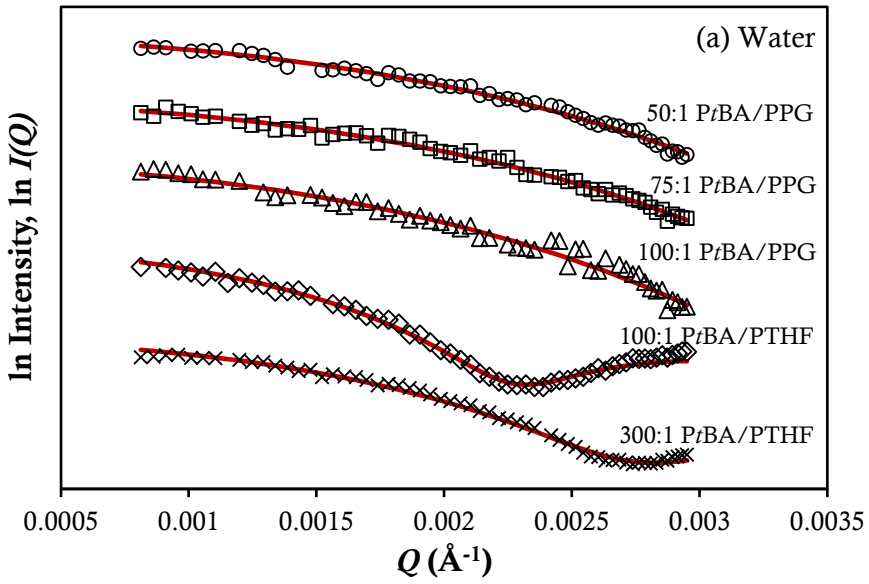

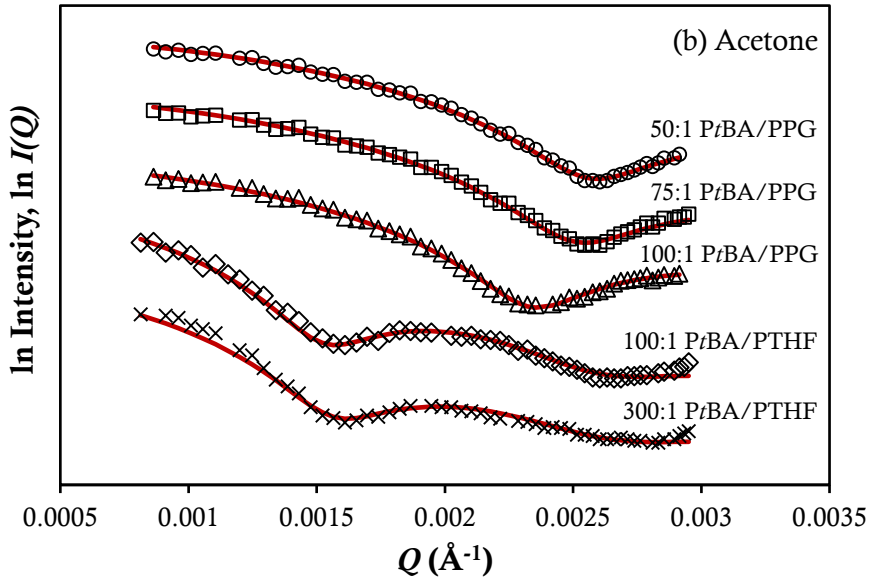

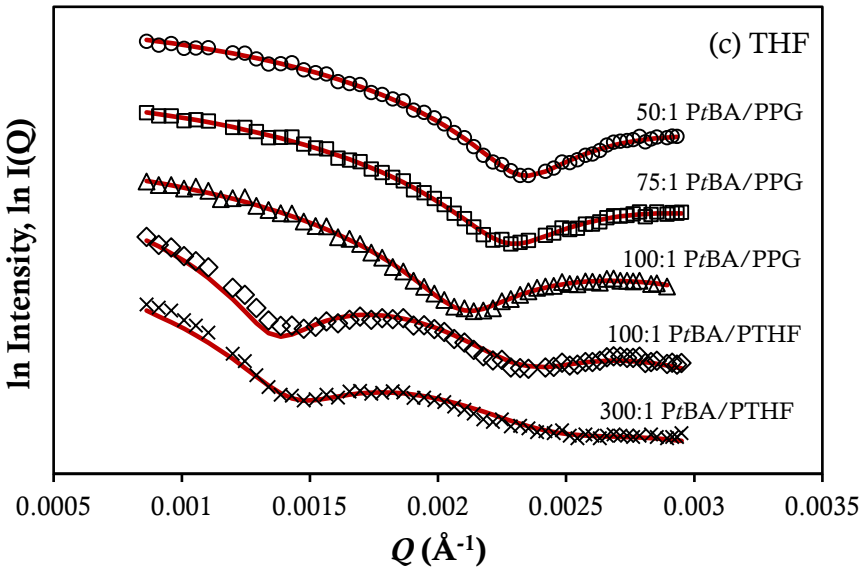

Figure 3.6 Intensity plots as a function of scattering vector (*Q*) of P*t*BA microgels cross-linked with PPG and PTHF dispersed in (a) water, (b) acetone and (c) THF fitted using the SasView program with polydisperse sphere model.

The fit results are collected in **Table 3.2**. The polydispersity (PD) of P*t*BA microparticles obtained from the SasView fits is rather low in all solvents. It is seen that these particles have low PD values with very small standard deviation (SD) indicating the narrow size distribution of these particles which is a benefit of using SFEP. However, larger PD values are found in acetone and THF which may reflect some inhomogeneity in the crosslinking and hence swelling of these particles.

Table 3.2 Polydispersity (PD) of P*t*BA microparticles dispersed in water, acetone and THF from SLS experiment analysed with the SasView program using the polydisperse sphere model.

Sample	Solvent		
	Water	Acetone	THF
50:1 P*t*BA/PPG	0.01±0.002	0.01±0.003	0.01±0.003
75:1 P*t*BA/PPG	0.02±0.004	0.08±0.001	0.06±0.003
100:1 P*t*BA/PPG	0.09±0.004	0.02±0.009	0.07±0.002
100:1 P*t*BA/PTHF	0.01±0.001	0.10±0.002	0.08±0.001
300:1 P*t*BA/PTHF	0.01±0.002	0.10±0.002	0.12±0.002

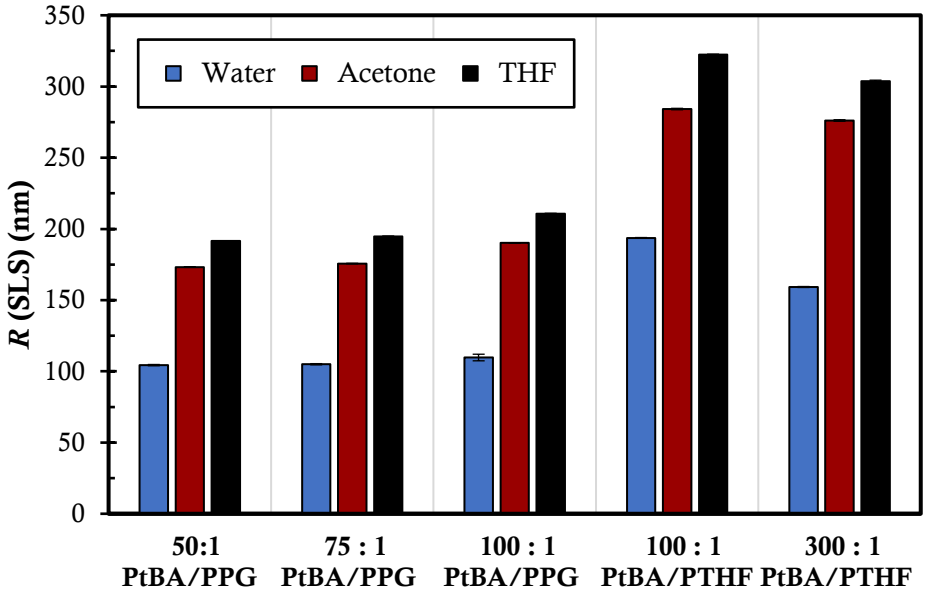

Figure 3.7 Radius of spheres (*R*) obtained from SLS (analysed with the SasView program and sphere model) of P*t*BA microparticles cross-linked with PPG at molar ratio of monomer to cross-linker = 50:1, 75:1 and 100:1, and cross-linked with PTHF at molar ratio = 100:1 and 300:1, respectively.

For SLS experiments, all P*t*BA microparticles are better swollen in organic solvents than in water, as we also found using DLS so that the increase of particle size of P*t*BA microparticles is related to the decreasing dielectric constant (ε) and Hansen solubility parameters of solvents: water > acetone > THF as expected. The particle size of 100:1 P*t*BA/PTHF microparticles is greater than that of 100:1 P*t*BA/PPG microparticles, consistent with the DLS result.

Table 3.3 Swelling ratios of P*t*BA microparticles cross-linked with PPG and PTHF in acetone and THF normalized with the radius of particles in water from DLS and SLS experiments.

Sample	Swelling ratio			
	DLS ($R_H/R_{H,water}$)		SLS ($R/R_{H,water}$)	
	Acetone	THF	Acetone	THF
50:1 P*t*BA/PPG	1.8 ± 0.1	1.5 ± 0.1	1.7 ± 0.01	1.8 ± 0.01
75:1 P*t*BA/PPG	2.1 ± 0.1	2.0 ± 0.2	1.7 ± 0.01	1.9 ± 0.01
100:1 P*t*BA/PPG	1.7 ± 0.1	1.7 ± 0.1	1.7 ± 0.04	1.9 ± 0.04
100:1 P*t*BA/PTHF	1.9 ± 0.1	1.8 ± 0.1	1.5 ± 0.01	1.7 ± 0.01
300:1 P*t*BA/PTHF	2.0 ± 0.2	2.1 ± 0.1	1.7 ± 0.01	1.9 ± 0.01

The relative swelling ratio from the radius of particles in acetone and THF normalized with the radius in water is listed in **Table 3.3**. For the DLS results, it is difficult to see a clear effect of the cross-linking density on the swelling ratio of P*t*BA/PPG microparticles in acetone and THF as a consequence of the somewhat noisy R_H values. However, a higher cross-linking density (molar ratio of monomer to cross-linker = 100:1 > 300:1) of P*t*BA/PTHF microparticles results in less swelling in acetone and THF. For the SLS results, we found the swelling ratio of P*t*BA/PPG in THF slightly decreases with increasing cross-linking density (molar ratio of monomer to cross-linker = 50:1 > 75:1 > 100:1) and the same is true for the P*t*BA/PTHF microparticles in acetone and THF. However, the swelling ratio of P*t*BA/PPG in acetone is independent of the cross-linking density. In summary, the SLS results show that the swelling of P*t*BA microgels is weakly dependent on the cross-linking density and the particles are somewhat better swollen in THF than in acetone.

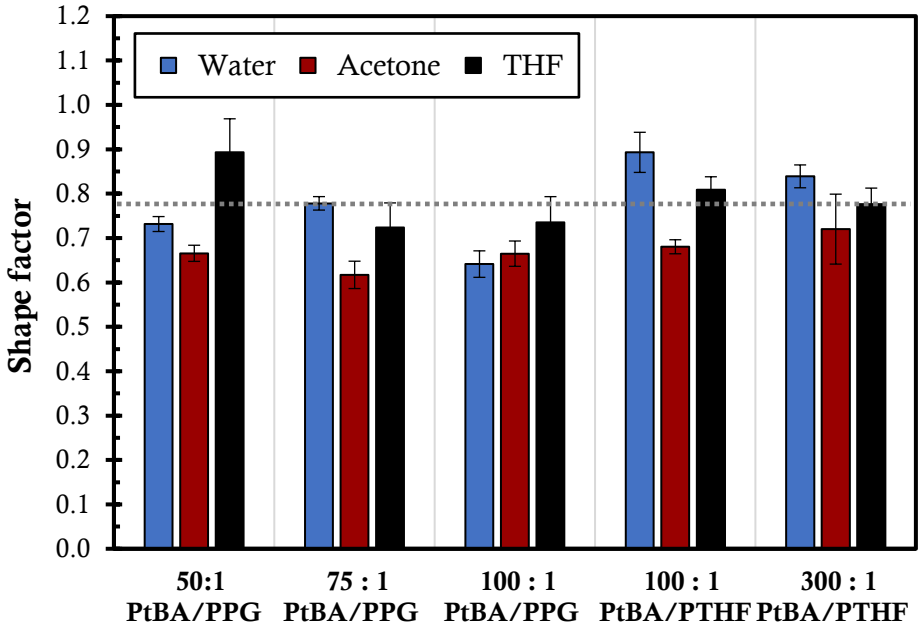

Figure 3.8 Shape factor (R_G/R_H) of P*t*BA microgels cross-linked with PPG at molar ratio of monomer to cross-linker = 50:1, 75:1 and 100:1, and with PTHF at molar ratio of monomer to cross-linker = 100:1 and 300:1, respectively.

Finally, in **Figure 3.8** we present the shape factor (ρ) which is the ratio of the radius of gyration ($R_{G,\,SLS}$) over the hydrodynamic radius ($R_{H,\,DLS}$), where R_G is calculated from the equation: $R_{G,\,SLS} = 0.775 * R_{SLS}$ for spherical particles and the radius of the sphere (R) was obtained from the SasView fits. The shape factor is a dimensionless parameter which can provide information on the particle shape and/or internal structure. Specific predictions are available for spherically symmetric particles. The shape factor of homogeneous hard spheres, hollow spheres, and polymer random coils are 0.775, 1, and 1.505, respectively.[29] Wolfe and Scopazzi[30] studied the effect of cross-linker content on the ρ value of PMMA microgels and found that the ρ value of the microgels is 0.55–0.67 which is lower than that of the hard sphere because the cross-linking density distribution of microgels is non-uniform as a result of the presence of dangling chains in the outer region. In addition, they found that the ρ value approaches the hard-sphere value with an increasing content of cross-linker. Such behaviour was also reported by Kunz[18] and Antonietti.[31]

The ρ value of our microgels is mainly in the range of 0.6 to 0.8, rather close to the prediction for homogeneous spheres. This is encouraging and suggests that these microgels are homogeneously swollen. Nevertheless, some ρ values are higher than the value of homogeneous spheres, but with a significant error bar. No systematic trends are visible for the ρ values as a function of cross-linking density or type of cross-linker. To some extent

this comparison is hampered by the noisy DLS data.

3.3.2 Swelling behaviour of PAA microgels

3.3.2.1 Effect of hydrolysis of P*t*BA to PAA microgels

To obtain pH-responsive PAA microgels, P*t*BA microparticles were freeze-dried and hydrolysed with TFA in DCM as described in Chapter 2. While P*t*BA microparticles are hydrophobic due to *tert*-butyl acrylate groups (-COOC-$(CH_3)_3$), PAA microgels are more hydrophilic as the acrylate groups are now converted to carboxyl groups (-COOH).

Table 3.4 Comparison of radius of particles and swelling ratio of P*t*BA microparticles in DI water and PAA microgels (after hydrolysis of P*t*BA microparticles) in pH 3.5 solution.

Sample	P*t*BA in DI water		PAA in pH 3.5 solution		R_{PAA}/R_{PtBA}	
	DLS (R_H, nm)	SLS (R, nm)	DLS (R_H, nm)	SLS (R, nm)	DLS	SLS
50:1 P*t*BA/PPG	111 ± 3	104 ± 0.4	156 ± 1	118 ± 0.5	1.4 ± 0.03	1.1 ± 0.01
75:1 P*t*BA/PPG	105 ± 2	105 ± 0.4	175 ± 1	123 ± 0.8	1.7 ± 0.03	1.2 ± 0.01
100:1 P*t*BA/PPG	133 ± 6	110 ± 2.3	185 ± 1	154 ± 0.3	1.4 ± 0.06	1.4 ± 0.03
100:1 P*t*BA/PTHF	168 ± 9	194 ± 0.3	290 ± 9	243 ± 0.5	1.7 ± 0.10	1.3 ± 0.01
300:1 P*t*BA/PTHF	147 ± 5	159 ± 0.3	-	-	-	-

Table 3.4 shows the particle radius of P*t*BA microparticles before and after hydrolysis to PAA microgels, and the ratio of these values. We assume that P*t*BA and PAA microparticles are both deswollen (in water and pH 3.5 solution, respectively) so we can investigate the effect of the hydrolysis reaction on the particle size. Theoretically, the hydrolysis will cause the decrease of molar mass per repeating unit by a factor of 1.8 for hydrolysing P*t*BA to PAA. By assuming that the bulk density before and after hydrolysis to PAA is stable, the volume should therefore decrease by a factor 1.8, equivalent to a factor 1.21 in the radius. Nevertheless, the particle sizes of PAA microgels are larger than those of the corresponding P*t*BA microparticles, judging by both the DLS and SLS experiments. We suggest that the hydrophilicity of PAA plays an important role so that

the PAA microgels are somewhat hydrated, even if they are in a collapsed state at low pH.

For the SLS experiments, it is obvious that the swelling ratio of PAA/PPG microgels decreases with increasing cross-linking density, whilst this trend is not clear in the DLS data. There is no marked difference in swelling ratio when comparing the 100:1 PAA/PPG microgels with the 100:1 PAA/PTHF microgels.

For 300:1 PAA/PTHF microparticles, we experienced difficulties measuring the particle size with DLS since the baseline of the correlation function was not a horizontal line and the resulting R_H has a very high error. Also, the SLS data could not be fitted well with the sphere model (discussed separately later). Therefore, we do not show the radii of these microgels in this table.

3.3.2.2 Effect of pH

As a result of the carboxyl groups, the swelling behaviour of PAA microgels is pH-sensitive. At low pH the carboxyl groups are protonated and when pH is above the pK_a (4.5 - 5) [12,32] of acrylic acid, the carboxyl groups are ionized to carboxylate anions so that the microgels will be swollen as a result of electrostatic repulsion between these anions. The effect of pH on the swelling of 100:1 P*t*BA/PPG, 50:1, 75:1 and 100:1 PAA/PPG, 100:1 P*t*BA/PTHF, 100:1 and 300:1 PAA/PTHF microgels is shown in **Figure 3.9**.

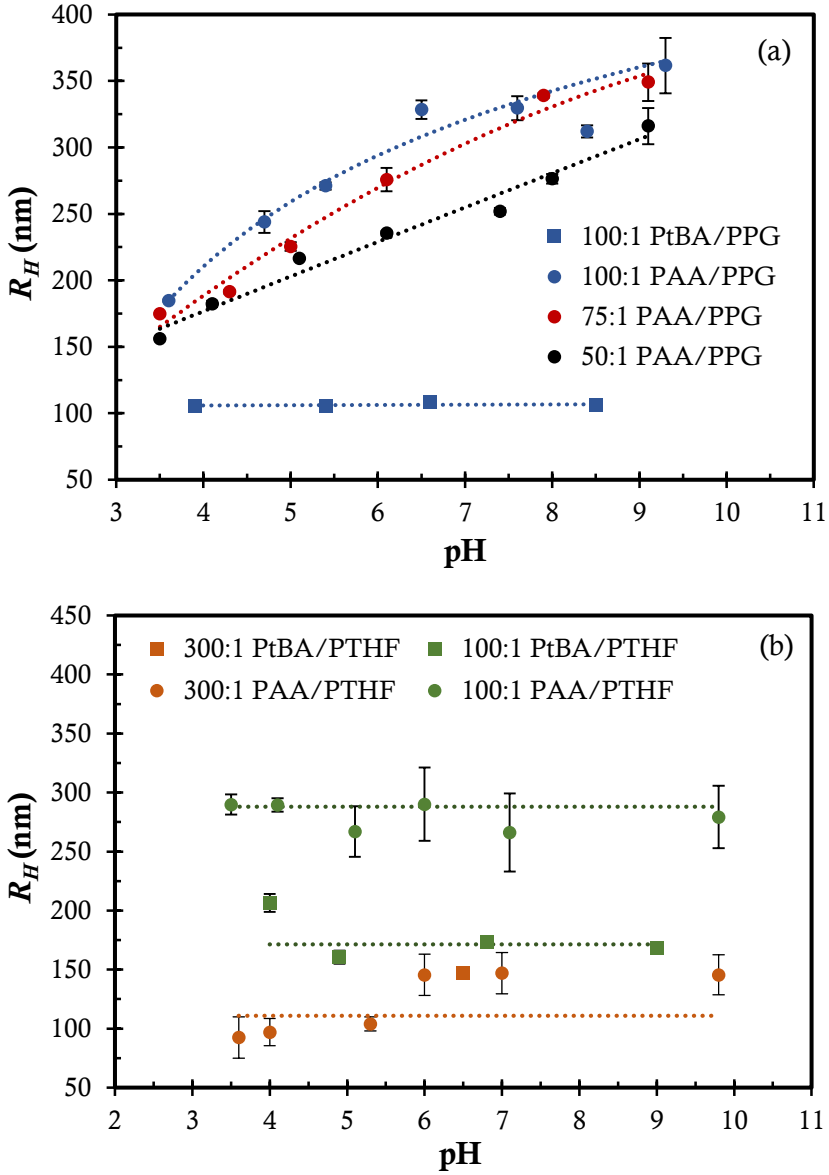

Figure 3.9 Hydrodynamic radius (R_H) of (a) 100:1 P*t*BA/PPG microparticles and 50:1, 75:1 and 100:1 PAA/PPG microgels, and (b) 100:1 P*t*BA/PTHF microparticles and 100:1 and 300:1 PAA/PTHF microgels measured with DLS.

As anticipated, the swelling of 100:1 P*t*BA/PPG microparticles is not dependent on pH. From the lowest pH (around 3.5), addition of NaOH solution into the PAA microgels solutions causes the microgels to swell and this continues until the highest pH (around 9). However, no sharp swelling transition is found as a function of pH. We found that the cross-linking density has a noticeable effect on the particle size of PAA/PPG microgels so that the particle size of 100:1 PAA/PPG at all pH is bigger than the other two, consistent with its cross-linking density being lowest. For 100:1 P*t*BA/PTHF, the particle size is around 171 nm and not sensitive to pH as found in 100:1 P*t*BA/PPG.

For PAA microgels cross-linked with PTHF, the particle size fluctuates around 290 nm and 111 nm with a large error for 100:1 and 300:1 PAA/PTHF, respectively, and there is no clear trend with pH. We noticed during the DLS experiments that the baseline of the correlation function is not a horizontal line and the uncertainties in the sizes of PAA/PTHF microgels are a result of this. Consequently, we do not use this result of PAA/PTHF microgels any further for calculating swelling ratio and shape factor.

We then studied the swelling behaviour of all samples using SLS as shown in **Figure 3.10**.

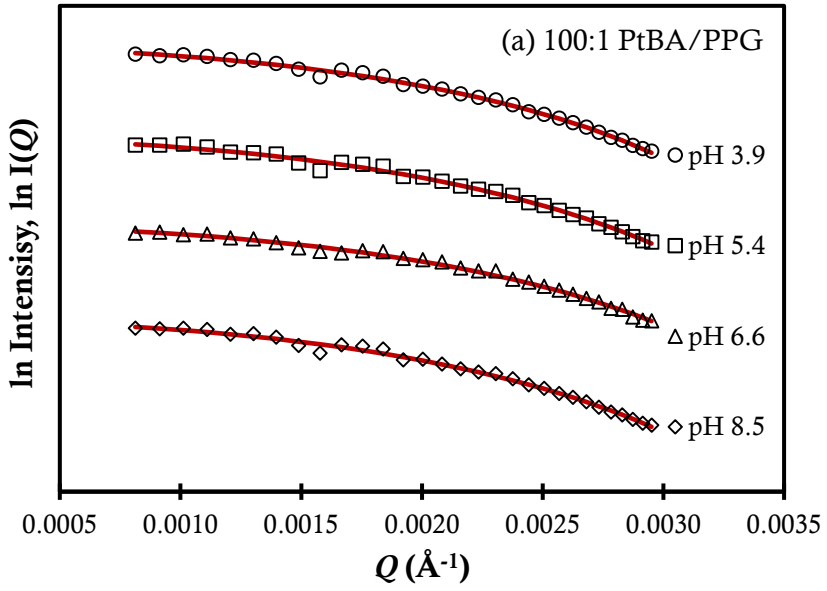

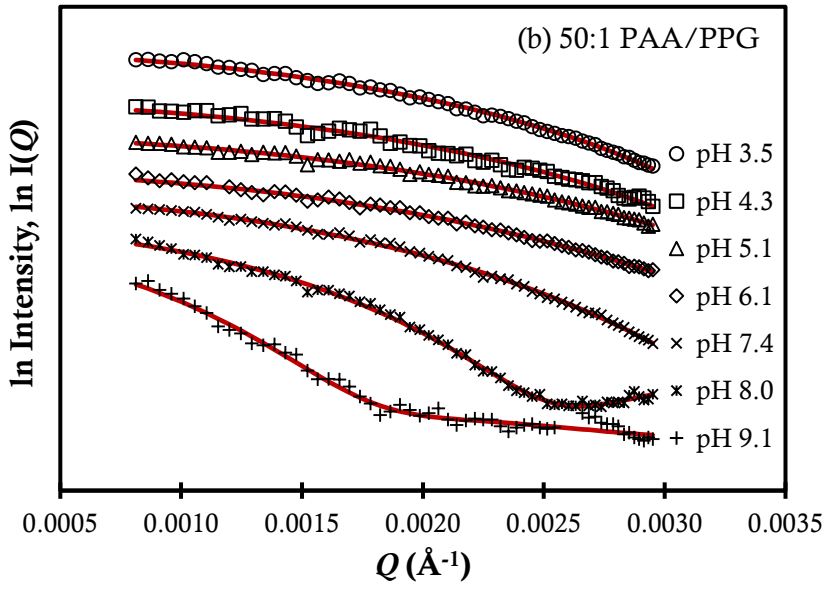

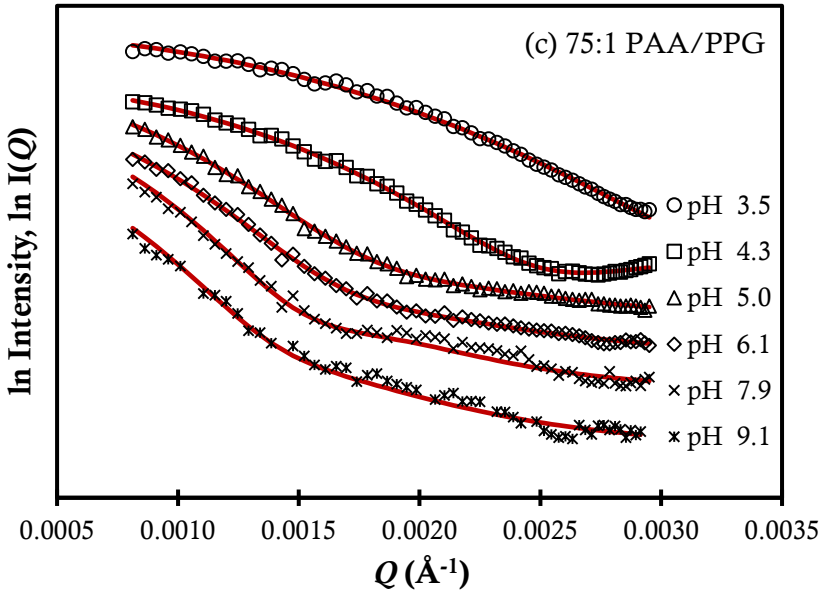
(c) 75:1 PAA/PPG
ln Intensity, ln I(Q)
pH 3.5
pH 4.3
pH 5.0
pH 6.1
pH 7.9
pH 9.1
0.0005
0.0010
0.0015
0.0020
0.0025
0.0030
0.0035
Q (Å-1)

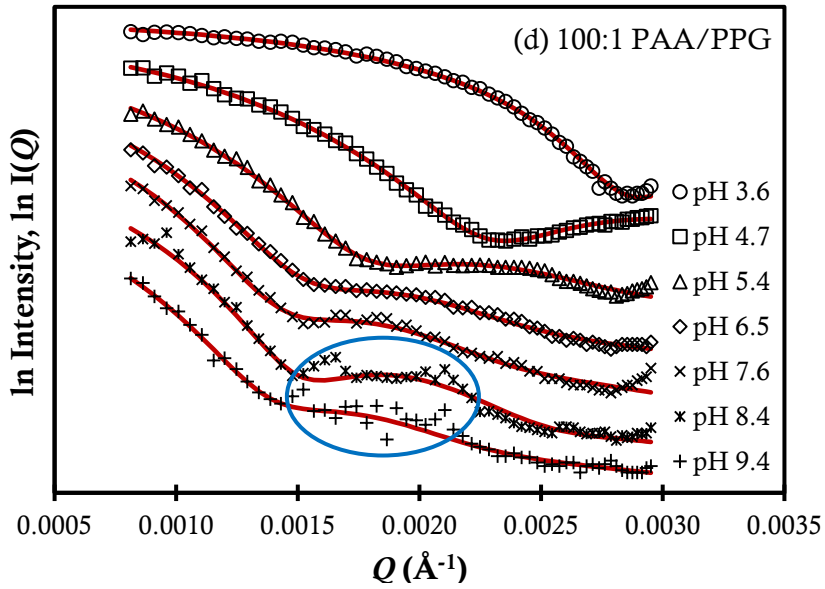
(d) 100:1 PAA/PPG
ln Intensity, ln I(Q)
pH 3.6
pH 4.7
pH 5.4
pH 6.5
pH 7.6
pH 8.4
pH 9.4
0.0005
0.0010
0.0015
0.0020
0.0025
0.0030
0.0035
Q (Å-1)

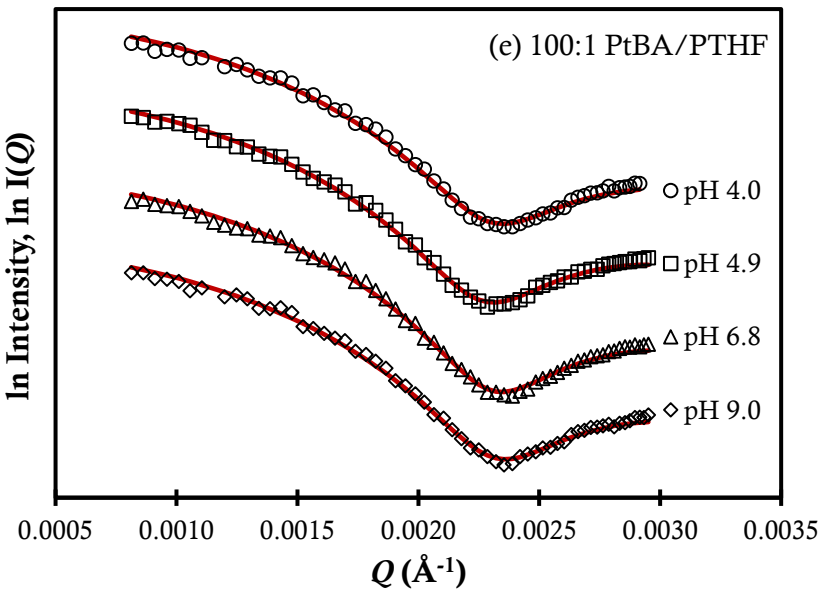
(e) 100:1 PtBA/PTHF
ln Intensity, ln I(Q)
pH 4.0
pH 4.9
pH 6.8
pH 9.0
0.0005
0.0010
0.0015
0.0020
0.0025
0.0030
0.0035
Q (Å-1)

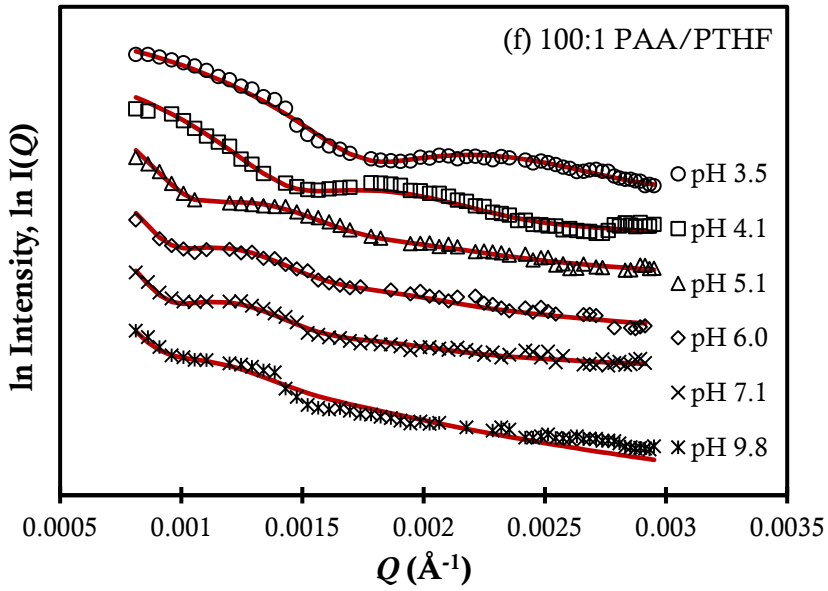

Figure 3.10 Scattering intensity profiles fitted using the SasView program with polydisperse sphere model of (a) 100:1 P*t*BA/PPG microparticles, (b) 50:1, (c) 75:1 and (d) 100:1 PAA/PPG microgels, (e) 100:1 P*t*BA/PTHF microparticles and (f) 100:1 PAA/PTHF microgels. (Parameters: sld_sphere = 1, sld_solvent = 0).

It is seen that the intensity curves of 100:1 P*t*BA/PPG, 50:1, 75:1 and 100:1 PAA/PPG, 100:1 P*t*BA/PTHF, and 100:1 PAA/PTHF microgels can be fitted very well with the polydisperse sphere model. However, the curves of 100:1 PAA/PPG microgels at pH = 8.4 and to a lesser extent at pH = 9.4 (see **Figure 3.10**(d)) have a few features around the first minimum of the form factor and beyond, that may be an indication of interparticle correlations/structure factor (not accounted for in the fitting process) becoming noticeable.

For 300:1 PAA/PTHF microgels, the polydisperse sphere model cannot fit the intensity curves properly, we therefore analysed this sample with a core-shell model and this will be discussed later.

The particle size of the microgels is as a function of pH illustrated by **Figure 3.11**(a), as expected, the 100:1 P*t*BA/PPG and 100:1 P*t*BA/PTHF particles are not pH-sensitive, while the swelling behaviour of PAA/PPG and PAA/PTHF microgels is pH-responsive. Moreover, a higher cross-linking density (50:1 > 75:1 > 100:1 PAA/PPG microgels) results in a smaller particle size consistent with the DLS experiments. The 75:1 and 100:1 PAA/PPG, and the 100:1 PAA/PTHF microgels gradually swell as the pH increases. Interestingly, the 50:1 PAA/PPG microgels only start to swell above pH 7. It is not clear why these particles should have a different swelling behaviour than the ones with lower crosslink densities.

In addition, considering the effect of the type of cross-linker, the particle size of 100:1 PAA/PTHF at all pH is a lot higher than the 100:1 PAA/PPG microgels as found previously in the section on the effect of hydrolysis.

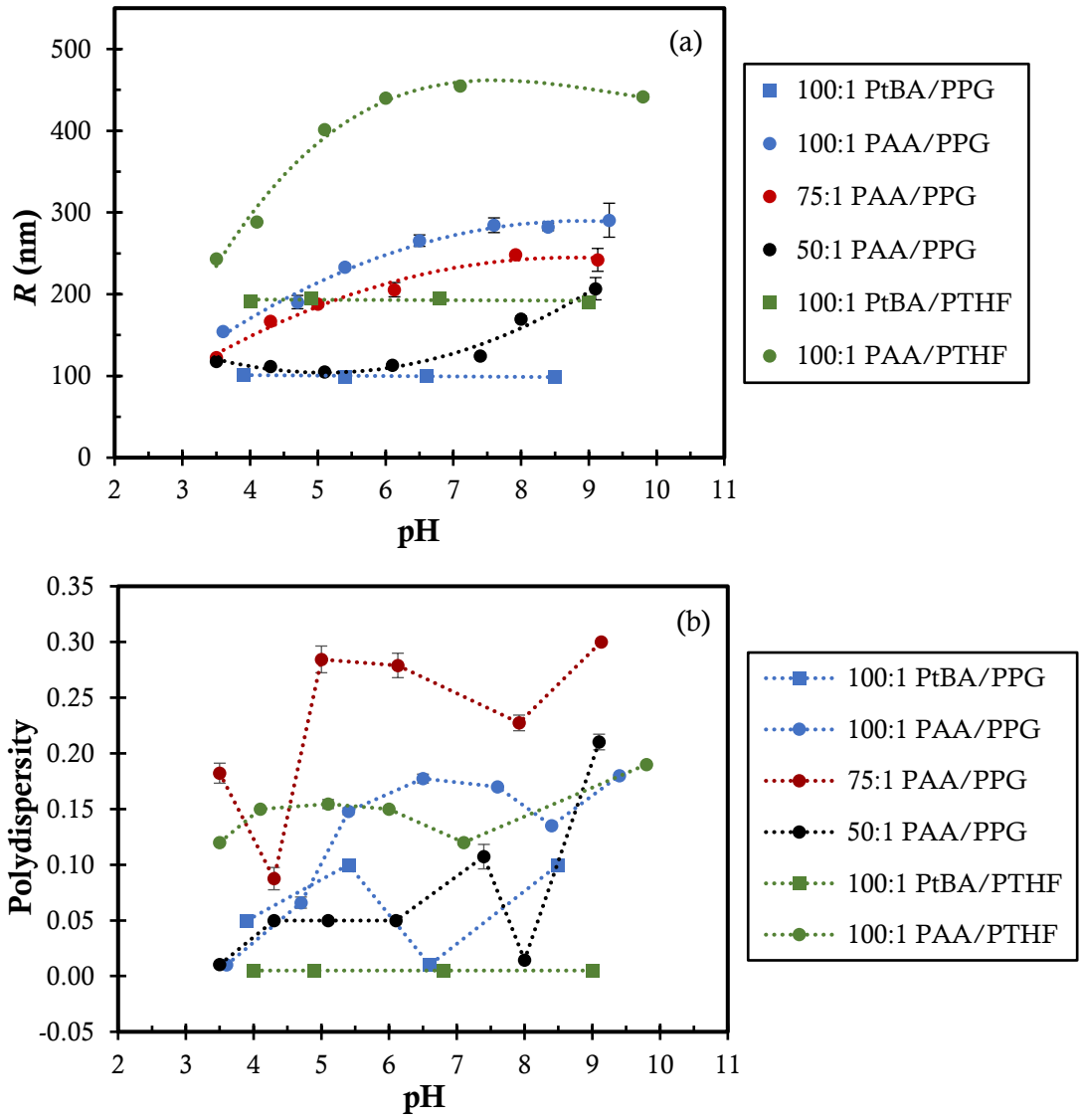

Figure 3.11 Effect of pH on (a) swelling behaviour and (b) polydispersity of 100:1 P*t*BA/PPG microparticles, 50:1, 75:1 and 100:1 PAA/PPG microgels, 100:1 P*t*BA/PTHF microparticle, and 100:1 PAA/PTHF microgels from SLS experiments, analysed with the SasView program using the polydisperse sphere model. (Parameters: sld_sphere = 1, sld_solvent = 0).

The polydispersity (PD; expressed as standard deviation in size divided by the mean size), which is a variable parameter during fitting the intensity curves as a function of pH is shown in **Figure 3.11**(b). The PD values of 100:1 P*t*BA/PPG, 50:1 PAA/PPG and 100:1 P*t*BA/PTHF are rather low in a range of 0 - 0.1, while the PD value of 100:1

PAA/PPG and 100:1 PAA/PTHF is higher mostly around 0.1 - 0.2 and the PD value of 75:1 PAA/PPG is very high up to 0.3. In section 3.3.1.1, we found that the PD value of swollen P*t*BA microparticles in organic solvents is in the range of 0.01 - 0.12. However, after hydrolysis of P*t*BA to PAA, the PD value of swollen PAA microgels is significantly higher than for the P*t*BA. We suggest that the hydrolysis reaction may cause a broader size distribution (or an inhomogeneous crosslink density) even though the hydrolysis reaction is highly successful according to ^{1}H-NMR results.

Moreover, we also attempted to analyse the SLS data using two other approaches: by determining the first minimum in the scattering curve and using Rayleigh-Gans-Debye (RGD) theory which predicts that the wave vector for the first minimum, Q_{min} is $4.49/R$; and using the Guinier approximation (see Appendix B). A limitation of this method is that we can calculate a particle size only when the plot of intensity vs angle shows the first angle of minimum intensity. Given the scattering angle range of 30 to 140 degrees, this limits this analysis to sphere radii ranging from 153 nm to 554 nm. Accordingly, from **Figure 3.10**(a) we cannot calculate the particle size of 100:1 P*t*BA/PPG microparticles at all pH and 50:1 PAA/PPG microgels at pH 3.5 – 7. For the Guinier approximation, a particle size is calculated from the slope of the linear region up to the limit $QR_G < 1$ in a plot of ln $I(Q)$ vs Q^2. Even although we only considered the slope of a linear relationship for scattering angles ranging from 30 to 60 degrees, we found that QR_G is often much higher than 1 since the particle sizes of the PAA microgels are too large in the swollen state.

We further considered the effect of cross-linking density and type of cross-linker on the swelling ratio of PAA microgels from the particle size in the swollen state (pH around 9) divided by the particle size at deswollen state (pH~3.5) as shown in **Table 3.5**.

Table 3.5 Particle size and swelling ratio of 50:1, 75:1 and 100:1 PAA/PPG microgels, and 100:1 PAA/PTHF microgels by comparing sizes at pH 9 and pH 3.5 using DLS and SLS experiments.

Sample	Radius at pH 3.5		Radius at pH 9		Swelling ratio ($R_{pH9}/R_{pH\ 3.5}$)	
	DLS (R_H, nm)	SLS (R, nm)	DLS (R_H, nm)	SLS (R, nm)	DLS	SLS
50:1 PAA/PPG	156 ± 1	118 ± 0.5	316 ± 14	207 ± 1.6	2.0 ± 0.1	1.8 ± 0.02
75:1 PAA/PPG	175 ± 1	123 ± 0.8	349 ± 14	242 ± 2.9	2.0 ± 0.1	2.0 ± 0.03
100:1 PAA/PPG	185 ± 1	154 ± 0.3	362 ± 21	291 ± 1.4	2.0 ± 0.1	1.9 ± 0.01
100:1 PAA/PTHF	-	243 ± 0.5	-	442 ± 3.3	-	1.8 ± 0.01

It is seen that the swelling ratio of PAA microgels is in a range of 1.8 – 2 consistent with the previous study of P*t*BA microparticles swollen in acetone and THF, given swelling ratios of 1.5 – 2.1. No effect of cross-linking density on the swelling ratio is visible here. Considering the effect of the type of cross-linker, 100:1 PAA/PPG microgels can swell better than 100:1 PAA/PTHF microgels.

In **Figure 3.12**, we present the shape factor (ρ) defined by R_G/R_H. Here, we did not further consider the shape factor of 100:1 P*t*BA/PTHF, 100:1 and 300:1 PAA/PTHF microgels since the results from DLS were erratic as mentioned previously. Theoretically, SLS is mainly sensitive to the size of the particle core (for particles with a dense core), while DLS will be more sensitive to any dilute "hairy" polymer shell around the centre of particle.

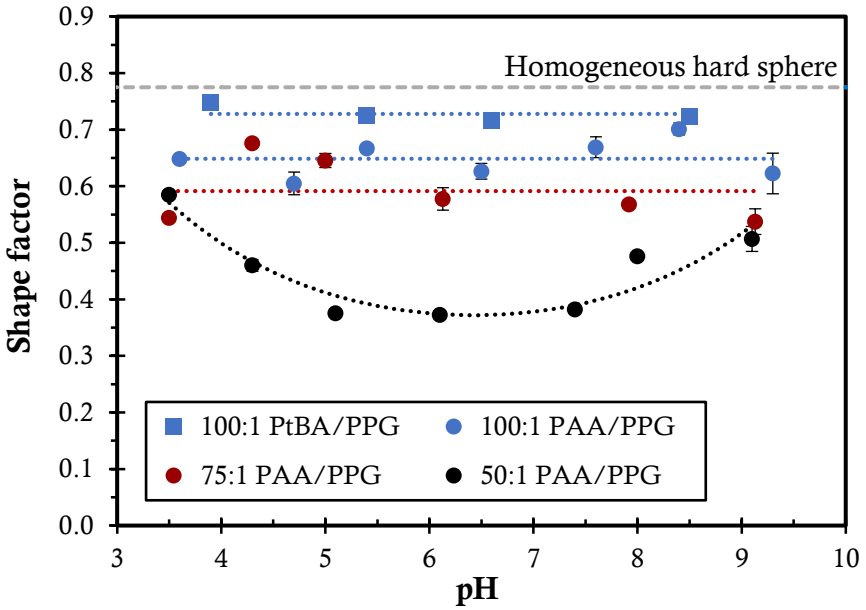

Figure 3.12 Shape factor (R_G/R_H) of 100:1 PtBA/PPG and 50:1, 75:1 and 100:1 PAA /PPG microgels calculated from DLS and SLS (analysing using with SasView software with polydisperse model).

The ρ value of P*t*BA microparticles is 0.72 - 0.75 which is very close to the homogeneous sphere value (0.775), whilst the value of 100:1 and 75:1 PAA/PPG microgels is 0.50 - 0.70 consistent with the typical value of microgels in which cross-linking density distribution is not similar throughout the particles or most likely the particles contain a dense core with a loose shell. Especially, the ρ value of 50:1 PAA/PPG microgels is rather low (0.37 – 0.6). Consequently, we suggest that PAA microgels have a core-shell structure and their swelling is heterogeneous.

As expected, the shape factor suggests that the structure of PAA/PPG microgels is a dense core with a loose shell but their scattering intensity can be fitted well with sphere model. However, as mentioned previously, the sphere model cannot fit the intensity curves of 300:1 PAA/PTHF microgels properly as shown in **Figure 3.13**(a). We first tried to analyse the intensity curves of 300:1 PAA/PTHF at pH 7 with a polydisperse core-shell model in which allows us to have two more variable parameters according to the additional shell layer. The values of sld_sphere and sld_solvent are set at 1 and 0, respectively so that when sld_shell is 0.5 or 2 it could be attributed to the dense core with loose shell or the capsule structure (loose core and dense shell), respectively.

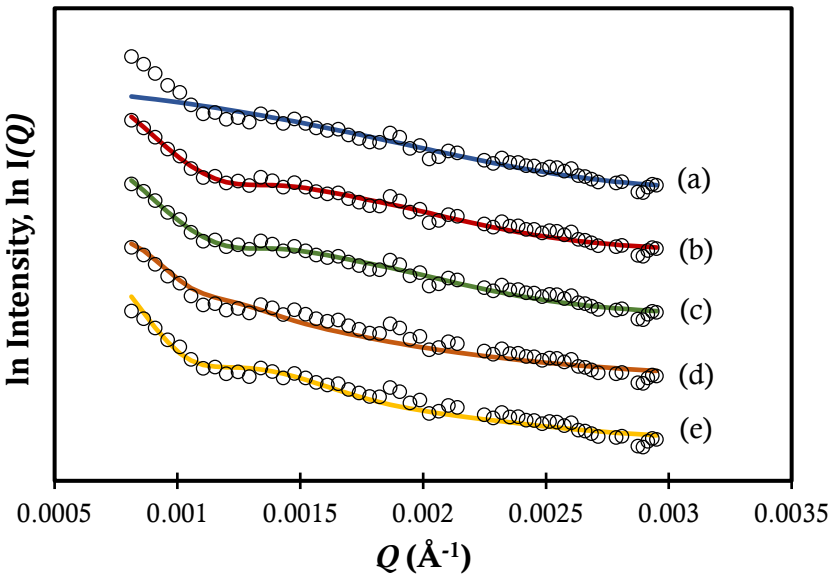

Figure 3.13 Scattering intensity profiles of 300:1 PAA/PTHF microgels at pH 7 fitted with the SasView program using polydisperse sphere model with (a) PD_sphere = 0.2, and polydisperse core-shell model with (b) sld_shell = 0.5, PD_core = 0.2, PD_shell = variable, (c) sld_shell = 0.5, PD_core = variable, PD_shell = variable, (d) sld_shell = 2, PD_core = 0.2, PD_shell = variable and (e) sld_shell = 2, PD_core = variable, PD_shell = variable. All conditions: sld_core = 1 and sld_solvent = 0.

In **Figure 3.13**(b-e), it is seen that the core-shell model can fit the 300:1 PAA /PTHF data at pH 7 very well for both values of sld_shell (0.5 and 2). Although the microgels could have a capsule structure, we consider it more likely that the structure of 300:1 PAA/PTHF microgels is a core-shell. Such a scenario with a denser particle core and a more dilute corona is often seen for microgels.[22]

The radius of core (R_{core}), shell thickness (T_{shell}) and polydispersity of core (PD_core) and shell (PD_shell) analysed with the core-shell model are listed in **Table 3. 6**. The core size fitted with the sphere model is much lower than the sizes fitted with the core-shell model. For fitting with a core-shell model (b) and (c), the total radius of 300:1 PAA/THF is very large about 720 nm (containing of the core 430 nm and the shell 290 nm), while the radius of 100:1 PAA/PTHF microgels from the sphere model is about 455 nm close to the core size of 300:1 PAA/PTHF at pH 7. However, for core-shell capsule (d) and (e), the total radius is different from each other depending on the PD value.

In addition, the PD value of all experiments is rather high (0.1 – 0.31) which could mean that the size of distribution of 300:1 PAA/PTHF is very broad.

Table 3. 6 Radius of core (R_{core}) and shell thickness (T_{shell}) for 300:1 PAA/PTHF microgels at pH 7.0 fitted with the SasView program using (a) polydisperse sphere model and (b, c) polydisperse core-shell model.

Model	sld_shell	R_{core} (nm)	T_{shell} (nm)	R_{total} (nm)	PD core	PD shell
(a) Sphere	0	119 ± 2	-	119 ± 2	0.20 (fixed)	-
(b) Core-shell (dense core-loose shell)	0.5 (fixed)	432 ± 9	290 ± 2	722 ± 9	0.20 (fixed)	0.25
(c) Core-shell (dense core-loose shell)	0.5 (fixed)	434 ± 14	290 ± 3	724 ± 14	0.19	0.25
(d) Core-shell (capsule)	2 (fixed)	504 ± 26	119 ± 28	623 ± 38	0.20 (fixed)	0.10
(e) Core-shell (capsule)	2 (fixed)	222 ± 25	125 ± 25	348 ± 36	0.31	0.10

We then further fitted the intensity curves of 300:1 PAA/PTHF at all pH following the same set-up conditions as pH 7 above and the total radius (R_{core}+T_{shell}) is plotted as a function of pH illustrated by **Figure 3.14**.

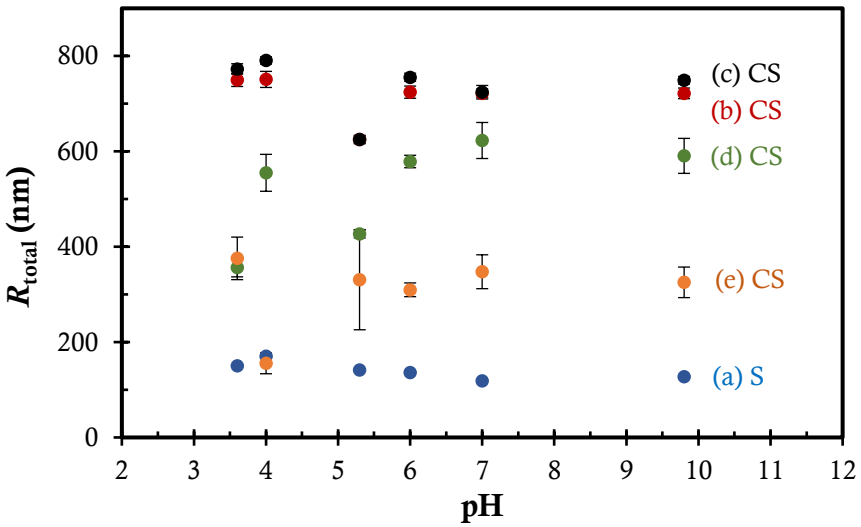

Figure 3.14 Total radius ($R_{total} = R_{core} + R_{shell}$) of 300:1 PAA/PTHF microgels as a function of pH fitted with the SasView program using polydisperse sphere model (S) with (a) PD_sphere = 0.2, and polydisperse core-shell model (CS) with (b) sld_shell = 0.5, PD_core = 0.2, PD_shell = variable, (c) sld_shell = 0.5, PD_core = variable, PD_shell = variable, (d) sld_shell = 2, PD_core = 0.2, PD_shell = variable and (e) sld_shell = 2, PD_core = variable, PD_shell = variable. All conditions: sld_core = 1 and sld_solvent = 0.

We here attempted to analyse the intensity curves of 300:1 PAA/PTHF microgels using the sphere and core-shell models with various set-up conditions, the results are still not promising. **Figure 3.14** reveals that the 300:1 PAA/PTHF microgels are not pH-responsive for all fitting conditions and the radius of particles is very high. In addition, we found that fitting with the core-shell model is rather complicated due to the larger number of parameters than for the sphere model. As a consequence, the fit results may be misleading, even although the curves can be fitted very well. Potentially, aggregates were present in this sample which hampered the data analysis.

Finally, a few additional experiments were carried out to explore the effect of salt and of adding free PEO on the swelling of PAA/PPG microgels.

3.3.2.3 Effect of salt

Apart from the pH response, the swelling behaviour of PAA microgels is also sensitive to the ionic strength. At swollen state of microgels, the addition of salt decreases the electrostatic repulsion between ionized groups which leads to a decrease of osmotic pressure difference between microgel networks and the external solution. However, at pH close to pK_a (around 5) it is possible that the addition of salt may initially swell the gels and at a high salt concentration the gels subsequently deswell as mentioned previously (see **Figure 3.2**).

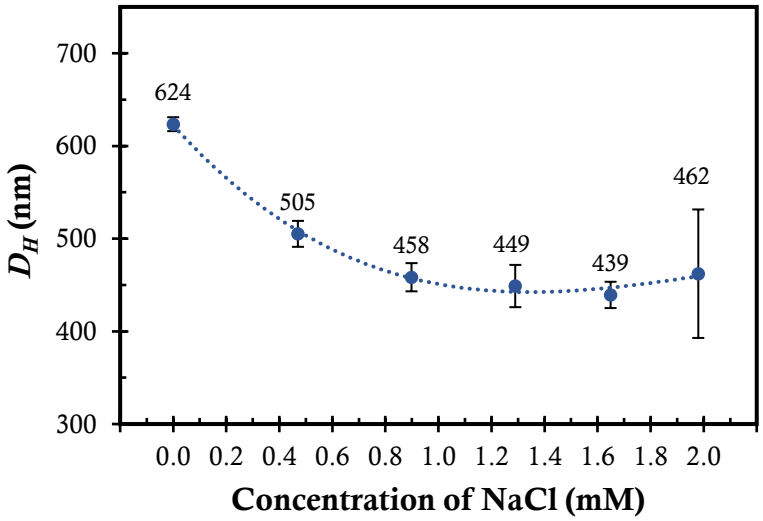

Figure 3.15 Effect of salt solution on hydrodynamic diameter (D_H) of 100:1 PAA/PPG microgels at pH 4.5.

In **Figure 3.15**, it can be seen that the increasing salt concentration causes a noticeable shrinkage of the PAA microgels even though at pH 4.5 and the NaCl concentrations are quite low (of order mM). However, when the salt concentration is above 0.9 mM, the PAA microgel size remains constant and the data point at 2.0 mM has a rather high standard deviation. It is however not likely that aggregation is already taking place at such a modest salt concentration.

3.3.2.4 Effect of PEO

This experiment was carried out to investigate the interaction between PAA microgels with PEO through hydrogen bonding so that to explore the possibility of PAA microgels to be used as carriers for small active ingredients.

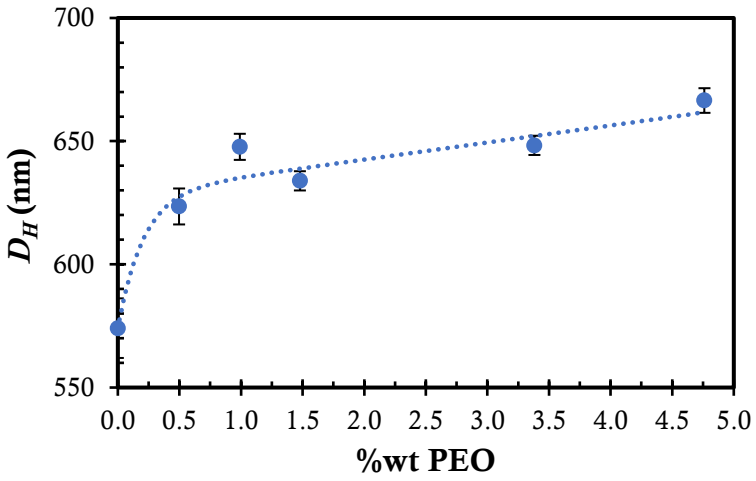

Figure 3.16 Effect of PEO M_w 200 on the swelling behavior of 100:1 PAA/PPG microgels at pH 4.5.

The hydrodynamic diameter (D_H) of PAA microgels dispersed in water is 574 nm was measured by DLS. We found a significant increase in the particle size of PAA microgels when 0.5%wt PEO is added, and further increasing the PEO content gradually increases the particle diameter of PAA microgels as shown in **Figure 3.16**. The initial increase in particle diameter could be due to association between the PAA microgels and PEO. However, when PEO is more added, the further increase in size may be in part due to an increasing viscosity of the solution (a constant viscosity was assumed in analyzing these DLS results). In addition, we suggest that the aggregation of the microgels due to depletion interactions induced by the added PEO is not likely here because of the low molecular weight of the PEO, and because this would give rise to a sudden onset of aggregation as a critical PEO concentration is reached.

3.3.3 Zeta potential

The zeta potential (ζ-potential) of microgels was measured as a function of pH. Results are presented in **Figure 3.17** for both P*t*BA/PPG and PAA/PPG microgels is investigated as a function of pH. It is seen that all samples have negative charges at all pH values (there is no isoelectric point visible in this experiment). Since we prepared the microgels via surfactant free emulsion polymerization using KPS (potassium persulfate) as an ionic initiator, the particles carry negative charges on their surface which is beneficial to stabilize the particles dispersed in water and prevent the agglomeration of particles. The ζ-potentials of P*t*BA microparticles are significantly higher than those of the PAA microgels. We suggest that the hydrolysis reaction of P*t*BA to PAA reduces the negative charges on the surface of PAA. In addition, when pH increases the ζ-potential of PAA microgels increases as a result of formation of carboxylate anions. There is only a slight dependence of ζ-potential on the cross-linking density, with the values for 50:1 PAA/PPG being slightly lower than for 75:1 and 100:1 PAA/PPG microgels. Above we also observed that the swelling as a function of pH of these PAA microgels is not very dependent on cross-linking density.

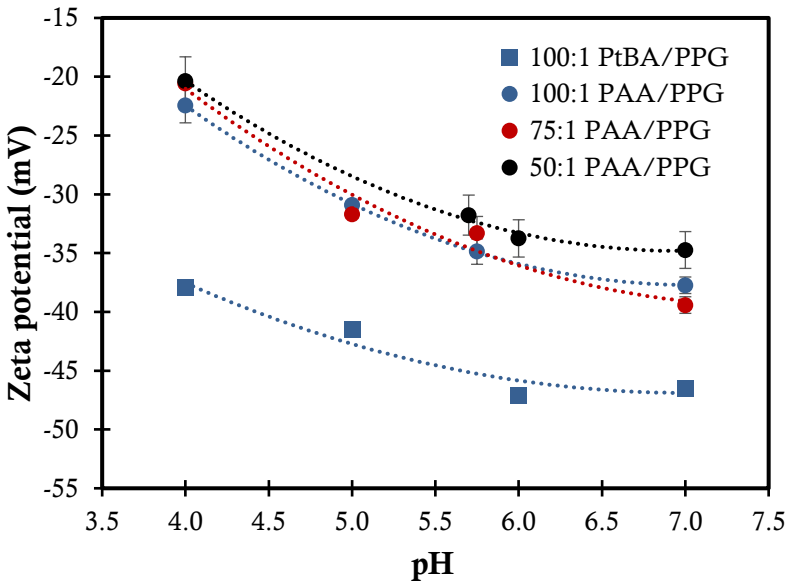

Figure 3.17 Effect of pH on zeta potential (ζ-potential) of 100:1 P*t*BA/PPG microparticles, 50:1, 75:1 and 100:1 PAA/PPG microgels.

Conclusion

In this chapter, we measured the particle size of P*t*BA and PAA microparticles using both DLS and SLS techniques. For the SLS experiments, the scattering intensity was analysed using the SasView program with a polydisperse sphere model except for the 300:1 PAA /PTHF microgels where we also used a core-shell model. In addition, with the combination of DLS and SLS, we can investigate the cross-linking density distribution of microgels through the dimensionless shape factor ($\rho = R_G/R_H$).

P*t*BA microparticles can swell in THF and in acetone but not in water, and the swelling ratio varied little across the fairly narrow range of cross-linking densities studied. The polydispersity (PD; expressed as standard deviation in size divided by the mean size) of P*t*BA microparticles in all solvents obtained from the SasView program was in the range of 0.01 - 0.12 indicating a narrow size distribution of the particles. In addition, the shape factor of P*t*BA was in the range of 0.6-0.8, close to the value for homogeneous sphere (0.775). This suggests that these P*t*BA microparticles are homogeneously swollen.

After that, we investigated the particle size of P*t*BA before and after hydrolysis to PAA microgels. Well-defined PAA microgels were obtained, and their sizes are larger than those of the P*t*BA precursors as a result of the PAA being hydrophilic and somewhat hydrated, even in the collapsed state at low pH.

Then we studied the swelling behaviour of P*t*BA and PAA microgels as a function of pH. P*t*BA particles are not sensitive to pH, whilst PAA microgels swell better at higher pH due to ionization of carboxylic acid as found in both SLS and DLS. Particles swell by at most a factor of 2.0 for PAA/PPG and by a similar factor of 1.8 for PAA/PTHF upon changing pH from 3.5 to 9. However, effect of cross-linking density on the swelling ratio is not visible for both DLS and SLS results. The PD values of most microgels were in a range of 0 - 0.2 except the PD value of 75:1 for PAA/PPG which is very high up to 0.3. The shape factor (ρ) of P*t*BA particles is consistent with homogeneous spheres as expected, while the ρ value of PAA microgels was in the range of 0.50 to 0.70, in line with other studies on microgels particles. The exception was the ρ value of 50:1 PAA/PPG which had a rather low shape factor (0.37 – 0.6).

Moreover, we found a difficulty in measuring the particle sizes of 300:1 PAA/PTHF using DLS and SLS; both gave erratic results. It is not clear what caused these issues, perhaps some aggregates were present.

In addition, we found that a small amount of salt reduces the swelling of 100:1 PAA/PPG microgels, while the addition of PEO increases the particle size of 100:1 PAA/PPG at pH 4.5 which might be due to association between the microgels with PEO through hydrogen bonding.

Bibliography

1. J. A. Bonham, F. Waggett, M. A. Faers, J. S. van Duijneveldt. *Colloid and Polymer Science* **2017**, *295*, 479-486.

2. A. K. Bajpai, S. K. Shukla, S. Bhanu, S. Kankane. *Progress in Polymer Science* **2008**, *33*, 1088-1118.

3. S. K. Ahn, R. M. Kasi, S.-C. Kim, N. Sharma, Y. Zhou. *Soft Matter* **2008**, *4*, 1151-1157.

4. W. A. Laftah, S. Hashim, A. N. Ibrahim. *Polymer-Plastics Technology and Engineering* **2011**, *50*, 1475-1486.

5. A. R. Khare, N. A. Peppas. *Biomaterials* **1995**, *16*, 559-567.

6. D. Klinger, K. Landfester. *Polymer* **2012**, *53*, 5209-5231.

7. R. Marcombe, S. Q. Cai, W. Hong, X. H. Zhao, Y. Lapusta, Z. G. Suo. *Soft Matter* **2010**, *6*, 784-793.

8. G. S. Longo, M. O. de la Cruz, I. Szleifer. *Macromolecules* **2011**, *44*, 147-158.

9. A. A. Polotsky, F. A. Plamper, O. V. Borisov. *Macromolecules* **2013**, *46*, 8702-8709.10. M. Y. Zhang, Z. Q. Cheng, T. Q. Zhao, M. Z. Liu, M. J. Hu, J. F. Li. *Journal of Agricultural and Food Chemistry* **2014**, *62*, 8867-8874.

11. O. E. Philippova, D. Hourdet, R. Audebert, A. R. Khokhlov. *Macromolecules* **1997**, *30*, 8278-8285.

12. Y. Guan, W. W. Jiang, W. C. Zhang, G. X. Wan, Y. X. Peng. *Journal of Polymer Science Part B: Polymer Physics* **2001**, *39*, 1784-1790.

13. L. Bromberg, M. Temchenko, T. A. Hatton. *Langmuir* **2002**, *18*, 4944-4952.

14. K. T. Oh, T. K. Bronich, V. A. Kabanov, A. V. Kabanov. *Biomacromolecules* **2007**, *8*, 490-497.

15. Y. Sun, 'Different particle information obtained from static and dynamic laser light scattering', Master of Science Thesis,Simon Fraser University, **2004**.
16. C. Fraschini, G. Chauve, J. F. Le Berre, S. Ellis, M. Methot, B. O'Connor, J. Bouchard. *Nordic Pulp & Paper Research Journal* **2014**, *29*, 31-40.
17. S. Bhattacharjee. *Journal of Controlled Release* **2016**, *235*, 337-351.
18. D. Kunz, A. Thurn, W. Burchard. *Colloid and Polymer Science* **1983**, *261*, 635-644.
19. B. M. Tande, N. J. Wagner, M. E. Mackay, C. J. Hawker, M. Jeong. *Macromolecules* **2001**, *34*, 8580-8585.
20. M. Dulle, S. Jaber, S. Rosenfeldt, A. Radulescu, S. Forster, P. Mulvaney, M. Karg. *Physical Chemistry Chemical Physics* **2015**, *17*, 1354-1367.
21. N. Boon, P. Schurtenberger. *Physical Chemistry Chemical Physics* **2017**, *19*, 23740-23746.
22. B. Sierra-Martin, J. R. Retama, M. Laurenti, A. F. Barbero, E. L. Cabarcos. *Advances in Colloid and Interface Science* **2014**, *205*, 113-123.
23. H. W. Chen, C. H. Tu. *Journal of Chemical & Engineering Data* **2005**, *50*, 1262-1269.
24. T. M. Aminabhavi, B. Gopalakrishna. *Journal of Chemical & Engineering Data* **1995**, *40*, 856-861
25. D. R. Lide. Handbook of chemistry and physics; CRC Press: Boca Raton, Florida, USA, **2004**.
26. A. Jouyban. Handbook of solubility data for pharmaceuticals; CRC Press: Boca Raton, Florida, USA, **2010**.
27. M. Mohsen-Nia, H. Amiri, B. Jazi. *Journal of Solution Chemistry* **2010**, *39*, 701-708.
28. P. C. Huang, J. P. Mata, C. M. Wu, C. T. Lo. *Langmuir* **2018**, *34*, 7416-7427.
29. W. Schärtl. Light scattering from polymer solutions and nanoparticle dispersions; Springer: Berlin, **2007**.
30. M. S. Wolfe, C. Scopazzi. *Journal of Colloid and Interface Science* **1989**, *133*, 265-277.
31. M. Antonietti, W. Bremser, M. Schmidt. *Macromolecules* **1990**, *23*, 3796-3805.
32. E. Jabbari, S. Nozari. *European Polymer Journal* **2000**, *36*, 2685-2692.

Chapter 4

The association of PAA and poly(ethers) in solution

Abstract

Polymer gels are three-dimensional networks formed by physical and/or chemical interactions. In our study, we are focusing on the physical association between the carboxylic acid of poly(acrylic acid) (PAA) and ether group of poly(ethers) which are poly(ethylene oxide) (PEO) and poly(tetrahydrofuran) (PTHF), via hydrogen bonding. In general, complexes of PAA and PEO can be formed by hydrogen bonding in acidic condition[1-4] while the use of PTHF is a new challenge as PTHF is almost insoluble in water. Instead of aqueous media, methanol is used as a solvent for the PAA/PTHF system. We also consider effects of concentration, weight ratio between PAA and poly(ethers), molecular weight, and types of polymer and solvent on the formation of hydrogen bonding. Apart from considering the chemical shift with ^{1}H-NMR, Diffusion Ordered NMR Spectroscopy (DOSY) and T_2 solvent relaxation are used to probe the hydrogen bonding of PAA and poly(ethers) from self-diffusion coefficients (D_s) and relaxation rates (R_2), respectively. From ^{1}H-NMR spectra, we only found a very small upfield shift to lower ppm due to hydrogen bonding from the low M_w PAA/poly(ethers) solutions. The first signs of hydrogen bonding are found in low M_w PAA (5000)/PEO (5000) in pH 3 solutions observed by DOSY-NMR. We found white aggregates formed by very high M_w PAA (4,000,000)/PEO (4,000,000) at volume ratios 20:80, 40:60, 50:50 and 60:40 which are evidence of strong hydrogen bonding in pH 3 solutions consistent with the results of DOSY and T_2 solvent relaxation.

4.1 Introduction

The preparation of polymer gels via physical interactions *i.e.* molecular entanglements, and/or secondary forces including ionic, hydrogen bonding or hydrophobic forces is of interest as the formation of such polymer networks is reversible by change in external conditions such as temperature,[5,6] pH and application of stress.[7,8] For example, protonated carboxymethyl cellulose (CMC) can form a three-dimensional network structure through hydrogen bonding and precipitate from the solution in acidic conditions and the network is broken at a high pH.[7] Kaushlendra and Asha[9] prepared a pyrene labelled polymer using short spacer pyrene monomer which was developed by coupling 2-isocyanatoethyl methacrylate with 1-pyrenemethanol. Self-association formed by hydrogen bonding between its urethane linkages (amine group (-N**H)** and carboxyl oxygen (C=**O**)) was investigated by ^{1}H-NMR. The peak of bonded amine protons (-N**H)** appears at 7.34 ppm at 25°C and when the temperature is increased, hydrogen bonding is weakening and thus the peak is shifted upfield to 7.07 ppm at 70 °C.

Hydrogen bonding is a non-covalent, attractive interaction between partial negative charges of electronegative atoms (containing lone pair electrons *i.e.* F, O, or N) and partial positive charges of hydrogen atoms (form polar covalent bond with high electron negativity *i.e.* F, O or N) in the same or in different molecule.[10]

$$\overset{\delta^{\ominus}}{X} - \overset{\delta^{\oplus}}{H} \bullet\bullet\bullet\bullet \overset{\delta^{\ominus}}{Y} \qquad (4.1)$$

Here the H atom is a hydrogen bond donor, the Y atom is a hydrogen bond acceptor, and the electron clouds on the X-H bond are pulled towards the X atom (higher electronegativity) resulting in a partial negative region on the X atom and a partial positive region on the H atom.

In our study, we are focusing on the complexation between poly(acrylic acid) (PAA) and poly(ethers) (poly(ethylene oxide), PEO and poly(tetrahydrofuran), PTHF). PAA is well known for self-association via hydrogen bonding of its carboxyl (-COOH) groups and it forms densely globular structures at low pH (below 3). When pH increases, the carboxyl groups are ionised to carboxylate anions (-COO^{-}) so the electrostatic repulsion between adjacent carboxylate groups leads to the decrease of self-hydrogen bonding and the expansion of the polymer chain into a fully solvated open coil conformation.[11-13] Especially, Swift *et al.*[13] found the pH-induced conformational change only occurs when the molar mass of PAA is greater than 16,500 g/mol, while low M_w PAA

exhibits only the extended conformation. Poly(ethylene oxide) (PEO) has a repeating unit with two methylene groups and one ether oxygen atom, [-$(CH_2)_2O$-]. PEO is water-soluble and its solubility relies on hydrogen bonding in aqueous solution. The conformation of PEO in water is still under study although a wide variety of data exists.[14-18] Karlstrom[14] studied the phase diagram of PEO in water using Flory-Huggins theory. Each segment of the PEO chains can take up one of two conformations, according to the rotation around C-C and C-O bonds. For the low-temperature forms, the C-C bonds are mainly gauche and the majority of C-O bonds are trans. This conformational form provides a rather large dipole moment which enhances the interaction with water. For the high-temperature forms, the other conformations providing a lower dipole moment will be more dominant resulting in a lower solubility in water. Tasaki[15] studied the conformation of PEO in water using computer simulations. The conformation of PEO is transformed from a collapsed coil in the gas phase to a helical structure in water as a result of hydrogen bonds of PEO/water and water/water including a bridged hydrogen bond of two protons of a water molecule bridging between oxygen atoms from two different ether units of PEO chains. Moreover, the end groups of PEO also play an important role in the solubility of PEO. Hammouda *et al.*[17] studied the effect of chain ends of PEO on the phase separation of PEO in aqueous solution. Three different chain ends of PEO: HO···OH, HO···CH_3 and CH_3···CH_3 were investigated. They found that for HO···OH chain ends PEO chains are soluble in water, whilst for CH_3···CH_3 chain ends PEO forms a network due to the hydrophobic interaction of –CH_3 end groups with other main chains of PEO, and HO···CH_3 end groups provide a branched structure of PEO.

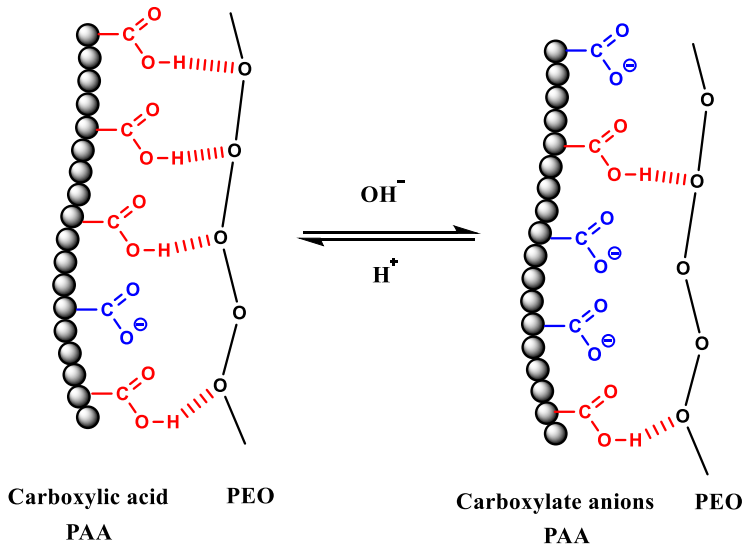

Figure 4.1 Effect of pH of solution on the hydrogen bonding between carboxyl (-COOH) groups of PAA and oxygen ethers $(-CH_2CH_2O-)_n$ of PEO.

The complexation between polyacids and PEO has been widely studied. For example, polycarboxylic acids such as poly(acrylic acid) (PAA) and poly(methacrylic acid) (PMAA), which contain carboxyl groups, can associate with ether oxygens of poly(ethylene glycol) (PEG) via hydrogen bonding in acidic condition as shown in **Figure 4.1**. Bailey *et al.*[1] investigated the influences of pH, temperature, composition and concentration on the hydrogen bonds of PAA and PEO by determining the viscosity of mixtures of PAA and PEO in solution. They found that the complexation between very high M_w PAA and PEO (M_v 1,000,000) induces the precipitation of PAA / PEO when the pH is below 3.8 and at a total polymer concentration of 2%w/v. The viscosity sharply decreases over the range of pH 4 to 6 and then remains stable from pH 7 to 12. At higher pH, the viscosity reduces again and precipitation is observed. In pH 4 solutions, the best condition for H-bonding causing a maximum viscosity is seen at the stoichiometric ratio of PAA and PEO = 1:1 with the total concentration = 0.5%wv and 6%wv for high M_w and low M_w PAA/PEO mixture, respectively. Pradip *et al.*[3] used fluorescence spectroscopy to determine the interaction of pyrene-labelled PAA with PEO in aqueous solution. They also asserted that H-bonding between PAA and PEO can be formed only under acidic conditions (below pH 4.5), and the most effective hydrogen bonding is at 1:1 stoichiometry. Recently, Swift *et al.*[19] studied the interpolymer complexes between PAA and various types of polymer such as PEO and PNIPAM with fluorescence anisotropy and light scattering. Although the calculated size of pure polymers in acid solutions has a large standard error due to their weak scattering signals compared to the complexes suspended

in the media, it is clearly seen that the particle size of the complexes is significantly larger than the pure polymers.

Even though PAA/PEO complexes have been widely reported, the study of the complexation between PAA and poly(tetrahydrofuran) (PTHF) is still limited. PTHF is a hydrophobic polymer having a repeat unit with four methylene groups and one ether oxygen atom, [-$(CH_2)_4O$-]. The ether oxygen improves the solubility in polar solvents including water for very low M_w PTHF. Typical solvents for PTHF are alcohols, benzene, toluene, THF, chlorobenzene, ethyl acetate, chloroform etc.[20] However, the PTHF used in our study is only sparingly soluble in water so for the PAA/PTHF system we cannot use water as a solvent. Considering the solubility of PAA and PTHF, methanol which is a weak proton-donating solvent could be a good candidate for being used as a solvent for association of PAA/PTHF system. However, we cannot find references for the complex of PAA/poly(ethers) in pure methanol, while the association of PAA/PEO in water/methanol mixed solvent has been studied previously. Ikawa *et al.*[2] found that PAA (M_n 100,000) or PMAA (M_n 147,000) can form a complex with PEO only when the PEO has sufficiently long chains, referred to as the critical chain length. For water-methanol mixed solvent (0, 25 and 50%wt methanol content), the critical chain length of PEO for PAA/PEO is with degree of polymerization (N) = 200 (M_w around 8,800) and independent of methanol content. However, the critical chain length of PEO for PMAA/PEO is increased from N = 40 (M_w around 1,800) in 0%metahnol to 120 (M_w around 5,300) in 50%wt methanol at 3 mM total concentration of mixed polyacid/PEO. This suggests that the interaction between PMAA and PEO is stronger than that between PAA and PEO as a result of hydrogen bonding as well as hydrophobic interaction in aqueous solution. However, the presence of methanol might weaken the hydrophobic interaction between PMAA and PEO. Ahn *et al.*[21] also reported that the complex of PAA and PEO in water is more favourable than in water/methanol mixed solvent because in water the complex formation is stabilized with hydrogen bonding and hydrophobic interaction, while in water/ methanol the complex is mainly stabilized by hydrogen bonding. Therefore, the association between PAA and PTHF in methanol might be feasible owing to the ether oxygen of PTHF and carboxyl group of PAA but it could be rather weak compared with PAA/PEO in aqueous solutions. The objectives of this chapter are to investigate the complex formation between PAA and PEO in acidic solution or methanol, and PAA and PTHF in methanol via hydrogen bonding as a function of concentration, M_w and polymer mixing ratio, and to evaluate the use of ^{1}H-NMR, DOSY and T_2 solvent relaxation techniques to characterise the hydrogen bonding.

4.2 Experimental

4.2.1 Materials

All polymers are listed in **Table 4.1** and were used without any further purification. Deuterium oxide (D_2O, 99.7%) and Deuterium chloride (DCl, 35%wt in D_2O) were obtained from Sigma-Aldrich. Polydispersity index ($\bar{M}_w/\bar{M}_n$) of PAA M_w 273,000 and PTHF M_w 6000 is 1.51 and 1.1, respective. All polymers were used without further purification.

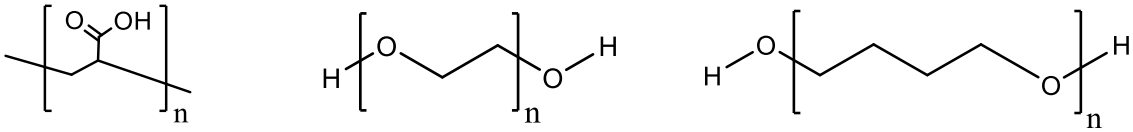

Poly(acrylic acid) (PAA) | Poly(ethylene oxide) (PEO) | Poly(tetrahydrofuran) (PTHF)

Figure 4.2 Chemical structures of PAA, PEO and PTHF.

Table 4.1 List of polymers and M_w of polymers.

Polymer	M_w of repeating unit (g/mol)	M_w (g/mol)	Number of repeating units (n)	Manufacturer
PAA	72	5000	69	Acros
		273,000	3,800	Polymer Laboratories
		4,000,000	56,000	Aldrich
PEO	44	200	5	Sigma-Aldrich
		5,000	120	Fluka
		300,000	6,800	Aldrich
		4,000,000	91,000	Aldrich
PTHF	72	250	4	Aldrich
		1,000	14	Aldrich
		6,000	83	Polymer Laboratories

4.2.2 ^{1}H-NMR and DOSY

Proton NMR (^{1}H-NMR) is very useful to observe hydrogen bonding providing both qualitative and qualitative information. In general, hydrogen bonding reduces the valence electron density around the bonded protons (the proton is deshielded) contributing to a downfield shift to a higher frequency (ppm).[22] However, the hydrogen bonding is highly dependent on concentration, temperature and solvent medium so these factors also affect the downfield and upfield shift of the bonded protons. For example, Bekiroglu *et al.*[23] found that at the mole ratio of methanol : water = 1:1, the –O**H** protons of methanol show a downfield shift (to higher ppm) with the chemical shift difference ($\Delta\delta$) = 0.15 ppm, while the –C**H**$_3$ protons of methanol slightly shift upfield (to lower ppm) with the $\Delta\delta$ value = 0.05 ppm compared to the proton peaks of pure methanol. However, the addition of solvents containing ether groups (*i.e.* THF, diethyl ether, and dioxane) results in a significant upfield shift of the –O**H** in methanol but the δ value of -C**H**$_3$ protons of methanol is unchanged.

Apart from considering the change of chemical shift in ^{1}H-NMR spectra, we also investigate the hydrogen bonds by diffusion ordered spectroscopy (DOSY NMR), which is a technique to identify NMR signals of mixed compounds in solution according to their different diffusion coefficients (D). The NMR signal intensity is attenuated depending on the diffusion time (Δ) and the gradient parameters (g, δ) as described by the Stejskal and Tanner equation:[24,25]

$$I = I_0 \exp(-D\gamma^2 g^2 \delta^2 (\Delta - \delta/3)) \qquad (4.2)$$

where I is the observed intensity, I_0 is the reference intensity (unattenuated signal intensity), D is diffusion coefficient (m^2 s^{-1}), γ is the gyromagnetic ratio of the observed nucleus (4257 s^{-1} G^{-1} for proton), g is gradient strength (G/m), δ is gradient diffusion length (s) and Δ is diffusion time (s). The DOSY NMR technique measures self-diffusion of particles in solution according to the self-correlation of particle velocity of the same nucleus at time t and at t+Δ.[26]

At infinite dilution, the self-diffusion coefficient (D) of polymer molecules depends on the friction coefficient according to the Debye-Einstein theory:[27-29]

$$D_0 = \frac{k_B T}{f_0} \qquad (4.3)$$

where D_0 is the diffusion coefficient (m^2/s), k_B is Boltzmann's constant (1.38065×10^{-23} J/K), T is absolute temperature (K), f_0 is the friction coefficient and $f_0 = 6\pi\eta a$ for the translational diffusion of a spherical particle of radius a in a continuum of viscosity η. The subscript '0' refers to infinite dilution.

The self-diffusion coefficient (D_s) in dilute solution can be approximated by Equation (4.4) under the condition that only translational self-diffusion is observed. However, if $R_g^2 \gg D_s\Delta$ then internal motion should be considered.[26]

$$D_s(c) = \frac{D_0}{(1+K_f^s c)} \qquad (4.4)$$

where K_f^s is the first virial coefficient and c is concentration.

All ^{1}H-NMR and DOSY-NMR measurements were performed on a Varian VNMRS 500 MHz Spectrometer with Agilent OneNMR probe. The NMR experiments were recorded at 25 °C. Typical conditions were as follows: number of scans = 16, number of increments = 20, lowest field gradient value = 2000 G/m and highest field gradient value = 25,000 G/m with diffusion time (Δ) = 50.0 ms. The ^{1}H-NMR spectra were processed by the MestReNova software (version 11.0.2-18153). The DOSY spectra were phased and baseline corrected before being processed to obtain the self-diffusion coefficient (D_S). The 2D-DOSY maps of low M_w (M_w 200 – 5000) and high M_w (M_w 4,000,000) polymers were processed with the DOSY Toolbox software (version 2.7) and MestReNova, respectively. For low M_w PAA/PEO systems, δ is set at 2 ms while for high M_w PAA/PEO and PAA/PTHF systems δ is set at 10 ms.

4.2.2.1 Low M_w PAA/PEO and PAA/PTHF

Pure polymer solutions of PAA M_w 5000, PEO M_w 200 and PEO M_w 5000 were prepared at 5 %wt, while the mixtures of PAA M_w 5000/PEO M_w 200 and PAA M_w 5000/PEO M_w 5000 were prepared at 10 %wt total concentration (weight ratio of PAA and PEO = 1:1) in deuterated water (D_2O) with deuterium chloride (DCl) to obtain a pH around 3. We also investigated the association of PAA M_w 5000 and PEO M_w 200 in methanol-d_4. For PAA/PTHF systems, the solutions of pure polymers and mixed polymers were prepared in the same way as the PAA/PEO systems except we used PTHF M_w 250 and PTHF M_w 1000 with methanol-d_4 as a solvent. All solutions were gently stirred on a roller mixer overnight before testing. The volume of solutions in a NMR tube was fixed at 0.6 ml.

4.2.2.2 Very high M_w PAA/PEO

Effect of concentration

The values for the self-diffusion coefficient (D_s) of PAA M_w 4,000,000 and PEO M_w 4,000,000 were collected at different concentrations (0.5, 1.25, 2.0, 5.0, 8.0, 10.0 kg/m^3) in deuterated water (D_2O) with deuterium chloride (DCl) to obtain pH around 3.

Effect of polymer mixing ratio

The values for the self-diffusion coefficient (D_s) of PAA M_w 4,000,000 and PEO M_w 4,000,000 and the mixed PAA/PEO at 1%w/v (or 10 kg/m^3) total concentration were collected at different volume ratios of PAA:PEO (100:0, 80:20, 50:50, 20:80 and 0:100) in deuterated water (D_2O) with deuterium chloride (DCl) to obtain pH around 3.

4.2.3 T_2 solvent relaxation

T_2 solvent relaxation NMR measures the spin-spin relaxation time of protons (^{1}H) of solvent. In a relaxation experiment, solvent molecules in a dispersion undergo a fast exchange between 'absorbed or restricted' solvent molecules on the surface phase with a short relaxation time, T_{2S} and the 'non-restricted or free' solvent molecules in bulk solution (distant from the surface) with a longer time, T_{2F}. The solvent relaxation can be determined in term of the relaxation rate (R_2): $T_2 = 1/R_2$ where R_2 is an average of relaxation rates of the surface phase (R_{2S}) and the bulk liquid phase (R_{2F}) obtained from Equation (4.5):[30,31]

$$R_{2(av)} = (1 - P_S)R_{2F} + P_S R_{2S} \qquad (4.5)$$

where P_S is the fraction of solvent molecules absorbed on a surface phase.

In addition, the relaxation data can be reported as a specific relaxation rate constant (R_{2sp}) which is the R_2 value normalized with the relaxation rate of a referent sample or bulk solvent (R_2°): $R_{2sp} = \left(\frac{R_2}{R_2^\circ}\right) - 1$. However, the T_2 value of solvent in a polymer solution may be only slightly different from the T_2 value of pure solvent. In comparison, the addition of particles with a high surface area (such as silica nanoparticles) can significantly enhance the number of solvent molecules in a "bound" environment so decreasing the average T_2 value or increasing the average R_{2sp}.[32]

The standard Carr-Purcell-Meiboom-Gill (CPMG) sequence was employed, and the transverse relaxation time (T_2) is generally obtained from a single exponential decay in Equation (4.6):[30,32,33]

$$M_{x,y}(t) = M_0 \exp\left(-\frac{t}{T_2}\right) + B \qquad (4.6)$$

where M_{xy} is the transverse magnetization between even pairs of 180° pulses separated by at time t, M_0 is the transverse magnetization immediately after the initial excitation of 90° pulse and B is a baseline offset. However, we found that a single exponential decay did not fit the relaxation curves well for all samples. At high concentration, polymer and solvent reveal independent relaxations so a double exponential is used to fit the curves:[31,34] $M(t) = M_0^1 \exp(-t/T_2^1) + M_0^2 \exp(-t/T_2^2)$, where the superscript 1 and 2 denote polymer and solvent, respectively.

T_2 solvent relaxation measurements were performed using the Acorn Area bench-top NMR supplied by XiGO Nanotools, Inc., USA, operating at 13 MHz. The Carr–Purcell–Meiboom–Gill (CPMG) pulse sequence was used to measure the magnetisation decay curve, M_{xy} as a function of time (t) and T_2 values were calculated by the AreaQuant program by fitting the magnetization decay curves with a single exponential (unless noted otherwise). Each experiment was repeated five times to obtain an average T_2 value. A recycle delay of at least $5T_1$ between scans was used to ensure full recovery of the magnetisation at temperatures 38-40 °C.

4.2.3.1 PAA/PEO

Low and high M_w

For PAA/PEO in methanol, we prepared pure PAA M_w 5000, pure PEO M_w 200 and PAA M_w 5000/PEO M_w 200 (weight ratio of PAA to PEO is 1:1) solutions in a range of 1-20%wt total concentration. For PAA/PEO in pH 3 buffer solution, we prepared pure PAA (M_w 5000 and M_w 273,000), pure PEO (M_w 5000 and M_w 300,000), PAA M_w 5000/PEO M_w 5000 and PAA M_w 273,000/PEO M_w 300,000 (weight ratio of PAA to PEO is 1:1) solutions at 5%wt total concentration. All solutions were gently mixed on a roller mixer overnight before testing.

Very high M_w

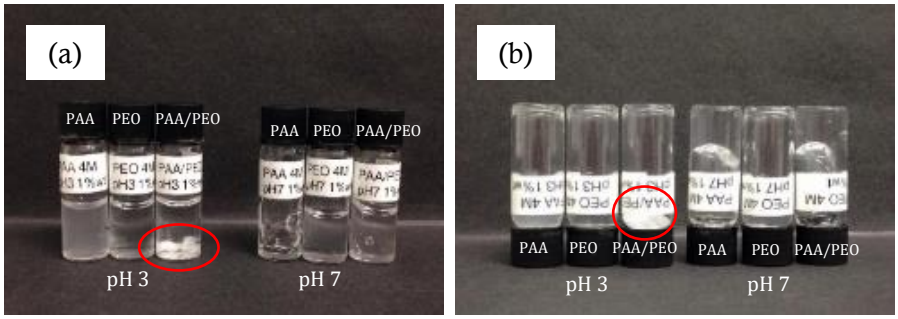

Figure 4.3 The solutions of pure PAA M_w 4,000,000, pure PEO M_w 4,000,000 and PAA/PEO solutions (volume ratio = 1:1) in pH 3 and pH 7 aqueous solutions at 1%w/v total concentration.

Interestingly, we found a white aggregate in a PAA/PEO M_w 4,000,000 solution mixture at pH 3, while the same PAA/PEO mixture is a bit cloudy at pH 7 as shown in **Figure 4.3**(a). Furthermore, **Figure 4.3**(b) shows that solutions of PAA and PAA/PEO at pH 7 are very thick. At low pH, the conformation of PAA is a compact globule which can be transformed into an expanded, fully solvated open coil as a result of carboxylic acid groups (-COOH) ionized to carboxylate anions ($-COO^-$) above its pK_a (pH = 4-4.5). As the PAA behaviour is pH dependent, the aggregate can be formed only at a low pH via hydrogen bonding between carboxylic acid groups of PAA and ether oxygens of PEO. At pH 7, the carboxyl groups are mostly ionized into carboxylate anions so the hydrogen bonding of PAA/PEO becomes weaker.

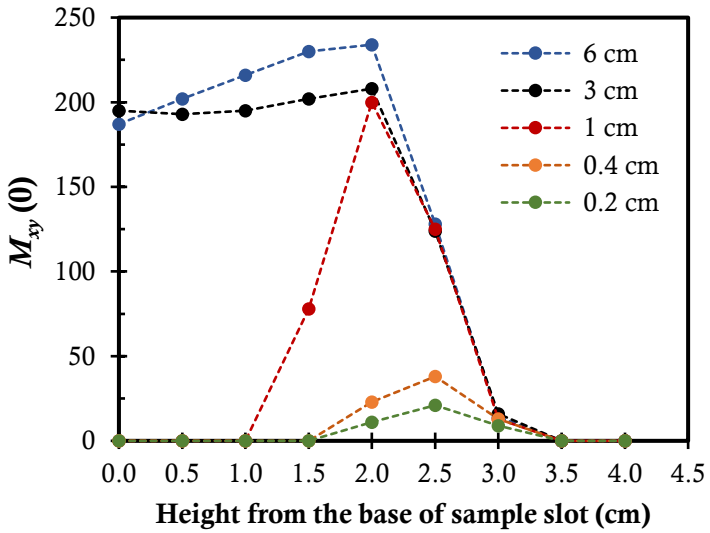

Figure 4.4 Effect of level of solutions in NMR tube (0.2, 0.4, 1, 3 and 6 cm) and the height of NMR tube from the base of sample slot on magnetization (M_{xy}) of 10 mM $CuSO_4$.

Due to the aggregate of PAA/PEO which settles at the bottom of the tubes, the volume of solution and location of NMR tube need to be optimised to ensure that the whole solution is located in the detection zone. We first examined the best condition for testing T_2 solvent relaxation by using 10 mM $CuSO_4$ which has a short relaxation time. From the results in **Figure 4.4**, the volume (or height of solutions in NMR tubes) and the location of NMR tube in the sample slot significantly affect the transverse magnetization (M_{xy}). Consequently, we prepared 0.12 ml (the height of solution at around 1 cm in NMR tube) of PAA/PEO M_w 4,000,000 solutions with various volume ratios of PAA to PEO from 100:0, 80:20, 60:40, 50:50, 40:60, 20:80 and up to 0:100. The total concentration of all solutions was 1%w/v in pH 3 solution. Then, the NMR tube was lifted from the base of sample slot at 2 cm before testing so the whole solution was exposed to the resonance magnetic and RF(pulses) fields.

4.2.3.2 Low M_w PAA/PTHF

The solutions of pure PAA M_w 5000, pure PTHF M_w 6000 and PAA M_w 5000/PTHF M_w 6000 (weight ratio of PAA to PTHF = 1:1) with a range of 5 – 50%wt total concentrations were prepared in methanol. We found that at high concentrations (over 20%wt) it took a long time to dissolve PAA in methanol. To ensure that the solutions were homogeneous, they were mixed by a probe sonicator (QSonica Q125, 125 Watt 20 KHz, amplitude 50%) in pulse mode (pulse on 5 sec/off 5 sec) for 15 mins and the concentrated solutions were extremely viscous. Then, the solutions were gently stirred by a roller mixer for 2 days before testing.

4.3 Results and Discussion

4.3.1 ^{1}H-NMR and DOSY-NMR

4.3.1.1 Low M_w PAA/PEO and PAA/PTHF

In this set of experiments, all low M_w PAA/poly(ethers) solutions were homogeneous and did not show any precipitate. In **Figure 4.5,** the association between PAA (M_w 5,000) and PEO with two different molecular weights (M_w 200 and M_w 5000) in D_2O (pH 3) is examined. The chemical shift (δ) of protons in PAA/PEO solutions at a total concentration of 10%wt is compared with the δ value of 5%wt pure PAA and 5%wt pure PEO solutions. Taking the signal of D_2O as a reference at 4.65 ppm, the δ value of PAA main chain protons in PAA/PEO solutions is similar to that in the pure PAA solution. The difference in chemical shift ($\Delta\delta$) of -C**H**$_2$ protons is 0.05 ppm (upfield shift to lower ppm) for PEO M_w 200 and PEO M_w 5000 in PAA/PEO solutions compared to the pure PEO solutions. Similarly, we only found an upfield shift to lower ppm with $\Delta\delta$ = 0.17 ppm of PEO M_w 200 in PAA M_w 5000/PEO M_w 200 in methanol-d_4 (MeOD).

Since PTHF is water-insoluble, methanol-d_4 (or MeOD) was used as a solvent and the methyl protons of MeOD appear at 4.87 ppm for PAA M_w 5000/PTHF M_w 250 and PAA M_w 5000/PTHF M_w 1000 solutions as shown in **Figure 4.6**. The chemical shifts (δ) of PAA/PTHF are compared to the δ values of the individual pure polymers. Similar to the PAA/PEO system, the main chain protons in PAA of PAA/PTHF appear at almost the same chemical shift as for the pure PAA, while the main chain protons in PTHF of all PAA/PTHF samples exhibit a small upfield shift to lower ppm with $\Delta\delta$ = 0.17 ppm.

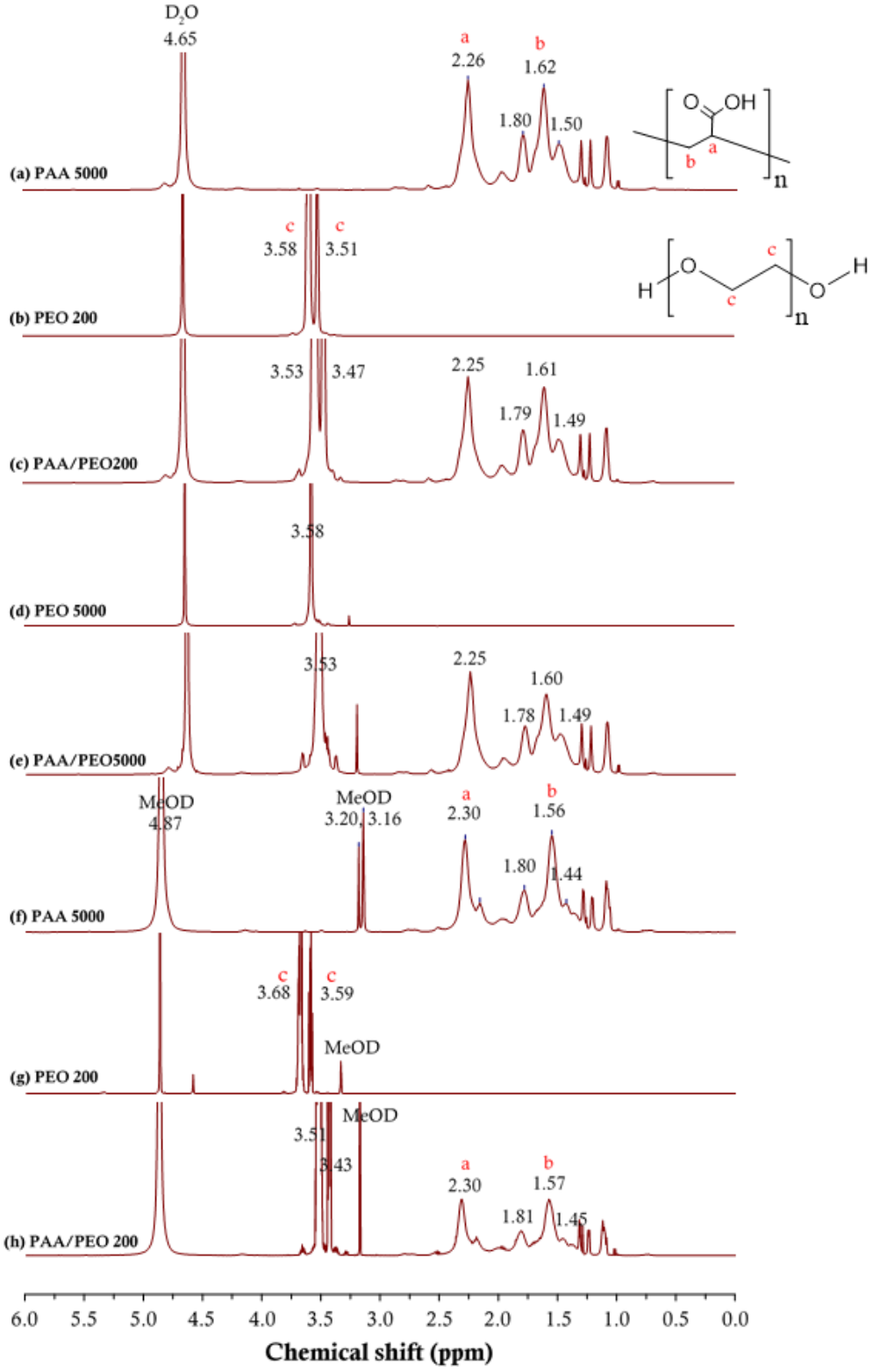

Figure 4.5 ^{1}H-NMR spectra of (a) 5%wt pure PAA M_w 5000, (b) 5%wt pure PEO M_w 200, (c) 10%wt PAA M_w 5000/PEO M_w 200, (d) 5%wt pure PEO M_w 5000, (e) 10%wt PAA M_w 5000/PEO M_w 500o in D_2O (PH 3), and (f) 5%wt pure PAA M_w 5000, (g) 5%wt pure PEO M_w 200 and (h) 10%wt PAA M_w 5000/PEO M_w 200 in methanol-d_4 (weight ratio of PAA to PEO = 1:1).

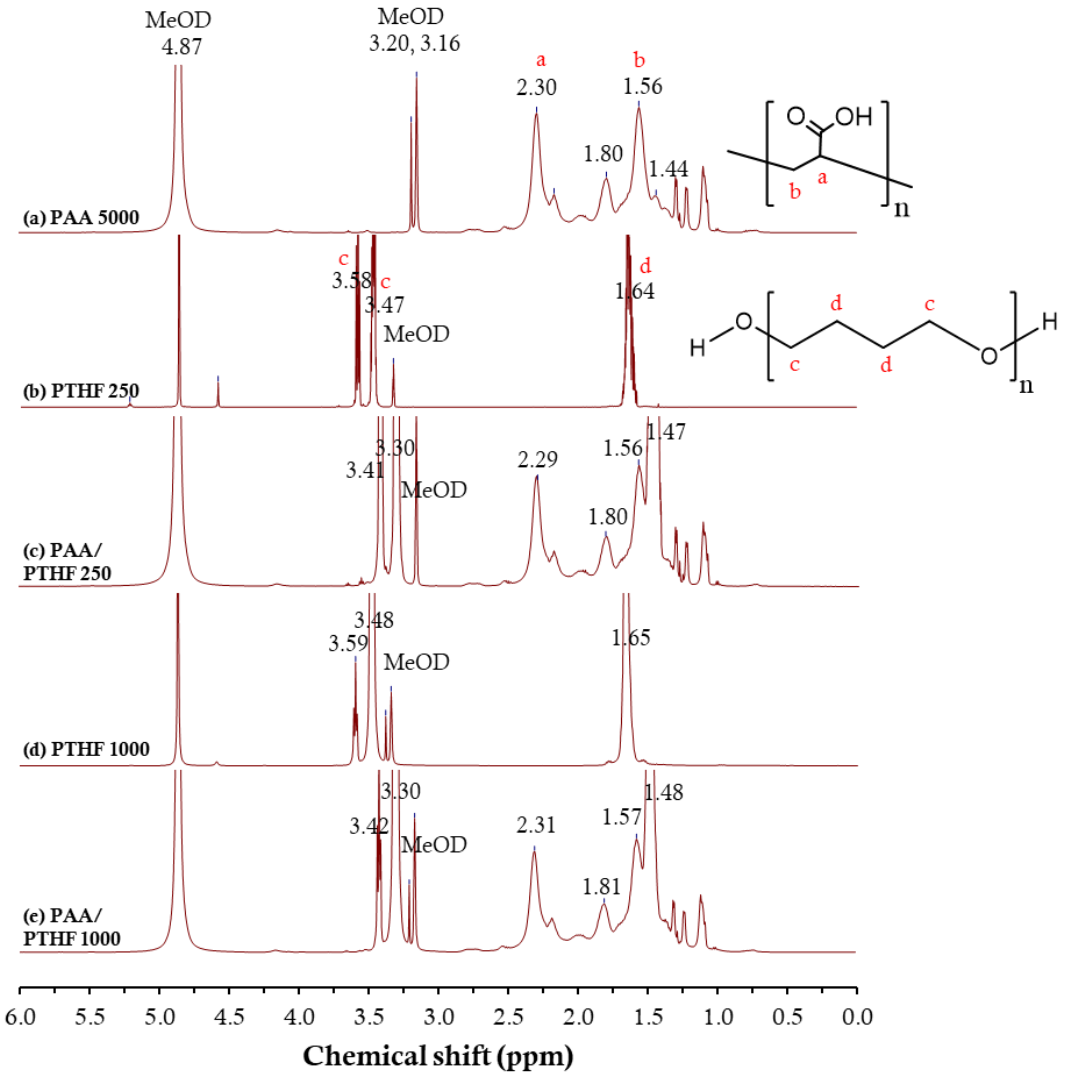

Figure 4.6 ^{1}H-NMR spectra of (a) 5%wt pure PAA M_w 5000, (b) 5%wt pure PTHF M_w 250, (c) 10%wt mixed PAA M_w 5000/PTHF M_w 250, (d) 5%wt pure PTHF M_w 1000, and (e) 10%wt mixed PAA M_w 5000/PTHF M_w 1000 in methanol-d_4 (weight ratio of PAA to PTHF = 1:1).

In general, hydrogen bonding decreases valence electron density around bonded protons, so the proton is deshielded and shifts downfield (to higher ppm) in the ^{1}H-NMR spectrum. Wang *et al.*[35] studied hydrogen bonding in polyacrylate solutions using chloroform as a probe molecule and TMS as a reference. Hydrogen bonding can be formed between the hydrogen atom of chloroform ($C\mathbf{H}Cl_3$) with the electronegative oxygen of polymethacrylate (PMA). With TMS as reference at 0 ppm, the δ value of chloroform protons is shifted downfield from 7.26 ppm (pure) to 7.39 ppm (for 20%wt PMA in chloroform). However, this study only considered the δ value of the chloroform proton and did not mention the δ value of PMA. For PAA, the carboxyl protons (-COO**H**) typically appear as broad singlets at 10-12 ppm and they may undergo a proton exchange

with D_2O and methanol-d_4 so these protons may not be detected easily in ^{1}H-NMR. In our experiment, we therefore cannot find these signals and only can consider the change in chemical shift (δ) of main chain protons to probe hydrogen bonding between PAA and poly(ethers).

The effect of hydrogen bonding on the δ value of the main chain protons of PAA or PEO has several origins because they are not directly affected by the shift of electron density from -COO**H** towards ether oxygens. Yokoyama and Yusa[36] studied the complex formed by poly(ethylene glycol) containing a triblock copolymer (PSS-PEG-PSS) and poly(methacrylic acid) (PMAA) via hydrogen bonding. The samples were dissolved in D_2O with 0.1 M NaCl at pH 3. The peak of the –C**H**$_2$ protons of PEG block in pure PSS-PEG-PSS solution appears at 3.7 ppm and it is unchanged when forming the complex with PMAA. The peaks of -C**H**$_2$ (main chain) and -C**H**$_3$ (pendant group) protons in pure PMAA solution appear at around 2.0 ppm and 1.0 ppm, respectively, whilst these protons of PMAA in the complex solution become broader and appear at a lower chemical shift (or upfield shift). The $\Delta\delta$ value is 0.36 ppm and 0.07 ppm for the peaks of -C**H**$_2$ and -C**H**$_3$ protons in PMAA, respectively.

Lu *et al.*[37] studied hydrogen bonding interactions between poly(ethylene glycol) (PEG) and poly(acrylamide) (PAM) in aqueous solutions. Theoretically, the peaks of amide protons (-CON**H**$_2$) should be shifted downfield when hydrogen bonding is formed between -CON**H**$_2$ of PAM and the ether oxygen of PEG. However, the amide peaks of 20% PAM in 28% PEG/PAM solution appear at the same chemical shift as 20% pure PAM solution but become broader than the pure PAM, while the main chain protons (-C**H**$_2$-O-C**H**$_2$-) of 8% PEG in the 28% PEG/PAM solution are clearly shifted downfield for 0.37 ppm compared to 8% pure PEG solution.

Liu *et al.*[38] prepared the zwitterionic ABC miktoarm star terpolymers consisting of PEG, PMAA and PDEA (poly(2-(diethylamino)ethyl methacrylate). The core-shell structure of PEG-*b*-PMAA-*b*-PDEA is investigated at different pH. At pH 10, PMAA segment is deprotonated so the hydrogen bonding between PMAA and PEG segments is absent. The broad peaks of main chain PMAA segments appear at around 1.6 ppm for –C**H**$_2$ and 1 ppm for -C**H**$_3$, while the sharp peak of PEG segments appears at 3.7 ppm. At pH 3, PMAA is fully protonated so the hydrogen bonding between PMAA and PEG segments should exist. The peak of –C**H**$_2$ of the PMAA segment shows significantly downfield shift but the δ value of -C**H**$_3$ in PMAA is almost unchanged, whilst the peak of PEO becomes broader and shows a slightly upfield shift (to lower ppm).

For our results, it is known that PAA can from a strong self-association via inter- and intra-hydrogen bonding between its carboxylic acid (-COOH) and can also interact with water or methanol. Consequently, it is possible that the δ value of the main chain protons of PAA in PAA/poly(ethers) solutions is similar to the δ value of such protons in pure PAA solution. On the other hand, the δ value of methylene protons (–C**H**$_2$) in the backbone of poly(ethers) (PEO and PTHF) in PAA/poly(ethers) solutions only shows the upfield shift from the δ value of such protons in pure poly(ether) solutions. Theoretically, the upfield shift to lower ppm occurs when the electron density around the proton is increased (or shielded). The presence of PAA to form hydrogen bonding with poly(ethers) may increase the electron density towards the ether oxygens of poly(ethers) and this may also shield the neighbouring atoms. Therefore, the upfield shift of –C**H**$_2$ main chain protons in poly(ethers) can be observed. However, the difference of chemical shift ($\Delta\delta$) value in our experiments is rather small which is 0.05 ppm and 0.17 ppm for low M_w PAA/PEO solutions in D_2O, and for low M_w PAA/PEO and PAA/PTHF in MeOD, respectively and the effect of M_w on the chemical shift is insignificant.

Using the same set of samples from the ^{1}H-NMR experiments, the self-diffusion coefficient (D_s) was measured with the 2D-DOSY NMR technique. For these diffusion experiments, we suggest that the association between PAA and poly(ethers) will lead to similar D_s values of each component in mixed solutions.

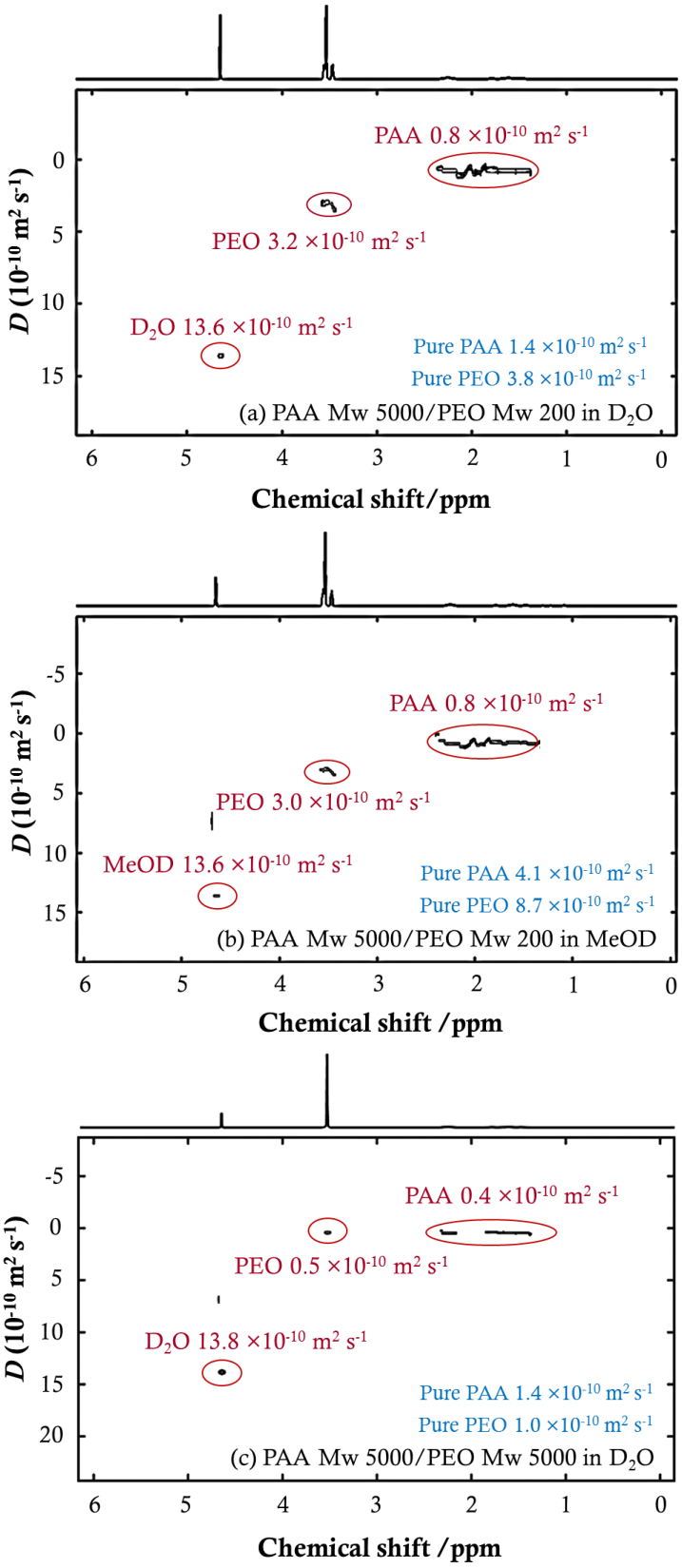

Figure 4.7 2D-DOSY NMR spectra of 10%wt PAA M_w 5000/PEO M_w 200 (a) in D_2O (pH 3) and (b) in methanol-d_4, and (c) 10%wt PAA M_w 5000/PEO M_w 5000 in D_2O (pH 3) and weight ratio of PAA to PEO = 1:1.

Considering PAA M_w 5000/PEO M_w 200 in D_2O at pH 3 (**Figure 4.7**(a)) and in methanol-d_4 (**Figure 4.7**(b)), we found that these two samples show two distinct diffusion signals of PAA M_w 5000 and PEO M_w 200. Nevertheless, the diffusion signal of PAA M_w 5000 and PEO M_w 5000 in the PAA M_w 5000/PEO M_w 5000 in pH 3 solution appears almost at the same value (0.4 and 0.5×10^{-10} $m^2\,s^{-1}$, respectively) as shown in **Figure 4.7**(c).

For PAA/PTHF solutions in methanol-d_4, we found that the PAA M_w 5000/PTHF M_w 250 shows two different diffusion peaks as shown in **Figure 4.8**(a) but the increase of M_w of PTHF from 250 to 1000 leads to fairly close values of D_s of PAA M_w 5000 and PTHF M_w 1000 (2.2×10^{-10} and 2.6×10^{-10} $m^2\,s^{-1}$, respectively) in the PAA M_w 5000/PTHF M_w 1000 solution as shown in **Figure 4.8**(b).

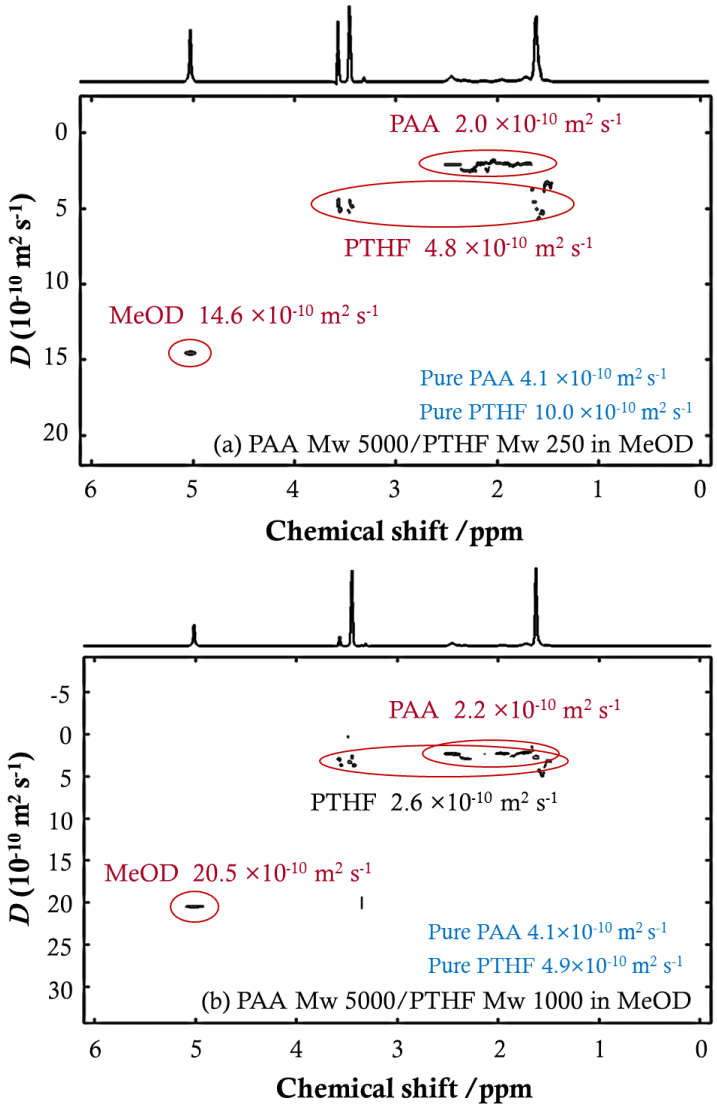

Figure 4.8 2D-DOSY NMR spectra of (a) 10%wt PAA M_w 5000/PTHF M_w 250, and (b) 10%wt PAA M_w 5000/PTHF M_w 1000 (weight ratio of PAA to PTHF = 1:1) in MeOD.

Consequently, focusing on the diffusion of the mixed PAA/poly(ethers) solutions, it is evident that the association between PAA and poly(ethers) can be found for PAA M_w 5000/PTHF M_w 5000 in D_2O (pH 3) and PAA M_w 5000/PTHF M_w 1000 in methanol-d_4.

Additionally, we considered the D_s values of pure polymers and mixed PAA /poly(ethers) as shown in **Figure 4.9**. From the Stokes-Einstein equation, the diffusion coefficient (D_s) is inversely proportional to the 'size' of the molecules. With hydrogen bonding, we suggested that the overall size of the PAA bonded with poly(ethers) should be larger than the pure polymers and thus the D_s value is decreased.

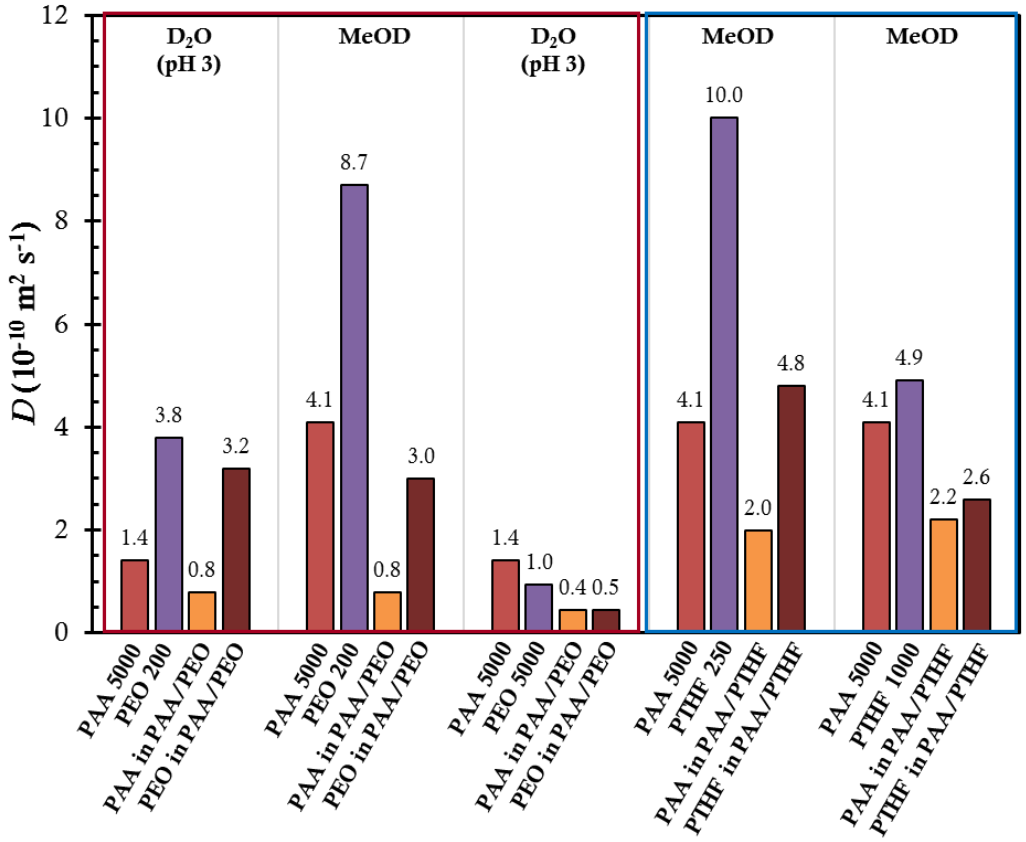

Figure 4.9 Self-diffusion coefficient (D_s) of polymer systems: 5%wt total concentration of pure polymer solutions and 10%wt total concentration of PAA M_w 5000/PEO M_w 200 and PAA M_w 5000/PEO M_w 5000 dissolved in D_2O (pH 3), PAA M_w 5000/PEO M_w 200 in MeOD, PAA M_w 5000/PTHF M_w 250 and PAA M_w 5000/PTHF M_w 1000 dissolved in MeOD (weight ratio of PAA to poly(ethers) is 1:1).

It is seen that the D_s values of PAA and poly(ethers) in PAA/poly(ether) mixtures are lower than the D_s value of pure polymer solutions. However, the D_s values of PAA and PEO in PAA M_w 5000/PEO M_w 200 in pH 3 solution are only slightly lower than the pure polymers so it could mean that there is no interaction between the PAA and PEO.

Similarly, the D_s values of each component in PAA M_w 5000/PEO M_w 200 in MeOD are different, although they are significantly lower than in the pure polymer solutions. For PAA M_w 5000/PEO M_w 5000 in pH 3 solution, the D_s values of individual polymers in the mixed PAA/PEO solution are lower than for the pure polymers and similar to each other, which might be due to the hydrogen bonding between the PAA and PEO. However, the decrease in D_s value will at least to some extent be due to an increase in viscosity, as we compared 5%wt pure polymers with 10%wt PAA/poly(ether) solutions (weight ratio of PAA to poly(ethers) = 1:1). Since we did not perform viscosity measurements, we instead measured the D_s values of 10%wt of pure polymer solutions as listed in **Table 4.2**.

Table 4.2 Comparison of the diffusion coefficient of PAA M_w 5000 and PEO M_w 5000 at 5%wt and 10%wt and mixed PAA/PEO at 10%wt total concentration in pH 3 solutions.

Sample	Diffusion coefficient (10^{-10} m^2/s)		
	5%wt pure polymer	10%wt pure polymer	Total 10%wt PAA/PEO
PAA M_w 5000	1.4	1.0	0.4
PEO M_w 5000	1.0	0.3	0.5

The D_s values of PAA (0.4×10^{-10} m^2/s) and PEO (0.5×10^{-10} m^2/s) in 10%wt PAA M_w 5000 /PEO M_w 5000 are 3.5 and 2 times lower than 5%wt of the pure polymers and they are also lower than an averaged D_s value (0.75×10^{-10} m^2/s) calculated from 10%wt pure PAA and pure PEO. Accordingly, it does not seem likely that the decrease in the D_s value of the 10%wt PAA/PEO solution is due solely to the increased viscosity.

In contrast, it is noticeable that both D values of PAA (2.2×10^{-10} m^2/s) and PTHF (2.6×10^{-10} m^2/s) in 10%wt PAA M_w 5000/PTHF M_w 1000 are about two times lower than in 5%wt of the pure polymers (4.1 and 4.9 $\times10^{-10}$ m^2/s, respectively). Interestingly, this decrease by a factor of two is also found in a PAA M_w 5000/PTHF M_w 250 solution. It seems the increase in concentration from 5%wt to 10%wt results in the D_s values decreasing by a factor of two for the PAA/PTHF system. This leads us to suggest that the decrease in diffusion coefficient for the PAA M_w 5000/PTHF M_w 1000 solution may not be completely attributed to hydrogen bonding but is at least in part due to the increase in viscosity.

In addition, the diffusion coefficient of a polymer in solution (D) generally scales with the molecular weight (M) as $D \sim M^{-\nu}$ so that the scaling exponent (ν) might be calculated by following equation:[39] $\left(\frac{D_1}{D_2}\right) = \left(\frac{M_2}{M_1}\right)^{\nu}$ for solutions at the same overall polymer concentration. Consequently, we found that the scaling exponent is 0.43 and 0.52 for PEO at pH 3 and PTHF in methanol, respectively, in reasonable agreement with the ν value (0.5) for a theta solvent. Considering the effect of solvent on the diffusion of pure polymer, we found that the D_s values of PAA M_w 5000 are 1.4 and 4.1 $\times 10^{-10}$ m^2/s and those of PEO M_w 200 is 3.8 and 8.7 $\times 10^{-10}$ m^2/s in D_2O (pH 3) and MeOD, respectively. It appears that both PAA and PEO can diffuse in methanol better than in water. In large part this is due to the difference in solvent viscosity which is 1.121 mPa.s[40] for D_2O (pH 3) and 0.602 mPa.s[41] for MeOD at 25 °C, respectively and from the Stokes-Einstein equation, the diffusion coefficient is inversely proportional to the viscosity of the solvent.

4.3.1.2 Very high M_w PAA/PEO

The association between PAA and PEO was only observed in PAA M_w 5000/PEO M_w 5000 in pH 3 solution by DOSY technique. In this section, we also investigate the association in pH 3 solution but used a very high M_w of PAA and PEO (M_w 4,000,000).

Effect of concentration

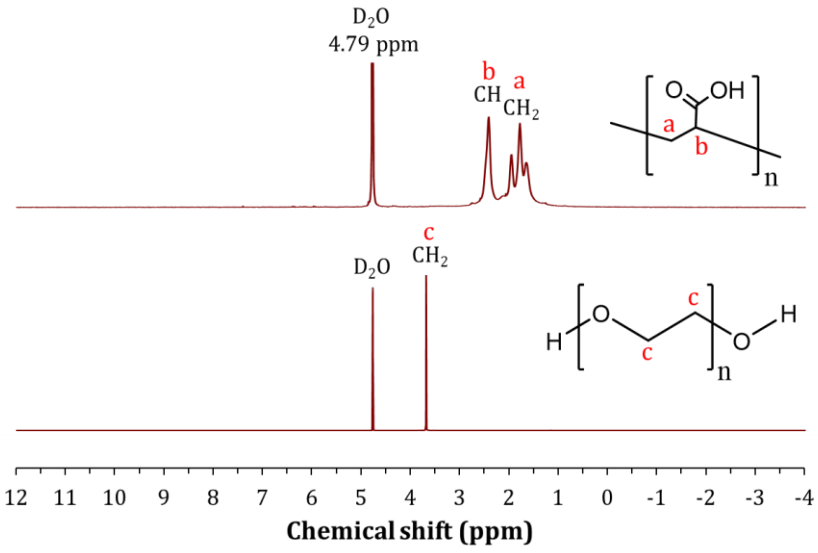

Figure 4.10 ^{1}H-NMR spectra of (a) PAA M_w 4,000,000 and (b) PEO M_w 4,000,000 at 1%w/v in D_2O (pH 3).

The ^{1}H-NMR spectra of PAA and PEO (M_w 4,000,000) dissolved in D_2O (pH 3) are shown in **Figure 4.10**. The peak of D_2O is set as reference at 4.79 ppm and therefore, the chemical shift (δ) value of –C**H** appears at 2.43 ppm and that of -C**H**$_2$ appears at 1.97, 1.79 and 1.66 ppm for PAA, while the δ value of –C**H**$_2$ in PEO appears at 3.72 ppm. However, the proton in the carboxylic acid groups (-COO**H**) of PAA cannot be seen due to proton exchange with D_2O. Similarly, there is no evidence of hydroxyl (-O**H**) end groups of very high M_w PEO.

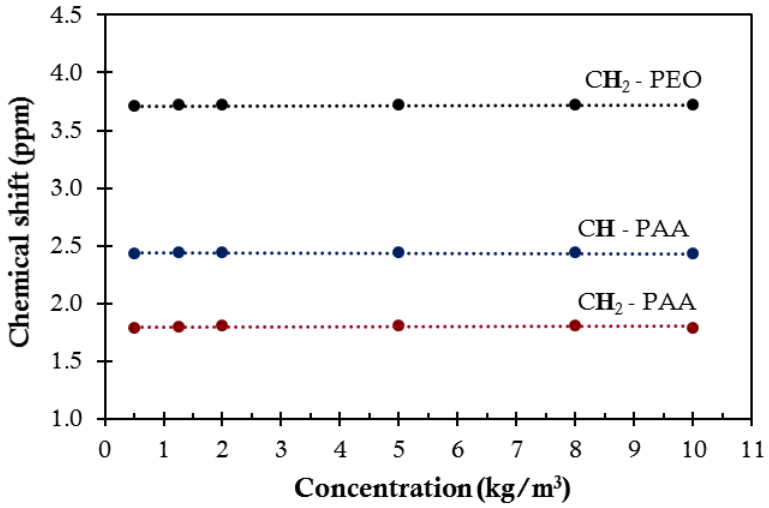

Figure 4.11 Plot of chemical shift (ppm) of -CH and -CH_2 protons for pure PAA M_w 4,000,000 solutions, and -CH_2 protons for pure PEO M_w 4,000,000 solutions as a function of concentration.

Using the peak of D_2O at 4.79 ppm as a reference, the chemical shift (δ) of proton signals of pure polymers can be investigated as a function of concentration (1 – 10 kg/m^3 or 0.05-1%w/v) as shown in **Figure 4.11**. However, the effect of concentration on the chemical shift of proton signals in PAA and PEO backbones is insignificant in our experiment.

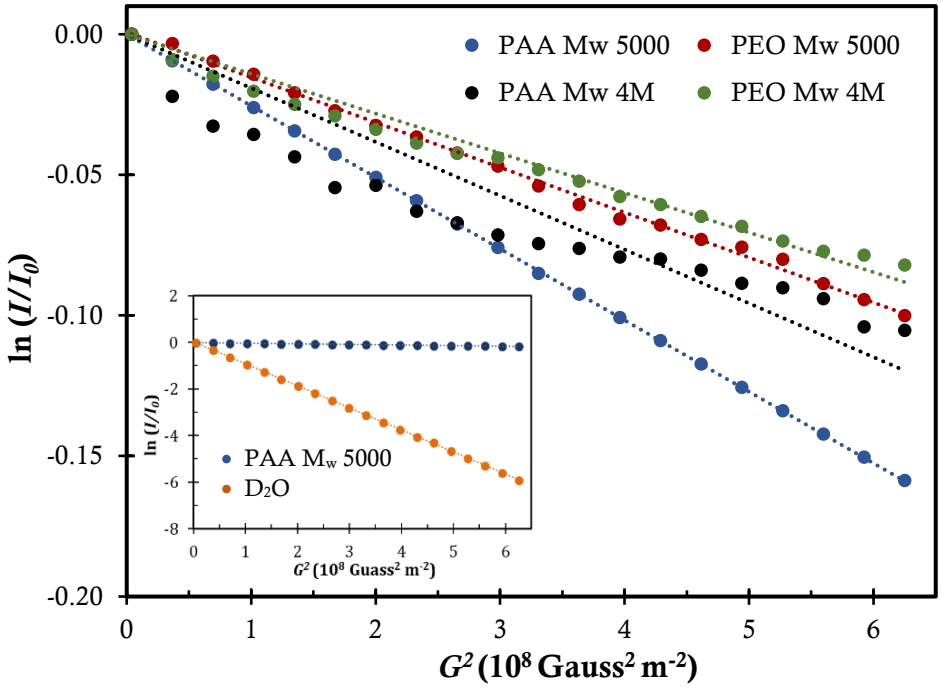

Figure 4.12 Plot of ln relative intensity (I/I_0) as a function of gradient strength squared (G^2) for pure PAA and pure PEO M_w 4,000,000 (4M) at 1%w/v and δ = 10 ms and for pure PAA, pure PEO M_w 5000 at 5%w/v and D_2O at δ = 2 ms.

Figure 4.12 shows the plots of intensity decay of polymers and D_2O as a function of gradient strength. It is seen that we only can measure an initial decay of polymers due to a limitation of the NMR machine hardware with gradient strength of 2,000 – 25,000 G/m, while the full decay of D_2O can be observed. Theoretically, the decays from a polydisperse sample are non-exponential and dependent on the polymer size distribution of the sample. Since we used very high M_w polymers in this section, polydispersity could be another factor to be concerned. The polydispersity was not stated for the polymers used here but may well be significant. It was reported that PEO M_w 3,160,000 (SWR-301, Dow Chemicals) has a rather large polydispersity (M_w/M_n) of 1.55±0.33.[42] Accordingly, the DOSY results of very high M_w polydisperse polymers in our experiment might be attributed to the diffusion of a population of shorter chains amongst longer entangled polymer chains.

Three regimes of polymer concentration are considered theoretically[43,44] as (i) dilute solution, the macromolecules do not overlap to each other so it can be considered as one macromolecule in a good or theta solvent, (ii) semi-dilute solution, the polymer chains start to overlap where the overlap concentration (c^*) [44-47] is defined as

$c^* = 3M/4\pi N_A R_G^3$ where M is the molar mass (g/mol), N_A is the Avogadro number, and R_G is the radius of gyration (nm) in a dilute solution, and (iii) concentrated solution (c^{**}), a polymer interacts with other polymer segments and also itself and the c^{**} is independent of molecular weight.

To calculate the overlap concentration (c*), we must first know the R_G of PAA and PEO M_w 4,000,000. Unfortunately, we did not find references for R_G of PAA in acidic solution. Instead, the following data may be instructive. Reith *et al.*[12] studied the structural properties of sodium polyacrylate (NaPAA) in aqueous solution with computer simulation and light scattering. The NaPAA with degree of polymerisation (N) of 8 – 3155 was dissolved in DI water with 1 M NaCl and the final pH was around 6-8. Whilst clearly this polymer will be ionised, the high salt concentration can effectively screen the electrostatic repulsion between ionized carboxyl groups, so chain dimensions may be similar to those of PAA at low pH. At $N > 100$, $R_H \; \alpha \; M_w^{\upsilon}$ where R_H is hydrodynamic radius (nm) and ν is the scaling exponent. The ν value for R_H and R_G is 0.55±0.02 and in a good agreement between the simulation and light scattering.

In our experiment, we used PAA M_w 4,000,000 (N = 56,000) dissolved in pH 3 solution in which the carboxylic acid of PAA is mostly protonated, thus we assume that electrostatic repulsion can be neglected. According to Reith's study:[12] $R_G \; \alpha \; M_w^{0.55}$, R_G of NaPAA M_w 296,600 (N = 3155) is 24.1 nm so the calculated R_G of NaPAA with N = 56,000 is 117 nm. Since we cannot find a reference for the R_G of PAA at low pH, we assume it is similar to the R_G of NaPAA at the same degree of polymerization (N). However, this value may be larger than the correct R_G of PAA at low pH since it is calculated on the basis of the swollen NaPAA chains at high pH although the electrostatic repulsion between ionized carboxyl groups is screened by the presence of salt.

PEO is a flexible polymer and its radius of gyration in water is as a function of molar mass: $R_G = 0.0215M^{0.583}$nm[46-48] so the R_G of PEO M_w of 4,000,000 is 152 nm. For the hydrodynamic radius, $R_H = 0.0145M^{0.571}$ nm[48] so the R_H of PEO M_w 4,000,000 is 85.3 nm. Consequently, we now can calculate the c^* for PAA and PEO M_w 4,000,000 which is 1.6 kg/m^3 (0.16 %w/v) and 0.45 kg/m^3 (0.045%w/v), respectively. Consequently, PAA and PEO solutions in our experiments are above c^* or in the semi-dilute regime.

For a dilute solution, a weak dependence of D with concentration (c) given by Equation (4.4) is expected.

For semi-dilute solution (c > c*), predictions are that $D_s \propto M^{-2}c^{(\nu-2)/(3\nu-1)}$ so for a good solvent ($\nu = 0.6$): $D \sim c^{-1.75}$, while for a theta solvent ($\nu = 0.5$): $D \sim c^{-3.0}$.[49]

For instance, Cosgrove and Griffiths[50] found that low M_w PS (M_w 435,500) solutions have a fairly weak dependence of D with concentration described as $D \sim c^{-0.91\pm0.04}$, whilst high M_w PS (M_w 1,030,000) solutions are in the semi-dilute regime with $D \sim c^{-2.25\pm0.10}$ which is in agreement with the predictions. Browns *et al.*[51] showed that PEO M_w 148,000 g/mol with $\overline{M_w}/\overline{M_n}$= 1.04 in the dilute regime (below c^*) is described as $D \sim c^{-0.5}$.

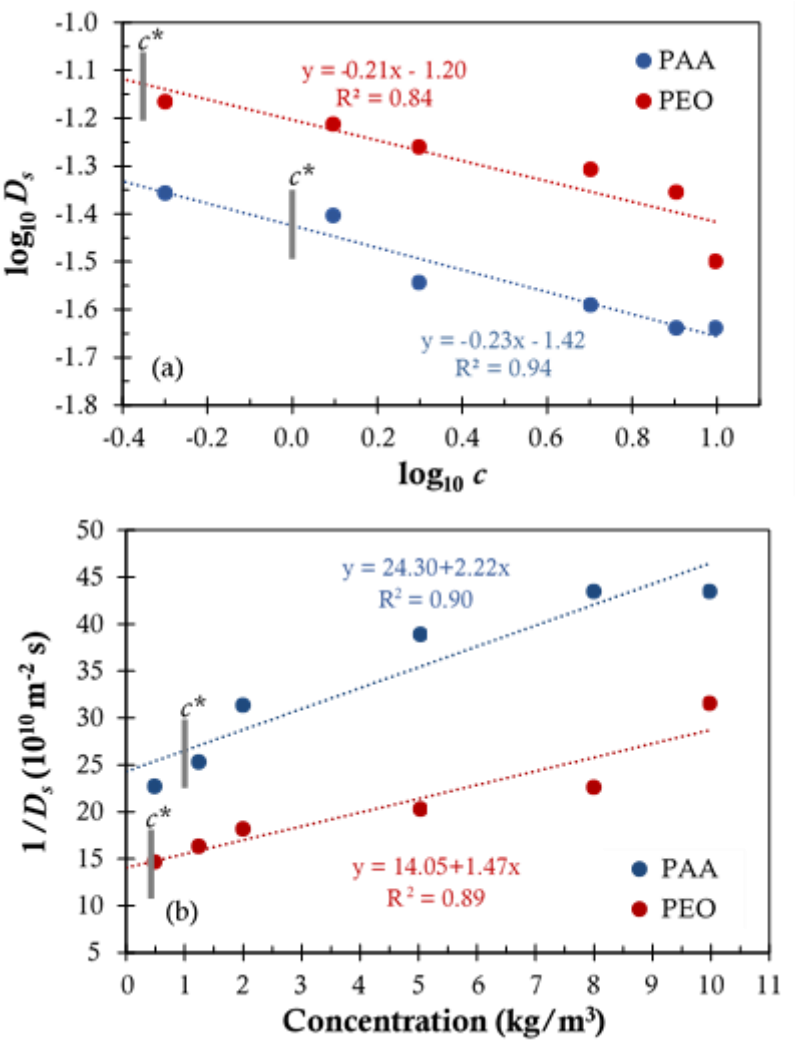

Figure 4.13 Plots of (a) $\log_{10} D_s$ vs $\log_{10}$ concentration (c), and (b) $1/D_s$ vs concentration (c) for PAA and PEO M_w 4,000,000 dissolved in D_2O (pH is around 3).

Here, we have very high M_w polymers (M_w 4,000,000) and as shown in **Figure 4.13**(a), essentially all the data were taken in the semi-dilute concentration regime, based on the c^* values calculated (above). However interestingly, the experimental D_s values show a very weak dependence on concentration indeed so that $D_S \sim c^{-0.23\pm0.03}$ and $D_S \sim c^{-0.21\pm0.05}$ for very high M_w PAA and PEO, respectively. The attenuation decay depends on the negative exponential of the diffusion coefficient times the gradient, G^2 by following Equation (2.2). Since the values of G are limited in the spectrometer, the sensitivity to small values of D, say less than 10^{-12}, is limited. In addition, it should be noted that the polymers used here are probably rather polydisperse. M_w is stated only in one significant figure, and no information is quoted on polydispersity. We therefore suspect that the data are dominated by the more mobile, low M_w components in the M_w distribution because we only measure the first part of the decay curves (- see **Figure 4.12**) arising from low M_w chains (rapid decay) and we do not detect the slower components in this experiment.

We then considered the self-diffusion for a dilute solution following Equation (4.4): $D_S(c) = \frac{D_0}{(1+K_f^S c)}$ where $R_g^2 < D_S\Delta$.[26] With diffusion time (Δ)=0.05 s and concentration = 0.5 kg/m^3, the D_s values of PAA and PEO are about 0.05 and 0.07 $\times10^{-10}$ m^2/s so the $D_s\Delta$ values of PAA and PEO are 25×10^{-14} and 35×10^{-14} m^2, respectively. Comparing with the R_G^2 of PAA and PEO (1.0×10^{-14} m^2 and 2.3×10^{-14} m^2), $R_g^2 \ll D_S\Delta$, then the Equation (4.4) should be valid in our experiments though we are still only measuring the more mobile chains in the mixture.

In **Figure 4.13**(b), the values for D_s of both PAA and PEO M_w 4,000,000 in acidic solutions decrease with the increase of concentration as predicted from Equation (4.4). The plot of $1/D_s$ as a function of concentration (c) is well fitted with a linear equation so the first friction coefficient, K_f^S, can be calculated from the slope and the intercept at $c = 0$ refers to the diffusion coefficient at infinite dilution, D_0. Therefore, the D_0 is 0.041 (±0.004) $\times10^{-10}$ m^2/s and 0.071 (±0.008) $\times10^{-10}$ m^2/s, and the K_f^S is 0.09±0.02 m^3/kg and 0.10±0.02 m^3/kg for PAA and PEO, respectively. The resulting D_0 can be further used to calculate the hydrodynamic radius (R_H) using the Stokes-Einstein equation for a spherical particle: $D = \frac{k_B T}{6\pi\eta R_H}$, where D is diffusion coefficient (m^2/s), k_B is Boltzmann's constant (1.38065×10^{-23} J/K), T is absolute temperature, η is solvent viscosity, and R_H is hydrodynamic radius. Consequently, the resulting R_H value from the DOSY experiment is 48.5±4.2 nm and 28.0±3.0 nm for PAA and PEO, respectively. For a random coil in a theta solvent, the

shape factor (R_G/R_H) is 1.73.[52] According to the R_G values from the literatures, the R_H values therefore would be around 68 nm and 88 nm for PAA and PEO, respectively. Consequently, the R_H of PAA from our experiment is greater than the PEO value and closer the theoretical value, while the R_H of PEO is much smaller which could be due to the polydispersity of the PEO samples and the intensity signal measured from the shorter and possibly less interacting chains.

Effect of polymer mixing ratio

In this section, the 1%w/v of PAA solution and 1%w/v of PEO solution in D_2O (pH 3) were mixed at various volume ratios of PAA to PEO (80:20, 50:50, and 20:80). After these two polymers were mixed, the solutions became cloudy and then precipitated from the solvent. We found the precipitate settled to the bottom of the tubes after few hours for 80:20 and 50:50 PAA/PEO solutions as shown in **Figure 4.14**. The precipitate is due to strong hydrogen bonding between the carboxyl groups of PAA and the ether groups of PEO illustrated by **Figure 4.1**.

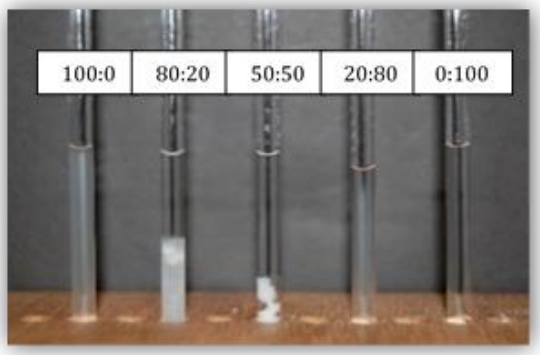

Figure 4.14 Photo of PAA and PEO (M_w 4,000,000) with the different polymer mixing ratio of PAA to PEO (100:0, 80:20, 50:50, 20:80, and 0:100) and the total concentration is 1%w/v.

Previously, we found that the δ value of main chain protons of pure PAA and pure PEO M_w 4,000,000 in D_2O is independent from the concentration in a range of 0.5 kg/m^3 (or 0.05%w/v) to 10% kg/m^3 (or 1%w/v), while the protons in carboxylic acid (-COO**H**) of PAA and hydroxyl group (-O**H**) of end group of PEO can exchange with D_2O and therefore the signal of these protons cannot be detected. **Figure 4.15** shows that the chemical shift (δ) of the main chain protons in the PAA/PEO solutions compared to the

individual polymer solutions does not change, although the aggregation is clearly observed in **Figure 4.14**.

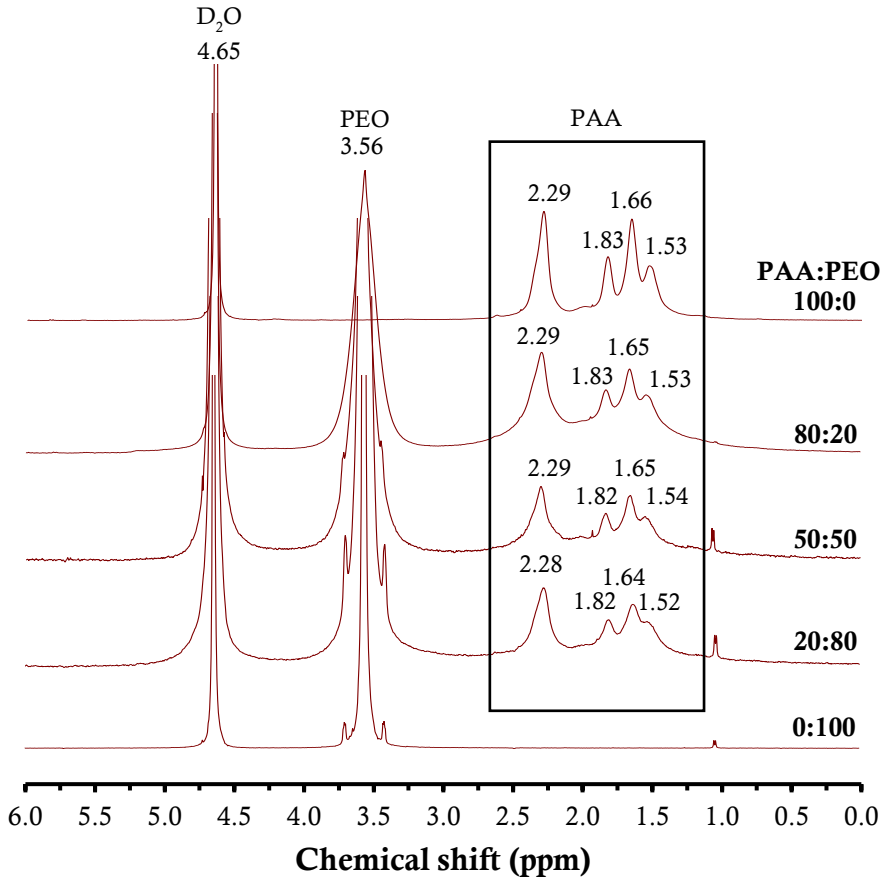

Figure 4.15 ^{1}H-NMR spectra of PAA M_w 4,000,000 and PEO M_w 4,000,000 with the different polymer mixing ratio of PAA a nd PEO (100:0, 80:20, 50:50, 20:80, and 0:100) and the total concentration is 1%w/v.

Consequently, we further determined the self-diffusion coefficient (D_s) of these solutions with DOSY-NMR to trace to the hydrogen bonding of PAA and PEO. Since the 20:80 PAA/PEO solution is rather cloudy but does not obviously show two-phase separation, we first measured the D_s value of this sample. Then, we tried to measure the D_s value of 80:20 and 50:50 PAA/PPO solutions but due to the aggregation we suggest that only some of polymer will be visible in DOSY data.

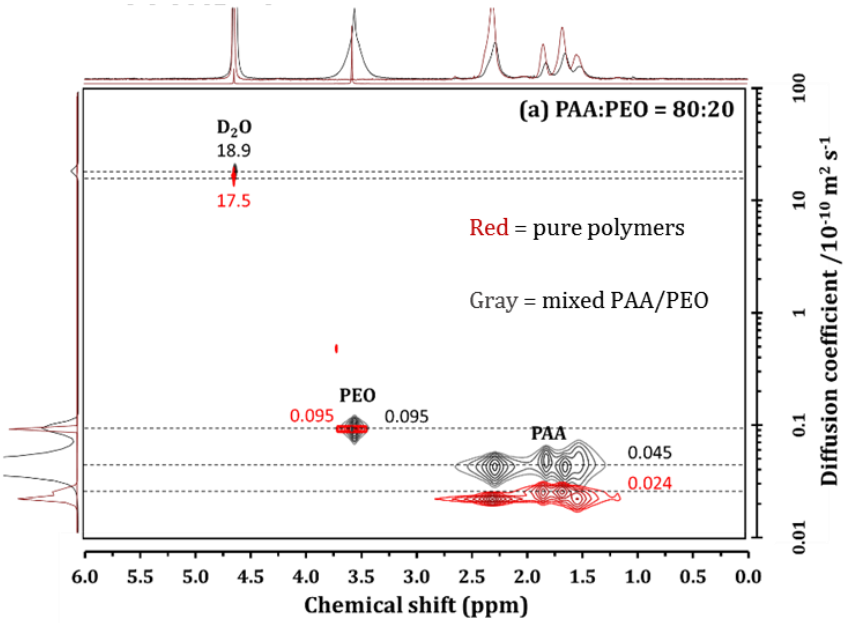
(a) PAA:PEO = 80:20
D2O
18.9
17.5
Red = pure polymers
Gray = mixed PAA/PEO
PEO
0.095
0.095
PAA
0.045
0.024
Diffusion coefficient /10-10 m2 s-1
100
10
1
0.1
0.01
6.0 5.5 5.0 4.5 4.0 3.5 3.0 2.5 2.0 1.5 1.0 0.5 0.0
Chemical shift (ppm)

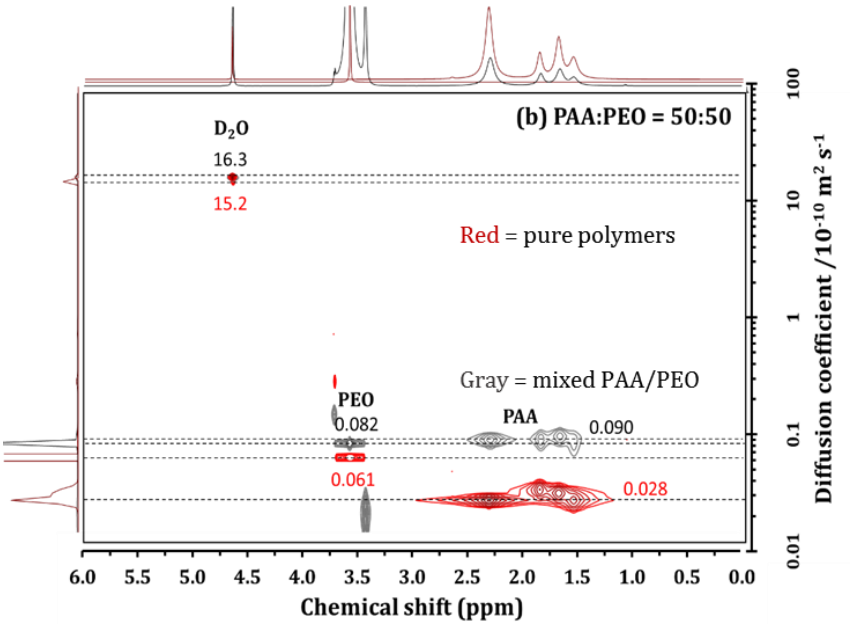
(b) PAA:PEO = 50:50
D2O
16.3
15.2
Red = pure polymers
Gray = mixed PAA/PEO
PEO
0.082
0.061
PAA
0.090
0.028
Diffusion coefficient /10-10 m2 s-1
100
10
1
0.1
0.01
6.0 5.5 5.0 4.5 4.0 3.5 3.0 2.5 2.0 1.5 1.0 0.5 0.0
Chemical shift (ppm)

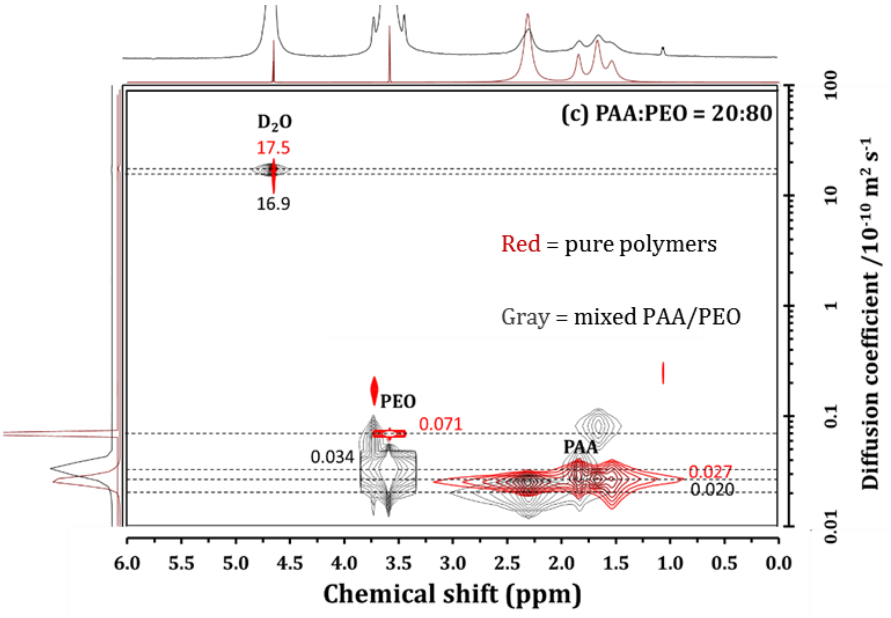

Figure 4.16 Self-diffusion coefficient (D_s) of pure PAA solutions (red, at 2.5-1.0 ppm) and pure PEO solution (red, at 3.57 ppm) and PAA/PEO solutions (gray) as a function of volume ratio between PAA and PEO solutions (a) 80:20, (b) 50:50 and (c) 20:80 with the total concentration = 1%w/v.

The D_s values of PAA and PEO in 20:80 PAA/PEO solution are lower than those values of individual pure polymer in solutions but the values are rather broad. Especially, each proton signal of PAA appears at different D_s values so here we only consider the D_s value of the peak at 2.29 ppm of -C**H** in PAA. This suggests that hydrogen bonding in the 20:80 PAA/PEO solution is rather weak. However, the D_s values of PAA and PEO in 80:20 and 50:50 PAA/PEO solutions are higher than the values for individual pure polymers as shown in **Figure 4.16**(a) and (b) since the aggregation found in both solutions causes a more dilute solution on the top and the aggregate settled at the bottom of the tubes. For 80:20 PAA/PEO solution, we found two separate D_s values of PAA and PEO in the mixed solution, while the 50:50 PAA/PEO solution has fairly close D_s values which might be the most promising evidence of the hydrogen bonding between these two polymers.

4.3.2 T_2 solvent relaxation

In this section, we use the T_2 solvent relaxation technique to probe the association between PAA and poly(ether) in solution. We consider whether or not an experimental R_2 value of mixed PAA/poly(ether) is different from a theoretical R_2 value which is calculated by Equation (4.7):

$$R_{2,cal} = 0.5R_{2,PAA} + 0.5R_{2,Poly(ether)} \quad (4.7)$$

where $R_{2,\mathrm{PAA}}$ and $R_{2,\mathrm{Poly(ether)}}$ are the relaxation rate of pure PAA and of pure poly(ether), respectively and the weight ratio of PAA to poly(ether) is 1 to 1. Total concentration of $R_{2,\mathrm{cal}}$ is the same as the pure polymer. It is expected that any association will cause a lower solvent T_2 value (or a higher R_2 value) than a calculated one because of decreased mobility of solvent molecules and increased viscosity of solution.

4.3.2.1 PAA/PEO

Low and high M_w PAA/PEO

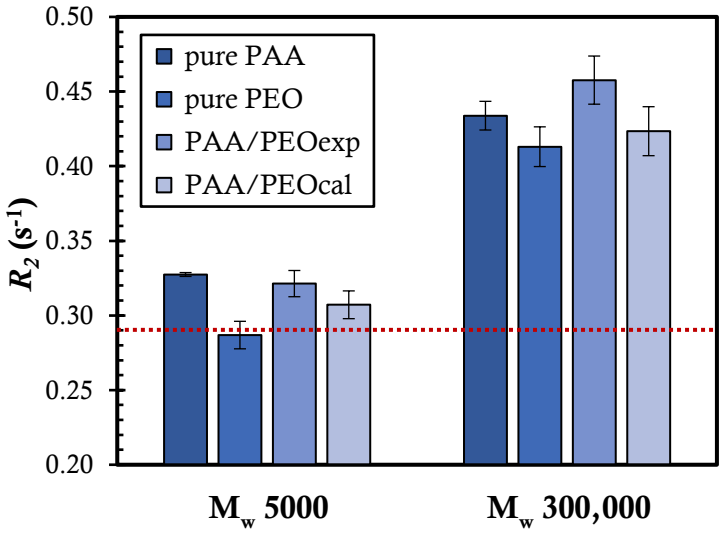

Figure 4.17 The relaxation rate (R_2, solvent) obtained from single exponential fit for pure PAA M_w 5000, pure PEO M_w 5000, PAA M_w 5000/PEO M_w 5000, pure PAA M_w 273,000, pure PEO M_w 300,000 and PAA M_w 273,000/PEO M_w 300,000 (weight ratio of PAA to PEO = 1:1) in aqueous solution at pH 3 and all samples are 5%wt total concentration. (Red-dotted line: R_2 of pH 3 aqueous solution = 0.29 s^{-1} at 38-40 °C)

For low M_w PAA (M_w 5000)/PEO (M_w 5000) and high M_w PAA (M_w 273,000) /PEO (M_w 300,000) in pH 3 solutions, a single exponential decay is used to fit all relaxation curves of polymer solutions at 5%wt total concentration. From **Figure 4.17**, it is seen that a higher M_w results in an increased R_2 value as a consequence of increasing viscosity. The R_2 value of PAA is higher than PEO which might be due to better solubility of PAA (more expanded chains) than PEO. The standard deviation (SD) of calculated R_2 values is obtained from error propagation of the SD of pure polymers. The experimental R_2 value of PAA/PEO (M_w 5000) in pH 3 solution is slightly higher than the calculated value within an error bar. For PAA/PEO (M_w 300,000), the experimental R_2 value is higher than the calculated one, however taking the size of error bars into account, the difference is not significant so there is no conclusive evidence for interaction between PAA and PEO.

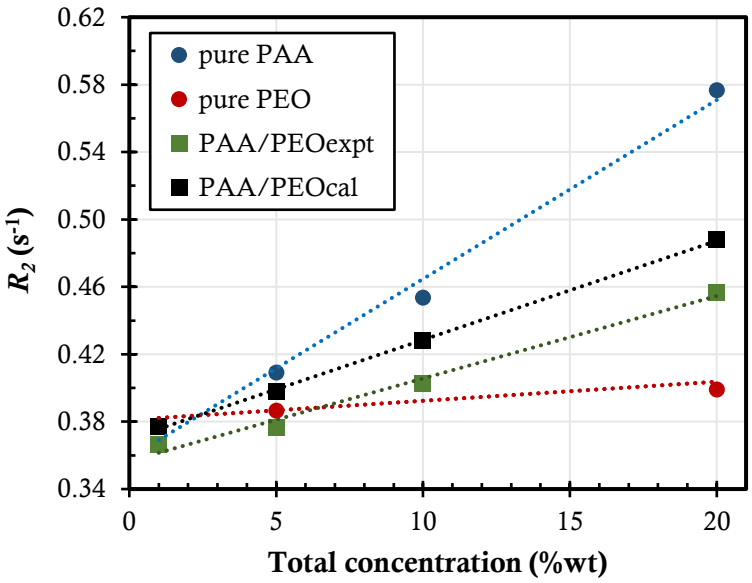

Figure 4.18 The relaxation rate (R_2, solvent) vs total concentration (%wt) obtained from a single exponential fit for pure PAA M_w 5000, pure PEO M_w 200, PAA M_w 5000/PEO M_w 200 solutions in methanol comparing with the calculated R_2 value of PAA M_w 5000/PEO M_w 200 (the weight ratio of PAA to PEO = 1:1).

Moreover, we investigated the association between PAA M_w 5000 and PEO M_w 200 in methanol. Since we used rather low M_w polymers, we prepared the solutions in a range of total concentration of 1-20%wt and all relaxation curves were fitted with a single exponential decay. In **Figure 4.18**, it is seen that the R_2 values of pure PEO of M_w 200 are significantly lower than for PAA of M_w 5000. It is possible that PEO chains are more collapsed in methanol so that they are only weakly dependent of concentration.

For 20%wt samples, we found that the relaxation curves cannot be fitted well with a single exponential. This means their relaxation decay is not only attributed to a long T_2 (low R_2 value) of the solvent but also a short T_2 (high R_2 value) of the polymer. However, we do not present the relaxation of polymer here as the R_2 value of polymer is independent of concentration in a range of 0-20%wt and has a large error, which we also found later for PAA/PTHF in methanol.

The experimental R_2 values (solvent) of low M_w PAA (M_w 5000)/PEO (M_w 200) are lower than the calculated ones for all concentrations. This could mean that there is no interaction between PAA M_w 5000 and PEO M_w 200 in methanol.

Very high M_w

Figure 4.19 Images of PAA M_w 4,000,000/PEO M_w 4,000,000 in pH 3 solution at different volume ratios of PAA to PEO (100:0, 80:20, 60:40, 50:50, 40:60, 20:80, 0:100) at 1 %w/v total concentration.

In this experiment, we mixed very high M_w PAA and PEO in pH 3 solution at various volume ratios (PAA:PEO = 80:20, 60:40, 50:50, 40:60 and 20:80) and 1 %w/v total concentration as shown in **Figure 4.19**. We observed white aggregates at the bottom of the NMR tubes in all mixed samples except the 20:80 solution which is only a bit cloudy. The aggregate is a strong evidence of the association between PAA and PEO and causes the remaining solutions to be more dilute. We therefore anticipate that the R_2 value of mixed PAA/PEO solutions should be lower than the calculated R_2 value (where $R_{2,cal} = V_{PAA}R_{2,PAA}+V_{PEO}R_{2,PEO}$ and V is volume ratio) or closer to the R_2 value of bulk solvent. Moreover, in principle one could use ^{1}H-NMR integration with D_2O peak as a reference to quantify the composition of the polymer solution above the aggregate (and thus potentially derive information on the composition of the aggregate itself) but that was not attempted here.

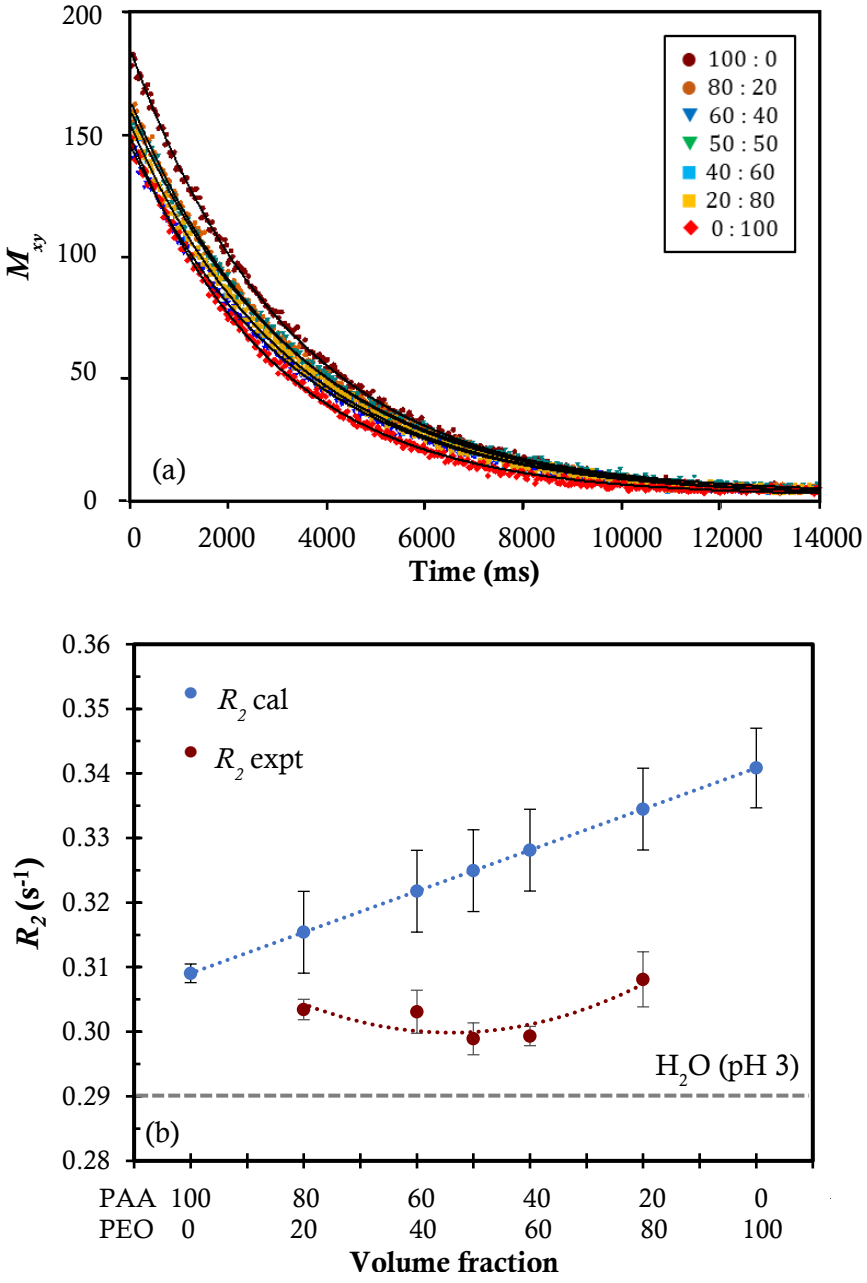

Figure 4.20 Solvent relaxation of PAA M_w 4,000,000/PEO M_w 4,000,000 in pH 3 solution at different volume ratios of PAA to PEO (100:0, 80:20, 60:40, 50:50, 40:60, 20:80, 0:100) at 1%w/v total concentration. (a) plot of transverse magnetization (M_{xy}) as a function of time, and (b) relaxation rate (R_2, solvent) vs volume fraction.

Figure 4.20(a) shows that the relaxation curves can be fitted well with a single exponential decay and **Figure 4.20**(b) shows the R_2 solvent values of PAA/PEO (M_w 4,000,000) solutions at the different volume ratios are in a range of 0.299 – 0.308 s^{-1} which is close to pH 3 solution (bulk solvent, R_2 = 0.290 s^{-1}) and lower than the calculated R_2

values as we expected due to the aggregation of PAA and PEO via hydrogen bonding. In addition, the optimum ratio for the hydrogen bonding is found at volume ratio = 50:50.

4.3.2.2 Low M_w PAA/PTHF

For the low M_w PAA/PTHF solution, we prepared pure PAA M_w 5000, pure PTHF M_w 6000 and mixed PAA M_w 5000/PTHF M_w 6000 in methanol at a range of concentrations of 5-50%wt. We observed that at above 10%wt the solutions became viscous. For mixed PAA/PTHF, the solutions were homogeneous without precipitate.

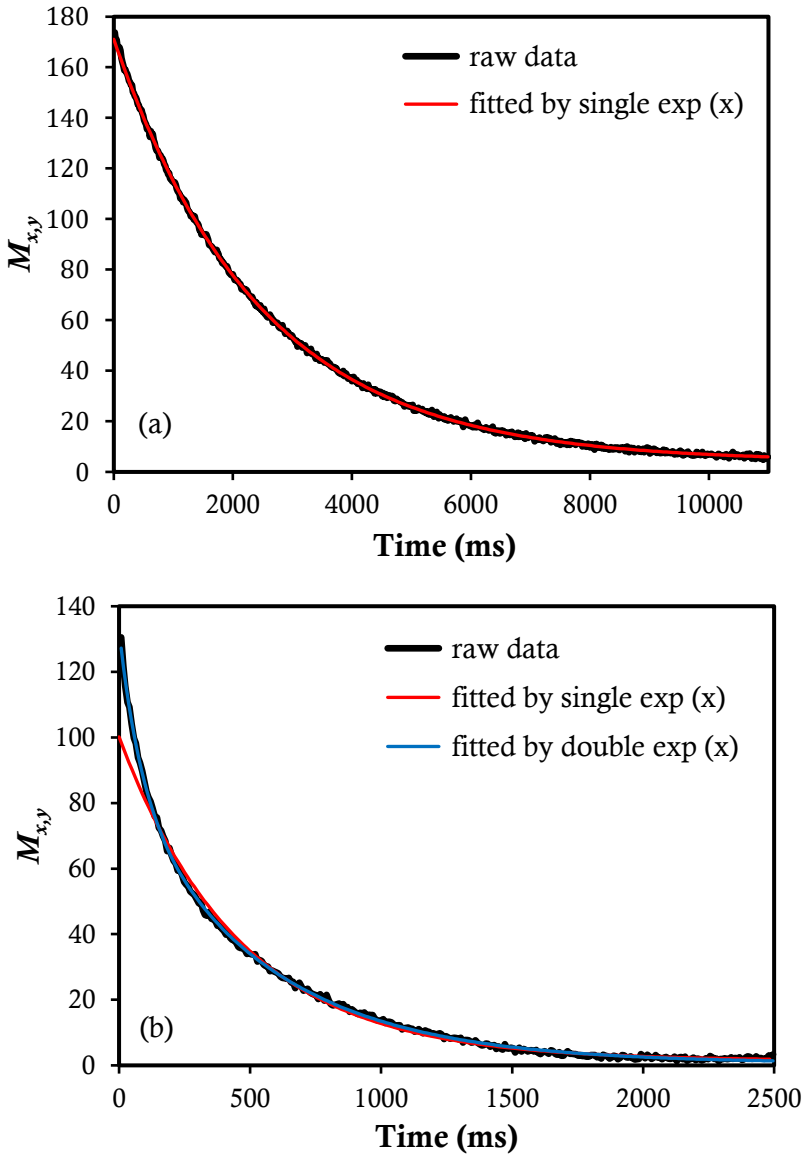

Figure 4.21 The relaxation curves of (a) 5%wt and (b) 50%wt of PAA M_w 5000 solution in methanol fitted by a single and double exponential, respectively.

We first obtained the values fitted by the AreaQuant program with a single exponential decay as Equation (4.6). However, we noticed that the single exponential cannot properly fit the relaxation decay curve of concentrated solutions at above 10%wt, while the double exponential can fit very well as shown in **Figure 4.21(**b**).** This indicates that at higher concentrations both polymer and solvent appear almost as independent relaxations. Therefore, we fitted all samples with a double exponential and the relaxation of polymer and solvent can be obtained.

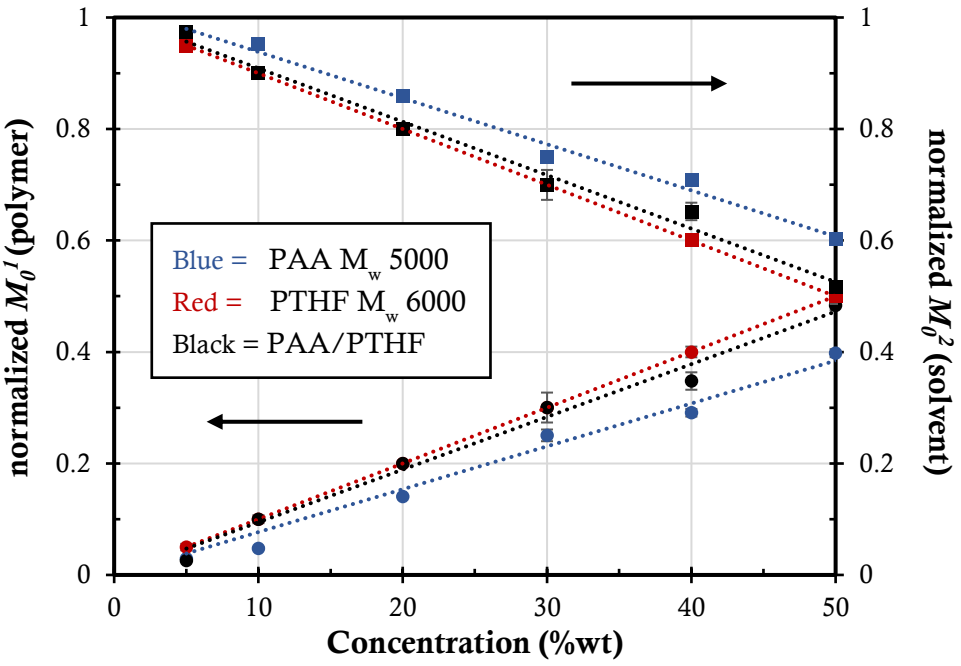

Figure 4.22 Normalized M_0^1 (polymer) and M_0^2 (solvent) constants obtained from double exponential fit as a function of concentration for PAA M_w 5000, PTHF M_w 6000 and PAA M_w 5000/PTHF M_w 6000 in methanol at the weight ratio of PAA to PTHF = 1:1.

M_0^1 and M_0^2 are attributed to the number of protons in polymer and solvent, respectively. Normalized M_0^1 and M_0^2 for each concentration are calculated using $M_0^1/(M_0^1 + M_0^2)$ and $M_0^2/(M_0^1 + M_0^2)$, respectively. In **Figure 4.22**, the consistency of the data above following a linear relationship between M_0 and concentration shows that the two components do originate from the polymer and solvent so that the increase of polymer concentration results in an increasing polymer proton number and a decreasing solvent proton number. In addition, the double exponential equation also gives the relaxation rates of protons involved with the two components: polymer (R_2^1) and solvent (R_2^2) as shown in **Figure 4.23**(a, b), respectively.

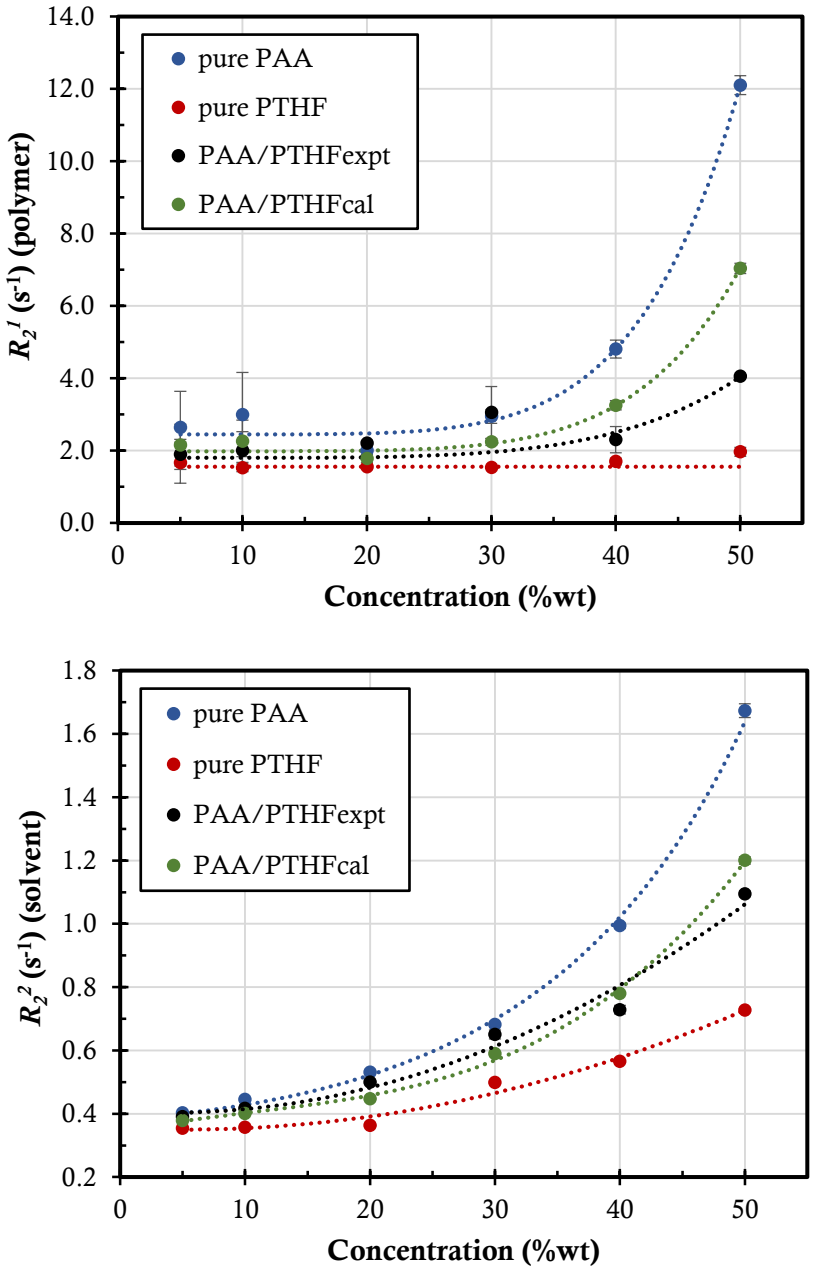

Figure 4.23 The relaxation rate (a) R_2^1 (polymer) and (b) R_2^2 (solvent) obtained from double exponential fit for pure PAA M_w 5000, pure PTHF M_w 6000, PAA M_w 5000/PTHF M_w 6000 solutions in methanol comparing with calculated values of PAA M_w 5000/PTHF M_w 6000 at the weight ratio of PAA to PTHF = 1 : 1. (R_2 of pure methanol = 0.36 s^{-1})

The value of R_2^1 (polymer) is significantly greater than that of R_2^2 (solvent) as expected because of size and mobility. The R_2 values of PAA are all greater and much more dependent on concentration than those of PTHF since perhaps PAA is more solvated (more extended) than PTHF (more collapsed chains) in methanol and PAA might have a stronger interaction as we found the higher R_2 values for both polymer and solvent.

In other words, we suggest that for PTHF solutions the solvent molecules may only pass through the coil-form of polymer chains and do not interact much with the polymer chains, which is called solvent free-draining.[53] In addition, the increase of R_2 values with increasing polymer concentration is because the mobility of the polymer protons and solvent become more constrained or the solutions become more viscous.

In **Figure 4.23**(a), it can be seen that the R_2^1 (polymer) values are significantly increased for PAA solutions over 30%wt, while the R_2^1 (polymer) values of PTHF and PAA/PTHF solutions are rather low in a range of 1 to 4 s^{-1}. In **Figure 4.23**(b), the R_2^2 (solvent) values at low concentrations are rather close to that of pure methanol (0.36 s^{-1}) and then they increased significantly above 20%wt. The figure also shows a calculated theoretical R_2 value, obtained from the R_2 value of pure polymer solutions at the same overall concentration and described as Equation (4.7). The calculated curve agrees well with the experimental data. There is therefore no evidence for association between PAA and PTHF in methanol, for the low molecular weights studied here.

Conclusion

The effect of the type of polymer, M_w, and solvent on the association between PAA and poly(ethers), observed with ^{1}H-NMR, DOSY and T_2 solvent relaxation, is summarized in the table below.

Table 4.3 Summary of techniques used to monitor the association between PAA and poly(ethers) in solution.

Techniques	PAA/PEO				PAA/PTHF
	Low M_w		High M_w	Very high M_w	Low M_w
	pH 3	methanol	pH 3	pH 3	methanol
Observation	soluble	soluble	soluble	aggregates	soluble
^{1}H-NMR	/	/	N/A	X	/
DOSY	/ (M_w 5000)	X	N/A	//	?
T_2 solvent relaxation	X	X	X	//	X

// = strong association, / = weak association, X = no association, and ? = inconclusive

Inspecting the ^{1}H-NMR spectra, an upfield shift to lower ppm is only found for low M_w samples: PAA (M_w 5000)/PEO (M_w 200 and M_w 5000) in D_2O at pH 3, and PAA (M_w 5000)/PTHF (M_w 250 and M_w 1000) and PAA (M_w 5000)/PEO (M_w 200) in methanol-d_4. We suggest that the upfield shift is due to H-bonding but it is not obvious here since the chemical shift difference ($\Delta\delta$) is very small (0.05 ppm for D_2O and 0.17 ppm for methanol-d_4). It is not clear why no such shift was observed for the very high M_w sample where macroscopic aggregation is visible. Comparison with the other two experimental techniques discussed below suggests that this approach was not helpful to identify cases of polymer association. Using DOSY-NMR, if the two polymers in a solution mixture have very similar values for the diffusion coefficient, this is taken as a strong indicator for association, especially if the pure polymer solutions have very different values. The

PAA/PEO mixtures investigated at pH 3 all showed evidence for such association (both at low and at very high M_w). The optimum hydrogen bonding is observed at 50:50 very high M_w PAA/PEO. No association was seen for a low M_w PAA/PEO mixture in methanol, whereas the results for PAA/PTHF mixtures were inconclusive.

Using the T_2 solvent relaxation technique, a marked difference of the experimental relaxation rates compared to predictions based on pure polymer solution data was taken as evidence for association. The low and high M_w PAA/PEO mixtures do not show such an effect (in water nor in methanol). The very high M_w mixtures however do show evidence of association. For very high M_w PAA/PEO (M_w 4,000,000), PAA can strongly associate with PEO at 1%w/v total concentration in pH 3 solution as we found white aggregates. This is consistent with the experimental R_2 values of PAA/PEO solutions being lower that the calculated ones (due to the remaining polymer concentration being lower), and a minimum value is observed at volume ratio of PAA to PEO = 50:50. In addition, for the PAA/PTHF in methanol, the relaxation curves were fitted with a double exponential decay so we obtained the relaxation signals from both components of polymer and solvent. However, we did not find evidence of association. In addition, we found that the R_2 values of PAA are greater and more dependent on concentration than the values of PTHF.

In conclusion, whilst ^{1}H-NMR does not appear to be too helpful to detect polymer association, both DOSY-NMR and T_2 solvent relaxation can be used to do so. DOSY already provided indications for association at low M_w, but the solvent relaxation approach required higher M_w samples for a clear effect to be visible.

Bibliography

1. F. E. Bailey JR, R. D. Lundberg, R. W. Callard. *Journal of Polymer Science Part A: Polymer Chemistry* **1964**, *2*, 845-851.

2. T. Ikawa, K. Abe, K. Honda, E. Tsuchida. *Journal of Polymer Science Part A: Polymer Chemistry* **1975**, *13*, 1505-1514.

3. Pradip, C. Maltesh, P. Somasundaran, R. A. Kulkarni, S. Gundiah. *Langmuir* **1991**, *7*, 2108-2111.

4. M. M. Zhao, S. A. Eghtesadi, M. B. Dawadi, C. Wang, S. Y. Huang, A. E. Seymore, B. D. Vogt, D. A. Modarelli, T. B. Liu, N. S. Zacharia. *Macromolecules* **2017**, *50*, 3819-3831.

5. Y. Hirashima, A. Suzuki. *Journal of Colloid and Interface Science* **2007**, *312*, 14-20.

6. A. Noro, Y. Matsushita, T. P. Lodge. *Macromolecules* **2008**, *41*, 5839-5844.

7. S. K. H. Gulrez, S. Al-Assaf, G. O. Phillips. Hydrogels: methods of preparation, characterisation and applications; Prof. Angelo Carpi (Ed.); In tech: UK, **2011**.

8. A. S. Hoffman. *Advanced Drug Delivery Reviews* **2012**, *64*, 18-23.

9. K. Kaushlendra, S. K. Asha. *Journal of Physical Chemistry B* **2014**, *118*, 4951-4962.

10. R. Parthasarathi, V. Subramanian. Characterization of Hydrogen Bonding: From van der Waals Interactions to Covalency; Grabowski, S. J. (Ed.); Springer: Netherlands, **2006**.

11. A. Katchalsky, H. Eisenberg. *Journal of Polymer Science* **1951**, *6*, 145-154.

12. D. Reith, B. Muller, F. Muller-Plathe, S. Wiegand. *Journal of Chemical Physics* **2002**, *116*, 9100-9106.

13. T. Swift, L. Swanson, M. Geoghegan, S. Rimmer. *Soft Matter* **2016**, *12*, 2542-2549.

14. G. Karlstrom. *Journal of Physical Chemistry* **1985**, *89*, 4962-4964.

15. K. Tasaki. *Journal of the American Chemical Society* **1996**, *118*, 8459-8469.

16. E. E. Dormidontova. *Macromolecules* **2002**, *35*, 987-1001.

17. B. Hammouda, D. L. Ho, S. Kline. *Macromolecules* **2004**, *37*, 6932-6937.

18. M. Winger, A. H. de Vries, W. F. van Gunsteren. *Molecular Physics* **2009**, *107*, 1313-1321.

19. T. Swift, C. C. Seaton, S. Rimmer. *Soft Matter* **2017**, *13*, 8736-8744.

20. P. Dreyfuss. Poly(tetrahydrofuran); Gordon and Breach Science Publishers, **1982**.

21. H. J. Ahn, E. C. Kang, C. H. Jang, K. W. Song, J. O. Lee. *Journal of Macromolecular Science: Pure and Applied Chemistry* **2000**, *37*, 573-590.
22. G. R. Bedford. General Reviews of Proton Magnetic Resonance. In Annual Reports on NMR Spectroscopy; Mooney, E. F. (Ed.); Academic press: London, **1971**.
23. S. Bekiroglu, A. Sandstrom, L. Kenne, C. Sandstrom. *Organic & Biomolecular Chemistry* **2004**, *2*, 200-205.
24. E. O. Stejskal, J. E. Tanner. *Journal of Chemical Physics* **1965**, *42*, 288.
25. P. Groves. *Polymer Chemistry* **2017**, *8*, 6700-6708.
26. T. Cosgrove, J. M. Sutherland. *Polymer* **1983**, *24*, 534-536.
27. H. J. V. Tyrrell, K. R. Harris. Diffusion in Liquids: A Theoretical and Experimental Study; Butterworths: London, **1984**.
28. C. S. Johnson. *Progress in Nuclear Magnetic Resonance Spectroscopy* **1999**, *34*, 203-256.
29. H. Weingartner, M. Holz. *Annual Reports Section "C" (Physical Chemistry)* **2002**, *98*, 121-155.
30. C. L. Cooper, T. Cosgrove, J. S. van Duijneveldt, M. Murray, S. W. Prescott. *Soft Matter* **2013**, *9*, 7211-7228.
31. D. Fairhurst, T. Cosgrove, S. W. Prescott. *Magnetic Resonance in Chemistry* **2016**, *54*, 521-526.
32. S. J. Mears, T. Cosgrove, L. Thompson, I. Howell. *Langmuir* **1998**, *14*, 997-1001.
33. G. P. Van der Beek, M. A. Cohen. Stuart, T. Cosgrove. *Langmuir* **1991**, *7*, 327-334.
34. M. R. Hossain, D. Wray, A. Paul, P. C. Griffiths. *Magnetic Resonance in Chemistry* **2018**, *56*, 251-256.
35. B. Wang, T. Yarnaquchi, S. Nakao. *Tsinghua Science and Technology* **2002**, *7*, 25 - 27.
36. Y. Yokoyama, S. Yusa. *Polymer Journal* **2013**, *45*, 985-992.
37. T. Lu, G. R. Shan, S. M. Shang. *Journal of Applied Polymer Science* **2010**, *118*, 2572-2581.
38. H. Liu, C. H. Li, H. W. Liu, S. Y. Liu. *Langmuir* **2009**, *25*, 4724-4734.
39. B. Hanley, M. Tirrell. *Polymer Engineering and Science* **1985**, *25*, 947-950.
40. C. Reichardt. Solvent and Solvent Effects in Organic Chemistry; Wiley-VCH: Weinheim, **2010**.
41. M. Holz, X. A. Mao, D.Seiferling, A. Sacco. *Journal of Chemical Physics* **1996**, *104*, 669-679.
42. B. D. Jones, 'Dilute solution molecular characterization and drag reduction studies of high molecular weight polyethylene oxide', Master of Science Thesis, Oregon State University, US **2002**.

43. Y. Uematsu. Electro-Osmosis of Polymer Solutions: Linear and Nonlinear Behavior; Springer, **2017**.

44. Q. C. Ying, B. Chu. *Macromolecules* **1987**, *20*, 362-366.

45. T. Coviello, W. Burchard, M. Dentini, V. Crescenzi. *Macromolecules* **1987**, *20*, 1102-1107.

46. R. Holyst, A. Bielejewska, J. Szymanski, A. Wilk, A. Patkowski, J. Gapinski, A. Zywocinski, T. Kalwarczyk, E. Kalwarczyk, M. Tabaka, N. Ziebacz, S. A. Wieczorek. *Physical Chemistry Chemical Physics* **2009**, *11*, 9025-9032.

47. N. Ziebacz, S. A. Wieczorek, T. Kalwarczyk, M. Fiakowski, R. Holyst. *Soft Matter* **2011**, *7*, 7181-7186.

48. K. Devanand, J. C. Selser. *Macromolecules* **1991**, *24*, 5943-5947.

49. S. Seiffert, W. Oppermann. *Polymer* **2008**, *49*, 4115-4126.

50. T. Cosgrove, P. C. Griffiths. *Polymer* **1994**, *35*, 509-513.

51. W. Brown, P. Stilbs, R. M. Johnsen. *Journal of Polymer Science Part B: Polymer Physics* **1983**, *21*, 1029-1039.

52. M. S. Wolfe, C. Scopazzi. *Journal of Colloid and Interface Science* **1989**, *133*, 265-277.

53. M. Chanda. Introduction to Polymer Science and Chemistry: A Problem-Solving Approach; CRC Press, **2013**.

Chapter 5

The use of PAA based hydrogels as controlled-release carriers triggered by pH

Abstract

Poly(acrylic acid) (PAA) is a hydrophilic and pH-responsive polymer due to the presence of ionisable carboxylic acid as pendant groups. Consequently, PAA has been widely used in controlled release applications. This chapter presents preliminary experiments using a dialysis method to investigate the release of active ingredients (AIs; benzyl alcohol (BnOH) and paracetamol) as a function of pH. Due to the limited amount of PAA/poly(ethers) microgels prepared previously, we instead used a commercial hydrogel, Carbopol® 690 from Lubrizol, US which is known to consist of highly cross-linked PAA hydrogels with allyl sucrose or allyl pentaerythritol as cross-linker. We have tried to identify the chemical structure of the Carbopol® 690 and compared it with linear PAA and our PAA microgels using FT-IR, ^{1}H- and ^{13}C- NMR. The results clearly show the existence of PAA as the main polymer component and the cross-linker is probably allyl sucrose. It is seen that the ionization of carboxylic acid to carboxylate anions in basic solutions increases the weight-swelling ratio of Carbopol® from 26 (pH 2) to 594 (pH 9). To investigate the possibility of using Carbopol® 690 as pH-responsive carriers, the AIs were loaded to the Carbopol® networks during the swelling of Carbopol® in methanol. The content of the AIs in solutions was measured using UV-Visible spectroscopy at different time intervals. %Loading of BnOH and paracetamol was 54% and 61%, respectively. It is seen that the release of the AIs from the Carbopol® was sustained but not pH-responsive.

5.1 Introduction

Hydrogels are of interest for pharmaceutical, biomedical and agricultural applications due to their significant swelling in aqueous medium and high biocompatibility. Especially, for stimuli-responsive hydrogels their volume transition is reversible and responsive to small changes in the surrounding environment such as temperature, pH, ionic strength, light and magnetic field.[1-3]

5.1.1 pH-responsive hydrogels for controlled release systems

Polyelectrolyte (PE) hydrogels are cross-linked polymer networks with anionic and / or cationic pendant groups providing pH-sensitivity. In general, anionic gels (such as PAA and PMAA) are swollen in basic solutions, while cationic gels (such as PAAm and poly(diethylaminoethyl methacrylate) (PDEAEMA)) swell in acidic solutions.[4-6] The swelling of PE gels is attributed to an increase in electrostatic repulsion between ionized groups. Apart from the pH-response, the swelling of PE gels is sensitive to salt concentration or ionic strength.[6] The pH in the human body varies depending on the tissue / cell compartment *i.e.* pH is 7.4-7.5 for blood, 7.0 -7.5 in the colon, 6.2-7.5 in the small intestine, 6.2-7.2 for tumors in extracellular milieu, and 1.0-3.0 in the stomach.[2,6,7] Due to the pH- and salt- responsive property of PE gels, they have been extensively studied and designed to be suitable for controlled-delivery systems targeting at a desired area. As shown in **Figure 5.1**, the drug release mechanism is controlled by pH-dependent swelling of PE gels. In the stomach (acidic condition), the drug can be only released from the swollen cationic hydrogel owing to increasing in positively charged groups, whilst in the intestine (basic condition) the drug release is seen from the swollen anionic hydrogel due to increasing in negatively charged groups.[2,8] In addition, in the colon the drug release mechanism is related to chemical reactions such as microbial biodegradation of polymer chains.[8]

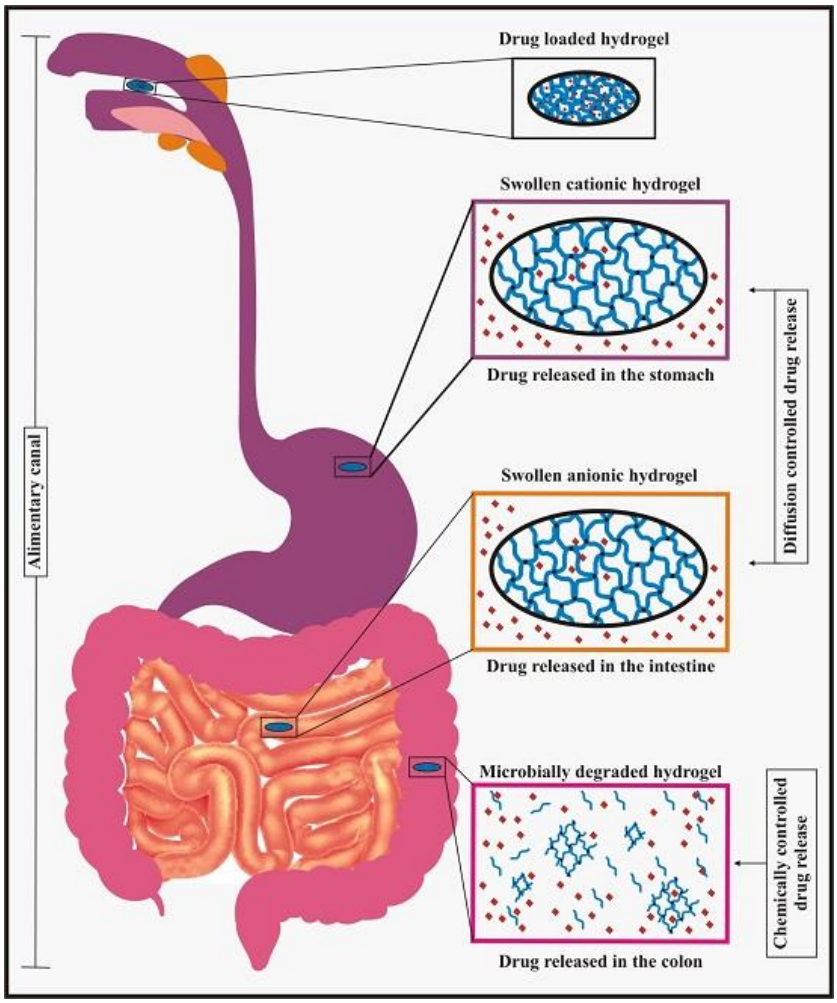

Figure 5.1 Drug release mechanism of anionic and cationic hydrogels for controlled delivery in the human body.[8] Reprinted from Graphical abstract of ref.[8]. Copyright (2017) by Polymers.

For example, Peppas *et al.*[9] studied the effect of pH on in vitro release of insulin from P(MAA-*g*-EG) hydrogels. The results show that the release of insulin is retarded in simulated gastric fluid (pH 1.2) due to interpolymer complexes between PEG grafts and carboxyl pendant groups of PMAA via hydrogen bonding. However, the insulin is suddenly released in phosphate buffered saline solutions (pH 6.8) since the hydrogen bonding is weakened due to the presence of negatively changed groups of PMAA leading to the expansion of cross-linked networks (increased correlation length, ξ and effective molecular weight between physical cross-links (M_e)) and the increase in drug diffusion coefficient (D) in the networks as illustrated by **Figure 5.2**.

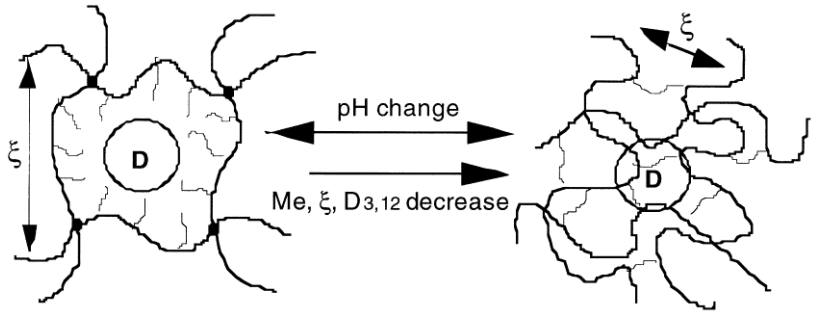

Figure 5.2 Effect of pH change on the complexation between PEG grafts and PMAA, the correlation length, ξ, the effective molecular weight between crosslinks, M_e, and the drug diffusion coefficient, $D_{3,12}$, in crosslinked, graft copolymer networks.[9] Reprinted from ref. [9]. Copyright (1999) by Journal of Controlled Release.

5.1.2 Commercial PAA based hydrogels

Carbopol® or Carbomer is a commercial range of PAA based hydrogels sold by Lubrizol. It is divided into three main categories: Carbopol® homopolymers are acrylic acid cross-linked with allyl sucrose or allyl pentaerythritol, Carbopol® copolymers are acrylic acid and C10-C30 alkyl acrylate crosslinked with allyl pentaerythritol, and Carbopol® interpolymers are Carbomer homopolymers or copolymers that contain a block copolymer of polyethylene glycol and a long chain alkyl acid ester.[10] In addition, each category has different grades varying in cross-linking density and polymerization solvent. Consequently, they have a wide range of applications such as pharmaceutical and multifunctional ingredients for controlled-release systems, bioadhesive formulation and rheology modifiers in a broad range of product types for household, industrial and institutional applications.

Parojcic *et al.*[11] investigated effect of dissolution media composition including water, buffered and unbuffered solutions at pH 4.5, 5.8 and 6.8 on drug release for paracetamol matrix tablets based on Carbopol® 970P and Carbopol® 71G which have identical chemical structures but different particle sizes. In-vitro drug release tests were performed in a paddle apparatus (Erweka DT70) at 200 rev min^{-1}. For Carbopol® 970P, the fastest release of paracetamol was observed in acidic media of 0.05 M KH_2PO_4 (pH ~ 4.5) and 0.1 M HCl (pH 1), approaching about 80-90% paracetamol released within 8 h, while the release in water and phosphate buffer was slower at 60-70%. In case of Carbopol® 71G, influence of dissolution media on the drug release profile is clearly seen so that the drug release was extremely rapid in 0.05 M KH_2PO_4 and 0.1 M HCl, and

complete within 2 h, whist the release in phosphate buffer pH 5.8 approached 100% in 8 h. In addition, the drug release was much slower in Ph Eur buffer solution pH 5.8 similar to pH 6.8 with about 50-55% released in 8 h. The results indicated that the dissolution media markedly affect the drug release so that high pH media induce the formation of gel layer on the surface tablet acting as the barrier for drug diffusion, and the drug release was therefore sustained. Conversely, in acidic dissolution media the gel swells less so the media can rapidly penetrate into the pores of the gel matrix, eventually the drug can diffuse through these pores faster than through the swollen gel.

This phenomenon was also observed by Bonacucina *et al.*[12] for paracetamol release from Carbopol® 974 (highly cross-linking), and Carbopol® 971 (lightly cross-linking) in water and water-miscible cosolvents (PEG 400 and glycerine). The release test was conducted in a paddle apparatus (Erweka DT6) with the use of the Enhancer Cell™ 4 cm^2 section.

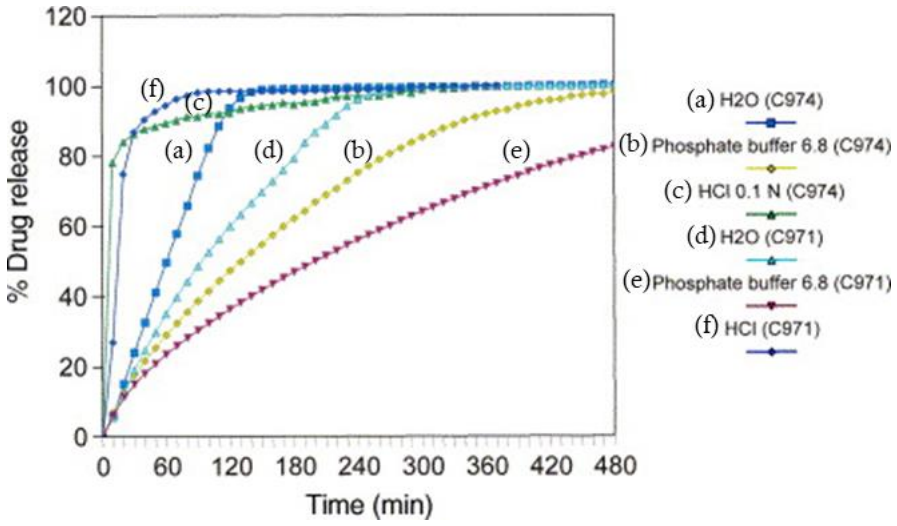

Figure 5.3 Release profiles of paracetamol from Carbopol® 974 (highly XL) and Carbopol® 971 (lightly XL) in H_2O, Phosphate buffer pH 6.8, and HCl 0.1 N.[12] Revised and Reprinted from ref. [12]. Copyright (2004) by International Journal of Pharmaceutics.

Figure 5.3 reveals the drug release in water at various pH values. The delayed release was observed following the order: phosphate buffer pH 6.8 > distilled water > HCl 0.1 N. This can be explained by the degree of ionization so that in high pH media carboxyl groups of Carbopol® were completely ionized causing the swelling of Carbopol® which limits the release of paracetamol, in water Carbopol® was partially neutralized, and in acidic solution Carbopol® was protonated and less viscous. In addition, they suggested

that in swollen state, Carbopol® 974 become the most rigid and channels were present causing the faster drug release than Carbopol® 971 which has homogeneous structure.

Noticeably, the release mechanism of drug from anionic hydrogels as mentioned above can be triggered by both acidic and basic conditions. Colombo *et al.*[13] suggests that the true swelling-controlled delivery system is a nonporous matrix in which the mobility of drug is restricted inside the gels in dry state, while in rubbery or hydrated state the mobility of drug is increased. However, for pharmaceutical applications the swellable matrix is typically porous since it is prepared by compressing a mixture of drug and excipient so the formation of a gel layer at the surface hinders the diffusion of drug.[13]

In our study, Carbopol® 690 was used as controlled-release carrier triggered by pH. Carbopol® 690 is a highly crosslinked poly(acrylic acid) powder polymerized in a toxicologically-preferred cosolvent system. It possesses relatively high viscosity, excellent stability in oxidizing systems, and shear thinning rheology so it is generally suitable for home cares such as creams and cleansers, dish care, laundry detergent. pH of un-neutralized PAA in aqueous dispersion is 2.5 – 3.5 and viscosity is 40,000 – 65,000 mPa.s (0.5%wt mucilage Brookfield RVT at 20 rpm at 25 °C).[14]

5.1.3 Model active ingredients

Properties of active ingredients (AIs) in our experiments are listed in **Table 5.1**. Benzyl alcohol and paracetamol were used as model AIs since they have rather similar in chemical structure with benzene ring and hydroxyl group and additional amide group for paracetamol.

Table 5.1 Physicochemical properties of model AIs.

Model AIs	Molecular structure	Molar mass (g/mol)	Solubility in water	pK_a	Log P	Other
Benzyl alcohol (BnOH) (liq.)	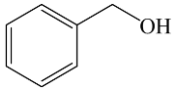	108.14	4.29 g/100 ml at 25 °C	15.4	1.1	B_p 209-205 °C
Paracetamol (solid)	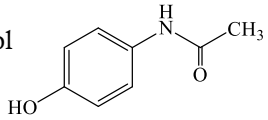	151.2	1.4 g/100 ml at 20 °C	9.5*	0.46	M_p 169 °C

*Paracetamol is present in a non-ionized form in the physiological range.[11]

In our experiment, we preformed preliminary experiments using a dialysis method to explore the ability of Carbopol® 690 being used as controlled-release carriers triggered by pH and UV-Visible spectroscopy was employed to measure %loading and %release of AIs from Carbopol® 690. Additionally, chemical structure of Carbopol® 690 comparing with linear PAA and PAA/PPG microgels was characterized using FT-IR, ^{1}H- and ^{13}C-NMR.

5.2 Experimental

5.2.1 Materials

Carbopol® 690 was kindly provided by Lubrizol. Benzyl alcohol (BnOH, anhydrous 99.8%) and paracetamol (or acetaminophen 98-102%) were purchased from Sigma-Aldrich. Poly(acrylic acid) (linear PAA M_w 5000, 50%wt solution in water) was purchased from Acros Organic. The PAA solution was dried with rotary evaporator and then vacuum oven at 60 °C until the weight was constant. Buffer solutions were prepared from potassium chloride (KCl, Merck) / hydrochloric acid (35% HCl, VWR) for pH 2, acetic acid (CH_3COOH, Fluka) / sodium hydroxide (NaOH, Fisher Scientific) for pH 4, potassium phosphate monobasic (≥98.0% KH_2PO_4, Sigma) / NaOH for pH 6 and 7, and sodium hydrogen carbonate ($NaHCO_3$, Fisher Scientific) / NaOH for pH 10, KCl / NaOH for pH 12. Deionized water (DI water) with a resistivity greater than 18.2 MΩ·cm was obtained from a Milli-Q Plus system from Millipore. Cellulose membrane dialysis tubing with a cut-off molecular weight of 14,000 (Sigma-Aldrich) was used for the release experiments of active ingredients. All chemicals were used without further purification.

5.2.2 Sample preparation

5.2.2.1 ATR-FTIR

Attenuated Total Reflection Fourier Transform Infrared (ATR-FTIR) spectra of solid samples were obtained with a Perkin Elmer spectrum 100 FTIR spectrometer in the wavenumber range 600–4000 cm^{-1} with a resolution of 8 cm^{-1}.

5.2.2.2 ^{1}H- and ^{13}C- NMR

Firstly, linear PAA and Carbopol® 690 were ionized in NaOH solution (pH 9.1) before drying. Proton (^{1}H-) NMR spectra of linear PAA, linear PAANa, Carbopol® 690, and

Carbopol® 690Na in D_2O were measured using a Bruker Advance III HD spectrometer operating at 500 MHz. The experiments were recorded at 25 °C and the number of scans was 64.

5.2.2.3 UV-Visible spectroscopy

UV-Vis absorbance was measured using an Agilent 8453 UV-Visible Spectrophotometer. All samples were contained within a quartz cuvette with an optical path length of 1 cm. DI water was used to run the background each time before measuring a new sample.

5.2.3.4 Determination of swelling ratio

0.01 g of Carbopol® 690 in 20 g of pH solutions (pH 2; HCl/DI water, pH 12; NaOH/DI water and DI water), and 0.3 g of Carbopol® 690 in 23.76 g methanol (30 ml) were added into centrifuge tubes before gently mixing on a roller overnight. Then, the mixtures were centrifuged at 10,000 rpm for 2 h, and the supernatant (unabsorbed solvent) was removed carefully with a syringe. The swollen gels were re-weighted, and the weight-swelling ratio (Q_w) defined as the ratio of W_{swollen} to W_{dry} was evaluated, here W_{swollen} and W_{dry} are the weight of swollen and dry gels, respectively.

5.2.3.5 Loading of AIs

In this study, benzyl alcohol (BnOH) and paracetamol were used as model active ingredients (AIs). Firstly, 5 ml of BnOH (l) or 0.03 g of paracetamol (s) was dissolved in 30 ml of methanol. Then, the AIs solution and 0.3 g of Carbopol® 690 were added into a Teflon centrifuge tube and they were gently mixed on a roller for overnight. To calculate %loading of the AIs trapped in Carbopol® 690, the mixture was centrifuged at 10,000 rpm using Sorvall Legend T Benchtop Centrifuge for 2 h. After that, volume of the supernatant was recorded, and the content of unloaded AIs was measured from the supernatant using UV-Vis spectroscopy together with the equations from the calibration curves in **Figure 5.9**. Carbopol® 690/AIs mixture was then air-dried in a fume cupboard until the weight was constant.

5.2.3.6 Release of AIs

To investigate the release of AIs from Carbopol® 690 as a function of pH, we prepared experiments using a dialysis method. Cellulose membrane dialysis tube with 33 mm in diameter was cut off the have the length of 20 cm in total, and 3 cm each side was left for

knotting. For control samples, 0.1 ml of BnOH and 20 ml of buffer solution at a desired pH value were poured into the dialysis tube, and then the closed tube was placed in a bottle filled with 150 ml of pH solution having the same pH value as inside the tube. For paracetamol, we used the same procedure as the BnOH samples, but 2.5 mg of paracetamol was pre-dissolved in 20 ml of buffer solution at a desired pH value before the paracetamol solution was poured in the tube. For the release from Carbopol® 690 carrier, 0.03 g of dried Carbopol® 690/AIs and 20 ml of buffer solution at a desired pH were added into the dialysis tube and then, the tube was placed into a bottle filled with 150 ml of external pH solution. All bottles were left on a roller and 3 ml of the external solution was taken from the bottom with a syringe at different time intervals to measure the extent of the AIs released from the Carbopol® 690 using UV-Vis spectroscopy together with the calibration curves in **Figure 5.9**. After measuring the absorbance, the solution was poured back into the bottle.

5.3 Results and discussion

5.3.1 Chemical characterization

Firstly, we would like to identify the chemical structure of Carbopol® 690. Although we have known that it is highly cross-linked poly(acrylic acid) (PAA), its cross-linker is not clearly informed whether allyl sucrose or allyl pentaerythritol.

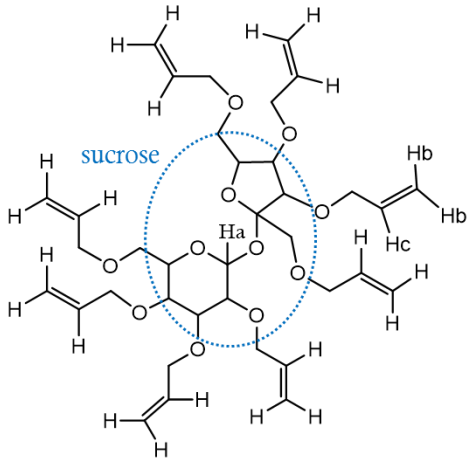

Allyl sucrose

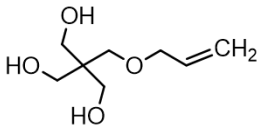

Allyl pentaerythritol

Figure 5.4 Chemical structures of sucrose and allyl pentaerythriol as possible cross-linkers for Carbopol® 690.

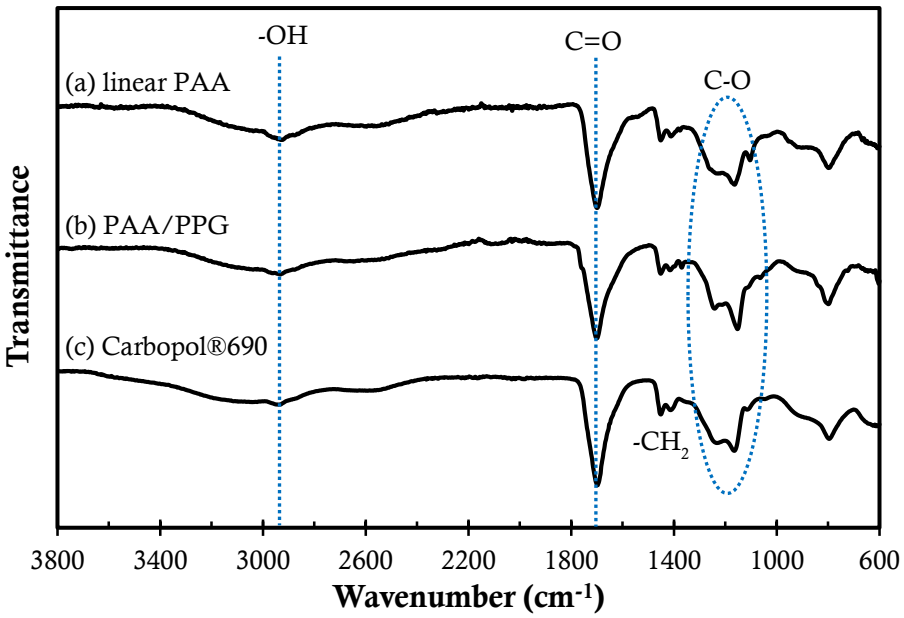

Figure 5.5 FT-IR spectra of (a) linear PAA, (b) 100:1 PAA/PPG microgels, and (c) Carbopol® 690.

Figure 5.5 illustrates that FT-IR spectra of linear PAA, 100:1 PAA/PPG microgels and Carbopol® 690 are very similar as we found the characteristic peaks of PAA appearing at 2938, 1698, 1451 and 1300-1100 cm^{-1} corresponding to -OH stretching, C=O stretching, $-CH_2$ bending, and C-O stretching, respectively. However, no evidence of cross-linker is seen, even though the product is listed as having a as high cross-link density.[14]

It is reported that proton signals of allyl sucrose[15] in $CDCl_3$ appear at 3.26-4.28 ppm for sucrose[s], at 5.23 ppm for glucopyranosyl moieties (Ha), at 5.24 ppm for geminal terminal olefin hydrogens (Hb), at 5.89 ppm for internal olefin (Hc), while the proton signals of allyl pentaerythritol[16] appear at 3.5 – 4.0 ppm for methylene protons ($–CH_2$), and 5.1-5.3 ppm and 5.8-6.0 for allyl protons. ^{1}H-NMR spectra of linear PAA and Carbopol® 690 are illustrated by **Figure 5.6**. It is seen that the characteristic structure of Carbopol® 690 is poly(acrylic acid) and the ^{1}H-NMR spectra of carboxyl groups of PAA are clearly different from ionized PAA with carboxylate groups. The carboxylate groups cause an upfield shift to lower ppm of methine (-C**H**-) and methylene protons (-C**H**$_2$-) in PAA main chains with the chemical shift change ($\Delta\delta$) = ~0.3 ppm[17] found in both linear PAA and Carbopol® 690. In addition, we found tiny peaks at 3.26, 3.38, 3.44, 3.49, 3.9, and 4.0 ppm, it is possible that the cross-linker might be allyl sucrose.

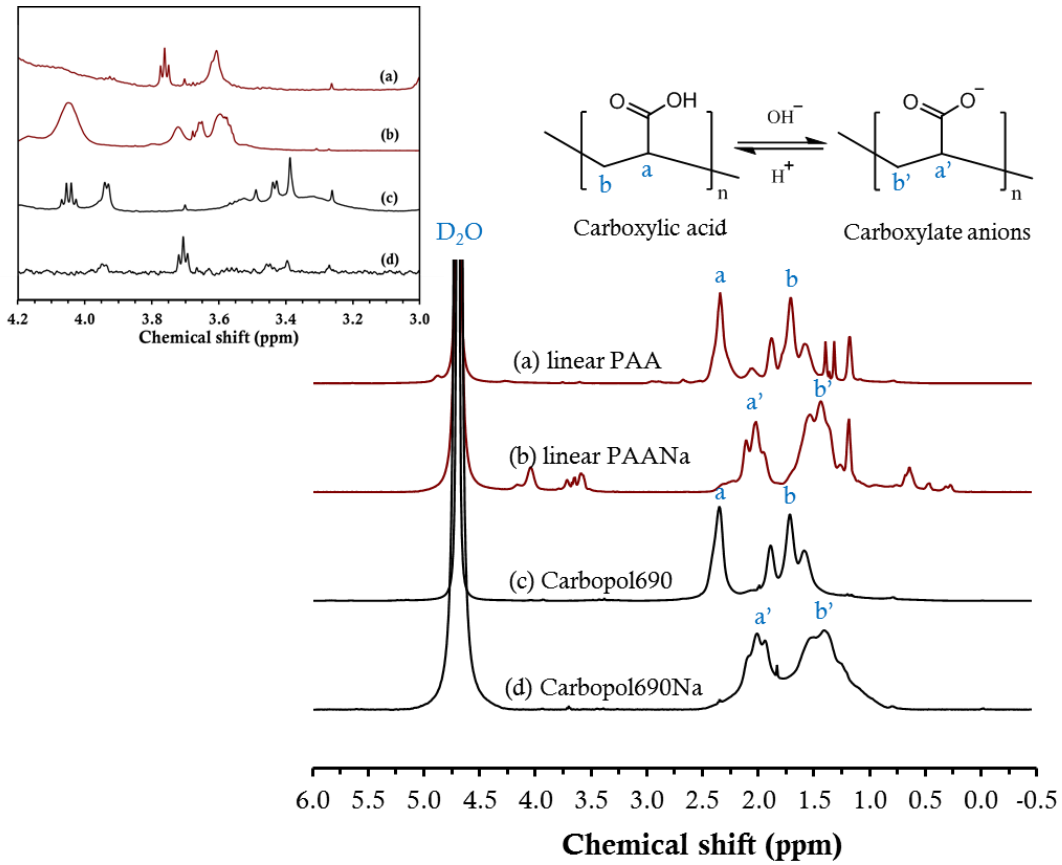

Figure 5.6 ^{1}H-NMR spectra of (a) linear PAA, (b) linear PAANa, (c) Carbopol® 690, and (d) Carbopol® 690Na.

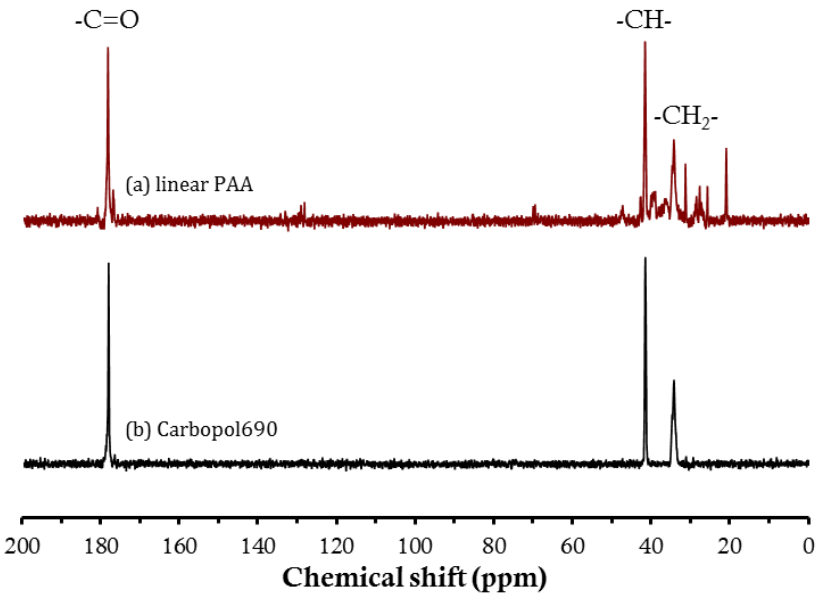

Figure 5.7 ^{13}C-NMR spectra of (a) linear PAA and (b) Carbopol® 690.

^{13}C-NMR spectra of linear PAA and Carbopol® 690 were illustrated by **Figure 5.7**. We only found the characteristic peaks of poly(acrylic acid) in Carbopol® structure appearing at 178.7 ppm for carbonyl group (–C=O), and at 41.5 and 34.1 ppm for -CH and $–CH_2$ in main chains, respectively.

5.3.2 Swelling ratio

The weight-swelling ratio (Q_w) of Carbopol® 690 in four different media was summarized in **Table 5.2**. It is seen that Carbopol® 690 significantly swells in higher pH solutions due to an increase in the difference of osmotic pressure between inside the gels and the surrounding solution as well as a rise in electrostatic repulsion between adjacent carboxylate anions of ionized Carbopol® 690. In addition, we measure the swelling ratio in methanol which is fairly similar to that of pH 2 solution and will be a helpful guidance on further experiments for loading of active ingredients (AIs).

Table 5.2 The weight-swelling ratio of Carbopol® 690 in pH 2 and pH 12 solutions, DI water and methanol.

Medium	Weight-swelling ratio (Q_w)
pH 2 solution	26
DI water*	195
pH 12 solution	594
Methanol	25

*pH of DI water is around 6 to 7.[18]

5.3.3 Calibration curves and loading of AIs

Figure 5.8 illustrates the maximum absorbing peaks of benzyl alcohol (BnOH) appear at 258 nm in methanol, at 257 nm in buffer pH 4, 7 and 10, and such peaks of paracetamol appear at 249 nm in methanol, at 244 nm in buffer pH 2 - 7, at 251 nm in buffer pH 10, and at 258 nm in buffer pH 12. This information will be further used to measure the amount of BnOH and paracetamol in the external solutions.

As shown in **Figure 5.8**(b), the absorbance peaks of paracetamol are shifted from 244 nm to 258 nm with increasing in pH of solutions. We suggest that it is due to the change of chemical structure of paracetamol resulting from the deprotonated phenyl groups at pH above its pK_a.[19] However, ^{1}H-NMR spectra of paracetamol in pH 4 (HCl/D_2O), D_2O, and pH 10 (NaOH/D_2O) show no difference (see Appendix B).

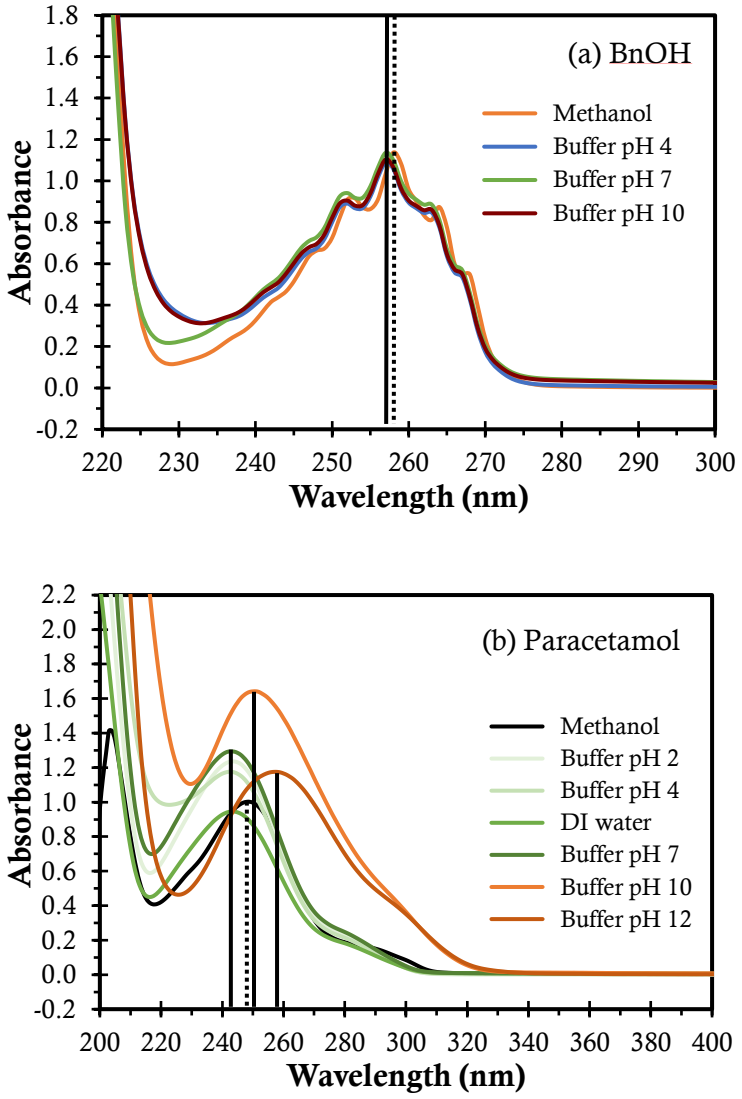

Figure 5.8 UV-Vis absorption spectra for (a) benzyl alcohol (BnOH) in methanol, buffer pH 4, 7 and 10, and (b) paracetamol in methanol, buffer pH 2, 4, DI water, pH 7, pH 10 and pH 12.

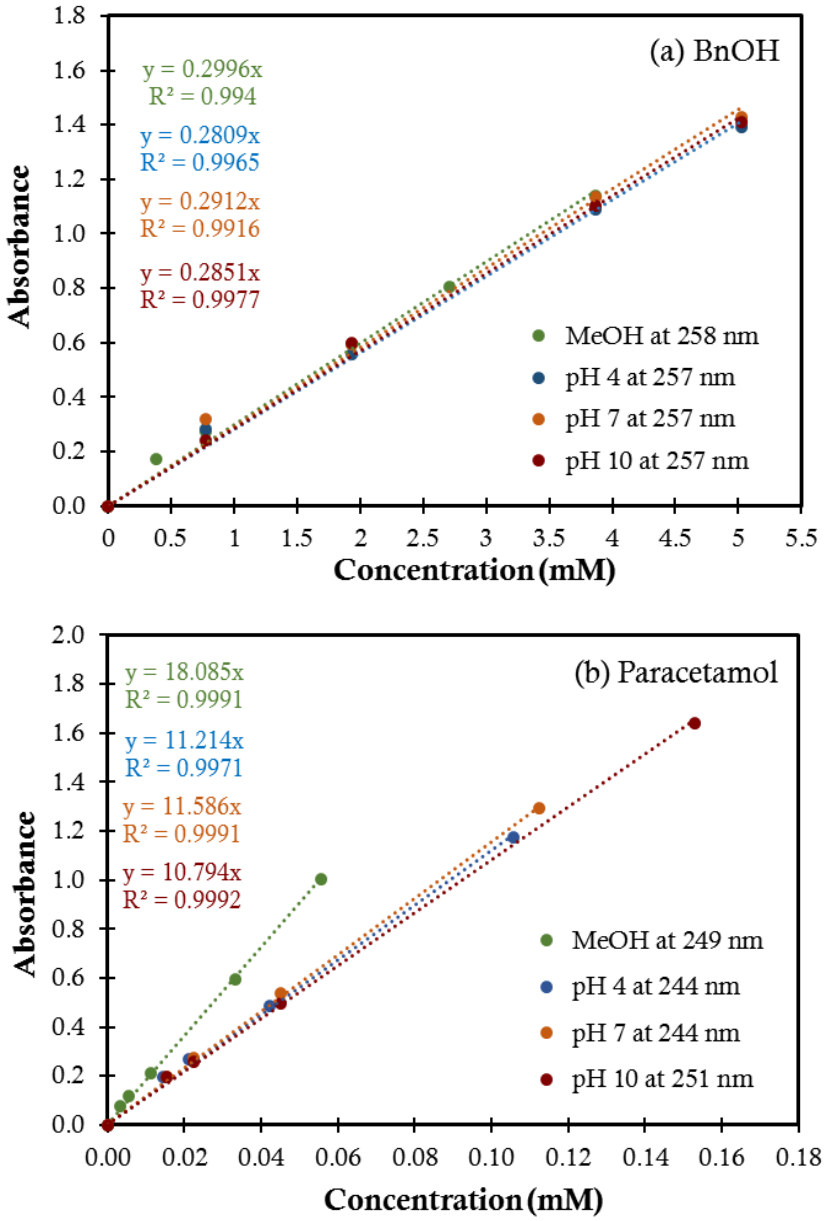

Figure 5.9 Calibration curves for (a) benzyl alcohol (BnOH) at a wavelength of 258 nm in methanol, and at 257 nm in buffer solutions of pH 4, 7 and 10, and (b) paracetamol at a wavelength of 249 nm in methanol and at 244 nm in buffer solutions of pH 4 and 7, and at 251 nm in buffer solution of pH 10.

Plots of absorbance as a function of concentration in **Figure 5.9** were used as calibration curves to determine %loading of AIs and %release of AIs as a function of time. To load AIs into Carbopol® 690 networks, AIs were first dissolved in methanol. We anticipate that the AIs will be trapped inside Carbopol® 690 networks during the swelling of the gels in methanol. From the supernatant of AIs/MeOH solutions, %loading of BnOH and paracetamol was 54% and 61%, respectively. Interestingly, these values are

rather high considering that the weight-swelling ratio of Carbopol® 690 in methanol is about 25 so that 0.3 g of Carbopol® 690 will be swollen to obtain approximately 7.5 g (or 7.2 g of methanol). However, we mixed 30 ml (23.76 g) of AIs/MeOH with 0.3 g of Carbopol® in the loading experiments, so we anticipated that the %loading might be around 30-40%.

5.3.4 Release of AIs

Considering the solubility of BnOH and paracetamol (P) in water, the concentrations we used in our experiments are very dilute and far from the solubility limit. Consequently, the release of AIs is independent from the solubility of AIs in various pH solutions assuming the concentration is the same.

Plots of %release of AIs illustrate the whole release profile of AIs after long times, while plots of normalized %release of AIs (with respect to the plateau value or 'upper limit value (a)' as listed below in **Table 5.3**) display a trend in the release rate of AIs more clearly. The release profiles of BnOH from Carbopol® 690/BnOH in pH 4, 6, 7, and 10 solutions are shown in **Figure 5.10**, and such profiles of paracetamol (P) from Carbopol® 690/P in pH 4, 7, and 10 solutions are shown in **Figure 5.11**.

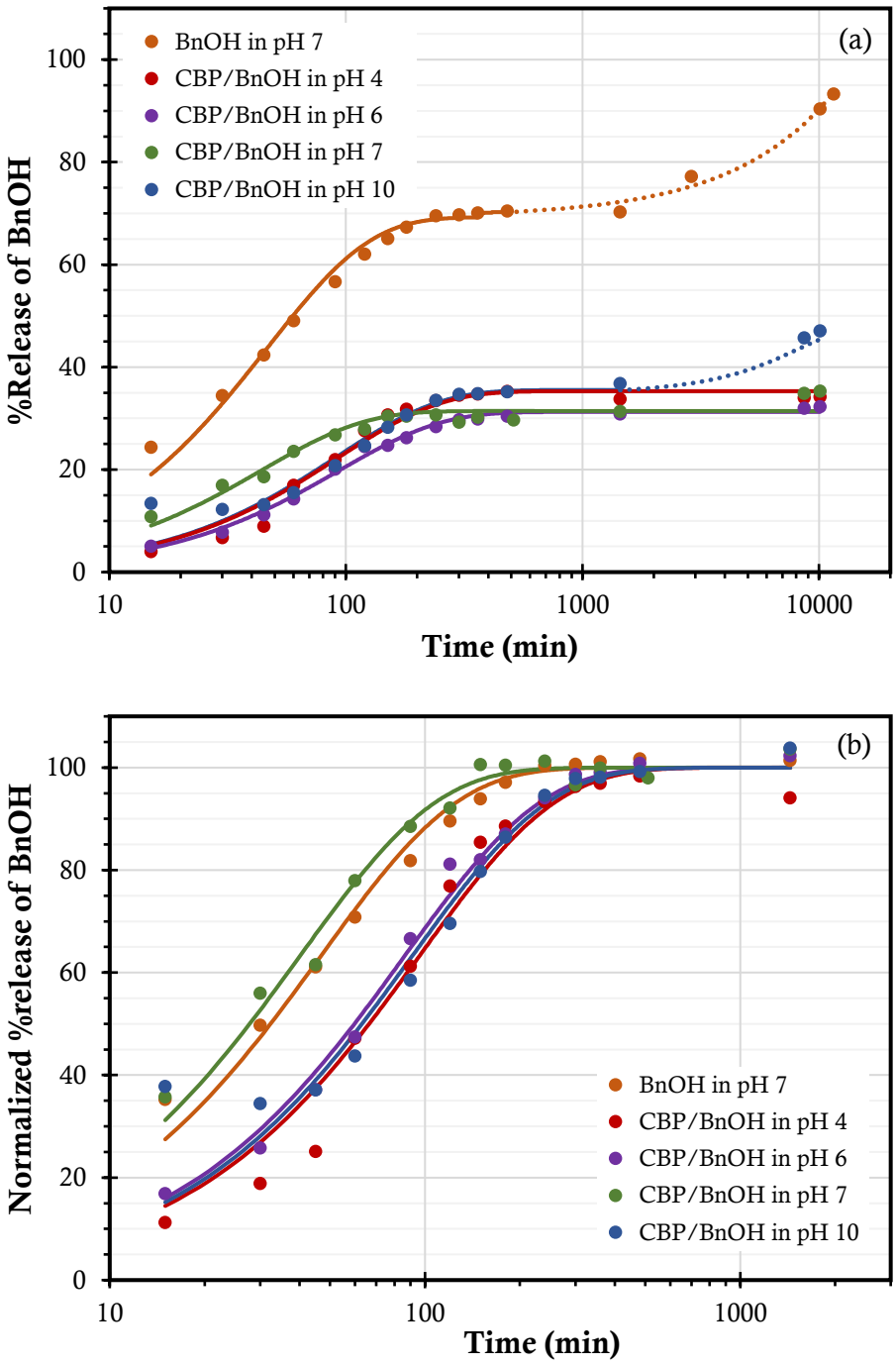

Figure 5.10 Plots of (a) %release and (b) normalized %release of benzyl alcohol (BnOH) (with respect to the plateau value at 1440 mins) from Carbopol® 690 in buffer solutions at pH 4, 6, 7 and 10.

In **Figure 5.10**(a), the initial release (15 mins) of BnOH from the CBP/BnOH is increased with increasing pH of external solutions, however, after that the effect of pH is insignificant. At 10,080 mins, the %release of BnOH from CBP/BnOH in pH 10 solution is about 46% which is slightly greater than the release in lower pH solutions (32-35%). For the control BnOH in buffer pH 7 solution, the majority of BnOH (70%) is released within 480 mins and approaching 100% in 11,520 mins. In **Figure 5.10**(b), the release of BnOH from the control sample and CBP/BnOH in pH 7 solutions are rather similar and significantly faster than the release in pH 4, 6, and 10.

From all release profiles in **Figure 5.11**(a), the release of paracetamol (P) is initially fast until after 480 mins the release is stable. The release of control samples is 96% and 60% within 480 mins for buffer solutions of pH 4 and 10, respectively, while the highest release from CBP/P is seen in buffer pH 4 solution (44%). In addition, the release of paracetamol from CBP/P show some dependence on the pH of the external solutions. The better release in acidic solutions is seen in the studies of Parojcic *et al.*[11] and Bonacucina *et al.*[12] on the release of paracetamol from Carbopol® 970P and 71G, and Carbopol® 974 and 971, respectively. It is evident that Carbopol® swell less in acidic media, and therefore the paracetamol (perhaps counterintuitively) can diffuse through the channels faster than the swollen Carbopol® acting as a barrier to retard the diffusion of AIs out of the gels. In **Figure 5.11**(b), the release of paracetamol from the control sample and CBP/P in pH 4 solutions is slightly faster than in other pH solutions.

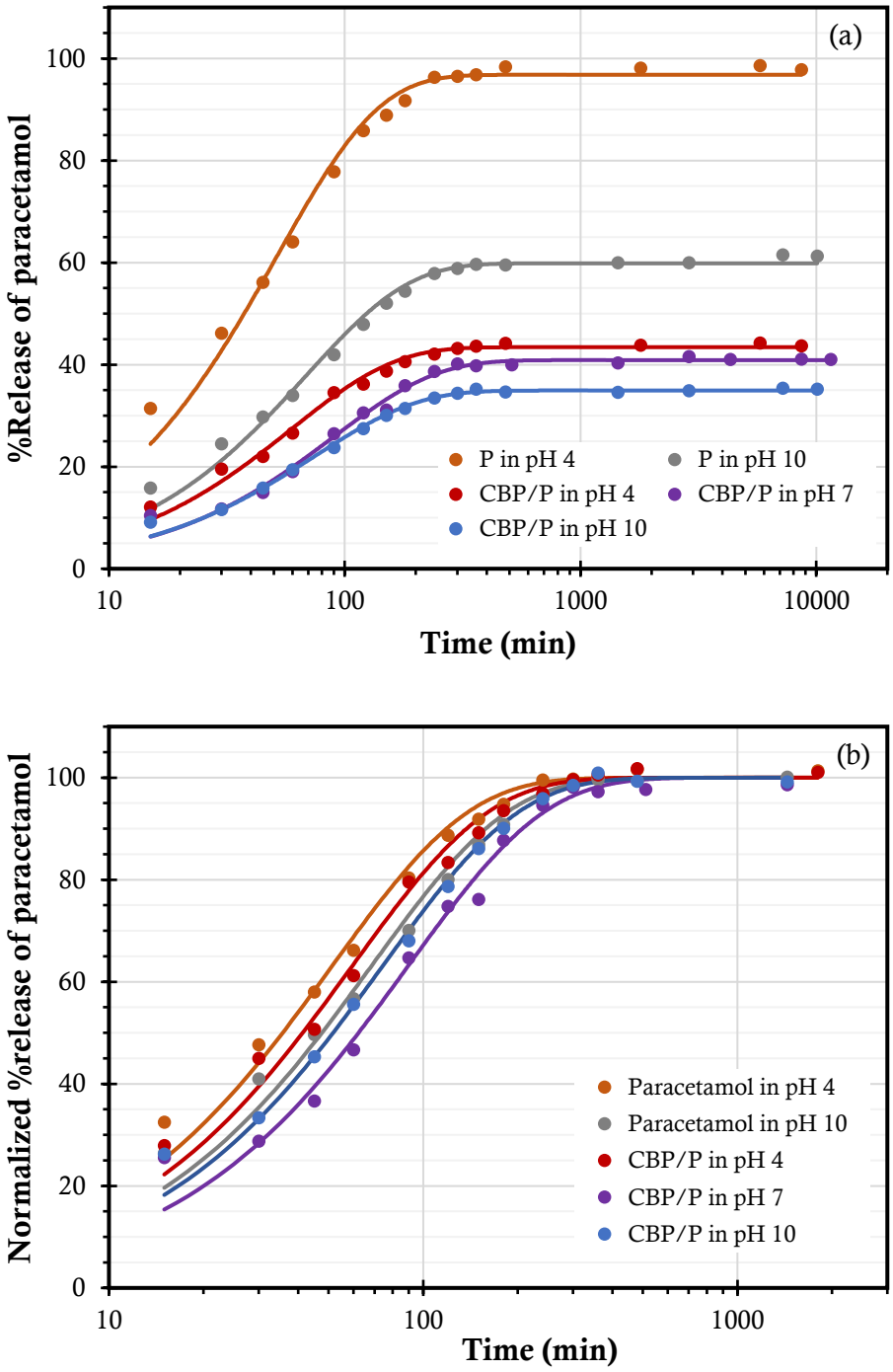

Figure 5.11 Plots of (a) %release and (b) normalized %release of paracetamol (P) (with respect to the plateau value at 1440 or 1800 mins) from Carbopol® 690 in buffer solutions at pH 4, 7 and 10.

To summarize, the release of AIs from Carbopol® is clearly sustained comparing with the control samples. However, the release of BnOH is independent of pH, while the release of paracetamol is only slightly higher at low pH. We suggest three possible reasons for insignificant influence of pH on the release of the AIs: 1) it is due to an association between Carbopol® and AIs, 2) we cannot identify that the AIs were trapped inside the Carbopol® networks and / or associated with the outer layer of Carbopol® so it is possible the release of AIs in the observed time might be attributed to the release of AIs on the surface of Carbopol® which is independent of the swelling of Carbopol®, and 3) it might be due to a volume change of the medium inside the dialysis tubing causing erratic results, however, we cannot prove this hypothesis since it is difficult to precisely weigh the wet tubing filled with Carbopol®/AIs before and after the release experiments.

Table 5.3 The release rate of benzyl alcohol and paracetamol from Carbopol® 690 at varying pH conditions.

Sample	**Solvent pH**	**y = a*(1-exp(-b*x))**	
		a = upper limit	b = release rate (min^{-1})
Benzyl alcohol (BnOH)	7	69.3	0.021±0.0011
Carbopol®690/BnOH	4	35.9	0.010±0.0010
	6	31.3	0.011±0.0004
	7	30.3	0.025±0.0013
	10	35.5	0.011±0.0014
Paracetamol	4	96.8	0.019±0.0008
	10	59.9	0.015±0.0006
Carbopol®690/paracetamol	4	43.4	0.017±0.0007
	7	40.9	0.011±0.0005
	10	34.9	0.013±0.0005

An exponential equation is used to fit the release profiles from 0 to 1,440 mins for CBP/BnOH and from 0 to 10,000 mins for CBP/P in **Figure 5.10**(a) and **Figure 5.11**(a), respectively. It is seen that the parameter 'a' is the upper limit rated to %release at equilibrium, and the parameter 'b' is the rate of growth (release rate, min^{-1}). From Carbopol®/BnOH, the %release at equilibrium is independent from pH values of surrounding solutions in the range of 30-36%, while the release rate in all pH solutions is

close at 0.01 min^{-1} except in pH 7 solution, 0.025 min^{-1}. For Carbopol®/paracetamol, the %release at equilibrium decreases with increasing pH values of surrounding solutions but the effect of pH on the release rate of paracetamol is invisible.

Conclusion

The release experiments of AIs (benzyl alcohol (BnOH) and paracetamol (P)) from Carbopol® 690 were conducted by the dialysis method with various pH buffer solutions. The content of released AIs in solutions was measured using UV-Visible spectroscopy.

The FT-IR and NMR results reveal that the Carbopol® 690 mainly consists of poly(acrylic acid) and it is feasible that the cross-linker is allyl sucrose, however at a low concentration. The weight of fully ionized Carbopol® 690 (pH 12) is about 23 times the weight in the collapsed state (pH 2). The AIs were loaded into the Carbopol® 690 during the swelling in methanol and %loading of BnOH and paracetamol were 54% and 61%, respectively, measured from the supernatant of Carbopol® 690/AIs/methanol. %Release of the AIs from Carbopol® 690 was measured from the external solutions (outside the tubing). In all experiments, the %release of AIs from Carbopol® was under 50% so that Carbopol® 690 can sustain the release of AIs comparing with the control samples. In addition, the effect of pH (or the swelling of Carbopol® 690) is insignificant for the release of BnOH and the release of paracetamol was only slightly slower in high pH media.

Bibliography

1. P. Gupta, K. Vermani, S. Garg. *Drug Discovery Today* **2002**, *7*, 569-579.

2. H. Almeida, M. H. Amaral, P. Lobão. *Journal of Applied Pharmaceutical Science* **2012**, *2*, 01-10.

3. N. Sood, A. Bhardwaj, S. Mehta, A. Mehta. *Drug Delivery* **2016**, *23*, 758-780.

4. W. A. Laftah, S. Hashim, A. N. Ibrahim. *Polymer-Plastics Technology and Engineering* **2011**, *50*, 1475-1486.

5. S.K. Ahn, R. M. Kasi, S. C. Kim, N. Sharma, Y. Zhou. *Soft Matter* **2008**, *4*, 1151-1157.

6. P. Bawa, V. Pillay, Y. E. Choonara, L. C. du Toit. *Biomedical Materials* **2009**, *4*, 15.

7. W. B. Liechty, D. R. Kryscio, B. V. Slaughter, N. A. Peppas, In Annual Review of Chemical and Biomolecular Engineering, Vol 1; Prausnitz, J. M., Doherty, M. F., Segalman, R. A., Eds.; Annual Reviews: Palo Alto, **2010**, pp 149-173.
8. M. Rizwan, R. Yahya, A. Hassan, M. Yar, A. D. Azzahari, V. Selvanathan, F. Sonsudin, C. N. Abouloula. *Polymers* **2017**, *9*, 37.
9. N. A. Peppas, K. B. Keys, M. Torres-Lugo, A. M. Lowman. *Journal of Controlled Release* **1999**, *62*, 81-87.
10. Carbopol-Polymers for Pharmaceutical Applications (Pharmaceutical Bulletin 1). [online] Available at: https://www.lubrizol.com/Life-Sciences/Literature/Pharmaceutical-Literature (accessed 08 August, 2018).
11. J. Parojcic, J. Duric, M. Jovanovic, S. Ibric, D. Jovanovic. *Journal of Pharmacy and Pharmacology* **2004**, *56*, 735-741.
12. G. Bonacucina, S. Martelli, G. F. Palmieri. *International Journal of Pharmaceutics* **2004**, *282*, 115-130.
13. P. Colombo, R. Bettini, P. Santi, A. N. Peppas. *Pharmaceutical Science & Technology Today* **2000**, *3*, 198-204.
14. Carbopol ® 690 polymer. [online] Available at: https://www.lubrizol.com/home-care/product-finder/products-data/59?productname=Carbopol%C2%AE%20690%20polymer (accessed 03 August, 2018).
15. F. J. Jaber, 'New routes for synthesis of environmentally friendly superabsorbent polymers', Master of Science Thesis, An-Najah National University, Palestine, **2012**.
16. A. Cornille, V. Froidevaux, C. Negrell, S. Caillol, B. Boutevin. *Polymer* **2014**, *55*, 5561-5570.
17. C. Dolce, G. Meriguet. *Colloid and Polymer Science* **2017**, *295*, 279-287.
18. The pH of Milli-Q® Water. [online] Available at: https://www.merckmillipore.com/GB/en/water-purification/learning-centers/applications/environment-water-analysis/ph-measurement/water-impact/7c2b.qB.xDkAAAFAdFsENFl2,nav?ReferrerURL=https%3A%2F%2Fwww.google.co.uk%2F&bd=1 (accessed 03 August, 2018).
19. V. Bernal, A. Erto, L. Giraldo, J. C. Moreno-Pirajan. *Molecules* **2017**, *22*, 14.

Chapter 6

Conclusions and future work

6.1 Conclusions

Polymer hydrogels are cross-linked polymer networks which can swell significantly in water. In this project, we have focused on hydrogels based on poly(acrylic acid) (PAA). In addition to the high water-absorption efficiency, the swelling behavior of PAA-based hydrogels is pH- and salt-sensitive. In order to explore a new polymer system having both hydrophobic and hydrophilic character, we decided to combine hydrophobic poly(ethers) *i.e.* poly(propylene glycol) (PPG) and poly(tetrahydrofuran) (PTHF), which are not widely used, into the PAA hydrogel networks. As mentioned in the introductory chapter, the cross-links of hydrogels can be formed by using either physical or chemical interactions. Both routes have been pursued in this thesis. We hypothesise that the resulting amphiphilic hydrogels may be applied as carriers which are suitable for both hydrophilic and hydrophobic active ingredients, with a release behaviour that can be controlled by pH, salt concentration, and type of solvent.

The experimental work was divided into four experimental sections as follows. Chapters 2 and 3 report on chemically cross-linked PAA based microgels. Two different poly(ethers) were used as macro cross-linkers to prepare the microgels. One is commercial PPGDA with M_n 800, whilst PTHF with divinyl acrylate end groups was prepared from PTHF with M_n 1000. The hydroxyl end groups of PTHF were modified to vinyl acrylate using two different esterification reactions: i) with methacrylic anhydride, trimethyl-amine and 4-dimethylaminopyridine (DMAP) as a catalyst to obtain PTHFDMA cross-linker, and ii) with acrylic acid and *p*-toluenesulfonic acid as a catalyst to obtain PTHFDA cross-

linker. According to the integration of ^{1}H-NMR, the PTHFDMA and PTHFDA were functionalised by 43% and 86%, respectively. We therefore used PTHFDA as a cross-linker to prepare the PAA microgels. We first prepared poly(*tert*-butyl acrylate) (P*t*BA) microparticles with PPGDA cross-linker (at mole ratios of monomer to cross-linker = 50:1, 75:1 and 100:1), and with PTHFDA cross-linker at mole ratios of monomer to cross-linker = 100:1 and 300:1) using surfactant free emulsion polymerization in aqueous medium with potassium persulfate (KPS) as initiator. Then, the *tert*-butyl groups of P*t*BA were converted to carboxyl groups using acid-hydrolysis (TFA in dichloromethane at room temperature), and consequently PAA microgels were obtained. The chemical structure of the resulting PAA microgels was confirmed by FT-IR and ^{1}H-, ^{13}C-, and HSQC-NMR. From TEM images, the dry sizes of 100:1 P*t*BA/PPG and 100:1 P*t*BA/PTHF microparticles were 212±18 nm and 380±25 nm in diameter, and after the acid-hydrolysis the dried sizes had slightly decreased to 189±7 nm and 369±39 nm, respectively. These results show that well-defined PAA micro-spherical particles were prepared successfully.

After that, the swelling behaviour of the resulting PAA/poly(ethers) microgels was investigated using light scattering techniques, as well as zeta potential measurements. The radius of gyration (R_G) and hydrodynamic radius (R_H) of the microparticles were obtained from SLS and DLS, respectively. For SLS, the raw data (scattering intensity vs scattering angle) were analysed using RGD theory, the Guinier approximation as well as the Sasview program to obtain the particle size. Due to some limitations of the RGD and Guinier approaches, the SasView program with a polydisperse sphere model was the preferred method to obtain the particle radius (R) and hence the radius of gyration (R_G) as $R_G = \sqrt{3/5}\,R$, as well as the polydispersity (PD; defined as standard deviation in size divided by the mean size of microparticles). In addition, the internal structure of microparticles can be evaluated from the 'shape factor (ρ)' defined as the ratio of R_G/R_H.

The P*t*BA microparticles are hydrophobic due to the presence of *tert*-butyl acrylate pendant groups, so they swelled considerably better in THF and in acetone than in water, consistent with the increasing polarity index of the solvents. However, the swelling ratio of these P*t*BA microparticles showed little dependence on the cross-linking density. The PD values in all solvents were in the range of 0.01-0.12, indicating a narrow size distribution of the particles. The shape factor of P*t*BA microparticles was in the range of 0.6-0.8, close to the value 0.775 expected for homogeneous, solid spheres. This indicates that the swelling of these P*t*BA microparticles is homogeneous.

Comparing the particles before and after hydrolysis of P*t*BA to PAA, the removal of the *tert*-butyl acrylate groups might be expected to lead to a decrease in particle size. However, we found that even in the collapsed state (pH 3.5) the particle size of PAA microgels was larger than that of the precursor P*t*BA ones. We ascribe this observation to hydration of the PAA groups, even under low pH conditions where the polymer is not ionised. In addition, we found that an increasing cross-linking density slightly reduces the swelling ratio of PAA microgels.

Considering the effect of pH, the P*t*BA microparticles as anticipated were not sensitive to pH, while the PAA microgels increasingly swell on increase of pH due to the ionisation of PAA. Interestingly, the swelling profile of 50:1 PAA/PPG microgels measured by DLS is markedly different from that observed with SLS. The DLS results suggest that the 50:1 PAA/PPG microgels start swelling as soon as NaOH solution is added, while the SLS results show that they will only swell when pH is greater than 7. In the swollen state (pH 9) the size of PAA/PPG and PAA/PTHF microgels is about 2 and 1.8 times the size in the collapsed state, respectively, and this swelling ratio was not dependent on the cross-linking. The PD values of most microgels were in the range of 0 - 0.2, and the ρ value of PAA microgels was in the range of 0.50 to 0.70, in line with previous work on microgels particles where the cross-linking distribution is non-homogeneous (dense core with hairy shell).[1-4] The peculiar pH dependence seen for 50:1 PAA/PPG particles (described above) resulted in rather low ρ values (0.37 – 0.6). Unfortunately, we faced a difficulty in measuring the particle size of 100:1 and 300:1 PAA/PTHF with DLS, and for 300:1 PAA/PTHF particles, the SLS results were also erratic, possibly due to some aggregation.

For particles in pH 4.5 solutions, adding 0.9 mM NaCl induced a shrinking of the 100:1 PAA/PPG microgels from 624 nm to 458 nm. However, upon further increase of salt concentration the particle size remained fairly stable in the range of 439 – 462 nm. In contrast, we found that the addition of PEO leads to a larger size of PAA microgels, perhaps due to an association between PAA microgels and PEO (at pH = 4.5). The ζ-potentials of P*t*BA microparticles were negative (-38 mV) due to the use of KPS as ionic initiator. After hydrolysis, the ζ-potentials of PAA microgels were around -21 mV at pH 4 and decreased to -39 mV at pH 7 due to an increase in carboxylate anions on PAA microgels. In addition, the ζ-potentials for 50:1 PAA/PPG were slightly lower than for 75:1 and 100:1 PAA/PPG microgels.

In summary, the swelling / de-swelling of PAA microgels are dependent on pH, salt and PEO concentrations. However, PAA microgels swell heterogeneously and the effect of cross-linking density on the swelling behaviour was limited in our experiments.

Chapter 4 covers the physical association between linear polymers of PAA and poly(ethers) in solution, characterised using three different techniques (^{1}H-NMR, DOSY, and T_2 solvent relaxation) as well as visual observations. We anticipate that the carboxyl groups of PAA can associate with the oxygen ethers of poly(ethers) *i.e.* PEO and PTHF via hydrogen bonding (H-bonding). This chapter considers the effect of M_w, type of poly(ethers), type of solvent, and concentration on the physical association. H-bonding between PAA and PEO in acidic solutions is well-known, but the study of PAA/PTHF solutions is limited. Since PTHF is hydrophobic, methanol was used as solvent for the PAA/PTHF solutions. For PAA/PEO in aqueous solutions, the pH of solution was kept around 3, since the carboxyl groups (-COO**H**) of PAA will be ionized (-COO^-) at high pH and consequently the hydrogen bonding between PAA and PEO is weakened. From our observation, only very high M_w PAA/PEO (M_w 4,000,000) in pH 3 solutions can form aggregates and separate from the aqueous media. This indicates a strong hydrogen bonding between these two polymers.

From ^{1}H-NMR spectra, protons in -COO**H** groups can be exchanged with D_2O so they cannot be detected easily. Thus, we cannot follow these protons to investigate the change of chemical shift ($\Delta\delta$) as a consequence of H-bonding. Instead, we examined protons in PAA main chains ([-C**H**$_2$-C**H**R-]; R = COOH) which are not directly affected by the H-bonding, and protons in PEO ([-C**H**$_2$C**H**$_2$-O-]$_n$) or in PTHF main chains ([-C**H**$_2$C**H**$_2$C**H**$_2$C**H**$_2$-O-]$_n$). We found a very small upfield shift to lower ppm in low M_w samples of PAA/PEO and PAA/PTHF solutions, while there is no evidence of the chemical shift change found in the very high M_w PAA/PEO solutions.

Using DOSY-NMR, the association between two polymers should lead to a decrease in self-diffusion coefficients (D_s) to two very similar values, and this would be especially noticeable for the case where the pure polymers have different D_s values. DOSY results gave such potential evidence for association both for low M_w and very high M_w of PAA/PEO solutions. In addition, the maximum hydrogen bonding formed by very high M_w PAA/PEO solutions was observed at volume ratio = 50:50, respectively. Furthermore, we did not see any evidence for the association between low M_w PAA/PEO

in methanol, and the result of low M_w PAA/PTHF in methanol was inconclusive. This is not a surprise as in aqueous solutions, the association between PAA and poly(ethers) is stabilized by the hydrogen bonding as well as the hydrophobic interaction but in methanol the main stabilizing force is hydrogen bonding alone.[5, 6]

For the R_2 solvent relaxation technique, we suggest that the association between the PAA and poly(ethers) might cause a significant difference of relaxation rate (R_2) compared with the R_2 value of the pure polymer solutions. Such a marked difference was only found for very high M_w PAA/PEO solutions, while the result of high M_w PAA/PEO solution is inconclusive. For low M_w PAA/PTHF in methanol, we varied the concentration up to 50%wt. Interestingly, at high concentration (above 20%wt) a single exponential cannot fit the relaxation curves properly due to the observation of the polymer signal. Therefore, a double exponential decay was used to fit the curves, so the relaxation of solvent and polymer components can be obtained. However, we did not observe a notable difference between the R_2 values of mixed PAA/PTHF and the pure polymer solutions. In conclusion, the results from ^{1}H-NMR may not be a helpful indicator for hydrogen bonding, while both DOSY-NMR and T_2 solvent relaxation can be used to do so.

Chapter 5 is the final experimental chapter. We performed preliminary experiments using a dialysis method to investigate whether the release of active ingredients (AIs) from commercial PAA based hydrogels or Carbopol® 690 can be controlled by pH. Benzyl alcohol (BnOH) and paracetamol were used as model AIs. We expect that these experiments will be a helpful guideline for further study using the PAA/poly(ethers) microgels prepared previously as carriers. In our experiments, the AIs were loaded into the Carbopol® 690 in the swollen state in methanol. UV-Visible spectroscopy was used to evaluate %loading and %release of AIs from the Carbopol® 690. The results show that the %loading of BnOH and paracetamol in the Carbopol® 690 was 54% and 61%, respectively. The release of BnOH from Carbopol® is clearly sustained so that the %release is around 32-46% at equilibrium (after 7 days), while the majority of BnOH from the control sample is released within 480 mins (70%) and approaches 100% after 7 days. However, the swelling of Carbopol® (effect of pH) has no marked effect on the release of BnOH. For Carbopol®/paracetamol samples, the release of paracetamol is about half the release of control samples at equilibrium (within 7 days).

Additionally, we found a higher release of paracetamol at low pH consistent with previous studies[7, 8] However, the difference of %paracetamol release in pH 4 and pH 10 is rather small (under 10%). Due to the unsuccessful results and the limited amount of PAA/poly(ethers) microgels prepared previously, we have not further applied this experiment with the PAA/poly(ethers) microgels.

6.2 Future work

The main reaction to prepare cross-linked microparticles in our project is surfactant free emulsion polymerization with KPS as initiator. The most important benefit of this method is that it only requires hydrophobic monomer and cross-linker, ionic initiator and water as medium, and spherical microparticles with a narrow size distribution can be achieved. After well-defined P*t*BA microparticles were prepared using SFEP, the particles were dried out using a freeze dryer, and a fine fluffy white powder of P*t*BA was obtained. Subsequently, a probe sonicator with a very high performance was used to re-disperse the P*t*BA powder in organic solvents, but the maximum volume of solution per time is rather small (5 ml). Among these attempts, we however still have difficulty dispersing the freeze-dried P*t*BA microparticles in organic solvents for acid-hydrolysis reaction to PAA microparticles. In addition, we tried to make a five-fold scale-up of the hydrolysis reaction, but the conversion of P*t*BA to PAA was incomplete confirmed from FT-IR results. These difficulties may eventually limit the preparation of the PAA microgels in a reasonable time. We suggest for future work that it would be worth trying other types of initiator.[9, 10] In addition, the effect of cross-linking density is insignificant in the swelling ratio of P*t*BA and PAA microgels at the mole ratio of monomer to cross-linker = 50:1, 75:1, and 100:1. To understand this effect more clearly, the cross-linking density might be widened by varying the mole ratio = 200:1, 300:1, and / or 500:1.

In chapter 4, it is suggested that the aqueous solution for PAA/PEO association should be acidic at pH around 3 to ensure that the carboxylic acid of PAA is protonated so it can strongly associate with the ether oxygen of PEO via hydrogen bonding as well as the mole ratio between PAA and PEO should be 1:1. From the results of chapter 4, ^{1}H-NMR may not be a good choice to probe the association as mentioned in the conclusion section. While DOSY-NMR can probe the association formed by low M_w PAA/PEO (M_w 5000) in pH 3 solutions at 10%wt total concentration, the results of T_2 solvent relaxation are unclear. We suggest that to strengthen the association, the concentration might have

to be increased for low M_w polymers. However, it may not work well for the association in methanol confirmed by the results of T_2 solvent relaxation for low M_w PAA/PEO (0-20%wt total concentration) and low M_w PAA/PTHF (0-50%wt total concentration). In this case, a water/methanol co-solvent might be a good candidate especially for PAA/PTHF solutions. Apart from concentration and solvent condition, the molecular weight of polymer is also a key factor for intermolecular H-bonding. As clearly observed, the strong H-bonding created by very high M_w PAA/PEO (M_w 4,000,000) in acidic solutions causes the aggregates to separate from the solutions which leads to the higher D_s value of mixed PAA/PEO than the value of pure polymers while we expect smaller D_s values due to the combination of two components. Consequently, we recommend that only homogeneous samples should be used, since the presence of aggregates may cause misleading results and affect the resolution of the DOSY spectra. Future experiments would benefit from much higher gradient strengths so that the complete attenuation functions can be measured.

As mentioned previously, we can only prepare a tiny amount (50-100 mg) of PAA microgels per time. Thus, we first tried to perform the controlled-release experiment as a function of pH using Carbopol® 690 as carrier, and UV-Vis spectroscopy was employed to measure the content of AIs (benzyl alcohol and paracetamol) loaded and released from the Carbopol® 690. However, Carbopol® 690 does not clearly show the anticipated controlled-release property triggered by pH. It might be possible that the active ingredients (AIs) were not incorporated inside the Carbopol® 690 but only attached on the surface, consequently the swelling / shrinking of the Carbopol® 690 did not affect the release of the AIs. Thus, it might be helpful if we can locate the AIs. For instance, we may try to use fluorescent dyes as AIs such as acridine orange[11] and rhodamine 6 G,[12] which can be observed with the naked eye or confocal microscopy. In addition, the property of AIs (*i.e.* solubility and disassociation) should be well-understood since the association between the AIs, carriers and medium is crucial for the release mechanism. Previously, we learned that DOSY and T_2 NMR relaxation techniques can be used to probe the association between polymers in solutions. It might be feasible to apply these techniques to investigate the controlled-release of AIs. For example, Alexander *et al.*[13] investigated the release of flurbiprofen (weakly acidic drug) from Pluronic micelles at various pH values using DOSY-NMR. While the D values of the micelles were stable, at above the pK_a of drug (~6.5) the D values of the drug were gradually increased attributing to the release of the drug from the micelles.

Also, we could use paramagnetic markers to enhance the relaxation rates inside the gels compared to the bulk solution as well as trapping silica nanoparticles inside the gel particles.

Bibliography

1. M. S. Wolfe, C. Scopazzi. *Journal of Colloid and Interface Science* **1989**, *133*, 265-277.

2. M. Antonietti, W. Bremser, M. Schmidt. *Macromolecules* **1990**, *23*, 3796-3805.

3. M. Reufer, P. Diaz-Leyva, I. Lynch, F. Scheffold. *European Physical Journal E* **2009**, *28*, 165-171.

4. J. Clara-Rahola, A. Fernandez-Nieves, B. Sierra-Martin, A. B. South, L. A. Lyon, J. Kohlbrecher, A. F. Barbero. *Journal of Chemical Physics* **2012**, *136*, 7.

5. T. Ikawa, K. Abe, K. Honda, E. Tsuchida. *Journal of Polymer Science Part A-Polymer Chemistry* **1975**, *13*, 1505-1514.

6. H. J. Ahn, E. C. Kang, C. H. Jang, K. W. Song, J. O. Lee. *Journal of Macromolecular Science-Pure and Applied Chemistry* **2000**, *37*, 573-590.

7. J. Parojcic, J. Duric, M. Jovanovic, S. Ibric, D. Jovanovic. *Journal of Pharmacy and Pharmacology* **2004**, *56*, 735-741.

8. G. Bonacucina, M. Cespi, G. Mencarelli, G. Giorgioni, G. F. Palmieri. *Polymers* **2011**, *3*, 779-811.

9. J. A. Bonham, M. A. Faers, J. S. van Duijneveldt. *Soft Matter* **2014**, *10*, 9384-9398.

10. J. A. Bonham, F. Waggett, M. A. Faers, J. S. van Duijneveldt. *Colloid and Polymer Science* **2017**, *295*, 479-486.

11. I. A. Gutowski, D. Lee, J. R. de Bruyn, B. J. Frisken. *Rheologica Acta* **2012**, *51*, 441-450.

12. M. Dinkgreve, M. Fazilati, M. M. Denn, D. Bonn. *Journal of Rheology* **2018**, *62*, 773-780.

13. S. Alexander, W. M. de Vos, T. C. Castle, T. Cosgrove, S. W. Prescott. *Langmuir* **2012**, *28*, 6539-6545.

Appendix A

Experimental techniques

A.1 Light scattering

Light scattering (LS) is a key technique in our experiments to measure the particle size, shape, polydispersity, thermodynamic properties of colloidal particles dispersed in solutions. In **Figure A.1**, LS technique is capable of measuring the particle size in the range of 10 nm – 10,000 nm [1,2] which covers the size range of microgels (10-1,000 nm).[3]

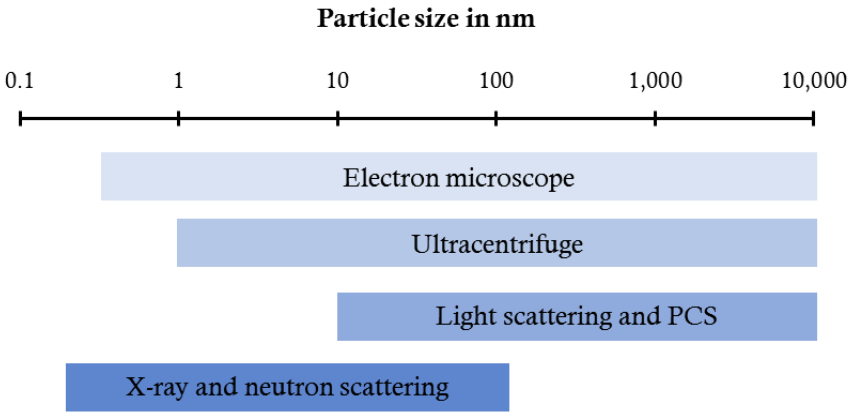

Figure A.1 Size ranges measured by different sizing techniques.[1] Modified from ref. [1]. Copyright (2010) by John Wiley and Sons, Ltd.

As show in **Figure A.2**, when a laser beam hits a target sample, the intensity of the scattered light (I) is measured by a photon detector as a function of time (t) at a fixed angle (θ) for dynamic light scattering (DLS) experiment, and as a function of degree of angle (θ) for static light scattering (SLS) experiments.

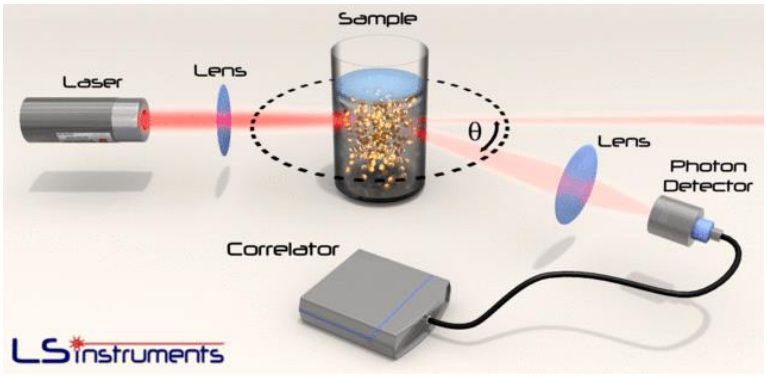

Figure A.2 Basic layout of a LS experiment.[4]

In our study, both DLS and SLS experiments were used to measure the particle size of microgels. Hydrodynamic radius (R_H) was obtained from the DLS, where the scattering angle (θ) is fixed at 90°. Static radius (R_S) and radius of gyration (R_G) were obtained from the SLS, where the θ was varied in the range of 30 – 140°.

A.1.1 Dynamic light scattering (DLS)

Dynamic light scattering (DLS) is also known as Photon Correlation Spectroscopy (PCS) or Quasi-Elastic Light Scattering (QELS). Fluctuations in the scattered intensity with time are observed due to a random and continuous movement (Brownian motion) of colloidal particles in a dispersion and accordingly, the faster movement (smaller size) of particles causes a more rapid fluctuation of the scattered intensity as shown in **Figure A.3**(a).[5,6]

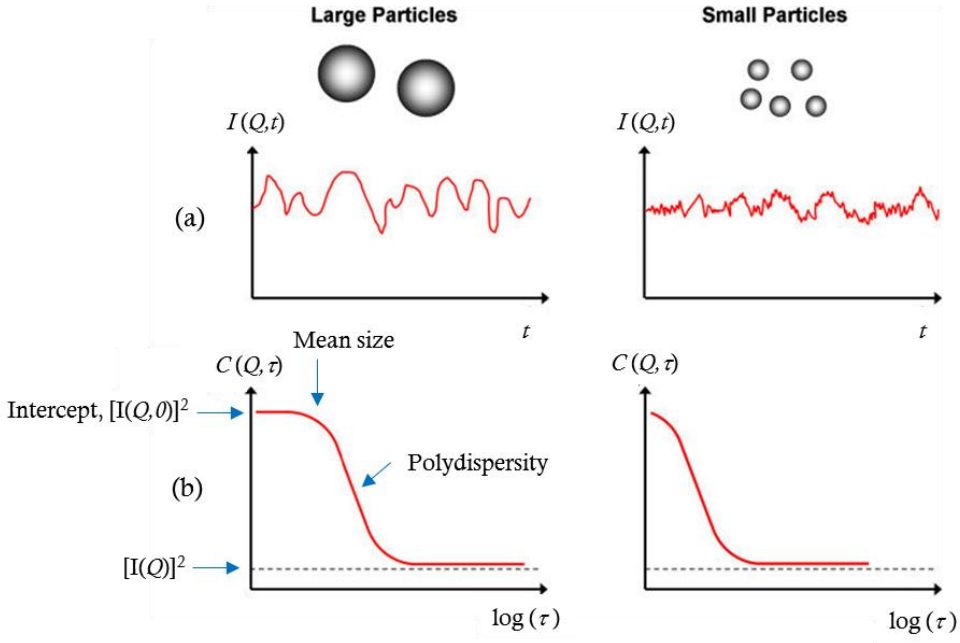

Figure A.3 Schematic illustrations of (a) the scattered light fluctuation ($I(Q,t)$) and (b) plots of correlation function ($g_2(Q,\tau)$ or $C(Q,\tau)$) as a function of lag time (delay time, τ) from small and large particles.[7] Revised and reprinted from ref. [7]. Copyright (2013) by Nanoscale Research Letters.

The time-dependent intensity fluctuation is measured directly, but it is generally expressed in terms of autocorrelation functions as shown in **Figure A.3**(b). Plot of correlation function vs delay time (τ) informs the mean size of particles from the start of the decay and the polydispersity from the gradient of the decay.[8]

The intensity correlation function (or the second-order correlation function), $g_2(Q,\tau)$ is defined as Equation (A.1):[5,6,9]

$$g_2(\tau) = \frac{\langle I(t)I(t+\tau)\rangle}{\langle I(t)\rangle^2} = \{1 + |g_1(\tau)|^2\} \qquad \text{(A.1)}$$

Where $I(t)$ and $I(t+\tau)$ represent the fluctuating intensity at time (t) and at delayed times ($t+\tau$), respectively. The braces represent the average of the intensity during the experiment time.

The electric field correlation function (or the first-order correlation function), $g_1(\tau)$ is defined as Equation (A.2): [5,9]

$$g_1(\tau) = \frac{\langle E(t)E(t+\tau)\rangle}{\langle E(t)\rangle^2} \quad \text{(A.2)}$$

Where $E(t)$ and $E(t+\tau)$ represent the scattered electric fields.

For monodisperse particles in Brownian motion, the $g_1(\tau)$ decays exponentially with the decay rate ($\Gamma=Q^2D_s$) as following Equation (A.3):[6,7,9]

$$g_1(\tau) = \exp(-D_s Q^2 \tau) \quad \text{(A.3)}$$

Where D_s is self-diffusion coefficient and the magnitude of the scattering vector (Q) is defined as Equation (A.4):[1,5,6,9]

$$Q = \frac{4\pi n_D}{\lambda} \sin\left(\frac{\theta}{2}\right) \quad \text{(A.4)}$$

Where n_D is the refractive index of solvent, θ is the scattering angle and λ is the wavelength of the laser light.

With the D_s calculated from the decay rate (Γ), the hydrodynamic radius (R_H) of an equivalent hard sphere diffusing at the same rate as the observed particles can be determined using the Stokes-Einstein equation as following Equation (A.5):[1,5,6,9]

$$D_S = \frac{kT}{f} = \frac{kT}{6\pi\eta R_H} \quad \text{(A.5)}$$

Where k_B is the Boltzmann constant, T is the absolute temperature and η is the viscosity of the solvent.

A.1.2 Static Light scattering (SLS)

Static light scattering (SLS) is similar to DLS, but the scattered light intensity ($I(Q)$) is measured as a function of degree of angle (θ) which is further represented by the scattering vector, Q (see Equation 3). The SLS data can be analysed with various approaches such as Zimm plot and Guinier plot, and consequently the weight average molecular weight (M_W), the radius of gyration, $\langle R_G^2 \rangle^{1/2}$ and the second virial coefficient (A_2) can be obtained.

The relationship of the dimension of a particle and the radius of gyration (R_G) depends on the size and shape of the particle. For example, $R_G = \sqrt{3/5}\, R$ for a solid sphere where R = radius, $R_G = \sqrt{2/3}\, R$ for a circular ring, $R_G = R/\sqrt{2}$ for a thin disk, and $R_G = l/\sqrt{12}$ for a thin rod where l is the rod length.[1]

In our study, the SLS data is analysed using three different approaches: the Rayleigh-Gans-Debye (RGD) theory, the Guinier approximation and the SasView software.

A.1.2.1 Rayleigh-Gans-Debye (RGD) theory

For homogeneous spheres with radius R in the RGD regime, the particle form factor, $P(Q)$ is given by Equation (A.6):[1,6]

$$P(Q,R) = \left[\frac{3}{(QR)^3}(\sin(QR) - QR\cos(QR))\right]^2 \qquad \text{(A.6)}$$

In the plot of $P(Q)$ as a function of scattering vector, Q, the radius of sphere (R) is determined from the position of the first minimum $P(Q)$ with a relationship of $Q_{min}R = 4.49$. In addition, effect of polydispersity, σ on the form factor curves is shown in **Figure A.4**. Increase in the polydispersity causes the minima to be filled in.

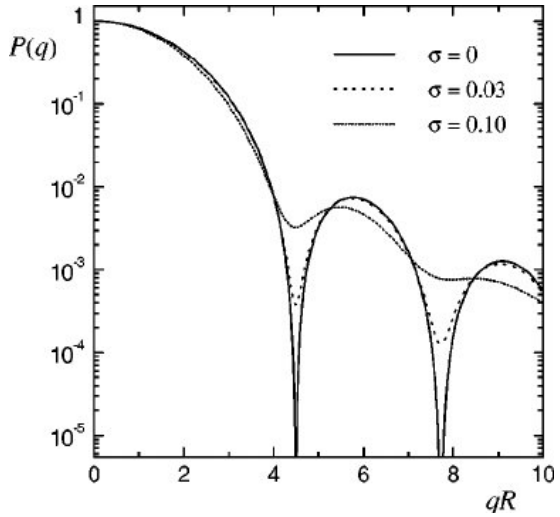

Figure A.4 Effect of polydispersity index, σ on the particle form factor, *P(q)* as a function of *qR.*[10] Reprinted from ref. [10]. Copyright (2000) by Physical review. E.

A.1.2.2 Guinier approximation

The Guinier approximation considers the scattering intensity $I(Q)$ at low values of Q, where $QR_G < 1$ for dilute systems and the scattering is independent of the shape of particles given by Equation (A.7):[1]

$$I(Q) = \Delta\rho^2 N_P V_P^2 \exp\left(\frac{-Q^2 R_G^2}{3}\right) \qquad \text{(A.7)}$$

Where $\Delta\rho$ is the contrast in scattering length density between a particle and the matrix ($\Delta\rho = \rho_P - \rho_M$), N_P is the number of particles in the sample, and V_P is the volume of a particle.

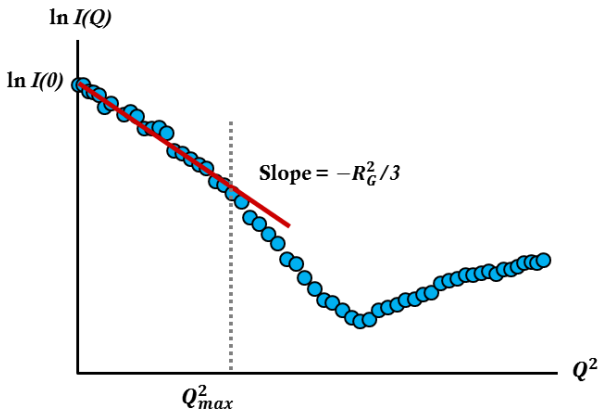

Figure A.5 Guinier plot of ln $I(Q)$ vs Q^2 with a slope of $-R_G^2/3$ and a linear up to the limit of $Q_{max}R_G < 1$.

From the plot of natural log of $I(Q)$ versus Q^2, a slope of $-R_G^2/3$ is then calculated to obtain the R_G for any isometric particles as shown in **Figure A.5**. It must be noted that this approach is only valid for a linear section up to the limit $Q_{max}R_G < 1$.

In our experiments, we found that the RGD theory and the Guinier approximation cannot analyse the SLS data for all conditions of microparticles, since these approaches are only valid for small QR_G. With the RGD theory, given the scattering angle range of 30-140°, the first minimum intensity can be found only for spheres with radii ranging from 153 nm to 554 nm. With the Guinier approximation, although we considered the slope in a small range of degree of 30-60°, the QR_G is often much higher than 1 due to the large size of PAA microgels in swollen states. Consequently, we then tried the SasView software to analyse the particle size of microgels.

A.1.2.3 SasView software

The SasView software with sphere model was used to analyse SLS data and the radius of sphere, *R* can be evaluated. The form factor for a monodisperse spherical particle with uniform scattering length density is normalized by the particle volume as following Equation (A.8):[11]

$$P(Q) = \frac{scale}{V}\left[3V(\Delta\rho)\frac{(\sin(QR)-QR\cos(QR))}{(QR)^3}\right]^2 + bkg \qquad (A.8)$$

where *scale* is a volume fraction, *V* is the volume of the particle, *r* is the radius of sphere, *bkg* is the background level, sld and sld_solvent are scattering length densities (SLDs) of the particle and the solvent respectively, whose difference is $\Delta\rho$.

The form factor for a spherical particle with a core-shell structure is normalized by the particle volume as following Equation (A.9):[11]

$$P(Q) = \frac{scale}{V_s}\left[3V_c(\rho_c-\rho_s)\frac{(\sin(QR_c)-QR_c\cos(QR_c))}{(QR_c)^3} + 3V_s(\rho_s-\rho_{solv})\frac{(\sin(QR_s)-QR_s\cos(QR_s))}{(QR_s)^3}\right]^2 + bkg \qquad (A.9)$$

Where *scale* is a scale factor, *V* is the volume, *r* is the radius, ρ is the scattering length density, *bkg* is the background level. The subscripts '*s*', '*c*', '*solv*' refer to shell, core, and solvent, respectively.

In addition, we allow the polydispersity (PD) to be additional for fitting the SLS data. However, the form factor equation for polydisperse sphere model is not given anywhere on the SasView documentations.[11] Polydispersity is represented by Gaussian distribution defined as Equation (10):[12]

$$f(x) = \frac{1}{Norm}\exp\left(-\frac{(x-x_{mean})^2}{2\sigma^2}\right) \qquad (A.10)$$

Where *Norm* is a normalization factor which determined during the numerical calculation, x_{mean} is the mean of the size distribution and the polydispersity (PD) is the ratio of standard deviation, σ to x_{mean}.

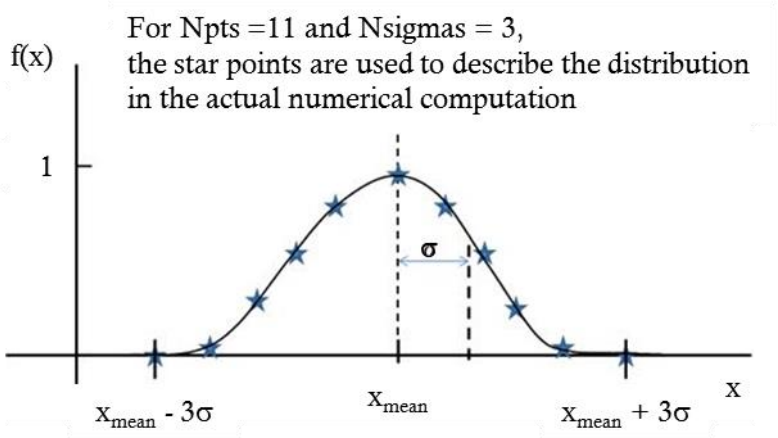

Figure A.6 Polydispersity represented by Gaussian Distribution.[12]

Table A.1 Parameter set up for sphere and core-shell models used to fit SLS data.

Model	Parameter	Value	Unit
Sphere	scale	variable	-
	radius	based on DLS	Å
	sld_sphere	1	$Å^{-2}$
	sld_solvent	0	$Å^{-2}$
	background	variable	cm^{-1}
	Polydispersity	0-0.3	-
Core-shell	scale	variable	-
	(core) radius	based on DLS	Å
	thickness	based on DLS	Å
	sld_core	1	$Å^{-2}$
	sld_shell	0.5, 2	$Å^{-2}$
	sld_solvent	0	$Å^{-2}$
	background	variable	cm^{-1}
	Polydispersity	above 0.1	-

A.2 Solvent Relaxation NMR

NMR spectroscopy is one of the most powerful techniques to identify molecular structures and dynamics. Particularly, NMR solvent relaxation is the measurement of the relaxation times of the proton in solvent molecules which is widely used to probe the strength and interaction of solid-liquid in dispersions such as polymer/solvent systems, an absorption of polymers or surfactants to colloidal particles in dispersions.[13-15] It is advantageous that deuterated solvents are not required.

NMR spectroscopy is based on the alignment of spin of atomic nuclei in response to the externally applied magnetic field. When the number of neutrons and protons are odd or the number of neutrons plus protons are odd, the nuclear spin is non-zero causing a spin angular moment with a magnitude of $J = \sqrt{I(I+1)}\hbar$ in an external magnetic field, B_0. For example, when the external magnetic field is applied in the z-direction, the proton (^{1}H) will have two spin states with magnetic quantum number of m = 1/2 and -1/2 leading to the difference in potential energy between two states, $\Delta E = \gamma \hbar B_0^Z$ where B_0 is the strength of applied filed in the z-direction, γ is the gyromagnetic ratio (for ^{1}H, γ = 2.675×10^8 rad T^{-1} s^{-1}) and $\hbar$ is the reduced form of the Planck constant, $\hbar = h/2\pi$. The relevant numbers of spins in each level are predicted by Boltzmann distribution given by Equation (A.11):[14]

$$\frac{N_{-1/2}}{N_{1/2}} = e^{-\Delta E/k_B T} \qquad \text{(A.11)}$$

Where k_B is the Boltzmann constant and T is the absolute temperature.

For relaxation NMR experiments, B_0 is applied on the z-axis so magnetic moment (M) rotates along the z-direction as shown in **Figure A.7**(a). When the 90° radiofrequency (RF) pulse (RF pulse is coherent) is applied along the x-axis (B_x), the spin population in upper state ($N_{-1/2}$) is slightly increased and greater than in lower state ($N_{1/2}$). After the pulse, the M is aligned along the y-axis (see **Figure A.7**(b)). Then, the system is allowed to relax for a time τ. During the relaxation process, the magnetization gradually decays to its equilibrium state, M_Z^0 and the precession of the spins releases radio frequency energy so-called Free Induction Decay, FID.

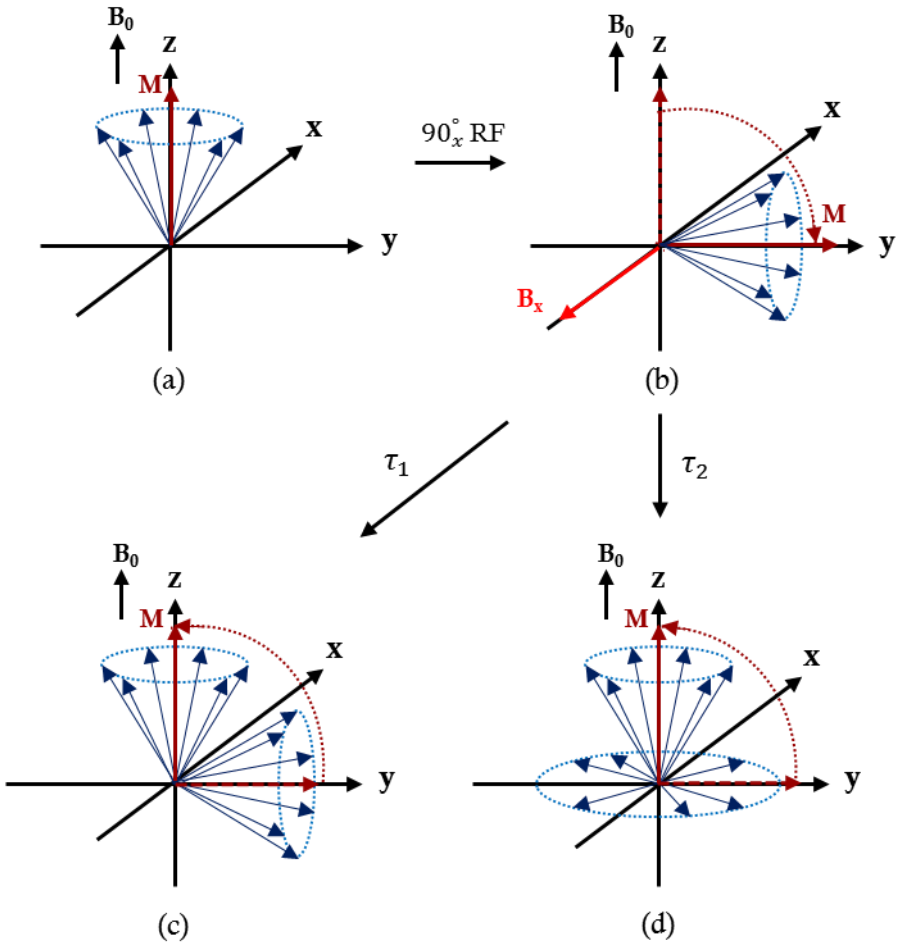

Figure A.7 Schematic illustration of (a) the magnetic moment (M) in the z-axis before applying the 90°_{x} RF pulse, (b) the magnetic moment (M) along the z-axis changed to the y-axis under the 90°_{x} RF pulse (B_x), and the rotation of the spins (c) along the z-axis (spin-lattice relaxation with a characteristic time, T_1) and (d) in the x-y plane (spin-spin relaxation with a characteristic time, T_2).

The spin-lattice or longitudinal relaxation is caused by the interaction of the nuclei and environment (lattice) and is often a first-order exponential recovery with a characteristic time, T_1, while the spin-spin or transverse relaxation is related to the decay of the coherent magnetization in the x-y plane, which is due to the field inhomogeneities and/or the interaction between the spins without the loss of energy to the surrounding, to the equilibrium state, M_Z^0 with a characteristic time, T_2.[14] In our experiments, only T_2 relaxation was considered. Since the field is not homogeneous, specific pulse sequences are generally used to measure the relaxation time. In our experiment, we used the Carr-Purcell-Meiboom-Gill (CPMG) sequence to determine the T_2 relaxation time described as a sequence of 90°_{x}-τ-180°_{x}-2τ-180-2τ..and so on.[13] Using an exponential equation to fit the

relaxation decay at time, t, the relaxation time (T_2) can be obtained given by Equation (A.12):[14]

$$M_y(t) = M_y(0)\exp\left(-\frac{t}{T_2}\right) \qquad \text{(A.12)}$$

Where $M_y(0)$ is the transverse magnetization immediately after the 90°_x RF pulse.

A.3 Diffusion Ordered NMR Spectroscopy (DOSY NMR)

DOSY NMR is a two-dimensional NMR which informs chemical shift (δ, ppm) and self-diffusion or translational diffusion coefficient (D_s). This technique is widely used to separate the NMR signals of different compounds in a mixture according to their different D_s values of each chemical component. This method is related to the Pulsed Gradient Spin Echo (PGSE) or Pulsed Field Gradient Stimulated Spin Echo (PFG-SSE or PFG-STE).

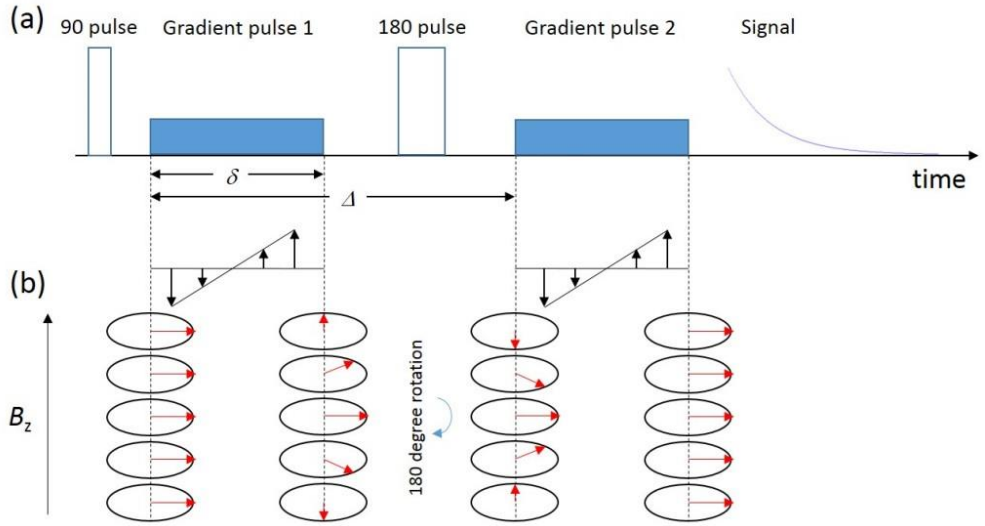

Figure A.8 Schematic diagram of (a) the PGSE pulse sequence with a pair of magnetic field gradient of duration time, δ, and (b) the phase evolution of the spins at different locations along the gradient direction.[16]

For example, the PGSE experiment is shown in **Figure A.8**. A series of diffusion spectra is recorded as a function of pulsed field gradient strengths (g), and the D_s value is calculated from the decaying signal intensity given by the Stejskal-Tanner equation (A.13):[17-19]

$$S(g) = S_0 e^{-D\gamma^2\delta^2 g^2 \Delta'} \qquad \text{(A.13)}$$

where S is the amplitude of spin echo or stimulated echo signal, S_0 is the amplitude in the absence of the diffusion (the reference intensity), D is diffusion coefficient ($m^2\ s^{-1}$), γ is the gyromagnetic ratio of the observed nucleus (4257 $s^{-1}\ G^{-1}$ for proton), g is gradient amplitude (G/m), δ is gradient diffusion length (s) and Δ' is the corrected diffusion time.

In our experiments, the DOSY NMR was performed by 'Doneshot' pulse sequence as illustrated by **Figure A.9**.

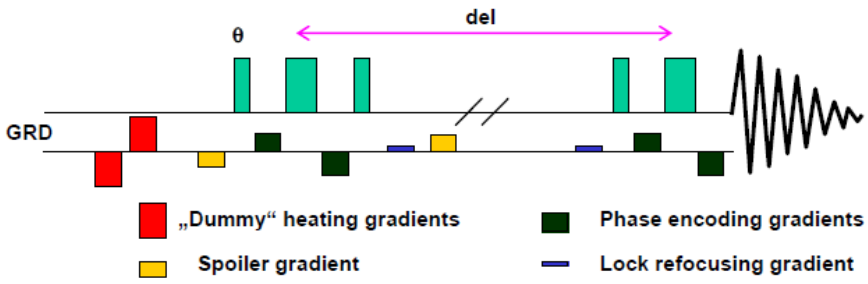

Figure A.9 Schematic illustration of Doneshot pulse sequence used in our experiment. Reprinted from Varian User Guide.

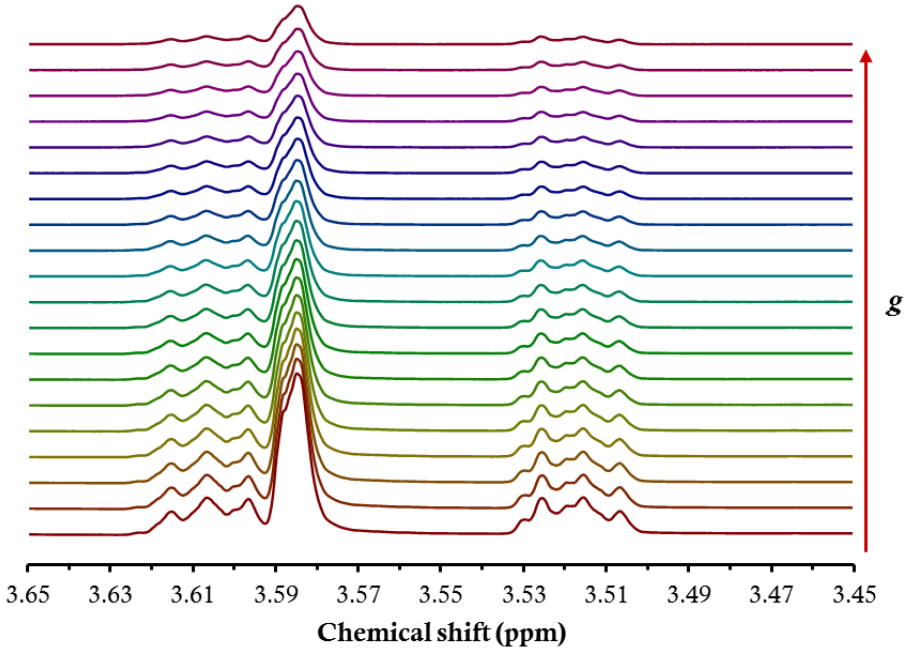

Figure A.10 The stacked NMR diffusion spectra of poly(ethylene glycol) (PEG; M_w 200) in D_2O measured by the Doneshot experiment at 25 °C, number of scans = 16, number of increments = 20, field gradient strength (g) in the range of 2000 to 25,000 G/m with diffusion time (Δ) = 50.0 ms and diffusion gradient length, δ=2 ms.

The DOSY Toolbox program was employed to evaluate diffusion coefficient that the decaying signal intensity was fitting with either Stejskal-Tanner Equation (A.13) or the NUG corrected Stejskal-Tanner equation given by Equation (A.14):[17]

$$S(g) = S_0 e^{-c_i \sum_{n=1}^{N} (D\gamma^2\delta^2 g^2 \Delta')^n} \qquad \text{(A.14)}$$

Bibliography

1. R. Richardson, In Colloid Science Principles, Methods and Applications; Cosgrove, T., Ed.; John Wiley & Sons Ltd: UK, **2010**, pp 273-298.
2. S. K. Brar, M. Verma. *Trac-Trends in Analytical Chemistry* **2011**, *30*, 4-17.
3. J. A. Bonham, M. A. Faers, J. S. van Duijneveldt. *Soft Matter* **2014**, *10*, 9384-9398.
4. Basic layout of a DLS experiment [online] Available at: https://lsinstruments.ch/en/technology/dynamic-light-scattering-dls (accessed 10 August, 2018).
5. P. N. Pusey, In Neutrons, X-rays, and Light: scattering methods applied to soft condensed matter; Lindner, P., Zemb, T., Eds.; Elsevier Science B.V.: Netherlands, **2002**, pp 203-220.
6. W. Schärtl. Light scattering from polymer solutions and nanoparticle dispersions; Springer: Berlin, **2007**.
7. J. Lim, S. P. Yeap, H. X. Che, S. C. Low. *Nanoscale Research Letters* **2013**, *8*, 14.
8. J. Moore, E. Cerasoli. In Encyclopedia of spectroscopy and spectrometry; Lindon, J. C. T., George E., Koppenaal, D. W., Eds.; Elsevier Ltd.: Netherlands, **2010**, p 2077-2088.
9. J. Stetefeld, S. A. McKenna, T. R. Patel. *Biophysical Reviews* **2016**, *8*, 409-427.
10. A. Heymann, C. Sinn, T. Palberg. *Physical Review E* **2000**, *62*, 813-820.
11. SasView model functions - Sphere Model. [online] Available at: http://www.sasview.org/sasview/user/models/model_functions.html?highlight=polydispersity#spheremodel (accessed 15 August, 2018).
12. Polydispersity distributions. [online] Available at: http://www.sasview.org/docs/user/sasgui/perspectives/fitting/pd_help.html (accessed 15 August, 2018).
13. S. J. Mears, T. Cosgrove, L. Thompson, I. Howell. *Langmuir* **1998**, *14*, 997-1001.
14. C. L. Cooper, T. Cosgrove, J. S. van Duijneveldt, M. Murray, S. W. Prescott. *Soft Matter* **2013**, *9*, 7211-7228.
15. D. Fairhurst, T. Cosgrove, S. W. Prescott. *Magnetic Resonance in Chemistry* **2016**, *54*, 521-526.

16. PGSE pulse sequence [online] Available at
: http://www.magritek.com/2016/07/18/gradients-in-nmr-spectroscopy-part-5-the-pulsed-gradient-spin-echo-pgse-experiment/ (accessed 16 August, 2018).
17. M. Nilsson. *Journal of Magnetic Resonance* **2009**, *200*, 296-302.
18. P. Groves. *Polymer Chemistry* **2017**, *8*, 6700-6708.
19. M. A. Connell, P. J. Bowyer, P. A. Bone, A. L. Davis, A. G. Swanson, M. Nilsson, G. A. Morris. *Journal of Magnetic Resonance* **2009**, *198*, 121-131.

Appendix B

B.1 Further attempts to fit scattering curves in chapter 3

The following section illustrates our attempts to analyse the SLS data of microgels at various pH using two approaches: Rayleigh-Gans-Debye (RGD) theory and Guinier approximation.

For the RGD theory, the scattering intensity (*I(Q)*) is plotted as a function of scattering vector (*Q*), and the radius of the particle (*R*) is obtained by determining the Q value at the first minimum in intensity, using the relationship, $Q_{min} = 4.49/R$. Since there is no first minimum intensity in the plot of 100:1 P*t*BA/PPG microparticles at all pH and 50:1 PAA/PPG microgels at pH 3.5 – 7, we cannot present the radii of these particles. In addition, we do not show the plot of *I(Q)* vs Q here as it can be seen in **Figure 3.11** and **Figure 3.14**.

For the Guinier approximation, ln intensity (ln *I(Q)*) is plotted as a function of scattering vector squared (Q^2) as shown in **Figure B.1**. The radius of the particle is obtained from the slope of the linear region up to the limit $QR_G < 1$ where the slope = $-R^2/5$. We typically determine the slope in a range of Q^2 = 0.66 – 2.45 $\times 10^{-4}$ nm^{-2} (or 30-60 degrees). However, we found that QR_G is often much higher than 1 due to very large size of PAA microgels in the swollen state. In addition, for 100:1 and 300:1 PAA/PTHF microgels, we calculate the radius of particles from the linear region which is found only in a more limited range of Q^2 than for other samples.

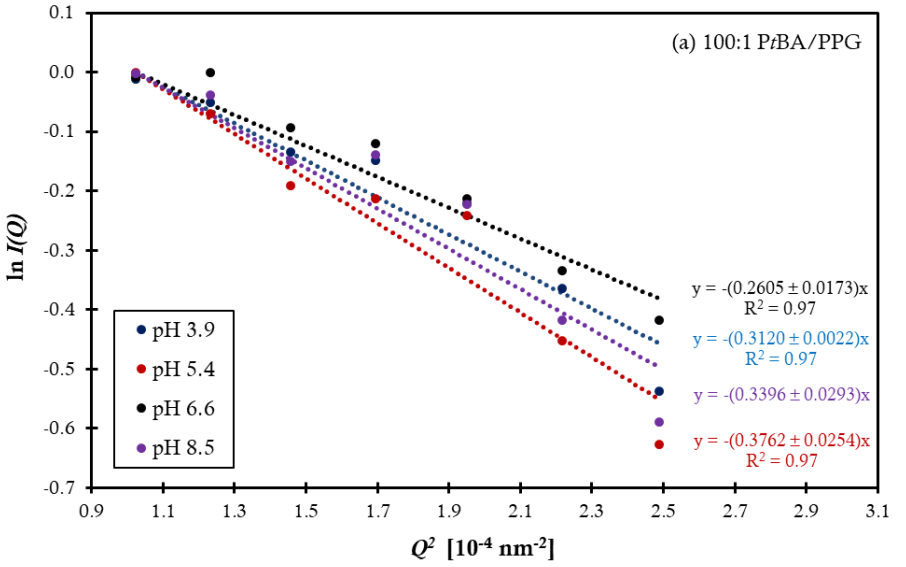
(a) 100:1 PtBA/PPG
ln I(Q)
Q² [10⁻⁴ nm⁻²]
pH 3.9
pH 5.4
pH 6.6
pH 8.5
y = -(0.2605 ± 0.0173)x
R² = 0.97
y = -(0.3120 ± 0.0022)x
R² = 0.97
y = -(0.3396 ± 0.0293)x
y = -(0.3762 ± 0.0254)x
R² = 0.97

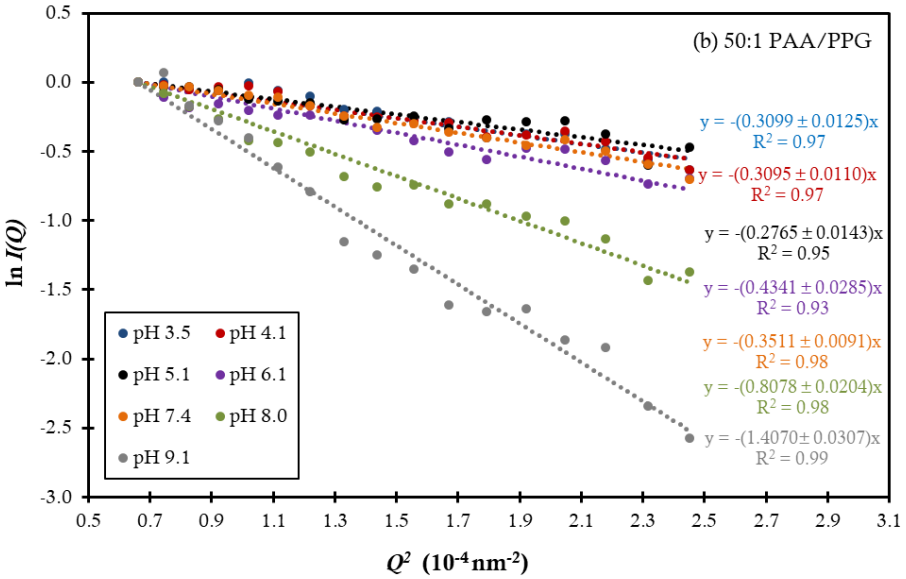
(b) 50:1 PAA/PPG
ln I(Q)
Q² (10⁻⁴nm⁻²)
pH 3.5
pH 4.1
pH 5.1
pH 6.1
pH 7.4
pH 8.0
pH 9.1
y = -(0.3099 ± 0.0125)x
R² = 0.97
y = -(0.3095 ± 0.0110)x
R² = 0.97
y = -(0.2765 ± 0.0143)x
R² = 0.95
y = -(0.4341 ± 0.0285)x
R² = 0.93
y = -(0.3511 ± 0.0091)x
R² = 0.98
y = -(0.8078 ± 0.0204)x
R² = 0.98
y = -(1.4070± 0.0307)x
R² = 0.99

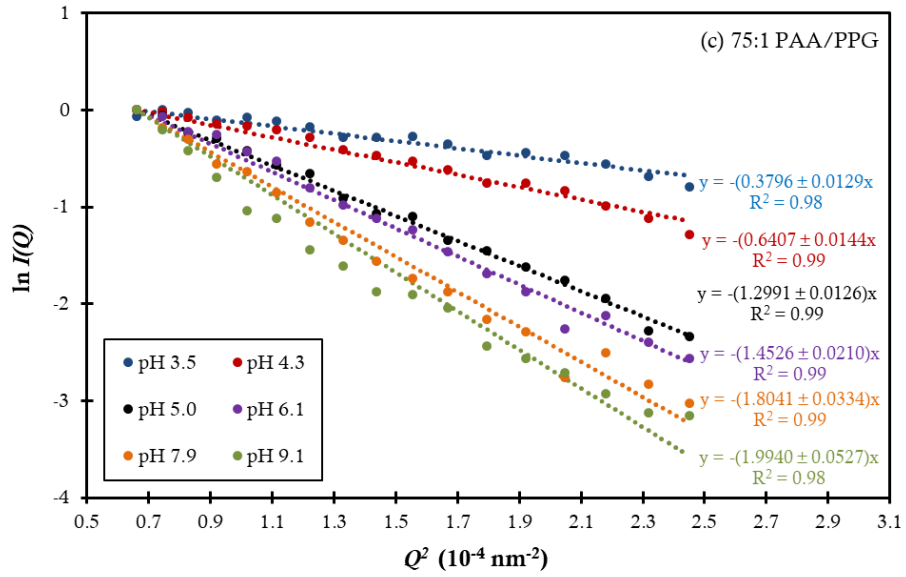
(c) 75:1 PAA/PPG
ln I(Q)
Q² (10⁻⁴ nm⁻²)
pH 3.5
pH 4.3
pH 5.0
pH 6.1
pH 7.9
pH 9.1
y = -(0.3796 ± 0.0129x
R² = 0.98
y = -(0.6407 ± 0.0144x
R² = 0.99
y = -(1.2991 ± 0.0126)x
R² = 0.99
y = -(1.4526 ± 0.0210)x
R² = 0.99
y = -(1.8041 ± 0.0334)x
R² = 0.99
y = -(1.9940 ± 0.0527)x
R² = 0.98

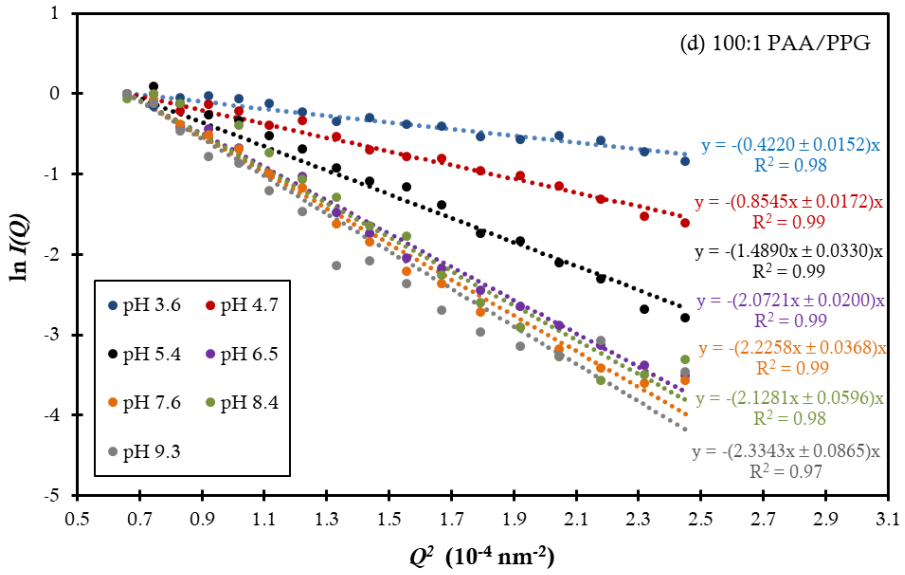
(d) 100:1 PAA/PPG
ln I(Q)
Q² (10⁻⁴ nm⁻²)
pH 3.6
pH 4.7
pH 5.4
pH 6.5
pH 7.6
pH 8.4
pH 9.3
y = -(0.4220 ± 0.0152)x
R² = 0.98
y = -(0.8545x ± 0.0172)x
R² = 0.99
y = -(1.4890x ± 0.0330)x
R² = 0.99
y = -(2.0721x ± 0.0200)x
R² = 0.99
y = -(2.2258x ± 0.0368)x
R² = 0.99
y = -(2.1281x ± 0.0596)x
R² = 0.98
y = -(2.3343x ± 0.0865)x
R² = 0.97

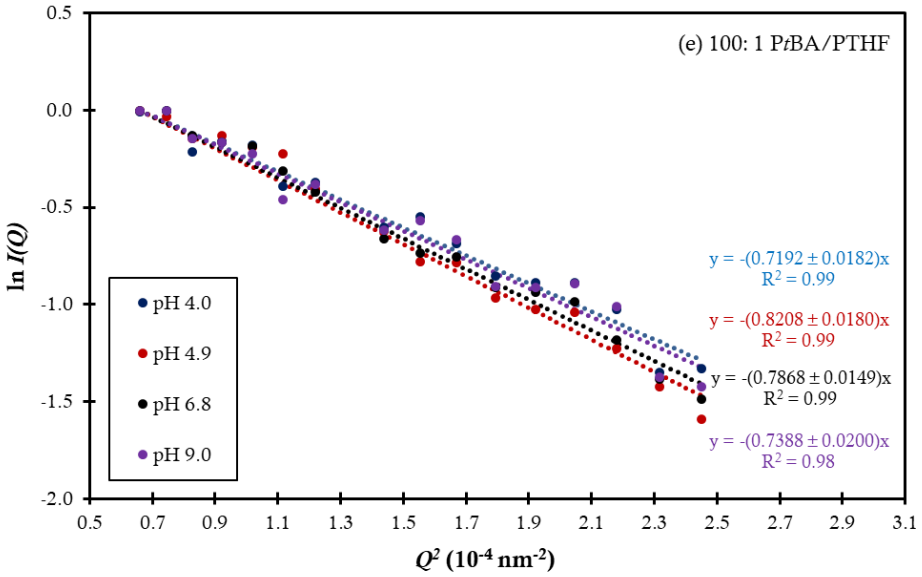
(e) 100: 1 PtBA/PTHF
ln I(Q)
Q² (10⁻⁴ nm⁻²)
pH 4.0
pH 4.9
pH 6.8
pH 9.0
y = -(0.7192 ± 0.0182)x
R² = 0.99
y = -(0.8208 ± 0.0180)x
R² = 0.99
y = -(0.7868 ± 0.0149)x
R² = 0.99
y = -(0.7388 ± 0.0200)x
R² = 0.98

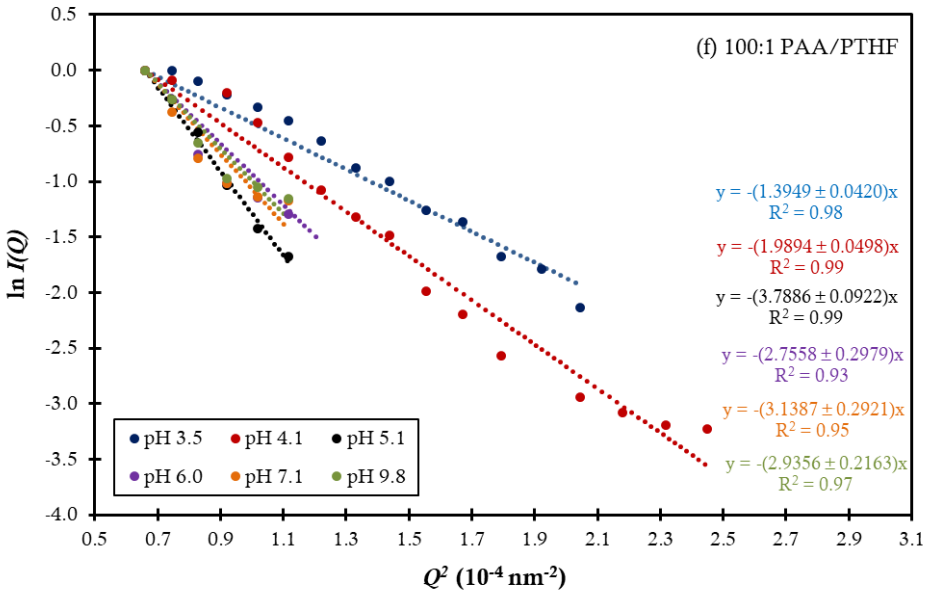

Figure B.1 Plot of ln intensity as a function of squared scattering vector (ln *I(Q)* vs Q^2) of (a) 100:1 P*t*BA/PPG, (b) 50:1, (c) 75:1 and (d) 100:1 PAA/PPG microgels, (e) 100:1 P*t*BA/PTHF microgels, and (f) 100:1, (g) 300:1 PAA/PTHF microgels.

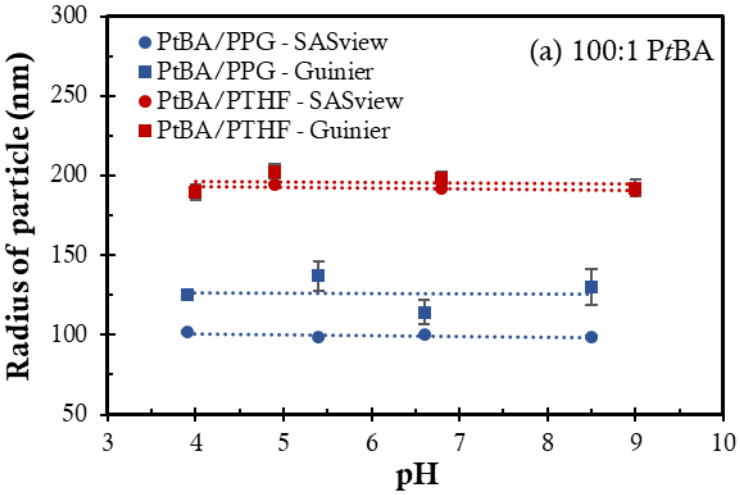
PtBA/PPG - SASview
PtBA/PPG - Guinier
PtBA/PTHF - SASview
PtBA/PTHF - Guinier
(a) 100:1 PtBA
Radius of particle (nm)
pH

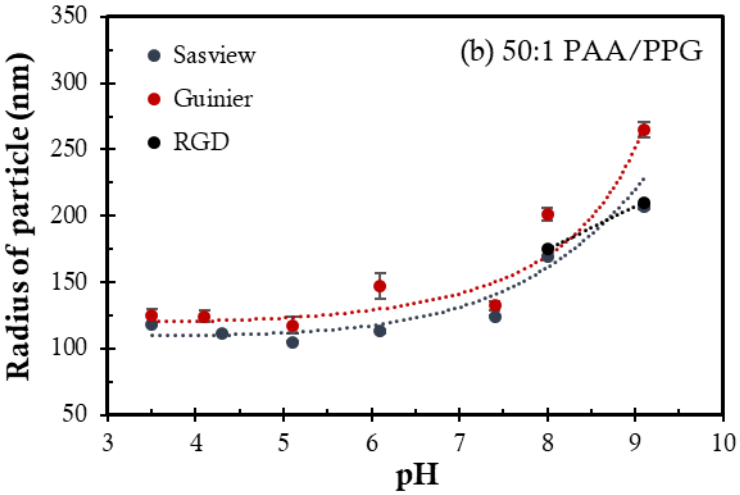
Sasview
Guinier
RGD
(b) 50:1 PAA/PPG
Radius of particle (nm)
pH

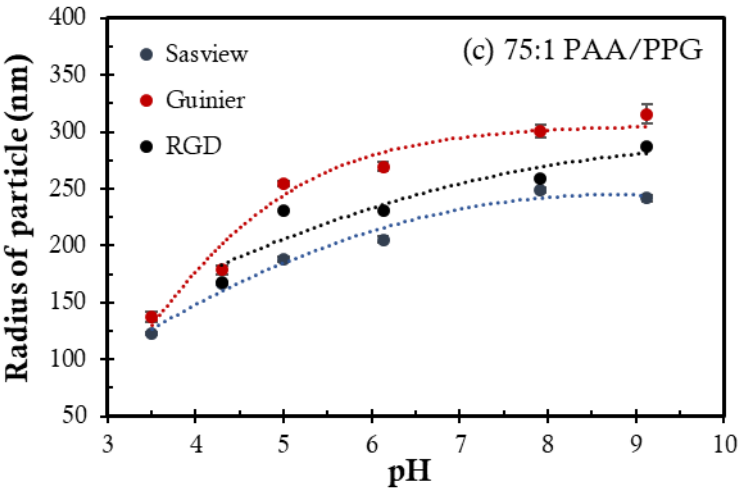
Sasview
Guinier
RGD
(c) 75:1 PAA/PPG
Radius of particle (nm)
pH

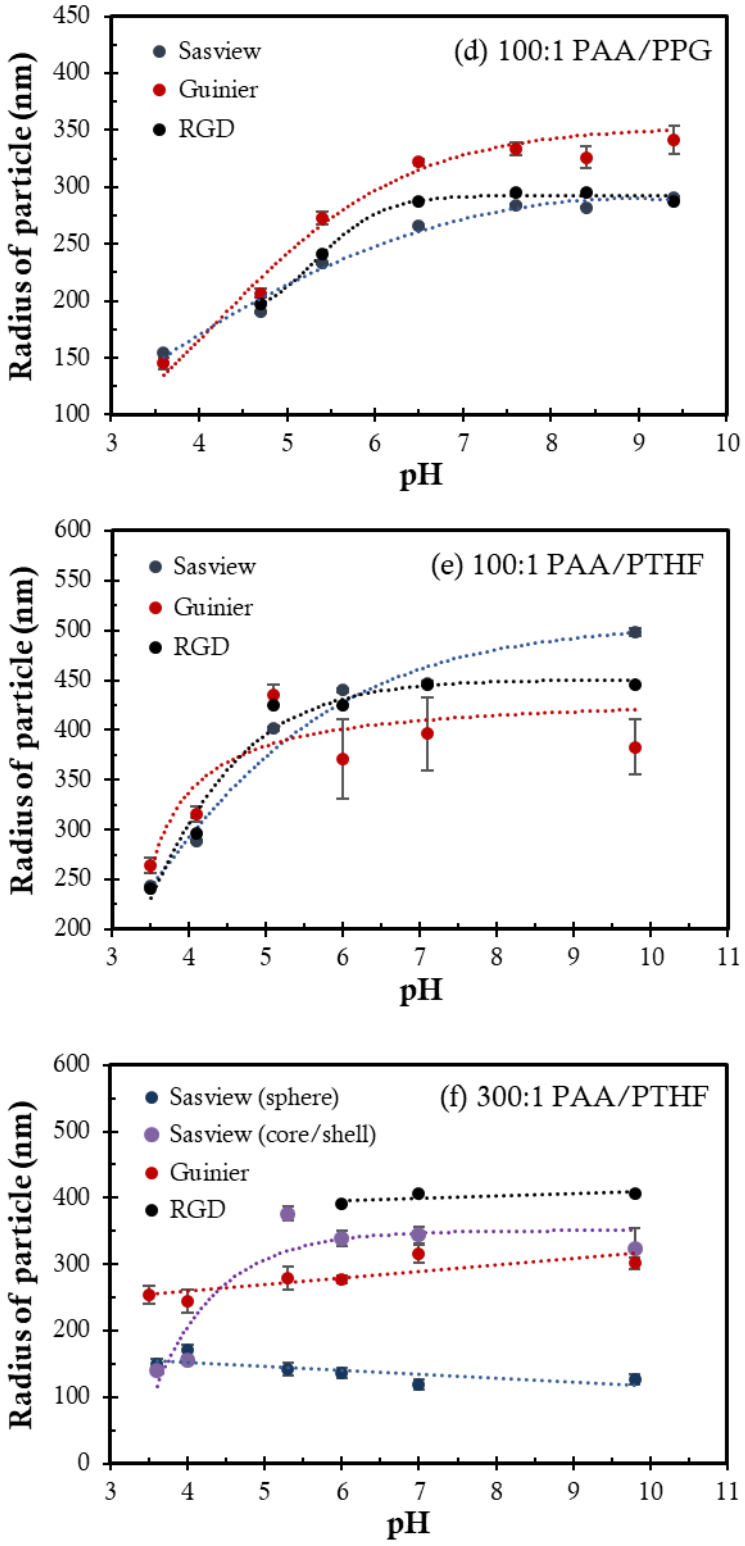

Figure B.2 Comparison of three different methods (the Sasview software with sphere model, RGD and Guinier) to calculate the radius of particle of (a) 100:1 P*t*BA/PPG and 100:1 P*t*BA/PTHF microparticles, (b) 50:1, (c) 75:1 and (d) 100:1 PAA/PPG microgels, and (e) 100:1, (g) 300:1 PAA/PTHF microgels.

B.2 Further experiments in chapter 4

From the Stejskal and Tanner equation (ST equation):

$S(g) = S_0 e^{-D\gamma^2\delta^2 g^2 \Delta'}$ where in Equation (4.2), the diffusion coefficient (D) depends on parameters: δ (gradient diffusion length) and Δ' (the corrected diffusion delay time). These parameters can be varied in the experiment set-up, while the gradient strength (g) depends on the specification of NMR machine. We once played with the parameter δ by varying the values = 2, 5 and 10.

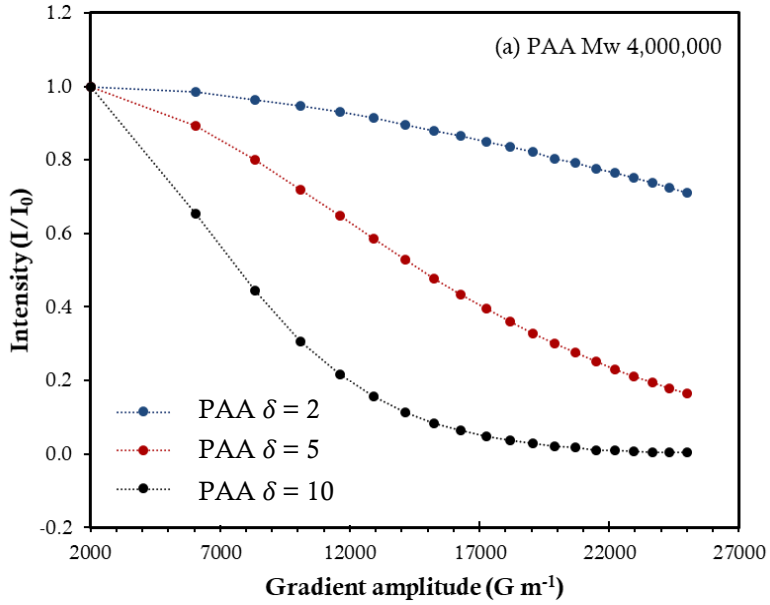

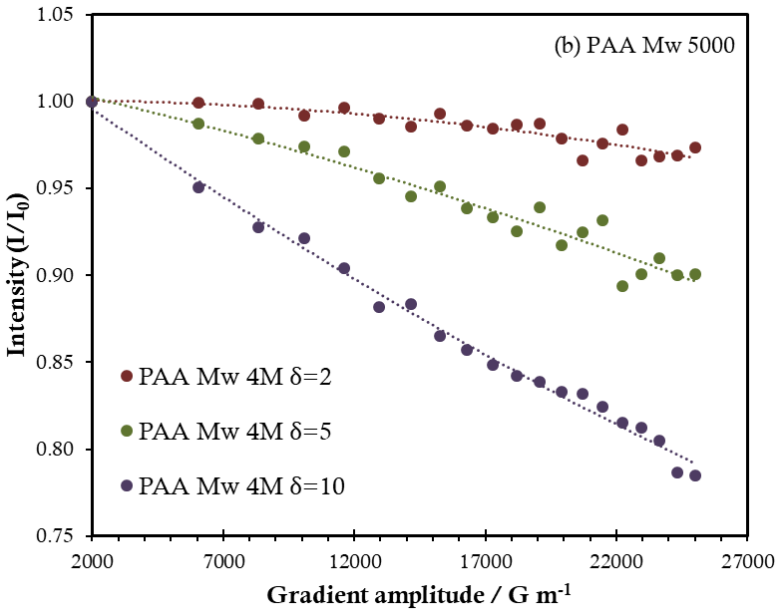

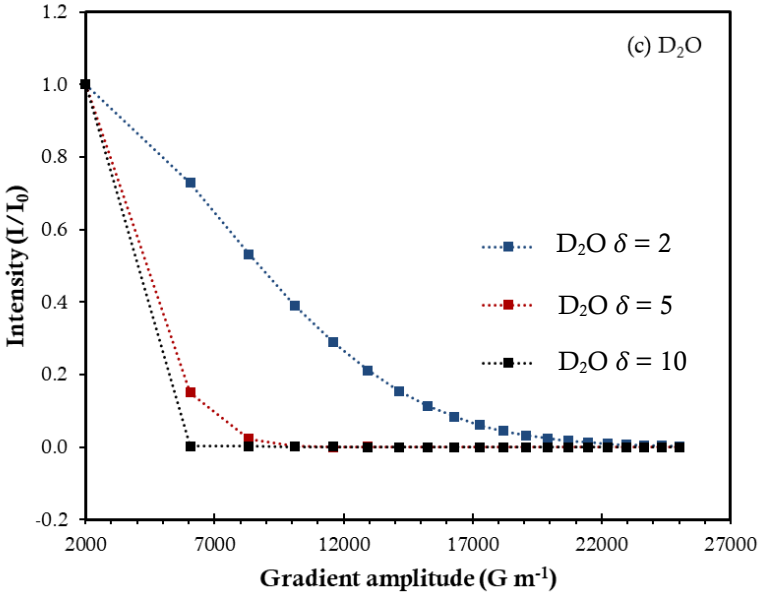

Figure B.3 Effect of diffusion gradient length (δ) on decay intensity (I/I_0) as a function of gradient strength (g) for (a) PAA M_w 4,000,000, (b) PAA M_w 5,000 in D_2O and (c) D_2O with the diffusion delay time = 50 ms (dotted lines are to guide the eye).

Figure B.3 shows the decay intensity of two different molecular weights of PAA and D_2O. The results indicate that the attenuation functions are not complete for polymer samples especially for PAA M_w 4,000,000. From the plot of ln (I/I_0) vs $g^2\gamma^2(\Delta-\delta/3)$ (s^{-1} m^{-2}), the D values (m^2/s) can be then calculated with the slope of $\delta^2 D$ where we used $\Delta' = \Delta-\delta/3$. Effect of δ on the D values obtained from DOSY Toolbox comparing to the ST equation fitting is illustrated by **Figure B.4**. As the equations used in the DOSY Toolbox program are also based on the ST equation (see Appendix A.4), the D values from our fits are rather in a good agreement with the results of the DOSY Toolbox program.

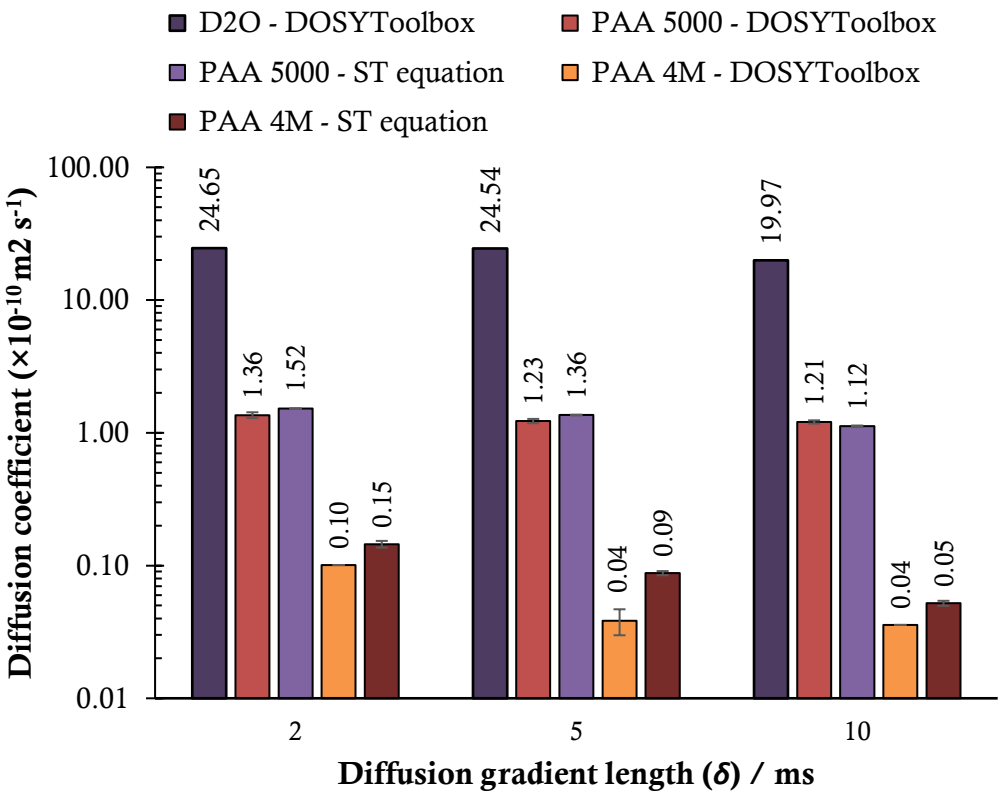

Figure B.4 Diffusion coefficient (*D*) for (a) PAA M_w 4,000,000, (b) PAA M_w 5,000 in D_2O and (c) D_2O with the diffusion delay time (Δ) = 50 ms fitted with the DOSY Toolbox and the ST equation.

B.3 Further chemical characterization in chapter 5

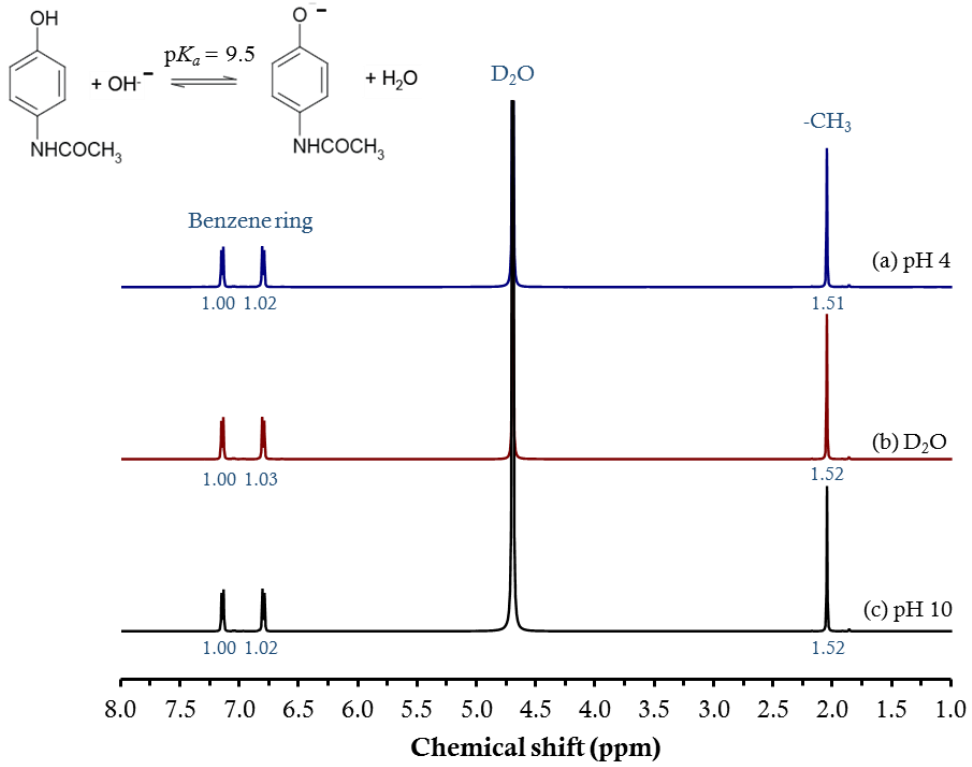

Figure B.5 ^{1}H-NMR spectra of paracetamol in (a) pH 4 (D_2O/DCl), (b) D_2O and (c) pH 10 (D_2O/NaOH).

Since we found a small shift of absorbing peak of paracetamol from 244 nm in buffer pH 2-7 to 251 nm and 258 nm in buffer pH 10 and 12, respectively, we suggest that this is due to the ionization of paracetamol with pK_a = 9.5. However, the ^{1}H-NMR spectra of paracetamol in different pH values of D_2O show no difference.